# *Degradable polyester sponges with tunable degradability made by sustainable methods*

Dissertation

submitted to obtain the academic degree of Doctor of Natural Sciences

(Dr. rer. nat.)

of the Bayreuth Graduate School of Mathematical and Natural Sciences

(BayNAT)

of the University of Bayreuth

submitted by

***Chengzhang Xu***

from *Yuxi, Yunnan Province, China*

Bayreuth, November 2023

This dissertation was prepared at the Chair of Macromolecular Chemistry II (MCII) of the Faculty of Biology, Chemistry and Geosciences at the University of Bayreuth from October 2018 to October 2023 under the supervision of Prof. Dr. Andreas Greiner with 1-year interruption.

This is a full reprint of the thesis submitted to obtain the academic degree of Doctor of Natural Sciences (Dr. rer. nat.) and approved by the Bayreuth Graduate School of Mathematical and Natural Sciences (BayNAT) of the University of Bayreuth.

Date of submission: 28.11.2023

Date of defense: 27.03.2024

Acting director: Prof. Dr. Jürgen Köhler

Doctoral committee:

Prof. Dr. Andreas Greiner (reviewer)

Prof. Dr. Andreas Möglich (reviewer)

Prof. Dr. Anna Schenk (chair)

Prof. Dr.-Ing. Holger Ruckdäschel

(additional reviewer: Prof. Dr. Markus Biesalski)

This dissertation is written as cumulative dissertation.
During my doctoral studies, the following two publications and one manuscript are part of my dissertation:

**(1) Thoroughly Hydrophilized Electrospun Poly(L-Lactide)/ Poly(ε-Caprolactone) Sponges for Tissue Engineering Application**
**Chengzhang Xu**, Jun Young Cheong, Xiumei Mo, Valérie Jérôme, Ruth Freitag, Seema Agarwal, Reza Gharibi, Andreas Greiner
Macromol. Biosci. **2023**, 2300143
https://doi.org/10.1002/mabi.202300143
Discussion in chapter 2.3, reprinted in chapter 3.1.

**(2) Investigation of the Thermal Stability of Proteinase K for the Melt Processing of Poly(L-lactide)**
**Chengzhang Xu**, Alexander Battig, Bernhard Schartel, Renée Siegel, Jürgen Senker, Inge von der Forst, Carlo Unverzagt, Seema Agarwal, Andreas Möglich, Andreas Greiner
Biomacromolecules **2022**, *23* (11), 4841-4850
https://doi.org/10.1021/acs.biomac.2c01008
Discussion in chapter 2.4, reprinted in chapter 3.2.

**(3) Cold processing of triblock copolymers under moderate pressure**
**Chengzhang Xu,** Chengwei Yi, Dipannita Ghosh, Anja Ramsperger, Julian Brehm, Christian Laforsch, Holger Schmalz, Sabine Rosenfeldt, Seema Agarwal, Andreas Möglich, Andreas Greiner (to be submitted)
Discussion in chapter 2.5, reprinted in chapter 3.3.

The following publications were achieved during my doctoral period but are not part of my dissertation:

**(4) Shape, Size, and Polymer Dependent Effects of Microplastics on *Daphnia magna***
Michael Schwarzer, Julian Brehm, Martina Vollmer, Julia Jasinski, **Chengzhang Xu**, Shakir Zainuddin, Thomas Fröhlich, Matthias Schott, Andreas Greiner, Thomas Scheibel, Christian Laforsch
Journal of Hazardous Materials **2022**, 426, 128136
https://doi.org/10.1016/j.jhazmat.2021.128136

**(5) Electrostatically Crosslinked Cellulose Nanocrystal and Polyelectrolyte Complex Sponges with pH Responsiveness**
Mor Boas, Patrick Martin, Gleb Vasilyev, Jong-Gun Lee, Rita Vilensky, **Chengzhang Xu**, Andreas Greiner, Eyal Zussman
Carbohydrate Polymers **2021**, 266, 118131
https://doi.org/10.1016/j.carbpol.2021.118131

# Contents

## List of abbreviations

| | |
|---|---|
| 2D | two-dimensional |
| 3D | three-dimensional |
| °C | degree centigrade |
| CD | circular dichroism |
| cm | centimeter |
| $CO_2$ | carbon dioxide |
| D-PFS | dip-coated PFS |
| DSC | differential scanning calorimetry |
| GPC | gel permeation chromatography |
| HDF | human dermal fibroblast |
| IM-PK | proteinase K immobilized with PAM |
| MOF | metal-organic framework |
| mPEG | methoxy-PEG |
| mPEG-*b*-PLA | methoxy poly(ethylene glycol)-*block*-polylactide |
| *N*-Suc-Ala-Ala-Pro-Leu-pNA | *N*-Succinyl-Alanine-Alanine-Proline-Leucine-*p*-nitroanilide |
| *N*-Suc-Phe-Ala-Ala-Phe-pNA | *N*-Succinyl-Phenylalanine-Alanine-Alanine-Phenylalanine-*p*-nitroanilide |
| *N*-Suc-Phe-pNA | *N*-Succinyl-phenylalanine-*p*-nitroanilide |
| NMR | nuclear magnetic resonance |
| PA | polyamide |
| PAA | poly(acrylic acid) |
| PAM | polyacrylamide |
| PCL | polycaprolactone |
| PDLA | poly(*D*-lactide) |
| PDLLA | poly(*D*,*L*-lactide) |
| PEDOT | poly(3,4-ethylenedioxythiophene) |
| PEG | poly(ethylene glycol) |
| PEO | polyethylene oxide |
| PFS | polymer fiber-based sponges |
| PI | polyimide |

| | |
|---|---|
| PIPP-*b*-PLLA | poly(2-isopropoxy-2-oxo-1,3,2-dioxaphospholane)-*block*-PLLA |
| PLA | polylactide |
| PLA-*b*-PEG | polylactide-*block*-poly(ethylene glycol) |
| PLA-*b*-PEG-*b*-PLA | polylactide-*block*-poly(ethylene glycol)-*block*-polylactide |
| PLLA | poly(*L*-lactide) |
| PS | polystyrene |
| PS-*b*-PBA | PS-*block*-poly(*n*-butyl acrylate) |
| ROP | ring-opening polymerization |
| SCD | supercritical drying |
| ss-NMR | solid-state NMR |
| $T_g$ | glass transition temperature |
| TGA-FTIR | thermogravimetric analysis coupled with Fourier transform infrared spectroscopy |
| TISA | thermally induced self-agglomeration |
| UV | ultraviolet |
| YPet | yellow fluorescent protein for energy transfer |

## Summary

This dissertation is aimed at the preparation and degradation of poly(*L*-lactide) (PLLA) sponge for tissue engineering. Three sub-aims, which are built up upon each other, could be branched from the main aim. The result of each sub-aim led to a new research field and resulted in sustainable processing. The first sub-aim is sponge preparation, including thorough hydrophilization. Surface modification methods were used for the hydrophilization of the sponges in order to conquer the inherent hydrophobicity of PLLA. Dip-coating is a well-known method for surface modification. In this work, dip-coating of a surfactant, Tween 20, was used in a sustainable way for sponge hydrophilization. The successful and efficient hydrophilization was demonstrated by hydrophilic dye staining. The strong hydrophilization was persistent even after storage in aqueous medium for a long time, favoring cell proliferation and penetration. A cell test showed the good cell compatibility of the hydrophilic sponges. Contrarily, low cell compatibility was observed in hydrophobic sponges. The hydrophilic PLLA sponges resolved the problem of the deep infiltration of cells into the sponge bulk, which was a remarkable challenge in the tissue engineering application of sponges. Hydrophilic PLLA sponges are favorable for not only biomedical applications, such as tissue engineering and drug delivery, but also other applications, such as agricultural materials.

Besides hydrophilization, the next challenge is to resolve the problem of the low degradation of PLLA to adapt to the requisites for tissue engineering application with different tissues. Hereby, the second sub-aim was proposed. In this sub-aim, an enzyme proteinase K, which was found to degrade PLLA effectively, was identified as a highly promising additive for PLLA to accelerate its degradation rate. However, the thermal processing of enzymes with PLLA might be a major issue due to their thermal sensitivity (such as with proteinase K). Therefore, new methods were established by cooperating with other groups to understand the structural changes of proteinase K at different temperatures, focusing mainly on the enzymatic activity of proteinase K. The result showed that the latter could retain its enzymatic activity in bulk state up to 130 °C. Nonetheless, proteinase K lost most of its activity once the temperature reached 150 °C or higher. The thermal processing temperature of PLLA is usually higher than 180 °C, therefore, the result clearly indicates that the encapsulation of proteinase K into PLLA during thermal processing will give rise to a limited success. This finding from the second sub-aim led to the third sub-aim: the development of the processing of proteinase K with baroplastic polymers at ambient temperatures. Utilizing baroplastic degradable polymers, it was shown that proteinase K could be processed in bulk with well-known poly(*L*-lactide)-*block*-

poly(ethylene glycol) block copolymers. It was found that poly(*L*-lactide)-block-poly(ethylene glycol)-*block*-poly(*L*-lactide) triblock copolymers with a specific ratio range of an LA/EG repeating unit (170/182 – 214/182) showed excellent baroplastic processability together with the formation of mechanically stable films. Following the baroplastic concept, polymer film could be processed with proteinase K at 37 °C under 10 MPa or higher pressure with a negligible loss of enzymatic activity. The preservation of protein functionality could be verified after processing with baroplastic by the encapsulation of a yellow fluorescent protein, yellow fluorescent protein for energy transfer (YPet), which was provided by Prof. Möglich's group. When being processed at 135 °C with baroplastic, YPet lost its yellow fluorescence. By contrast, the yellow fluorescence was maintained when processed at 37 °C. The degradation test of baroplastic film in proteinase K buffer solution showed a rather slow degradation rate, which was in accordance with the sludge water degradation result. Additionally, baroplastic displayed little toxicity against cells and Daphnia, indicating the biocompatibility of the baroplastic material in the environment. The overall result of the thesis transported a comprehensive understanding of the processing and tailored degradation of PLLA-related materials, which is promising for applications where tailored degradation is required, such as tissue engineering and agricultural materials.

## Zusammenfassung

Das Hauptziel dieser Dissertation ist die Herstellung und der Abbau von PLLA-Schwämmen für Anwendungen in der Geweberekonstruktion. Die drei aufeinander aufbauenden Teilziele der Dissertation leiten sich direkt vom Hauptziel ab. Das Ergebnis jeden Teilziels, führte zu einem neuen Forschungsgebiet und schließlich jeweils zu einer nachhaltigen Verarbeitungsmethode. Das erste Teilziel ist die Herstellung von Schwämmen und deren komplette Hydrophilisierung. Um die inhärente Hydrophobie von PLLA zu überwinden, wurden für deren Hydrophilisierung Methoden zur Oberflächenmodifizierung eingesetzt. Die Tauchbeschichtung ist eine bekannte Methode zur Oberflächenmodifizierung welche in dieser Arbeit mit dem Tensid, Tween 20, zur Hydrophilisierung der Schwämme als schonende Methode eingesetzt wurde. Die erfolgreiche und effiziente Hydrophilisierung wurde durch Färbung mit einem hydrophilen Farbstoff nachgewiesen. Die starke Hydrophilisierung blieb auch nach längerer Lagerung in wässrigem Medium bestehen und begünstigte so die Zellproliferation und -penetration. Untersuchungen mit Zellen bestätigten die gute Zellverträglichkeit der hydrophilen Schwämme. Im Gegensatz dazu wurde bei den hydrophoben Schwämmen eine geringere Zellkompatibilität festgestellt. Die hydrophilen PLLA-Schwämme lösten das Problem der Infiltration von Zellen in das Innere der Schwämme, was eine besondere Herausforderung bei der Anwendung von Schwämmen in der Geweberekonstruktion darstellte. Hydrophile PLLA-Schwämme eignen sich nicht nur für biomedizinische Anwendungen, wie für die Geweberekonstruktion und die Wirkstofffreisetzung von Medikamenten, sondern auch für andere Anwendungen als landwirtschaftliche Materialien.

Neben der Hydrophilisierung besteht die nächste Herausforderung darin, das Problem des geringen Abbaus von PLLA zu lösen, um die Anforderungen für die Geweberekonstruktion von verschiedenen Geweben zu erfüllen. In diesem Zusammenhang wurde das zweite Teilziel formuliert. Im Rahmen der Arbeiten zum zweiten Teilziel, wurde das Enzym Proteinase K, das bekannterweise PLLA effektiv abbaut, als vielversprechendes Additiv für PLLA identifiziert, um dessen Abbaugeschwindigkeit zu beschleunigen. Allerdings könnte die thermische Verarbeitung von Enzymen mit PLLA aufgrund ihrer thermischen Empfindlichkeit (wie bei Proteinase K) problematisch sein. Daher wurden in Zusammenarbeit mit anderen Gruppen neue Methoden entwickelt, um die strukturellen Veränderungen der Proteinase K bei verschiedenen Temperaturen zu untersuchen, wobei der Schwerpunkt auf der enzymatischen Aktivität der Proteinase K lag. Das Ergebnis zeigte, dass die Proteinase K ihre enzymatische

Aktivität im festen Zustand bis zu 130 °C beibehalten konnte. Ab 150 °C jedoch, verlor Proteinase K den größten Teil seiner Aktivität. Die Temperatur bei der thermischen Verarbeitung von PLLA liegt in der Regel über 180 °C, sodass das Ergebnis eindeutig darauf hinweist, dass die Mischung von Proteinase K mit PLLA in der Schmelze nur wenig erfolgversprechend ist. Die Ergebnisse des zweiten Teilziels führten zum dritten Teilziel: der Verarbeitung von Proteinase K mit baroplastischen Polymeren bei Raumtemperatur. Durch die Verwendung baroplastischer abbaubarer Polymere konnte gezeigt werden, dass Proteinase K mit bekannten Poly(*L*-Lactid)-*block*-Polyethylenglykol Diblockcopolymeren im Festkörper verarbeitet werden kann. Es wurde festgestellt, dass Poly(*L*-Lactid)-*block*-Polyethylenglykol-*block*-Poly(*L*-Lactid) Triblockcopolymere mit einem bestimmten Verhältnis der LA/EG-Wiederholungseinheiten (170/182 - 214/182) eine ausgezeichnete baroplastische Verarbeitbarkeit, zusammen mit der Bildung mechanisch stabiler Filme ergaben. Dem baroplastischen Konzept folgend, konnte der Polymerfilm mit Proteinase K bei 37 °C unter 10 MPa oder höherem Druck mit einem vernachlässigbaren Verlust an enzymatischer Aktivität der Proteinase K verarbeitet werden. Die Erhaltung der Proteinfunktionalität konnte nach der Verarbeitung mit Baroplastik auch durch die Verkapselung des gelb fluoreszierenden Proteins YPet, das von der Gruppe von Prof. Möglich bereitgestellt wurde, nachgewiesen werden. Während YPet bei der Schmelzeverarbeitung mit dem Baroplastikpolymer bei 135°C YPet seine gelbe Fluoreszenz verlor, blieb die gelbe Fluoreszenz erhalten, wenn die Verarbeitung unter Baroplastikbedingungen bei 37 °C erfolgte. Der Abbautest von Baroplastikfilmen in Proteinase-K-Pufferlösung zeigte einen eher langsamen Abbau, was mit dem Ergebnis des Abbaus in Klärschlammwasser korrelierte. Darüber hinaus zeigte Baroplastik eine geringe Toxizität gegenüber Zellen und Daphnien, was auf dessen Umweltverträglichkeit hinweist.

Das Gesamtergebnis der Arbeit vermittelt ein umfassendes Verständnis der Verarbeitung und des maßgeschneiderten Abbaus von PLLA und dessen Derivate. Daraus ergeben sich vielversprechende Ansätze für Anwendungen, bei denen ein maßgeschneiderter Abbau erforderlich ist, z. B. in der Geweberekonstruktion und bei landwirtschaftlichen Materialien.

# 1. Introduction

The aims of the thesis are the preparation, characterization and degradation of three-dimensional (3D) scaffolds made of degradable materials. Three aspects: porous materials, the preparation of polymeric sponges and degradation of polymer materials will be addressed in this chapter. The first aspect is about different types of porous materials. Next, different methods for the preparation of electrospun polymeric sponges will be discussed as representative examples of porous scaffolds. Finally, the degradation of polymer materials will focus on different methods of degradation, including hydrolytic and enzymatic degradation, together with important aspects of accelerated degradation.

## 1.1. Porous materials

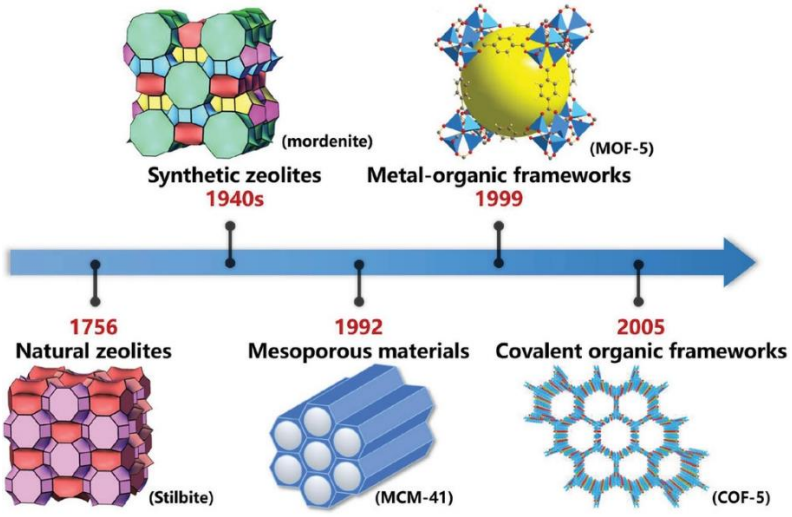


**Figure 1-1**. Milestones in the history of functional porous materials (reprinted with permission, © 2020 John Wiley and Sons).[1]

Porous materials have drawn great interest in versatile application fields, such as sensing, adsorption, separation, insulation, catalysis, energy storage and medical applications.[2, 3] The wide application of porous materials is due to their large portion of empty space, resulting in a relatively high specific surface area. Guest molecules can be efficiently absorbed, diffused or transferred.[4] The International Union of Pure and Applied Chemistry defined materials with pores less than 2 nm in size as microporous materials. Materials with a pore size between 2 and 50 nm are defined as mesoporous materials, while those with a pore size above 50 nm are defined as macroporous materials.[5] The family of porous materials has been growing rapidly

since mesoporous silica was invented in 1992 (**Figure 1-1**).[6] Nowadays, different types of porous materials have been utilized, for example, zeolite,[7] metal-organic frameworks (MOFs),[8] and polymeric porous scaffolds.[9] From a chemistry point of view, porous materials could be classified into three main categories (**Scheme 1-1**): (1) inorganic, (2) inorganic-organic and (3) polymeric, i.e. organic.[4]

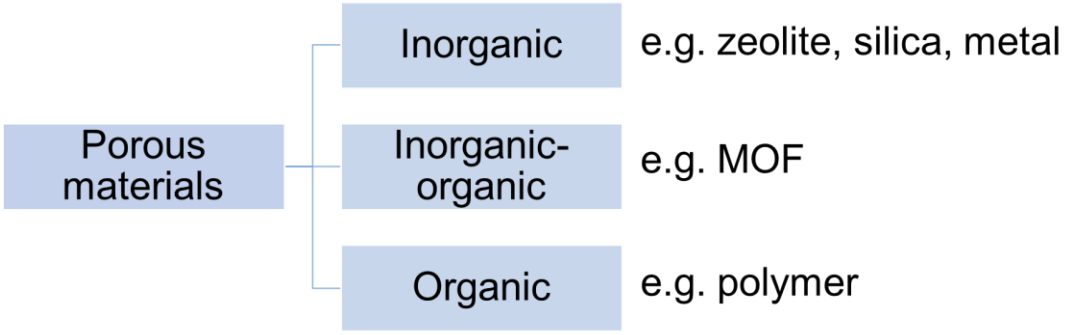


**Scheme 1-1.** Different types of porous materials.

### 1.1.1. Inorganic porous materials

#### 1.1.1.1. Zeolite

Inorganic porous materials have been used for a long time. Zeolites are representative materials of inorganic porous materials. They could be found in nature with a microporous structure,[10] and are aluminosilicates with alkaline or alkaline-earth cations.[11] Zeolite was first described by Axel Cronstedt in 1756.[12] Owing to its porous structure, zeolite has great potential in applications such as catalysis and gas adsorption.[13] After the discovery of zeolites A and X by Breck *et al.* in 1956,[14] the methods of synthesizing zeolites have been investigated intensively. Zeolites are mainly synthesized by hydrothermal treatment.[15] New methods of synthesizing zeolites have been developed over the past few decades which have led to the discovery of zeolites with novel structural features.

Catalysis is a major application of zeolites in the petrochemical industry for the degradation of long chain hydrocarbons.[16] Zeolites are also used for gas separation, where microporous architectures are necessary. In the gas separation application, zeolites are used to separate molecules of different shapes and sizes.[13] Synthetic and modified zeolites exhibit great potential in the market due to adjustable properties. However, the high manufacturing and operation costs still remain a hinderance to the application of zeolites.[17]

#### 1.1.1.2 Porous metallic materials

Porous metallic materials are commonly known as metallic foams, and have been under development for over 90 years.[18, 19] They have been widely applied due to their good mechanical properties.[20] The metal framework shows shape stability, high temperature resistance, thermal shock resistance and machinability, befitting a favorable material for the applications. Representative applications are energy and environmental protection, biological, medical and in the chemical industry. Typical metals used for the preparation of porous materials are aluminum, gold and magnesium. Aluminum is the most commonly researched metal with the longest history. Due to its light weight and good mechanical stability, porous aluminum material or its composite is widely used for energy adsorption, linkage, space frame nodes and car components in different fields, such as architecture and the automotive industry.[21] Gold has a long history in human development. It has also been intensively studied over the past twenty years due to its catalytic activity and electrical conductivity.[22] The high-surface area of porous gold has attracted a lot of attention for applications, such as in electrocatalysis, fuel cells and biosensors.[23] In addition to aluminum and gold, magnesium is also a commonly used member of porous material. Magnesium has a density similar and an elastic modulus close to human bone, and good ductility. These features can reduce the chance of bone fractures.[24] Moreover, magnesium can promote bone growth for bone healing after degradation.[25] Those properties make magnesium a benign member for tissue healing where mechanical stability is required, such as bone tissue healing.[26]

Even though porous metallic materials have been extensively studied in different fields, there are still some drawbacks and challenges remaining. The service condition, for example, in the field of energy and environmental protection is not predictable, restricting the application of porous metallic materials. Moreover, even though the latter show good prospects in medical applications, such as an artificial skeleton, the corrosion resistance and biocompatibility still need improvement.[18]

#### 1.1.1.3 Silica porous materials

In comparison with other materials, porous silica materials have the advantage of being nontoxic, and mechanically, chemically and thermally stable (not swelling).[27] They feature a high surface area, large pore volume and large fraction of pores.[28] Due to those characteristics, porous silica materials are attractive in fields such as catalysis, sensing, separation, adsorption and drug delivery.[29]

Silica materials are usually prepared as layered silicas,[30] hollow silica spheres[31] and silica nanoparticles.[32] Those structural modifications could provide stable innovative silica structures and versatile properties for numerous applications. Taking silica nanoparticles as an example, mesoporous silica nanoparticles have attracted special attention for various applications.[33] They are produced by the condensation of silica precursors using a surfactant as a template, the network of cavities forms by the removal of template molecules.[34] This kind of silica material does not only display homogeneously distributed pores but also a high density of silanol groups on the surface of the particles, favoring the subsequent modification and functionalization process. Silica nanoparticles have numerous potential applications owing to their benign properties. When being used in the catalysis field, the high surface area of silica nanoparticles could support highly accessible active sites compared with bulk silica nanoparticles.[35] The inertness, multifunctionalities and solvent-resistant properties make silica nanoparticles a preferable choice as a catalyst support material. Due to its porous structure and stability, silica nanoparticles are also used as a protein encapsulation medium. Cai *et al*., for example, encapsulated green fluorescence protein in silica nanoparticles by covalent interaction.[36] The protein was encapsulated during the silica nanoparticle preparation step in a reverse emulsion. The encapsulated green fluorescence protein showed a higher resistance against protease as well as denaturant and heat. Despite all promising properties, silica nanoparticles also have drawbacks in some applications. When being applied in the tissue engineering field, for example, the rich silanol groups on the surface might cause hemolysis due to the interaction with the surface of the phospholipids.[37] The brittleness of the silica material also limits its application in some areas where impact resistance is required.[38]

### 1.1.2. Inorganic-organic porous material

In the past few decades, reticular chemistry has opened up the space for the synthesis of porous frameworks with designed chemical composition and incorporated various functionalities on the backbone. Among those materials, the MOF and covalent organic framework are relatively young members of the family of porous materials (**Figure 1-1**). The MOFs are zeolite-related crystallized hybrid inorganic-organic frameworks with a high surface area, which allows the combination of properties of inorganic and organic porous materials.[39] The maximum degree of porosity and pore size of MOFs apparently exceed those of zeolite.[40] The porosity of MOFs measured by Brunauer–Emmett–Teller analysis could reach up to 10000 $m^2/g$, which is significantly higher than the porosity of zeolites.[41] The MOFs are constructed by secondary

building units, metal ions/clusters and multidentate organic linkers *via* coordination bonds. The building blocks and underlying topology could be specifically selected to control the pore size and shape of MOFs.[1] Due to the combination of metal ions and the relatively small organic linkers, the majority of MOFs are microporous.[42] The open channels also expedite mass transfer, facilitate substance exchange and also provide enough surface area for abundant active sites. The shapes and sizes of the pores designed make MOF a promising material for applications where defined pores are required, such as catalysis. When being used as catalysts, MOFs could be combined with other nanomaterials, such as graphene. They could be calcinated to acquire metal-carbons and heteroatoms with catalytical efficiency.[41] The metal center and organic linkage, which are located in the cavity of the MOF, synergize with a guest catalyst material. The MOFs could also be heterometallic and the metal ions in MOFs could be substituted by Earth-abundant transition metals.[39, 43, 44] Thermal stability and solvent resistance are two important factors for MOFs used as catalysts. In the early stage of MOF research, MOFs such as MOF-5[45] and MOF-77,[46] which are representative, have extraordinary surface areas. They have been applied as catalysts. However, their sensitivity to moisture and poor thermal stability limits their application. More MOFs have been chosen in the catalysis field in recent years, such as UIO-66[47] and ZIF-8.[48] The newly developed MOFs possess thermal robustness and prolonged water resistance, as verified by X-rays before and after water treatment.[49, 50]

The tunable properties of MOFs, such as designed flexibility, porosity and pore structure, make them ideal candidates for specific applications, for example, in biomedicine. They have been used in magnetic resonance imaging as contrast agents due to their high metal content, resulting in a high loading capacity of magnetic centers.[51] They are also widely used as drug carriers because of their high capacity for the storage of guest molecules provided by their high porosity. MIL-100(Cr) and MIL-101(Cr), for example, with large pores (25–34 Å) and high surface areas (3100–5900 $m^2/g$), were first utilized as drug carriers to load the analgesic model drug ibuprofen.[52] Both MIL-100 and MIL-101 showed a high drug load capacity and sustained release of ibuprofen due to the host-guest interaction.

The MOFs have been also widely used in some other research fields in the past few decades, such as energy conversion, gas storage and chemical sensing. However, the remaining criterion for the industrial application of MOFs is the rather high cost. Compared to some other porous materials, such as zeolite, which usually cost several euros per kilogram, this crucial aspect should be taken into consideration.[53] The design of MOFs with low production and

regeneration costs is essential for future industrial applications.

### 1.1.3. Polymeric porous material

Polymeric porous materials, among all the porous materials, have also received high research interest due to the manifold combination of porous structures and the properties of polymers. The shape of polymeric porous material and defined porosity can be designed flexibly.[54-56] The facile processability is another asset of porous polymers. Polymers can be processed in molded form with pores, which benefits numerous practical applications, for example, energy storage, filtration and gas separation.[57-60] Furthermore, they can be processed by solvent-based techniques while the pore structures are maintained.[61-63] These unique properties are hard to achieve utilizing other porous materials, such as zeolites or porous silicas. In addition, diverse routes of polymer synthesis make polymer porous material capable of adjusting the surface functionality in the pores or at the surface.[64-66] Another advantage of polymer materials is the light weight of elements in polymers, such as hydrogen, carbon and oxygen, that provide polymer porous materials which are competent in many applications.[67, 68] Polymeric porous materials can be divided into two main categories based on the pore geometry: closed or open cellular structure (**Figure 1-2**). In this chapter, three different types of polymer porous materials will be discussed: polymer foam, aerogel and sponge.

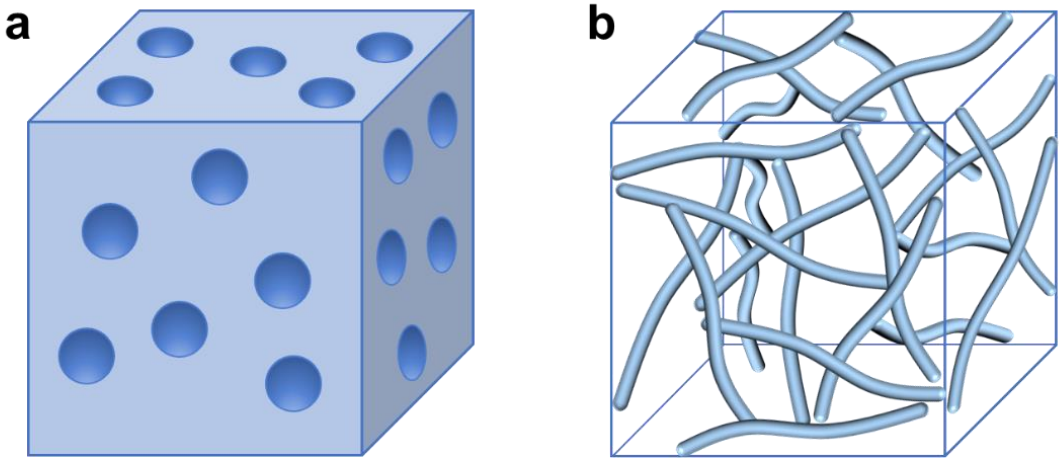


**Figure 1-2.** Polymeric porous materials with (a) a closed and (b) open cellular structure.

#### 1.1.3.1 Polymer foam

Polymer foam is an important material class characterized by closed pores.[69] Polymer foams are lightweight, have thermal insulation capacity, a sound insulation effect and the potential

for impact resistance.[70-72] They are mainly prepared by extrusion or foam injection molding using mechanical, physical and chemical foaming.[69] The foam structure can be achieved with a supercritical fluid, such as carbon dioxide ($CO_2$), endowing the polymer foam materials with a light weight and dimensional stability compared with their counterpart bulk materials.[73-75]

Polymer foam materials can be processed by three main steps: cell formation, growth and stabilization. In the cell formation step, a cell growth agent is added to a polymer melt, followed by a large amount of gas production to form a polymer-gas mixture. An increasing gas amount saturates the mixture and the gas leaches out to form cell nuclei.[76, 77] In the cell growth step, the cells close to each other will merge to form larger cells. Consequently, the cell expands and the amount of cell volume increases.[78, 79] The cell formation and growth makes the cell wall thinner. Thus, the addition of surfactants or cooling is required to stabilize the polymer foam.[80, 81]

The application of polymer foams has increased vigorously in recent years. Albeit polymer foams have benign characters, one remaining critical issue is that it is hard for them to meet high-performance requirements. Foaming, for example, introduces lightweight polymer materials, but it also causes a simultaneous loss of mechanical properties. Thus, other high-performance engineering polymer foams are attracting more attention nowadays.[82] Polyamide 6 (PA6), for example, was used by Yuan *et al.* to study the correlation between the microstructure and mechanical property using nanoclay as a reinforcement filler.[83, 84] The mechanical property (toughness) of PA6 nanoclay composite foam is improved by promoted crystallization behavior. Another common filler to increase the mechanical properties of polymer foams is glass fiber.[85] Volpe *et al.* prepared PA66 foam with a sandwich structure reinforced by glass fiber. The mechanical properties of PA66-glass fiber composite foam are remarkably enhanced because of the increased gas pressure of the fine-formed core layer. The addition of reinforcement in applications can significantly tune the functionality of polymer foams by synergies of foaming and fillers or polymer blends. The functionality desired is tailored by the dispersion, arrangement and networking of the reinforcement fillers during the foaming step.[86, 87] Due to the light weight of polymer foams, they are attracting increasing attention in the field of electric vehicles, targeting the reduction of vehicle mass to achieve less environmental pollutant and a lower fuel consumption.[88, 89] The polymer foams are applied to reduce weight and improve properties, such as impact properties.[90] The lightweight parts are of great significance not only in the automotive field but also in other fields, such as thermal and sound insulation in construction[91, 92] and aerospace.[93]

Besides their preferable properties, including the light weight, good sound absorption and low thermal conductivity, there are still challenges remaining when using polymer foams. Packing foams made from petroleum-based polymers, for example, might cause environmental debris when being discarded after use.[94-96] In addition, most of the polymers used as foams have poor flame retardation and breathability.[97-99] Regarding solutions, recent research is focusing on the preparation of biodegradable polymer foams to solve environmental issues.[100, 101] In order to improve the flame retardation, flame retardants are added to the polymer foam, by either physical blending[102] or the addition of reactive flame retardants to the foaming formulation.[103, 104]

#### 1.1.3.2 Polymer aerogel

Aerogels are a kind of porous material which have attractive features, such as low density (the density of aerogel could reach as low as 0.003 g/cm$^3$),[105] a high surface area, high porosity and low thermal conductivity.[106-110] The first aerogel was synthesized by Kistler in 1931,[111] where a supercritical drying (SCD) method was applied for the conversion from aquagel to aerogel. The definition "gels in which the liquid phase is replaced by air phase with an unchanged volume of the solid network" was first proposed by Kistler. In recent decades, aerogels are more commonly accepted as a "gel comprised of a microporous solid in which the dispersed phase is a gas," as defined by the International Union of Pure and Applied Chemistry.[112] Research into aerogels expanded in 1960s, when sol-gel technology was applied in silica aerogel preparation, which simplified the preparation process.[113] Aerogels were prepared from various materials with different entities by the sol-gel method. Nevertheless, silica aerogel is attracting a lot of research attention and still remains the only aerogel which can be commercially produced on a large scale.[114] However, silica aerogel faces the challenge of poor mechanical properties, which limits its function in applications.[115-119] The next upsurge of aerogel occurred in the 1990s, when organic aerogels were developed.[120] Polymers have also been used to prepare aerogels in recent years, which, due to their exceptional properties, have the potential to be applied in fields of drug delivery, wound healing, environmental mitigation, sensors, filtration, catalysis, thermal insulation and aerospace.[121-125] Compared with traditional inorganic aerogels, organic aerogels feature better mechanical properties. Thus, polymers are commonly used in aerogels to adjust the latter's physical behavior. Moreover, polymers feature modifiable chemical structures, which are preferable to functional blocks for aerogels. The controllable molecular weight of polymers also broadens

the usage of polymer aerogels.[126-130] Nowadays, biopolymers, such as polysaccharides, including starch, alginate and chitosan, are widely used in biomedical applications due to their biocompatibility.[131] The biodegradability and -compatibility of polymer aerogels also make them preferable candidates for various biomedical applications, such as wound healing and drug delivery. The low density and elevated surface area enable aerogels to be applied as drug carriers.[132] Utilized in drug carrying systems, polymer aerogels have excellent characteristics, such as effectiveness and enhanced protection. In addition, the surface modification of polymer carriers can lead to drug selectivity.[133] Nowadays, aerogels made of synthetic polymers, such as polydimethylsiloxane and aliphatic polyesters, are also used as drug carriers.[134, 135] Based on their biocompatibility and -degradability, they are also prospective materials which can be applied in the field of tissue engineering. Polylactic glycolic acid aerogels, for example, have been used for the seeding of bone marrow mesenchymal stem cells.[136] The potential of hepatocytic differentiation of the cells was investigated after the cell proliferation.

Aerogels featuring high porosity, a large surface area and low density are also widely applied in non-biomedical fields, such as sorbents. They have been applied as environmental mitigation for the clean-up of oil leakage, and the remediation of toxic metals and organic compounds.[137] Polymer aerogels, such as cellulose-graphene aerogel, could effectively absorb heavy metals, such as copper, zinc, cadmium and chromium, due to the relatively high porosity.[138] These kinds of benign properties makes the cellulose aerogel a potential green absorption material for water purification.

Based on those satisfactory characteristics, polymer aerogels have been applied in versatile fields. On the other hand, there are still restrictions which prevent the polymer aerogel from being widely used in daily life. An example is the connection between laboratory research and industrial production, which remains a hinderance to the application of polymer aerogels. This gap still needs to be overcome for the future commercial utilization of polymer aerogels.[139]

#### 1.1.3.3 Polymer sponge

Among 3D porous scaffolds, man-made polymers sponges made of polymer fibrous materials have also attracted significant research interest in recent years. Polymer sponges mimic natural sponges, which can be found, for example, in wood, bamboo, cork and coral.[140] Both man-made polymer sponges and natural sponges are open cellular porous materials. Man-made sponges, which are formed by either top-down or bottom-up methods, feature compressibility,

high porosity, low density and breathability due to the interconnected pores.[141] In comparison to two-dimensional (2D) materials, mass transfer and diffusion make sponge an important candidate for various applications. Porous sponges have been used in versatile fields, such as for organic compound removal,[142, 143] in filtration and separation,[144] as catalyst carriers,[145] for thermal insulation,[146] and for biomedical applications, such as tissue engineering[147] and drug carriers.[148]

Polymer foams, which have closed cellular structure, have to be distinguished in structure and preparation from polymer sponges. Commercial methods for the preparation of polymer foams, for example, polyurethane[149] and melamine-formaldehyde foams,[150] cannot be applied for the preparation of sponge. However, other techniques, such as the template growth method, the sol-gel method and the self-assembly of electrospun fibers in dispersion, could be applied for the preparation of sponges.

1.1.3.3.1. Preparation of polymer sponges

1.1.3.3.1.1 Template growth

Sponges prepared by the template growth method are formed by using a sacrificial material as a template. After the successful construction of the sponge, the template material will be removed by some other techniques, such as freeze-drying, dissolution or pyrolysis. Ice, colloidal or emulsion particles, and polymer are the most popular template agents.[151, 152] Starch aerogel, for instance, was used as a template for the preparation of poly(3,4-ethylenedioxythiophene) (PEDOT) aerogel with the aid of supercritical $CO_2$.[151] The PEDOT was then synthesized using the starch aerogel as a template medium. After the successful acquisition of PEDOT aerogel, the starch template was removed by washing. The starch was used as a template during preparation to avoid organic gelation, which was published in a previous work.[153] As a result, the PEDOT aerogel could be controlled well. Template growth was described by Schaedler *et al*. as an elegant method.[154] In this work, the authors used a self-propagating photopolymer as a template. Under exposure to ultraviolet (UV) light, the monomer formed a patterned interconnected 3D polymer structure, whose dimensions could be adjusted by different parameters, such as a mask pattern and the angle of incidental light. After deposition of conformal nickel-phosphorous on polymer lattices, the polymer was etched out. With the help of polymer lattices, the nanoscale film deposited was translated into a 3D macroscopic structure, where the base materials were hollow tubes. Similarly, Jang *et al*. prepared a titanium nitride 3D porous sponge by the template growth method,[155] In this

publication, free-standing 3D polymer skeletons were prepared by direct laser writing using two-photon lithography. The next step was the creation of a titanium nitride deposition by atomic layer deposition, followed by the formation of hollow ceramic nanolattices after etching out the polymer core. The nanolattices could be kagome or octahedral unit cells. Compared with the previous method,[154] the two-photon lithography fabrication method described in this article enabled more than two orders of magnitude smaller feature resolution. Both template growth methods described the preparation of 3D inorganic sponges, which could also be applied for the preparation of polymer sponges.

Ice is frequently used as a template for the preparation of sponges, except when polymers are used as templates. A novel type of funnel-like chitosan sponge, for example, was prepared by Ko *et al*. using embossed ice particulates as a template.[156] The ice template was removed by freeze-drying after the solidification of the chitosan sponge. The sponge had a hierarchical porous structure, which was beneficial for tissue engineering applications with human dermal fibroblast cells. Other templates which are regularly used for template growth sponges are easily removable particulate agents, such as salts and gases. Nam *et al*. prepared PLA sponges with interconnected pores using ammonium bicarbonate particles as a porogen generation medium.[157] The sponge was prepared by casting of a binary mixture of poly(*L*-lactide) (PLLA) solvent gel and ammonium bicarbonate particles in a paste state. The molded PLLA paste with ammonium bicarbonate particles was incubated in hot aqueous medium. The gases ammonia and $CO_2$ were released from ammonium bicarbonate upon contact with acidic aqueous solution at an elevated temperature. The salt particles were removed by water during the solidification of the polymer. Using this method, sponge could be shaped according to the choice of mold. The resulting sponge showed an interconnected porous structure. The shape and dimension of the sponge could be adapted to match tissue defects. The cell viability test showed that the cells grew efficiently on the sponge after seeding.

Utilizing the template growth method, the porosity and cellular structure can be controlled by the amount of template material relative to that of the polymer and the size of the template material. However, the porogen applied for sponge preparation should be adapted to the application of the sponge, which depends on the toxicity and the residual content of the porogen material.

1.1.3.3.1.2 Sol-gel method

The sol-gel method is widely applied in the preparation of sponges.[143] Three main steps are required for the sol-gel method: (a) sol-gel process, (b) aging and (c) drying. In the sol-gel process, a sol (colloidal suspension) is formed by hydrolysis or partial condensation of alkoxides. Afterwards, a gel forms by polycondensation through a catalyst or temperature change. The solid particles dispersed merge to form a 3D network during the gel formation step.[158] Depending on the type of dispersion medium, either water or organic solvent, the gels formed are called hydrogel[159] or organogel,[160] respectively. In the aging step, complete polycondensation or reprecipitation is allowed with sufficient time that an interconnected network can form. The drying step, which allows the solvent to be substituted by air, is critical for the formation of the porous structure. Three main methods are normally used in the drying step: SCD, freeze-drying and ambient pressure drying.[161] The SCD is a general method for the preparation of aerogels. The solvent is removed by SCD with the help of supercritical liquid. During SCD, supercritical $CO_2$ is a commonly used liquid to replace the solvent from the gels and form the pores in the 3D scaffold.[158]

Ambient pressure drying takes a longer time compared to the other two (usually several days to weeks), making it hard to retain the porous structure of the 3D scaffolds. However, ambient pressure drying is considered to be a safer and less expensive way for large productions.[162]

Cryogels have been widely used to prepare polymer sponges.[163] They form by introducing a continuous liquid phase to crystallization by freezing. The polymeric phase undergoes gelation in the frozen domains by either physical or chemical cross-linking. A stable sponge is produced by the removal of the solvent, such as by sublimation. Preparation of silk-fibroin sponges from cryogel and hydrogel was reported by Okay *et al*., while comparing the two formation methods.[164] The cryogel and hydrogel were made at -18 °C and 50 °C, respectively. The cryogel showed a high compressive stability and could be compressed up to 100 % without any cracks. It recovered to its original height after unloading. The subsequent sponge obtained from cryogel had 90 % porosity and showed a regular, interconnected porous structure. By contrast, fibroin hydrogel showed weak and brittle properties. This study showed the large potential of cryogels in the preparation of sponges.

Polymers are also applied in the preparation of sponges from organogels, using other dispersion media.[165] Different from cryogels, the dispersion medium, i.e. organic liquid phase, remains liquid in the process. The sponge forms by the removal of the dispersion medium. The preparation process of sponges from organogels is similar to those from cryogels. The polymer

undergoes a gelation step in organic dispersion medium, which is induced by a parameter change, such as pH, light or temperature. Polymers are known to be used as organogelators in the preparation process of organogels.[166] When polymers are used as organogelators, one of the important features is that the polymer can form physical cross-linking by relatively strong supramolecular interactions. It has been found that helical conformation of polymers favors the formation of cross-linking points due to their strong interaction. Polystyrene (PS), for example, has different stereoisomers. However, atactic PS does not show the properties of organogelators. Stereoregular PS, such as isotactic or syndiotactic PS, possesses a gelation feature in some organic solvents. Kobayashi *et al.* found out that syndiotactic PS showed an organogelation property in a solvent mixture of chloroform, carbon tetrachloride and benzene.[167] Poly(methyl methacrylate) also shows similar properties to syndiotactic conformation, which was proven to show an organogelation property in various solvents, such as bromobenzene, chlorobenzene and toluene.[168] The biodegradable poly(3-hydroxybutyrate-*co*-3-hydroxyvalerate) was also reported to form thermoreversible organogel by dissolution in toluene at 90 °C.[169] The helical structure formed during the cooling process after dissolution. Organogelation was induced by a 3D network structure formed by the interaction between the helical segments.

1.1.3.3.1.3 Melt process

The 3D printing method has also attracted a lot of attention recently regarding the preparation of sponges. Three-dimensional printing was first investigated by Kodama *et al*. using a photo-hardening thermoset as an additive manufacturing method in 1981.[170] In 1986, “stereolithography” was proposed as a 3D printing methodology using layer-by-layer printing and UV curing.[171] The 3D printing techniques can be applied in biomedical fields, depending on the materials selected.

The 3D printed sponges featuring specificity, controlled internal geometry and appropriate pore interconnectivity are favorable in some application areas, such as tissue engineering.[172, 173] This method can be used with resins as sacrificial molds to prepare biological sponges, which enables the direct printing of 3D frameworks from solvent-free, aqueous-based systems for transplantation with or without cells.[174] Combined with modern techniques in cell biology and material science, 3D printing has become an attractive method for preparing implantable sponges for the reconstruction of injured organs.[171, 175, 176]

The completely biomedical method is called 3D bioprinting. There are three main techniques for this: laser-assisted, inkjet and extrusion.[176] Nowadays, 3D bioprinting has been developed to fit medical applications such as skin, blood vessels, cardiac tissue, heart valves and bone.[177] Materials which can be applied for bioprinting include both natural and synthetic materials. Among the natural materials, collagen, an abundant and ubiquitous protein derived from animal and human tissues, is commonly used for 3D bioprinting. Akkineni *et al*., for example, reported that if a soft core biopolymer hydrogel, such as collagen hydrogel, is combined with alginate as a shell material, the sponge is mechanically stable and robust.[178] Sorkio *et al*. prepared a recombinant human-sourced collagen I and human laminin 3D corneal using laser-assisted 3D bioprinting.[179] Yang *et al.* used collagen I or an agarose/sodium alginate mixture for 3D bioprinting.[180] The *in vitro* 3D cartilage tissue was then constructed by incorporating the sponges with chondrocytes.

Synthetic materials are also widely used in 3D bioprinting. Kesti *et al*., for instance, reported that a high-resolution scaffold which was printed by mixing thermoresponsive poly(*N*-isopropylacrylamide)-grafted hyaluronan with methacrylated hyaluronan had good cell viability.[181] The authors demonstrated that poly(*N*-isopropylacrylamide)-grafted hyaluronan is supportive of a range of polymers which undergo tandem gelation during extrusion. Cell-laden printed and stratified cartilage constructs were thereby facilitated.

However, considering features such as cross-link ability, cell viability, mechanical stability and processability, bioprinted single material sponges often hardly meet the requirements for biological application fields.[181] Therefore, the development of different materials for 3D bioprinting is essential for versatile applications. Moreover, a lack of precision in droplet placement and size remains a challenge in 3D bioprinting. More advanced techniques are required to optimize the preparation process of polymeric sponges. In the past few years, for example, electrospun polymeric sponges have drawn of lot of research attention.[182-184] The sponge is prepared by the self-assembly of electrospun short fibers, which will be discussed in the next chapter.

### 1.2. Electrospun fibers

Electrospinning is a state-of-art technique which allows the preparation of nano- and microfibers. An electrical charge effect on liquid droplets had already been observed in the 1700s. In 1745, Bose demonstrated that water aerosol could be obtained by applying

electrostatic charges.[185] Electrospinning was then systematically studied by Rayleigh in 1885.[186] In 1887, Charles V. Boys found that fibers were yielded by an apparatus with an insulated disk incorporating an external electrical field.[187] This study indicated that a viscous liquid could be stretched into fine fibers. Electrospinning was patented by Formhals Anton between 1931 and 1944 in different countries, such as America, France and Germany.[188, 189] Cellulose acetate electrospun fibers were processed during this time. Based on the electrospinning technique, Bernard Vonnegut and Raymond L. Neubauersome also produced liquid jets using electrostatic force in 1952.[190] In this study, uniformly sized droplets formed and the size of the droplets could be estimated. In 1964, Sir Geoffrey Ingram Taylor made significant progress on electrospinning by modeling the shape of a droplet cone under electrostatic force using mathematical methods.[191] This cone became well-known later as the Taylor cone. However, the production rate of electrospinning is relatively low compared with conventional methods.[192] Therefore, despite the early studies on electrospinning, it was not widely applied as an industrial fiber production technique.[188]

The electrospinning technique has been developed intensively in the past few decades. Starting in the 1990s, several research groups began research on electrospinning by introducing electronic microscopes to characterize the nanoscale property of the fibers.[193-198] During this time, versatile polymers were reported to be possible for electrospinning. Continuous fibers on a nanometer scale could be obtained by electrospinning. Electrospinning attracted a lot of conspicuous research attention at the beginning of the 21st century. Based on the electrospinning technique, electrospun fiber composites, including organic and inorganic materials, opened up a new research field for versatile applications.[199] Since then, with the modern and advanced technique of electrospinning, various forms of fibers, such as yarn, aligned fibers and coaxial fibers, have been investigated.[200-204] The application of electrospinning has been dramatically enhanced in different fields, such as biomedicine, energy, environment and electronics, utilizing the tailored size, morphology, composition, structure and porosity of the electrospun fibers.

### 1.2.1. Electrospinning principle and process

The electrospinning setup usually consists of a spinneret (normally a hypodermic needle with a blunt tip), a high-voltage power supply, a syringe pump to feed the solution, and a collector connected to either a negative electrode or the ground, as illustrated in **Figure 1-3a**. During the electrospinning process, a pendant droplet is extruded from the spinneret. When an electric

field is applied to the droplet, it is elongated and forms a Taylor cone (**Figure 1-3b**). Afterwards, the surface tension of the solution droplet is overcome by the electrostatic repulsion force among the surface charges. This step results in the whipping (bending) instability, which could, finally, result in Raleigh instability and droplet formation. A fine jet then ejects from the cone and is gathered by a collector while the solvent evaporates.[205, 206]

There are several parameters which can influence the electrospinning process and, thereby, the fiber formation. There are three main categories of parameters which affect the electrospinning process: environmental conditions, processing setup and solution formulation.[207] Environmental factors are mainly temperature and relative humidity. Temperature affects the viscoelasticity of the solution and the evaporation of solvents, and can also change the thickness of the fibers.[208] As an example, when the temperature increases, the viscosity reduces. Consequently, fibers are formed with a smaller diameter.[209] If the solvents evaporate faster, the elongation of the fibers reduces.[210] Humidity can also affect the morphology of the fibers. When relative humidity is high, water vapor from the air might penetrate the solution jet, introducing a pore structure onto the surface of the fibers.[205] Contrarily, if the relative humidity is low, solvent evaporation is faster, thus, a clot might form easily at the tip of needle.

Electrospinning can be done in solution, emulsion, suspension or melt. The characteristics of these formulations and other processing parameters govern, to a large extent, the formation of fibers. Processing parameters are the manipulation parameters, such as the flow rate, voltage, and distance between the needle and the collector. Voltage is an important parameter, which influences the formation of fibers. An electrical field can form between the needle and the collector and, therefore, initiate the formation of fibers due to voltage.[211] The electrostatically charged solution has to overcome the viscosity and surface tension of the solution or melt in the initial state of fiber formation. The voltage also plays a role in the morphology of fibers. Regarding some polymers, when the electrical static force is increased on the ejected jet, the latter is stretched more, thus, thinner fibers form.[212] However, the effect of the voltage also depends on different polymers. The voltage, for example, has no effect on the polyethylene oxide (PEO) fiber diameter.[186] Similarly, for some polymers, a higher flow rate generates fibers with a larger diameter, such as for PS.[213] However, it is favorable for the electrospun system to form bead-free fibers with a rather low flow rate.[214] Additionally, the distance between the needle tip and the collector influences the evaporation time of solvents. Thus, it is important to optimize the distance between the needle tip and the collector to obtain the fiber diameter required.[215]

One of the most important solution parameters is viscosity. Other parameters, such as the molecular weight of the polymer, together with the concentration of the electrospun solution, determine the extent of chain entanglement, correlating to the viscosity of the solution. If the molecular weight of the polymer or concentration is too low, a solution with a low extent of chain entanglement cannot form a proper polymer network, which results in a viscoelasticity which is too low. Consequently, fibers with micro- or nanobeads are formed.[216] However, a solution viscosity which is too high leads to clogging on the needle tip during electrospinning, and the solution flow is hindered.[217] The viscosity also affects the fiber morphology. A high viscosity solution results in ribbon-like fibers. Another important solution parameter is the electrical conductivity of the electrospun solution, because it is essential for Taylor cone formation, leading to the initiation of fiber ejection.[218, 219] If the electrostatic forces caused by the voltage cannot overcome the viscosity of the surface tension, no fiber jet formation is observed.

### 1.2.2. Electrospinning methods

Electrospinning is a sophisticated method, which enables the production of versatile nonwovens. The conventional electrospinning setup is equipped with a single nozzle (depicted in **Figure 1-3a**). The traditional electrospinning technique has a relatively low production efficiency. The nozzle can be improved to increase productivity. Exemplarily, multiple needles arranged side by side, as shown in **Figure 1-3c**, are used to increase the electrospinning efficiency.[220] The production capacity of polyimide (PI) nonwoven, which is used in lithium battery and high-temperature filtration applications, is enhanced significantly by using multichannel needles to around 2000 $m^2$ per day.[221] However, some undesirable problems are caused by this kind of multichannel needle. Inhomogeneously distributed nonwoven, for example, is collected due to the instability resulting from the jet interaction, and an unsought merging of jets occurs during the electrospinning. Thus, the multichannel needle still needs investigation to solve these unexpected problems.[222] A secondary electrical field generated by auxiliary electrodes can be introduced between the needle and connected electrode to neutralize the repulsion between the needles, thus, reducing the instability of the jets.[223, 224] In addition to multichannel needles, other forms of needles, such as flat plate, solid pin, hollowed tube and metal string, have been used for the improvement of electrospinning productivity.[225-227] Those processing methods are summarized as needleless electrospinning. However, control of the flow rate and uniform jets remain a big challenge in needleless electrospinning. It was

discovered that the utilization of a moving spinneret can improve the homogeneity of the jets. In 2005, Elmarco s.r.o. (Liberec, Czech Republic) first patented and commercialized the needleless electrospinning setup, which is well-known as the "Nanospider".[228] A rotating cylinder is used as a spinneret in Nanospider. A thin layer of solution forms on the surface of the cylinder by immersing the rotating cylinder in solution. When an electrical field is applied to the cylinder, spikes form on the cylinder surface, thus, initiating the electrospinning. Since then, papers about needleless electrospinning have been published worldwide, including recent techniques such as the toothed wheel,[229] linear flume[230] and shear-aided spinneret.[231]

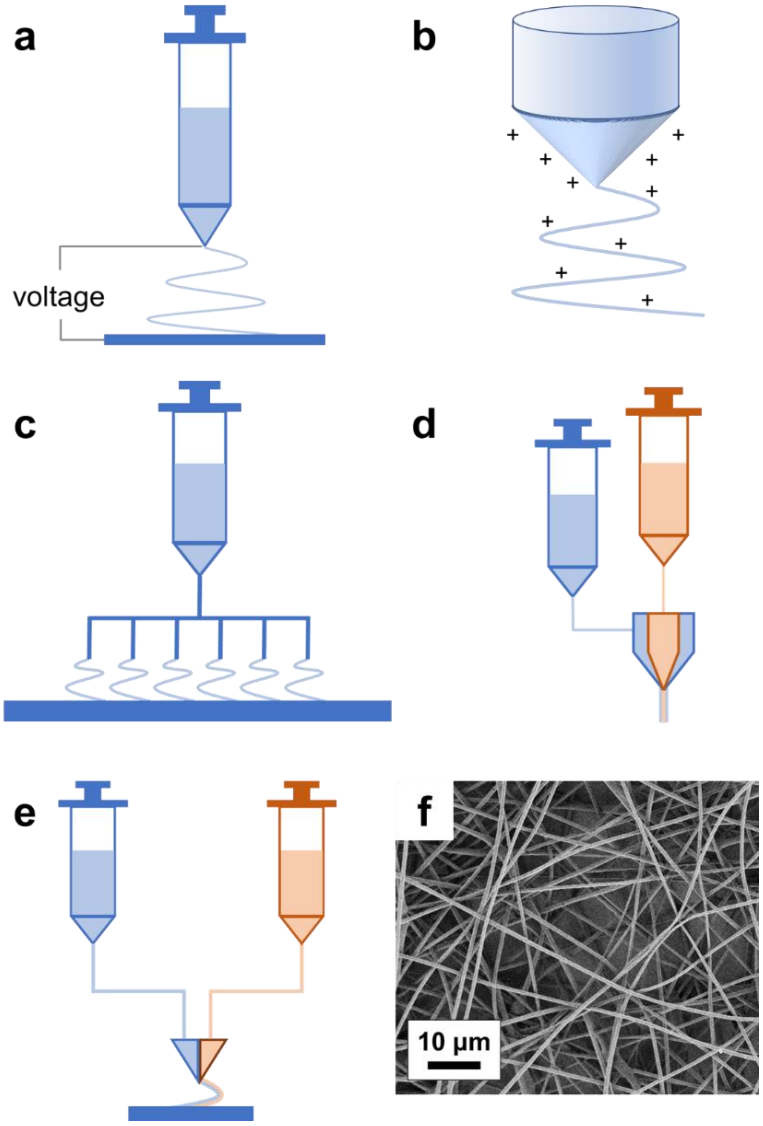


**Figure 1-3**. (a) Conventional electrospinning setup, (b) Talyor cone, (c) side-by-side electrospinning, (d) multichannel electrospinning, (e) coaxial needle and (f) morphology of electrospun fiber prepared by (a), taken by scanning electron microscope.

In addition to the requirement of productive capacity, composite materials using different solvent systems are also required for electrospinning. Electrospinning multiple solutions simultaneously cannot be satisfied by a single spinneret. In this case, a multiaxial spinneret is a feasible concept. A coaxial needle is often used in electrospinning for the preparation of bicomponent fibers.[204] Compared with a single needle, the coaxial needle is configured by inserting an inner needle into an outer needle (**Figure 1-3d**). This needle allows the feeding of two different solutions by two syringe pumps at different flow rates. When the two fluids meet at the tip of the coaxial needle, the inner fluid is wrapped by the outer fluid to form a coaxial Taylor cone. In the presence of an electrical field, a coaxial jet ejects from the cone, and coaxial fibers are obtained with a core-sheath structure. Coaxial electrospinning is usually applied for the fiber production of materials which are not suitable for electrospinning,[232, 233] or different types of materials, such as oil, oligomer, liquid crystals, protein, bacteria and viruses, which have to be encapsulated as a core material in a core-sheath form.[234-238] Ethylene/propylene/diene terpolymer rubber[239] and epoxy resin,[240] for example, have been prepared by coaxial electrospinning as core material. The as-spun core-shell fiber was cross-linked thermally, and the shell material was removed afterwards. Triaxial needles can be also obtained by increasing the number of concentric needles.[241] This kind of needle is used for the preparation of three-layer structured fibers by feeding three different solutions simultaneously.[242]

A side-by-side needle (**Figure 1-3e**) is also used for electrospinning different solution systems, in addition to core-shell structured fibers.[243] Fibers consisting of a split of different components can be obtained by side-by-side electrospinning. This kind of electrospinning allows both components to be exposed equally to the environment. Janus electrospun fibers are prepared by side-by-side electrospinning.[244] Antibiotic (ciprofloxacin)-loaded polyvinylpyrrolidone and silver nanoparticle-loaded cellulose polymer matrices are used as two components for side-by-side electrospinning,[245] and the properties of both components can be expressed in a wound dressing application. The immediate release of ciprofloxacin allowed a strong initial antibacterial effect, while long-term sustained anti-bacterial action was provided by the silver nanoparticles from the other side of the Janus fiber.

The distance between the needle and the collector can be also investigated for new forms of electrospinning. The needle to collector distance in conventional electrospinning is usually 5 – 15 cm, and the voltage applied is between 10 and 20 kV. This conductive mode is called far-field electrospinning.[205] The latter has difficulty in the precise control of fiber deposition. This

difficulty can be conquered by near-field electrospinning, which is conducted by a reduced needle to collector distance (0.5 – 5 cm).[246] At this distance, straight electrospun jet deposits directly on the collector before starting the instable whipping. Due to the reduced distance, the electrical field, in that case, is highly concentrated between the needle and the collector.[247] Thus, a reduced voltage is required (0.6 – 3 kV). With a moving collector, the fibers can be deposited precisely as patterns. However, compared to far-field electrospinning, near-field electrospinning has a relatively low production capacity. In addition, the complexity of the setup remains a challenge for mass production, which limits its applications where large-scale product is required.[248, 249]

The development and expanded techniques of electrospinning has drawn increasing research interest of many researchers and become a prosperous research field. Compared with other materials, electrospun nonwoven has different advantages, such as a high aspect ratio, malleability and porosity.[186] Due to those advantages, electrospun nonwoven has been applied to different fields, such as energy, tissue engineering and catalysis.[250-252] However, electrospinning nonwoven is the assembly of loosely overlaid 2D fibers (**Figure 1-3f**). The increased collected nonwoven thickness during electrospinning causes the electrical conductivity to reduce. A greater thickness of nonwoven is hard to reach due to the reduction in conductivity.

Nowadays, the requisite of 3D scaffolds, namely sponges, is increasing. Thus, methods for electrospun sponge preparation are widely studied.[253] Compared to 2D electrospun nonwoven, sponges can broaden the application of electrospinning due to a greater thickness, which allows applications where the third dimension is required.[254] Diffusion and mass transfer are important for these kinds of applications.[146] Thus, it is crucial to develop advanced methods for the preparation of sponges.

### 1.3. Electrospun sponges

Efforts have been made in the past few decades to obtain a sponge structure during the electrospinning process. With adjusted parameters, a 3D fibrous structure can be achieved by direct electrospinning instead of a 2D nonwoven using conventional electrospinning.[255] Sponge preparation by direct electrospinning is still a challenge. The shape and porosity of such sponges can be only minimally controlled. Furthermore, the mechanical stability of the direct electrospun sponges is rather weak.[253] A more advanced technique was introduced by

Duan *et al*. and Si *et al*. in 2015 to prepare sponges by the short fiber assembling and freeze-drying method.[182, 184] In contrast to foams, which have a closed cellular structure, these sponges possess interconnected pores with an open cellular structure with a well-controlled density. This open cellular structure provides the possibility of infiltration into matter and mass transfer, allowing their application in some fields where these features are important, such as tissue engineering. This kind of scaffold, which is also called sponge, has been studied intensively in the last few years. Two different methods are mainly being used to prepare electrospun sponges: the thermally induced self-agglomeration (TISA) method and short fiber assembling/freeze-drying method.

### 1.3.1. Thermally induced self-agglomeration method

A new approach to prepare 3D electrospun scaffolds was first demonstrated by Xu *et al*. in 2015.[183] In this publication, the TISA approach consisted of the following steps: (1) electrospun polycaprolactone (PCL) nonwoven was soaked in ethanol, then cut by mechanical grinding, in the presence of liquid nitrogen, into short fibers; (2) the short fibers were dispersed in a water/gelatin/ethanol mixture; (3) the short fiber dispersion was immersed in a water bath at a temperature around 55 °C, which is the melting point of PCL, and self-agglomeration was induced thermally; after several minutes a 3D polymer hydrogel formed; finally, (4) the aerogel was freeze-dried after being rinsed in deionized water.

The PCL sponge obtained by the TISA method had an interconnected porous structure with a porosity of around 95 %, which favors the later tissue engineering application. In order to optimize the mechanical property of the TISA sponge, PLA can also be blended with PCL for sponge preparation, which has been published by the same group.[256] After blending 20 % weight percent PLA, the bioactivity and stiffness improved, which is beneficial to the tissue engineering application. Because the 3D polymer network already forms before freeze-drying in the TISA method, there is no shrinkage of the sponge after freeze-drying and the shape can be maintained, which is a big advantage of the TISA method. However, the design of the sponge shape by TISA is a challenge, because the short fibers self-agglomerate during thermal treatment, which is hard to adjust. Meanwhile, the short fibers assemble spontaneously, making the porosity uncontrollable. If the sponge shape needs adjusting for some specific applications, the short fiber assembling and freeze-drying method could be a good choice.

### 1.3.2. Short fiber assembling and freeze-drying method

Since the short fiber assembling and freeze-drying method was first proposed in 2014, it has become a conventional technique for electrospun sponge preparation.[146, 257-259] This method includes the following steps: (1) electrospun nonwoven is fragmented into short fibers; (2) the short fibers are dispersed in a non-solvent; (3) the dispersion is transferred into a mold; (4) freezing; and, finally, (5) removal (drying) of the solvent by sublimation. Compared with the TISA method, the porosity of sponges prepared by the short fiber assembling and freeze-drying method can be tailored during the short fiber dispersion step. The shape of the sponge can be designed by using different molds at the freezing-drying step. However, a cross-linking step is required after the formation of the sponge to assure the mechanical stability.

The short fiber assembling and freeze-drying method can be used to prepare both inorganic and organic sponges. In one of the earliest publications about the short fiber assembling and freeze-drying method, poly(methylacrylate)-*co*-methyl methacrylate-*co*-4-methacryloyloxy-benzophenone sponge was prepared.[184] The density and shape of the resulting sponges were tunable. Large-scale production was also possible. The sponges displayed low density and repeated compressibility, opening up a new type of electrospun sponge for application in versatile fields, such as sound adsorption, thermal insulation and responsive electrical conduction.

Jiang *et al*. prepared PI sponges using the method above. The PI sponge showed high reversible compressibility, thermal stability and low thermal conductivity. Thus, this kind of PI sponge was used in the thermal insulation field. In 2018, the same group prepared poly(bis(benzimidazo)benzophenanthroline-dione) sponges by the short fiber assembling and freeze-drying method.[259] These low-density sponges had a high compressibility, low thermal conductivity and high pyrolytic stability. Their compressibility and flame retardancy made it possible to separate waste solvent and reuse the sponge afterwards by ignition.

Electrospun sponges prepared by the short fiber assembling and freeze-drying method using biodegradable polymers have also been studied intensively in recent years. Chen *et al*. prepared biocompatible PLA/gelatin sponges by this method.[260] The short fibers were chemically cross-linked by glutaraldehyde to achieve mechanical stability of the sponges. These sponges were hydrophilic. Cell culture tests showed that the sponge enabled relatively high cell viability. The same group reported on a PLA/hyaluronic acid sponge.[258] The latter sponge showed superabsorbent features and benign cytocompatibility. An *in vivo* study of the sponge exhibited that it had good cartilage repair affinity, which makes it promising in the tissue engineering

field. Mader *et al*. prepared a PLA/PCL electrospun sponge,[147] wherein the PCL was used as a cross-linking agent. The density and porosity of the sponge were tunable by the fiber dispersion concentration in the sponge preparation step. Rapid cell proliferation onto the sponge was confirmed using Jurkat cells. Similarly, a pure PLA sponge was prepared by the same group.[261] However, the as-prepared PLA sponge was hydrophobic, which hindered the cell infiltration. In this work, a block copolymer containing polysaccharide was used as a surface modification agent for hydrophilization. The dynamic human hepatic cell culture result revealed that the surface modification significantly enhanced the cell adhesion and distribution throughout the sponge.

There are many features affecting the application of electrospun sponges. Since 3D electrospun sponge is usually lightweight with a high number of pores, porosity is one of its key properties. Berhan *et al*. proposed a method to calculate the porosity of sponge based on the length and diameter of the short fibers.[262] The calculation is described by the following equations:

$$\Phi_c = \frac{V}{V_{ex}} \tag{1}$$

Where $\Phi_c$ is the volume fraction of short fibers, $V$ is the bulk volume of short fibers and $V_{ex}$ is the excluded volume. $V$ and $V_{ex}$ are calculated by equations (2) and (3):

$$V = \frac{4\pi r^3}{3} + \pi L r^2 \tag{2}$$

$$V_{ex} = \frac{32\pi r^3}{3} + 8\pi L r^2 + \pi r L^2 \tag{3}$$

However, this method is based on the assumption that all short fibers are ideal rods. The following method is used more often for porosity calculation in real sponge applications:[146]

$$P\,(\%) = (1 - \frac{\rho_{SG}}{\rho_{bulk}}) \times 100 \tag{4}$$

Where $\rho_{SG}$ represents the density of the electrospun sponge and $\rho_{bulk}$ is the bulk density of the material used for sponge preparation.

Another important property is mechanical stability, which is highly relevant for the cross-linking step during preparation. Duan *et al*. cross-linked the polymethacrylate by UV light,[184] or a coated shell of poly(p-xylylene).[263] Jiang *et al*. applied a “self-gluing” method by using the PI precursor, poly(amic acid), in the short fiber dispersion step. A fibrous skeleton network formed after the imidization of the poly(amic acid).[146] After cross-linking, the sponge

assembled by electrospun short fibers gains interconnected junctions and is, therefore, mechanically stable, which is crucial for some applications, such as being used as a catalyst carrier.[145]

The hydrophilicity of sponge is essential to allow cell infiltration for some medical applications, such as tissue engineering. Hydrophilization can be introduced during the sponge preparation steps. For the PLA/gelatin and PLA/hyaluronic acid sponges mentioned above, for example, gelatin and HA had already been blended in the electrospinning step to provide the hydrophilicity of the sponges.[258, 260] Sponge can also be hydrophilized posttreatment. Mader *et al*., for example, hydrophilized PLA sponges by plasma-treatment after the sponge formation.[147] Another PLA sponge was hydrophilized by the dip-coating of amphiphilic material.[261] The efficient hydrophilization of sponge allows cell adhesion and further penetration into the sponges.

Other important properties of sponges in tissue engineering applications are biocompatibility and -degradability. Biocompatibility means low cell toxicity to provide a suitable environment for cell attachment and growth in the scaffold. Degradable polymer is favorable for tissue engineering applications, because it allows the physiological degradation of the scaffold in the human body after the repair and regeneration of the injured tissue.[264] In addition to tissue engineering applications, sponge is also of interest regarding daily life applications, such as packaging and microplastic filtration. Degradability is considered to be an important characteristic of polymers in daily life applications. The polymer should serve for a certain time to fulfill its function, then should degrade and eventually be bio-inspired in mineralization.[265] Polymers with degradability are encouraged to prevent environmental pollution.[266] Thus, degradable polymers have attracted a lot of research interest in various applications. The topic of degradability, which is complex, will be discussed in the next chapter to establish the context.

### 1.4. Degradable polymers

Among all the features of polymers, degradability is a special property compared with other materials, such as metals, ceramics and glasses.[265] Based on the fact that polymers are built up by organic compounds, degradation of polymers can be achieved by different methods: polymer samples can be fragmented by light, mechanical stress, hydrolysis, enzymes or microbes. After fragmentation, polymer chains could be further degraded to oligomers or

monomers, which could be, thereby, bioavailable. The process of the metabolization of bioavailable oligomers or monomers by organisms (mostly by the action of a set of enzymes) is called biodegradation. Carbon dioxide and water are the final products of biodegradation occurring under aerobic conditions. By contrast, methane and water could be the possible degradation products under anaerobic conditions. Polymers following this process are called biodegradable polymers. The latter should be strictly distinguished from hydrolytically or enzymatically degradable polymers as the final products are different.[266, 267]

There are two main types of degradable polymers: natural and synthetic polymers. Natural polymers can also be called biopolymers, such as gelatin, collagen, chitosan, cellulose, silk fibroin and poly(*β*-hydroxyalcanoate).[268] Natural polymers are widely applied as tissue engineering materials.[269] However, their rather weak mechanical properties still restrict the utilization of natural polymers in versatile applications. Synthetic biodegradable polymers usually contain a heteroatom in the polymer backbone, such as ester bonds, which hinder the stability of C-C bonds, thus, offering cleavage points in the polymer chains.[270] Typical synthetic biodegradable polymers are poly(*α*-hydroxy acids), such as polylactide (PLA), poly(glycolic acid) and poly(lactic-*co*-glycolic acid), a copolymer of them. Other famous synthetic biodegradable polymers are PCL and Ecoflex® (poly(butylene adipate-*co*-terephthalate).[271] The PCL has high processability due to its solubility in common solvents.[272] However, its slow degradation rate and poor mechanical property have limited its application.[273] Thus, it is normally used with additives or as a fraction of a polymer blend.[147]

Compared with PCL, PLA is a more frequently used biodegradable polyester due to its rather good mechanical properties and better degradability.[274] It is polymerized from renewable agriculture resources, such as corn and other polysaccharides.[274] It has been the most promising polymer among all the technical biodegradable polymers. The monomer of PLA, lactic acid, has two optical forms, *L*- and *D*-lactic acid. When polymerizing PLA from lactic acid or lactide, three forms are possible: PLLA, poly(*D*-lactide) (PDLA) or poly(*D*,*L*-lactide) (PDLLA).[275] The PLA is polymerized by either polycondensation from lactic acid or ring-opening polymerization (ROP) from lactide. Nowadays, commercially available PLA is usually made by ring-opening polymerization from lactide derived from corn. Due to it being a sustainable resource, it has the potential to reduce petroleum-based materials. Furthermore, degradation of PLA generates environmentally friendly products, including lactic acid, or $CO_2$ and water as end products. The PLA has been widely used in different fields, such as agriculture, biomedicine and packaging.[276]

### 1.4.1. Degradation of PLA-type polymers

#### 1.4.1.1 Hydrolytic degradation

Because of their bio-friendly characteristics, PLA and related polymers have been seen as a promising solution for plastic pollution. They have been widely used as biodegradable fiber, plastics, agriculture films, for tissue engineering, and biomedical or pharmaceutical devices. If PLA is unintendedly disposed of in nature, it could possibly biodegrade and transform to biomass. Thus, it would be sustainable.[277, 278] However, PLA is classified as a slow biodegradation rate plastic. It has a weight loss of 5 % after 90 days, which can cause a microplastic debris problem, where microplastic is defined as plastic particles that have a size smaller than 5 mm.[279] The occurrence of the degradation of PLA depends greatly on environmental factors and is extremely slow in natural seawater.[280]

Depending on its application, PLA is in contact with different media. When being used as a pesticide release medium, for example, in agricultural fields, PLA serves in a relatively high humidity environment, where it is in direct contact with water.[281] Water generates the slow hydrolytic degradation of PLA. The hydrolysis reaction contains two main steps.[282] In the first step, water diffuses into the amorphous part of the PLA, and a random cleavage of ester linkage in the PLA chain is generated by hydrolysis, resulting in the formation of shorter chains by chain scission. Following the latter, the carboxylic end group works as a catalyst for an autocatalysis reaction to accelerate the hydrolytic degradation.[283] In the second step, water-soluble oligomers or monomers form. The weight loss of PLA begins in the second step. Afterwards, with the existence of biomass, the oligomers or monomers are degraded further into end products, such as $CO_2$ or water. The first step is so slow that it is a rate decisive step in PLA degradation.[284] It should be mentioned here that the hydrolytic and enzymatic degradation of amorphous polymers is generally by orders of magnitude faster than the degradation of corresponding crystallites. In the worst case, only the amorphous part of a polymer sample is degraded, but the crystallites remain as small microplastics particles with unknown environmental consequences.

There are generally two types of degradation: surface and bulk degradation.[285] The mechanism of both kinds of degradation is illustrated in **Figure 1-4**. The surface degradation takes place mainly on the outer layer of polymers. Surface degradation is a heterogeneous process, because the erosion affects only the polymer surface, not the inner part. By contrast, bulk degradation is rather slow, and the cleavage occurs throughout the whole device. Thus, bulk degradation is a homogenous process, which is not restricted to only the surface of a polymer sample.

The hydrolytic chain cleavage of PLA occurs preferably in the amorphous region. Thus, amorphous PDLLA is found to degrade faster interiorly than outside.[286] The reason behind is the large contribution of interior autocatalysis. The latter is attributed to two main parts: the first is the carboxylic end group engendered by the hydrolysis reaction; the second is the oligomers, which escape from the polymer matrix but are still close to the polymer, yielding a low pH value, which accelerates the degradation of PDLLA.

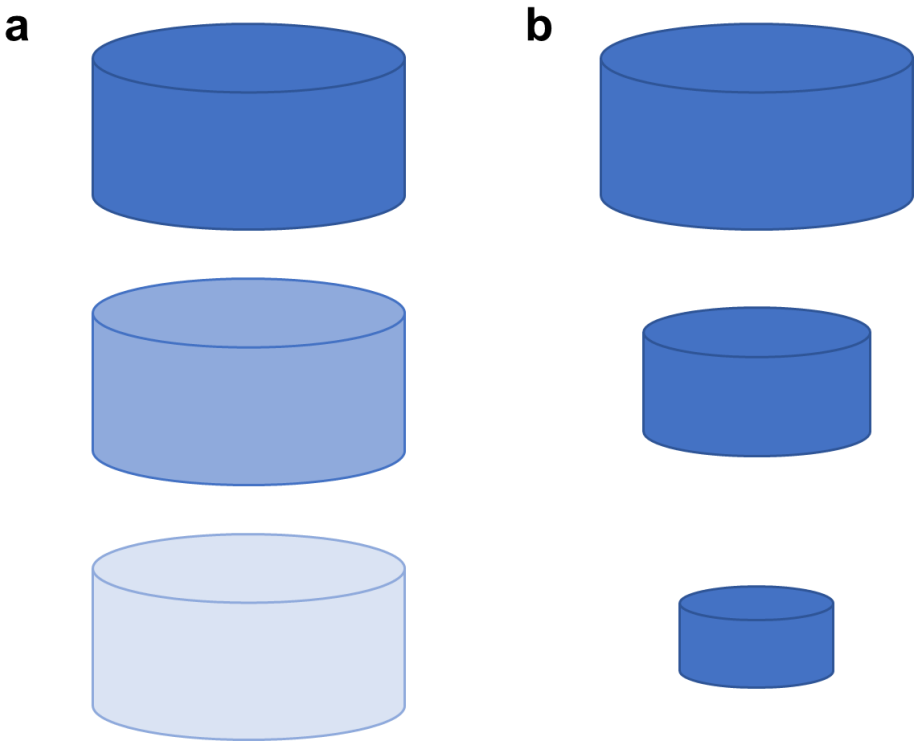


**Figure 1-4**. (a) Bulk degradation, and (b) surface erosion of polymers.

In the case of semi-crystalline PLLA, the degradation is more complex. The hydrolytic degradation is generated by a chain scission by diffused water in the amorphous region. After the chain scission, the crystallinity tends to increase.[287] The hydrolytic attack then occurs in the center of the crystalline domain. In most of the publications, the degradation rate is reported to be affected by crystallinity.[288] Higher crystallinity restricts the hydrolytic degradation of PLLA.

Various studies have been reported concerning the hydrolytic degradation of PLLA. Example include using titanium oxide nanoparticles as an additive,[289] the effect of nanocomposites affected by a water-ethanol system,[290] different temperatures[291] and organic modifiers,[292] which have been studied to tailor the degradation rate of PLLA. A study showed that the

polymer chain is more flexible and water adsorption increases at a rather high temperature, which is above the glass transition temperature ($T_g$) of PLLA, resulting in the acceleration of the hydrolytic degradation.[293] In another study, the PLLA degradation rate was found to be higher in a 1:1 mixture of water and ethanol.[294] The reason behind this is the higher diffusion rate of ethanol in polymer chains. However, due to the intrinsic hydrophobicity of PLLA, the hydrolytic degradation rate in the environment is hard to control. Previous research has shown that the degradation of PLLA remains in water or the human body for a long time.[295] Without enzymatic degradation, the crystalline of PLLA remains in the human body for more than five years.[296]

#### 1.4.1.2 Enzymatic degradation

Enzymatic degradation has been widely applied for the degradation of PLLA. Enzymes, such as lipase, alcalase and esterase, have been used to hydrolyze PLLA.[297] Factors such as the stereochemistry of the PLLA chain, pH, temperature and crystallinity have an effect on the enzymatic degradation of PLLA.[298] Therefore, environmental conditions and proper microorganisms are important for the biodegradation of PLLA in the environment. The enzymatic degradation of PLLA can be either surface erosion or bulk degradation, depending on the location and reaction rate of enzymes.[299] However, due to the intrinsic hydrophobicity of PLLA, diffusion of water is usually slower than the ester bond cleavage. Thus, surface erosion is the dominant degradation mechanism.

The first paper about the enzymatic degradation of PLLA was published in 1981 by Williams *et al*.[300] In this paper, proteinase K from *Tritirachium album* was assessed to degrade PLLA enzymatically. Since then, research has been done about the enzymatic degradation of PLLA, including the work of Oda *et al*., who tested 56 commercially available proteases for PLA degradation.[301] Enzyme catalyzed degradation of polymer is specific. Experiments showed, for example, that alkaline proteases are efficient enzymes for PLA degradation.[302] Among the commercial enzymes, proteinase K is an intensively used enzyme for different studies.[303, 304] It belongs to the serine proteases.[305] Serine residue plays an important role in the active site in proteinase K. The catalytic triad of proteinase K consists of three residues: serine, histidine and aspartate.[306] Before the enzymatic hydrolysis reaction, the PLA chain is recognized by the catalytic triad.[298] Due to the stereochemistry mismatch, PDLA cannot react in the active site of proteinase K.[307, 308] Instead, PLLA can orient and be recognized well by the proteinase K active site for further enzymatic hydrolysis.

1.4.1.3. Tailoring degradation of PLLA

As a biodegradable polymer, PLLA is already applied in fields of daily life, such as packaging materials, to solve the plastic pollution problem of polymers after their service period.[309] When applying biodegradable materials, the first concern is the environmental degradability. However, due to the rather low degradation rate of PLLA in the environment,[310] modification of PLLA is still required. The additives for PLLA which can tailor the degradation of PLLA have been published. Citrate additive, for example, might prohibit the environmental degradation when being used as a plasticizer of PLLA.[311] By contrast, additives such as oligolactic acid can hypothetically accelerate the hydrolysis rate of PLLA.[310] Additionally, blending starch with PLLA can also increase the latter's degradation rate, which was showed to be 100 – 150 % higher than the previous study.[312] Rather than an addition of additives, it is more direct to introduce another block into the backbone of PLLA to tailor the degradation rate. Tang *et al*. introduced carbohydrate lactone into the PLLA backbone.[313] The hydrophilicity of the modified polymer was found to be higher and the degradation rate is four times higher.

Moreover, due to the high specificity and higher efficiency of enzymes for PLLA degradation, it is more straightforward to use a specific enzyme as an additive for the accelerated degradation of PLLA. The specific enzyme proteinase K was blended into PLLA by melt extrusion to improve the degradation rate of the latter enzymatically.[314] In this research, cross-linked polyacrylamide (PAM) was introduced into the extrusion process as a thermal insulation material to protect the proteinase K from heat-induced deactivation. The degradation test shows that the polyacrylamide-protected enzyme partially survived the heat processing, and the enzyme-immobilized PLLA showed accelerated degradation. This research indicated that enzyme processing is theoretically possible with a protective medium.

However, due to the heat sensitivity of the enzyme, it is crucial to use proteinase K for PLLA thermal processing, which is normally done at a temperature higher than 180 °C. Moreover, the mechanical stress during processing has to be considered.[315] There has already been some research done to study the enzymatic activity.[316, 317] Bajorath *et al*., for example, demonstrated that the $Ca^{2+}$ ions could form a secondary structure hydrogen bond with proteinase K,[316] which is between the Ca1 binding site and the substrate-recognition site, and could, therefore, enhance the enzymatic activity of proteinase K. When the calcium ions were removed by ethylenediaminetetraacetic acid, the enzymatic activity dropped significantly within several hours. The reason behind this was a conformation change of the recognition site produced by the removal of $Ca^{2+}$. By contrast, when calcium ions were again added into proteinase K, the

enzymatic activity was raised slightly. Similarly, another study about proteinase K enzymatic stability was done by Yazawa *et al*. In this research, the thermal stability of proteinase K was checked for the existence of heavy metal ions.[317] It was found that the denaturation temperature in the presence of praseodymium (Pr) was 16.2 °C higher than that without Pr ions. The enzymatic activity of Pr-derivatized proteinase K at 70 °C was found to be 46-fold higher than the nitroanilide substrate.

Nonetheless, up to now, most of the studies about the thermal stability of proteinase K concern aqueous media. Very little research has been done about the thermal stability of proteinase K in bulk state. However, if proteinase K is used as an additive to tailor the degradation rate of PLLA, bulk state is more relevant to the real processing condition. Regarding the thermal processing of PLLA, other factors which affect proteinase K activity, such as shear force, pressure and temperature, have to be considered. To check whether proteinase K is still enzymatically active after processing, it is essential to develop new methods to investigate the enzymatic activity of proteinase K in bulk state.

In addition to the thermal processing using proteinase K as an additive, another possibility is to process PLLA together with proteinase K under mild conditions. However, the processing temperature for normal PLLA (beyond 180 °C) is devastating for proteinase K. The processing of enzymes or protein generally with polymer melts is still a mega problem. The solution for this challenge will enable the processing of polymer with enzymes or proteins. Therefore, I have explored in the thesis a relatively unknown method for the processing of polymer in the liquid state far below its softening or melting point. This kind of material is referred to in literature as "baroplastic," which will be introduced in the next chapter.

### 1.5. Baroplastic

The term "baroplastic" was first proposed and patented by Russel *et al.* in 2001,[318, 319] in which "baro" originates from the Greek *baros* (pressure). Baroplastic is a kind of copolymer or polymer blend, which can be processed under pressure instead of temperature. The concept of baroplastic is a block copolymer of two segments: a soft component a, of which $T_{ga}$ is lower than room temperature; and a hard component b, of which $T_{gb}$ is higher than room temperature, so that the flow of component 2 is negligible at room temperature. The two covalently bonded polymer segments can undergo order-to-disorder transition upon heating (upper order-to-disorder transition), displaying liquid- or solid-like behaviors.[320] Phase separation by induced

upper order-to-disorder transition normally occurs together with a change in volume, which results in a substantial effect of pressure on this transition.[321] As an example of a copolymer, the order-to-disorder transition of a weakly interacting block copolymer, PS-*block*-poly(*n*-butyl methacrylate), was found to be 150 °C/kbar (the order-to-disorder transition is 150 °C lower with 1 kbar increase of pressure). In research done by Ryu *et al.*, the transition of PS-*block*-poly(*n*-pentyl methacrylate) was found to be 725 °C/kbar,[322] indicating a significant effect of hydrostatic pressure on the phase transition of the polymer. There are already several models describing the baroplastic behavior. Dudowicz *et al.*, for example, introduced a lattice cluster theory to predict the interaction between two segments of the block copolymer.[323] González-León proposed an order-to-disorder transition shift induced by pressure.[324] The shift is schematically illustrated in **Figure 1-5**.

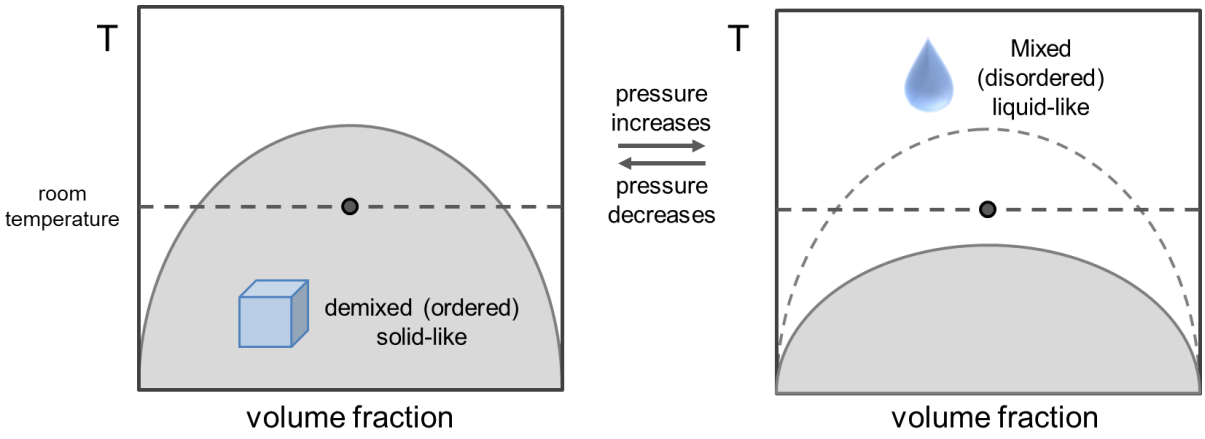


**Figure 1-5.** Illustration of pressure-induced disorder-to-order transition.

Based on this model, it is also demonstrated that low temperature processing can be achieved if the order-to-disorder transition takes place under the $T_g$ of the hard block in the block copolymers.[324] In this model, the free energy change is correlated to the mixing volume, which can be expressed by equation (5) below:[325]

$$\frac{\partial \Delta G_{mix}}{\partial P} = \Delta V_{mix} \tag{5}$$

When the $\Delta Vmix$ has a positive value, this segment occupies more volume when mixing. By contrast, when applying pressure, the segments has less volume, indicating that this segment tends to demix under this condition. In the other situation, when $\Delta Vmix$ has a negative value, the segment prefers to mix when applying pressure. The value $\Delta Vmix$ depends on several factors, such as the difference in thermal expansion, thermal compressibility and the structure

of the component. This equation can also be applied to describe polymer blend systems.

The shift induced by pressure was observed experimentally as a phase boundary correlating to temperature and the phase diagram of composition. The pressure coefficient, $dT_{ODT}/dP$, can determine the shift boundary effected by pressure. Those parameters are described in the Clausius-Clapeyron equation:

$$\frac{dT_{ODT}}{dP} = \frac{T\Delta V_{mix}}{\Delta H_{mix}} \tag{6}$$

Where $\Delta H_{mix}$ is the mixing enthalpy, which is usually positive. This equation indicates that the effect of pressure on miscibility is derived from $\Delta V_{mix}$.

With the development of baroplastics in the past few decades, Ruzette and Mayes introduced a new model to predict the miscibility of compressible block copolymers. The model is called the compressible regular solution, which is depicted as the equation below:

$$\Delta G_{mix} = kT\left[\frac{\Phi_a\tilde{\rho}_a}{N_a v_a} ln\, a + \frac{\Phi_b\tilde{\rho}_b}{N_b v_b} ln\, b\right] + \Phi_a\Phi_b\tilde{\rho}_a\tilde{\rho}_b\left(\delta_{a,0}-\delta_{b,0}\right)^2 + \tilde{\rho}_a\tilde{\rho}_b\left(\tilde{\rho}_a-\tilde{\rho}_b\right)\left(\delta_a^2-\delta_b^2\right) \tag{7}$$

Where $\Phi_i$ is the volume fraction of polymer block $i$, $\tilde{\rho}_i$ is the bulk density of the polymer block, $N_i$ is the number of repeating units of each chain, $v_i$ is the bulk molar volume, and $\delta_{i,0}$ and $\delta_i$ are solubility parameters at 0 K and specific temperature T, respectively. Knowing the parameters of the polymer segments, this equation can be used to predict the phase behavior of the polymer components. Baroplastics are expected to be phase separated under ambient conditions, and with the increasing of pressure, the mixed state boundary shifts below room temperature, thus, the baroplastic is processible at room temperature.

However, this equation only offers a qualitative prediction of the phase behavior of block copolymers, and is still not yet a complete model to be applied under all conditions. Nonetheless, a guideline to the phase behavior of polymer components can be provided by the parameters, especially the densities of polymers. Polymer components with similar densities are observed to have pressure-induced miscibility.[326] By checking the pressure-induced miscibility of a n-alkyl methacrylate/PS system with a range of density, Ruzette *et al.* determined that $\rho_a$ and $\rho_b$, which represent the densities of component a and b at 25 °C, should match the following relationship:

$$0.94\,\rho_a < \rho_b < 1.06\,\rho_a$$

Along with the guideline model, miscibility under pressure of a series of block copolymers can

be estimated. However, other practical criteria of the polymers, such as the availability of monomers, cost of monomers, feasibility of the polymerization and ease of production must be considered. The promising finding of baroplastic material, thereby, allows the reduction of energy consumption during processing. The low-temperature processing also prevents the decomposition of polymers during processing and, therefore, makes recycling possible.[327] In addition, the processing of baroplastics also provides the possibility of using thermal-sensitive material as an additive, such as proteins.

### 1.5.1. Processing of baroplastic

At the beginning of the 21st century, with the proposal of the term "baroplastic," several block copolymers have been observed to have pressure-induced miscibility, such as PS-*block*-poly (*n*-butyl methacrylate),[321] PS-*block*-poly(hexyl methacrylate)[328] and PS-*block*-poly(*n*-pentyl methacrylate),[322] and the phase behavior of these polymers has been studied empirically. However, the order-to-disorder transition temperatures of those polymers are still far above the $T_g$ of both polymer components. In 2003, González-León *et al*. published an article about baroplastic processing at a rather low temperature.[329] In this article, PS-*block*-poly(*n*-butyl acrylate) (PS-*b*-PBA, **Scheme 1-2a**) and PS-*block*-poly(2-ethylhexyl acrylate) were used to investigate the low-temperature processing capability.

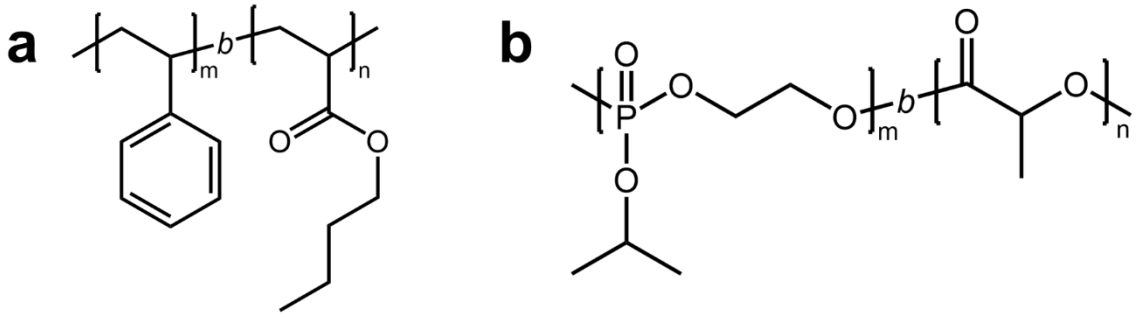


**Scheme 1-2.** Chemical structure of (a) PS-*b*-PBA and (b) poly(2-Isopropoxy-2-oxo-1,3,2-dioxaphospholane)-*block*-PLLA.

Despite the PS segments, of which the $T_g$ is relatively high, it is still possible to process PS-*b*-PBA by compression molding into a rigid transparent item using normal hydraulic pressure. The as-prepared polymer and compression-molded products are displayed in **Figure 1-6**. Remarkably, the processing temperature of 25 °C used was far below the normal processing temperature of PS.[330] A significant advantage of this kind of block copolymer is that once the

pressure is released after processing, the $T_g$ of the polymer blocks remains the same, providing the mechanical property for future applications.

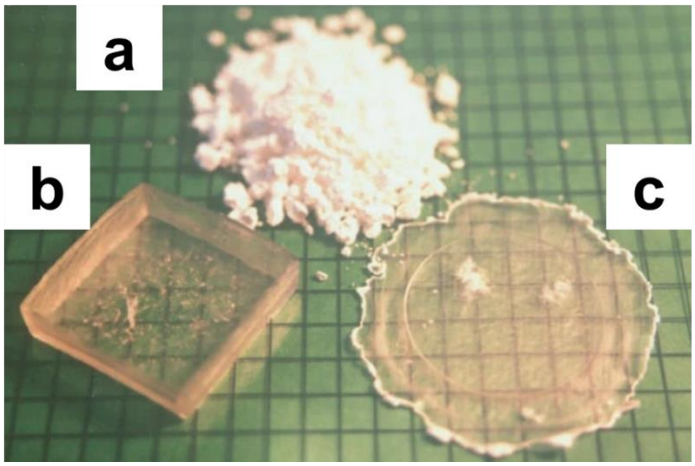


**Figure 1-6.** Polystyrene-*block*-poly(*n*-butyl acrylate) (PS-*b*-PBA), with 45 wt.% PBA (a) as-prepared, (b) and (c) after processing by compression molding at 25 °C using a pressure of 34.5 MPa (reprinted with permission, © 2003 Springer Nature).[329]

As a comparison, PS-*block*-polyisoprene was used in this article to study the pressure-induced behavior during processing. Contrarily, compression molding of PS-*block*-polyisoprene at room temperature was not successful. Similarly, Ruzatte *et al*. demonstrated that with PS-*block*-n-alkyl methacrylate block copolymers, pressure-induced miscibility was found only with the polymers with an n number ranging from 2 to 6,[331] indicating that the low-temperature processability is relevant to the polymer components, which correlates to the molecular structure. With the discovery of room temperature-processable baroplastic, this article transported the theory of baroplastics to real processing applications, and opened up a new gate to the investigation of a series of block copolymers which can be processed at a rather low temperature.

Since the publication of low temperature-processable PS-*block*-alkyl methacrylate block copolymers, there has been a few more such polymers used for reduced-energy consumption processing with enhanced properties. Lv *et al*., for example, synthesized PS-*b*-PBA core-shell polymer,[332] which can be processed at room temperature, but usually with poor mechanical properties. In this work, hydrogen bonding was introduced by a mixture of poly(acrylic acid) (PAA) and PEO. After blending the core-shell baroplastic with a PAA-PEO mixture and drying, the polymer blend could be processed at room temperature (25 °C) under 10 MPa pressure, and

compared with the baroplastic without the PAA-PEO mixture, namely, without the introduction of hydrogen bonding, the reinforced baroplastic exhibited higher mechanical strength and modulus. Similarly, Qiao *et al*. prepared reinforced PS-*b*-PBA.[327] The reinforcement was also achieved by the introduction of hydrogen bonds. Instead of a PAA-PEO polymer blend, agar was used as an additive in this work to enhance the mechanical property of PS-*b*-PBA. The PS-*b*-PBA/agar composite film showed significant optimized tensile strength and Young's modulus. Moreover, this composite material could be repeatedly processed at 100 °C several times without any notable loss of mechanical property, which favors the recycling of the composite material in real applications.

In addition to the well-known PS-*block*-alkyl methacrylate baroplastics, degradable polymer can be used as baroplastic. Taniguchi *et al*. synthesized poly(*L*-lactide)-*block*-poly(*ε*-caprolactone-*r*-5 ethylene ketal *ε*-caprolactone) and poly(*L*-lactide)-*block*-poly(1,5-dioxepan-2-one) copolymer.[333] The high $T_g$ segment PLLA and low $T_g$ segments poly(*ε*-caprolactone-*r*-5 ethylene ketal *ε*-caprolactone) ($T_g$ ranges from -60 to -40 °C) or poly(1,5-dioxepan-2-one) ($T_g$ = -38 °C) allow the polymer processing at 25 °C with 34.5 MPa hydraulic pressure. By monitoring the molecular weight of the polymers before and after processing, the degradation of polymers caused by processing was negligible, implying the potential of recyclability of these baroplastics.

### 1.5.2. Processing of baroplastic with additives

Due to the low energy consumption and high recycling ability of baroplastics, they have been used for processing with other additives to meet the requisites in applications. Lv *et al*., for example, synthesized PS-*b*-PBA.[334] Having a low $T_g$ segment PBA ($T_g$ = -40 °C) and a high $T_g$ segment PS ($T_g$ = 109 °C), the block copolymer could be processed at room temperature (25 °C). With the incorporation of carbon nanotubes, the highly conductive PS-*b*-PBA/carbon nanotube composite could be applied as an efficient electromagnetic interference shielding material. Repeated processing tests showed that the composite could retain its electromagnetic interference shielding effectiveness after ten cycles of processing, indicating the good durability and recyclability of the composite material.

Furthermore, due to the low temperature processability of baroplastics, it is a promising material for the processing of thermal-sensitive materials. An important application is the encapsulation of enzyme, which can degrade the baroplastic itself, to tailor the degradation rate

of the matrix. A typical example is using proteinase K as an additive to degrade the PLLA matrix. In the work of Iwasaki *et al*., PLLA was synthesized using polyphosphoester as an initiator.[335] The as-synthesized poly(2-Isopropoxy-2-oxo-1,3,2-dioxaphospholane)-*block*-PLLA (PIPP-*b*-PLLA, **Scheme 1-2b**) could be pressed at ambient temperature, thus, favoring the processing of heat-sensitive biomolecules, such as proteinase K. The latter was then used as an additive during the processing, and the activity was retained after pressing. The proteinase K-encapsulated PIPP-*b*-PLLA film pressed at a lower temperature (35 °C) has a self-accelerated degradation property, compared with that pressed at 130 °C. A significant disintegration of the film pressed at 35 °C was observed after 30 days. Nonetheless, the synthesis of PIPP-*b*-PLLA is complicated and has not achieved technical relevance, which hampers its application as a degradable baroplastic. Thus, a baroplastic which is easy to synthesize is essential for the encapsulation of proteinase K to tune the degradation rate of the PLLA matrix. This baroplastic is described in this thesis.

# 2. Synopsis

## 2.1. Aim of the thesis

The overall aim of the thesis is to prepare porous sponges made from degradable polyesters with tunable degradability. The achievement of the overall aim is based on three sub-aims: (1) the hydrophilization of sponges, (2) understanding of the thermal stability of enzymes, which can degrade PLLA, and (3) the processing of PLLA-type polymers at an ambient temperature. In the first sub-aim, sponges were prepared by assembling PLLA/PCL electrospun short fibers. The as-prepared sponges are hydrophobic due to the intrinsic hydrophobicity of PLLA/PCL, thus, it is important to modify PLLA sponges to benefit the applications where hydrophilicity is essential. Relevant applications for hydrophilic sponges could be, for example, drug release, tissue engineering (e.g. for cell adhesion and cell penetration) and agriculture materials (e.g. for mulch films). However, the low degradation rate of PLLA could be detrimental for these applications (e.g. the PLLA biodegradation for tissue generation could be asynchronous and persistent PLLA microplastic particles could be formed from PLLA mulch films). Thus, it is important to adapt the degradation rate of the PLLA/PCL sponges to the demands of the target applications. One possible solution is to encapsulate PLLA-degrading enzymes in the PLLA material in order to accelerate the degradation. Proteinase K is a well-established enzyme for the degradation of PLLA. Thus, the encapsulation of proteinase K during the bulk processing of PLLA could be a promising concept. Th latter leads to the second sub-aim of the thesis: the investigation of the thermal stability of proteinase K as a processing additive. The enzymatic activity of proteinase K has been well investigated in aqueous solution under various conditions, but investigations of its thermal stability in a bulk state are, to the best of my knowledge, unknown. Therefore, it is important to establish new methods for the analysis of the thermal stability of proteinase K and to gain an understanding of the enzymatic activity as a function of thermal treatment during bulk processing. The impact of mechanical stress on proteinase K during bulk processing is known and, therefore, not in the focus of my thesis. It became clear from the results of sub-aim 2 that the thermal bulk stability of proteinase K is limited and surely not given during the thermal processing of PLLA in the melt state (bulk). Therefore, it is necessary to protect proteinase K during processing, or a low-temperature processing method should be used in bulk. Hence, PLLA-type polymers are required for enzyme processing under ambient conditions. To achieve this, the third sub-aim is introduced: the utilization of a degradable baroplastic polymer, typically block copolymers, which allow the processing of proteinase K at ambient conditions. The achievement of the three sub-aims directly target the

overall aim of this thesis. The fulfillment of the overall aim of this thesis would enable the preparation of a degradable scaffold with tunable degradability by thermal processing, which could lead to new solutions for advanced applications.

### 2.2. Overview of dissertation

The fulfillment of the overall aim of this dissertation is based on three chapters (**Figure 2-1**). Firstly, the preparation of a hydrophilic electrospun sponge from the PLLA/PCL blend. Secondly, the investigation of the thermal behavior of proteinase K, and thirdly, the protection of proteinase K by low temperature processable degradable polymers.

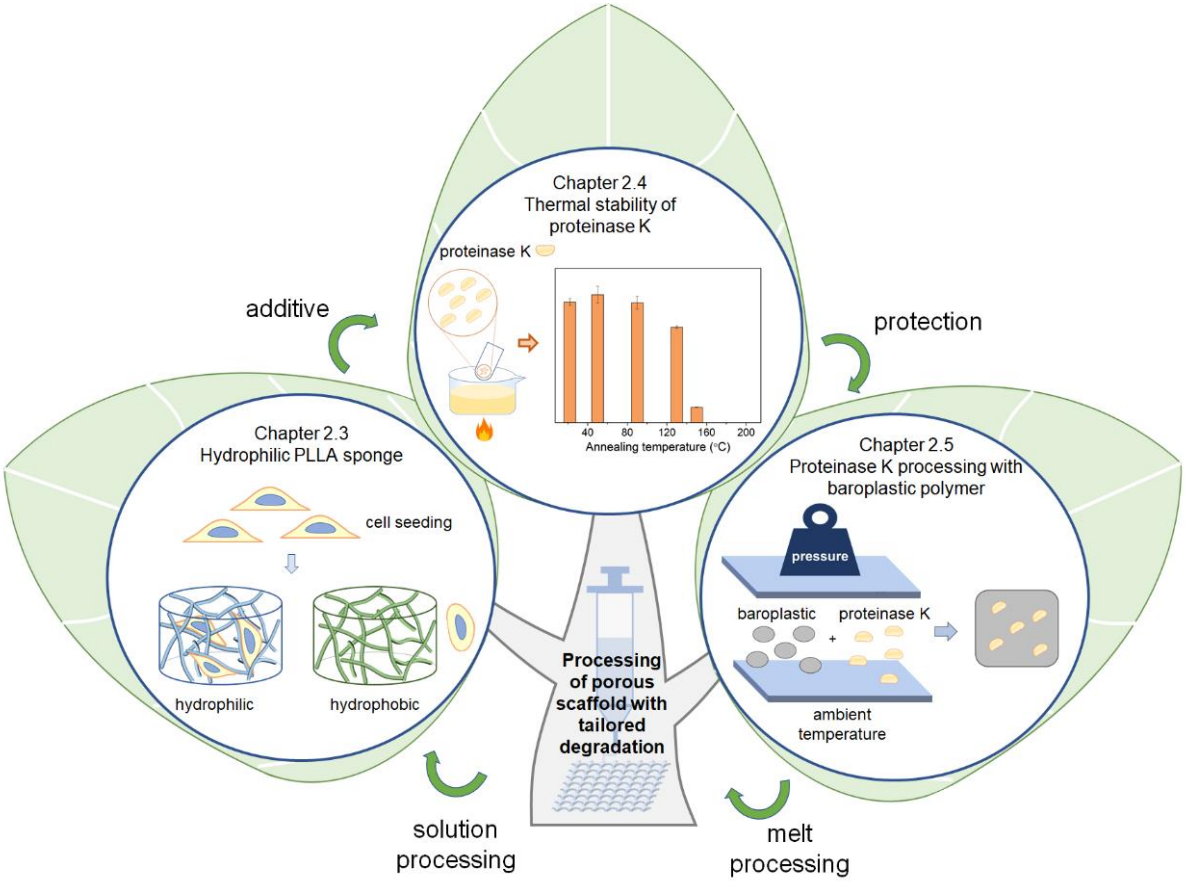


**Figure 2-1**. Table of contents image of the dissertation.

The results of the chapters led to two publications and one manuscript to be submitted, which are described briefly below.

The first publication, referring to chapter 2.3, is about hydrophilic PLLA/PCL sponge preparation. The hydrophilicity and biocompatibility of sponge to human cells is the essential

requirement for many applications, such as tissue engineering. However, the efficient and sustainable hydrophilization of PLLA/PCL sponge remains a big challenge. This challenge is the topic of chapter 2.3. In this chapter, the surface hydrophilization of sponges was conducted by a straightforward modification method. The characterization of the sponge focused on the investigation of the hydrophilization and cell compatibility of sponges. The hydrophilized PLLA/PCL sponge has the potential to be applied as a tissue engineering scaffold, drug loading medium and agriculture material.

Tailoring the degradation rate is the next important step for a successful polymer-based degradation system. Consequently, in chapter 2.4, the potential for a tailored degradation of PLLA sponges was investigated. The enzymatic degradation of PLLA is a promising concept for the control of the degradation rate. Proteinase K has been found previously to degrade amorphous and crystalline PLLA rapidly. However, the handling of proteinase K under the processing conditions of PLLA far above 150 °C could lead to the complete loss of its structure and enzymatic activity. Therefore, in chapter 2.4, the enzymatic activity of proteinase K at different temperatures was investigated thoroughly to simulate different processing scenarios. Other advanced methods for the structural characterization of annealed proteinase K were established. It was clearly proven that the handling of proteinase K at temperatures above 130 °C leads to the significant denaturation and reduction of its enzymatic activity. However, the processing of PLLA occurs under standard melt-processing conditions at about 180 °C, which does not match the thermal limitations of proteinase K.

The limited thermal stability result, shown in chapter 2.4, clearly calls for a new solution. A potential solution could be the solvent-free polymer encapsulation of proteinase K at ambient temperatures, which is shown in chapter 2.5, where the "baroplastic" concept is applied. In this chapter, it was found that polylactide-*block*-poly(ethylene glycol) (PLA-*b*-PEG) block copolymers could be processed at ambient temperatures following the baroplastic concept. This property of PLA-*b*-PEG was utilized to encapsulate proteinase K at ambient temperatures. In order to explore their potential for processing with proteinase K and gain a fundamental understanding of this promising approach, a series of PLA-*b*-PEG block copolymers were synthesized and characterized to translate it to practical applications in the sense of the overall purpose of this dissertation.

## 2.3. Thoroughly Hydrophilized Electrospun Poly(*L*-Lactide)/ Poly(*ε*-Caprolactone) Sponges for Tissue Engineering Application

Chengzhang Xu, Jun Young Cheong, Xiumei Mo, Valérie Jérôme, Ruth Freitag, Seema Agarwal, Reza Gharibi, Andreas Greiner

https://doi.org/10.1002/mabi.202300143

Macromol. Biosci. **2023**, 2300143

Polymer fiber-based sponges (PFSs) for tissue engineering could be prepared by different methods, for example, by 3D printing from melt or self-assembly of electrospun short fibers in dispersion. I have chosen the self-assembly approach for the first step. This work aims particularly at the preparation of hydrophilic degradable PFSs for tissue engineering applications. The degradable polymer used for PFS was PLLA, with a small amount of PCL (as a melt glue for the mechanical stabilization of PFS). The PLLA/PCL PFSs were inherently very hydrophobic, which is inappropriate for their application as a scaffold in tissue engineering. Our group recently reported surfactants for the modulation of the hydrophilicity of electrospun PFSs.[336] However, the concept has not been applied for PLLA PFSs. The surfactants (sodium dodecyl benzenesulfonate: SDBS) used in our recent work are certainly inappropriate for tissue engineering. Therefore, the surfactant concept was probed for the hydrophilization of PLLA/PCL PFSs using the biocompatible nonionic surfactant Tween 20. The preparation procedures are shown illustratively in **Figure 2-2**. The PLLA/PCL blend was processed by solution electrospinning (Step A in **Figure 2-2**). Afterwards, the electrospun nonwoven was cut into short fibers mechanically (Step B in **Figure 2-2**). The PFSs were formed by assembling the short fibers, followed by the self-assembly of short fibers in an aqueous dispersion. Due to the hydrophobicity of PLLA and PCL, the short fibers tended to agglomerate in aqueous medium. The problem of agglomeration was solved by the addition of a small amount of Tween 20 (0.01 wt.%). After the latter, a homogeneous short PLLA/PCL fiber dispersion was obtained, which could be freeze-dried to remove the dispersion medium. Smooth PFSs were formed as a result of this process. Annealing at 60 °C was essential in order to obtain mechanically stable PFSs. The thermally annealed PFSs had overlapped joints, which were formed by the physical cross-linking of PCL due to its melting during the annealing step.

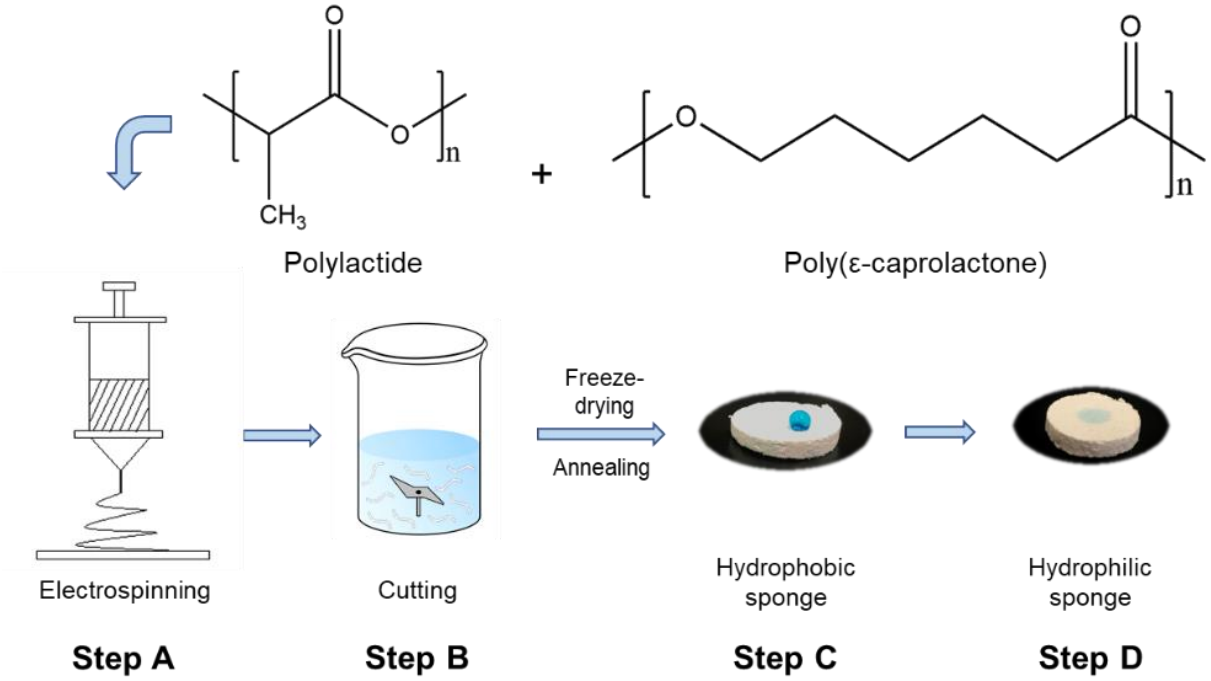


**Figure 2-2**. Schematic illustration of the PFS preparation process (step A: electrospinning of the PLLA/PCL blend; step B: cutting nonwoven short fibers and their dispersion; step C: freeze-drying and thermal cross-linking of PFS; step D: hydrophilization of PFS).

The as-prepared PFS is hydrophobic due to the intrinsic hydrophobicity of PLLA and PCL, even though a small amount of Tween 20 was applied to the dispersion medium. The deposition of a droplet of a hydrophilic dye (Wusitta Blau) on the surface of the PFS showed its hydrophobicity (Step C in **Figure 2-2**). The hydrophilization of PFSs was accomplished by dip-coating in an aqueous solution of Tween 20. After dip-coating, the PFS showed significantly improved hydrophilicity, which was also confirmed by treatment with an aqueous solution of Wusitta Blau. The drop of Wusitta Blau solution was rapidly soaked up by the hydrophilic PFS (Step D in **Figure 2-2**). The hydrophilic PFSs obtained by coating with Tween 20 were compared to those which had been hydrophilized by plasma treatment (P-PFS-3, PFS-3 is prepared by short fiber dispersion with 0.01 wt.% Tween 20; the density of the PFS is 54 mg/cm$^3$). The analysis of cross-sectional cuts of PFS after dipping in an aqueous solution of Wusitta Blau clearly showed that the hydrophilization of the PFS by plasma treatment occurred only on the surface of the PFS (**Figure 2-3**, its cross-section is not dyed by Wusitta Blau). By contrast, the surface and the cross-section of the PFS coated with Tween-20 is dyed by Wusitta Blau, which clearly indicates its thorough hydrophilization.

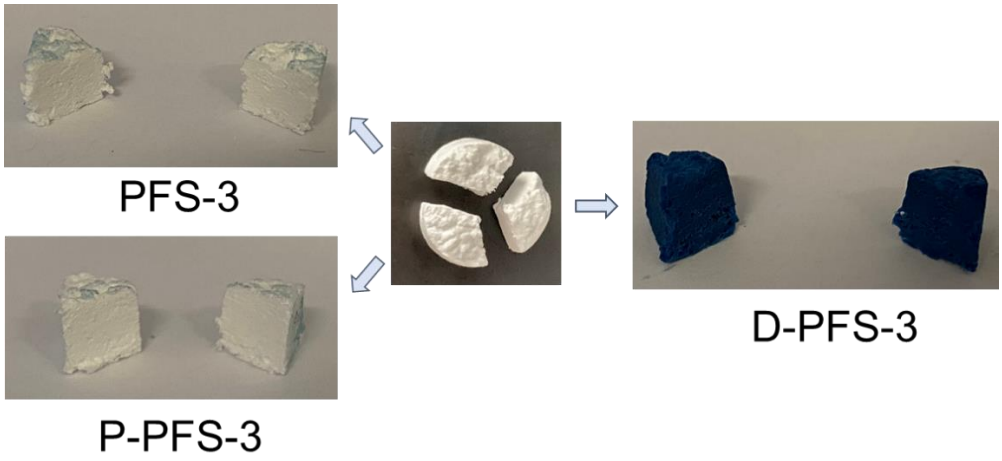


**Figure 2-3**. Cross-section of PFS-3 (left), P-PFS-3 (center) and D-PFS-3 (right) after immersing in hydrophilic dye (Wusitta blau) for 30 min.

The thorough hydrophilicity of PFS could facilitate the cell adhesion and penetration in a tissue engineering application. Notwithstanding, the cytotoxicity of Tween 20 needs verification. Thus, MG63 and human dermal fibroblast (HDF) cells (HU02) were used to determine the toxicity of the leaking substance from a PFS in cell culture medium. Leachates from dip-coated PFS (D-PFS-3) and original hydrophobic PFS (PFS-3) were used for MG63 and HDF cell culture in the cytotoxicity test. After 24 h, both cell types still had a high viability in the leachates from both hydrophilic and hydrophobic PFSs, and no significant reduction was observed (**Figure 2-4a** and **b**). This result implied the nontoxicity of leachates from the PFSs. Furthermore, the cell viability of HDF cells was monitored for a further 10 days. The cell viability of both hydrophilic and hydrophobic samples after 10 days showed only a slight decrease, indicating that the incorporation of Tween 20 on the PFS did not exceed the toxicity level of MG63 and HDF cells.

In addition to the cytotoxicity test, cell adhesion results showed that only a few cells adhered to the surface of the hydrophobic PFS. Meanwhile, a significantly larger population of cells was observed on the hydrophilic PFS. Moreover, the adhered cells on the hydrophilic PFS surface maintained their spindle-like shape for up to 48 h. The cell adhesion result revealed the preference of cell proliferation on hydrophilic PFS surfaces. Furthermore, the cell penetration in both hydrophilic and hydrophobic PFSs was detected using MG63 and HDF cells. After 48 h of the cell seeding test, the histological analysis by H&E staining showed that hardly any penetration was detected in the hydrophobic PFSs for either cell line. Contrarily, the proper

penetration of both MG63 and HDF cells was detected in hydrophilic PFSs (**Figure 2-5**). In addition, cells also spread on the surface of hydrophilic PFSs but not on hydrophobic ones.

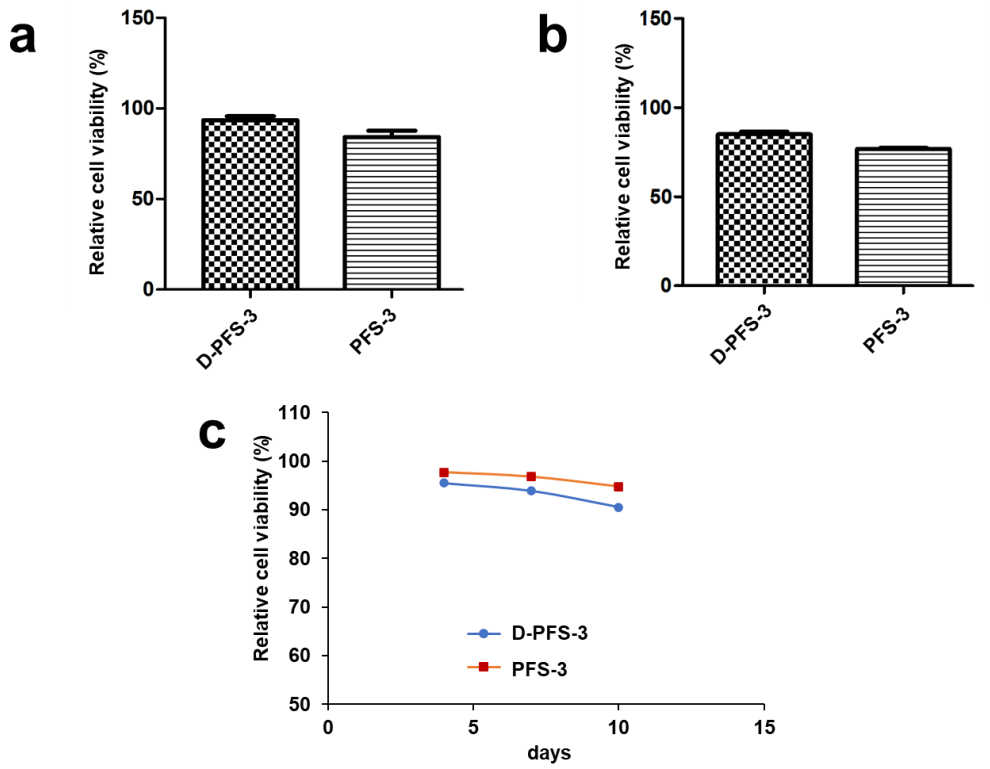


**Figure 2-4**. (a) The cytotoxicity analysis of MG63 cells on leachate extracted from the D-PFS-3 and PFS-3 after 24 h. (b) The cytotoxicity analysis of HDF cells on leachate extracted from the D-PFS-3 and PFS-3 after 24 h (control: cell culture plate = 100 % cell viability). (c) HDF cell viability monitoring on leachate extracted from the D-PFS-3 and PFS-3 over 10 days.

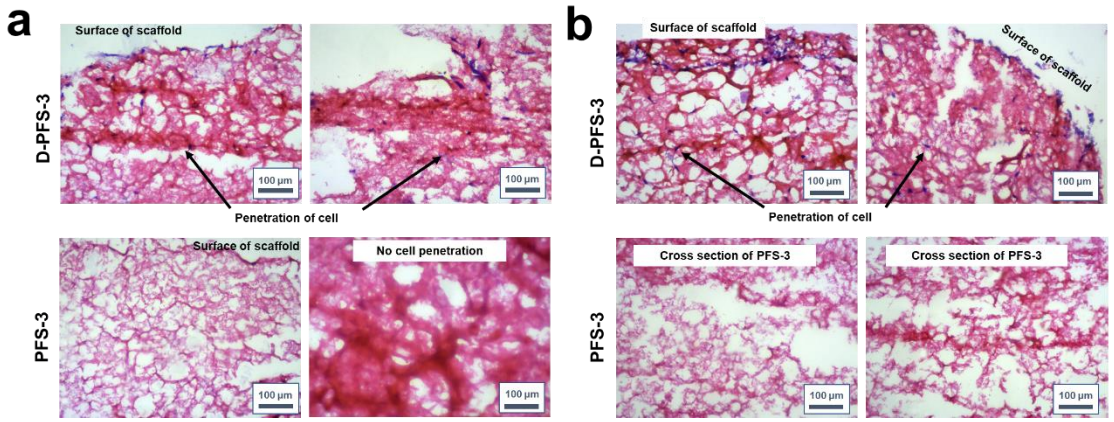


**Figure 2-5**. The representative images of H&E-stained histological sections of seeded (a) MG63 cells and (b) HDF cells on the surface and cross-section of PFSs after 48 h cultivation.

In conclusion, PLLA PFSs were successfully prepared under sustainable conditions by the self-assembly of short electrospun fibers. Aqueous medium could be used as a dispersion medium in the short fiber dispersion step to get a homogeneous dispersion with the application of surfactant Tween 20, which is a sustainable system. After freeze-drying, the mechanical stability of PFS could be achieved by the physical cross-linking of PCL in the polymer blend. The surface modification of PFS was done by a coating of Tween 20, which significantly improved the hydrophilicity of the PFS. A cell toxicity test confirmed the nontoxicity of the PFSs to MG63 and HDF cells. The cell proliferation and penetration were found to be more suitable with hydrophilic PFSs, which made the hydrophilic PLLA PFS a promising candidate for tissue engineering applications.

## 2.4. Investigation of the Thermal Stability of Proteinase K for the Melt Processing of Poly(*L*-lactide)

Chengzhang Xu, Alexander Battig, Bernhard Schartel, Renée Siegel, Jürgen Senker, Inge von der Forst, Carlo Unverzagt, Seema Agarwal, Andreas Möglich, Andreas Greiner

https://doi.org/10.1021/acs.biomac.2c01008

Biomacromolecules **2022**, *23* (11), 4841-4850

As mentioned previously, polyesters such as PLLA degrade slowly under environmental and physiological conditions. However, some applications might need faster degradation. Enzymes incorporated in the bulk of the polyesters could accelerate their degradation following the scheme of enzymatic degradation of polyesters. However, the incorporation of enzymes into the bulk of polyesters could occur with technical relevance only by polyester melt (bulk) processing. Since the polyester melt processing occurs at high temperatures, it is of outmost importance to understand the thermal stability of enzymes and, with this, the correlation of enzymatic activity in the bulk state with temperature. This understanding is the scope of chapter 2.4 and published in the second paper of this thesis. One of the key requisites of using proteinase K as a processing additive is that the enzymatic activity should be maintained after thermal processing to warrant PLLA enzymatic degradation in relevant applications. Hence, it is essential to establish an enzyme activity assay of proteinase K in a dry state to evaluate its behavior under different conditions and for the understanding of the methods for the analysis of structural changes of proteinase K induced by external factors.

Proteinase K powder was annealed in a dry state in order to simulate the thermal processing conditions. The annealing was done in a preheated vial immersed in a water or oil bath at different temperatures to mimic the thermal processing conditions. The structure of the annealed, partially water-insoluble proteinase K was conducted by multinuclear magic-angle-spinning ss-NMR spectroscopy. The NMR spectrum showed, in contrast to the native sample, a weaker hydrogen-bond network, which could be due to the denaturation and change of secondary and tertiary structure of proteinase K. The thermal response of proteinase K to high temperatures was also studied by TGA-FTIR spectroscopy. The isothermal analysis at 200 °C showed a mass loss of around 10 % after 6 min (**Figure 2-6a** and **b**). The FTIR spectrum of effluents from proteinase K at 200 °C demonstrated its decomposition products, consisting of water, acetic acid, ammonia and carbon dioxide. In accordance with the NMR result, TGA-

FTIR revealed the denaturation of proteinase K at high temperatures (200 °C).

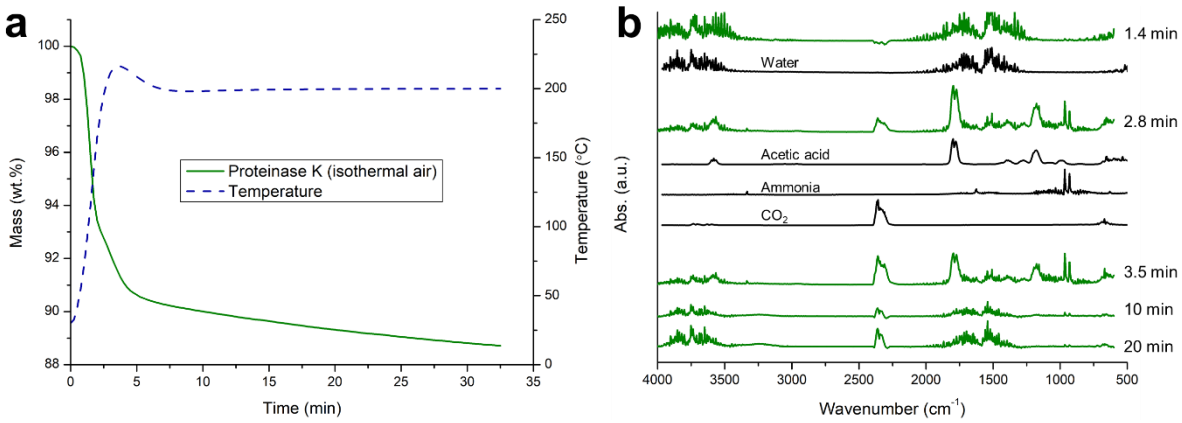


**Figure 2-6**. (a) Mass of the proteinase K sample (green solid line) and temperature (blue dashed line) over time from isothermal gravimetric measurements under air flow. (b) The FTIR spectra of the effluents at different time points in isothermal gravimetric measurements on proteinase K under air (green lines). Reference spectra of small molecules (water, acetic acid, ammonia and $CO_2$) are shown as black lines for comparison.

The enzymatic activity of proteinase K is highly dependent on the native 3D folded structure. Far-UV circular dichroism (CD) spectra of native and annealed proteinase K were recorded to analyze the folded structure of proteinase K. Solutions of proteinase K in tris buffer were used for the CD analysis. As reported previously, the annealed proteinase K dissolved only partially in the buffer solution. Therefore, only the soluble fraction could be analyzed by CD spectroscopy. The CD spectrum of native proteinase K displayed a mixture of α/β fold. By contrast, the peak at 208 and 222 nm reduced dramatically after annealing, indicating the damage of the secondary structure of proteinase K (**Figure 2-7**), therefore, the denaturation, probably resulting in the loss of enzymatic activity.

An enzyme activity assay has been established for the quantitative determination of the enzymatic activity of proteinase K. *N*-Suc-Ala-Ala-Pro-Leu-pNA was identified as a substrate for the proteinase K assay. Thereby, a reliable protocol of the proteinase K assay is now available. Based on the assay, the specific activity of native proteinase K is (6.5 ± 0.2) U/mg, where U refers to one enzyme activity unit and is defined as the hydrolysis of 1 μmol substrate per minute.

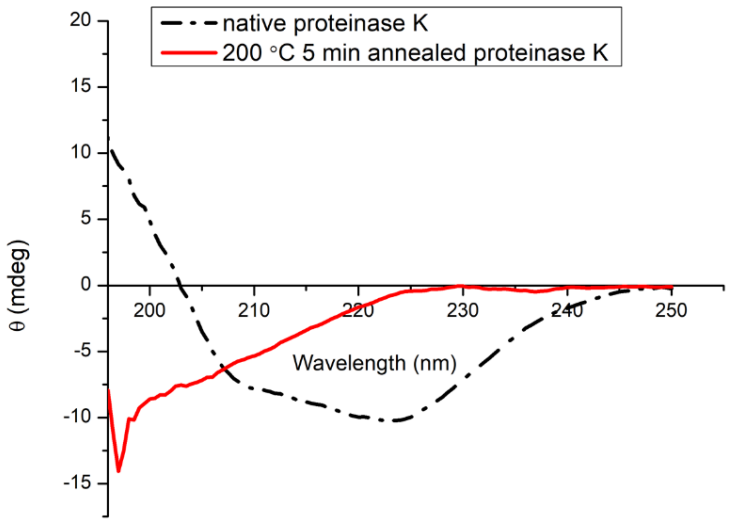


**Figure 2-7**. Far-UV circular dichroism spectra of native (black) and annealed proteinase K (red, 200 °C for 5 min).

Using this assay, the enzymatic activities of proteinase K annealed at different temperatures in bulk state were calculated (**Figure 2-8**). Surprisingly, there was no significant loss of enzymatic activity till the annealing temperature of 130 °C for 5 min. While being annealed at 150 °C, the specific activity was (0.85 ± 0.02) U/mg, implying a big loss of activity. When the annealing temperature was higher than 150 °C, namely, 180 and 200 °C, the proteinase K had only negligible activity left. It is very clear from these results that proteinase K cannot be used for the thermal bulk processing of PLLA. However, a sound ensemble of methods has now been established for the verification of different concepts for the processing of proteinase K and related enzymes with PLLA and other polymers.

The activity assay mentioned above was performed with bare enzyme without any protection. The limitations of the thermal bulk processing of proteinase K with PLLA and related polymers could be overcome by its protection via encapsulation. Hence, polyacrylamide particles were used to immobilize proteinase K.[337] We have reproduced this encapsulation method and analyzed the enzymatic activity of the encapsulated and annealed proteinase K. The proteinase K immobilized with PAM (IM-PK) particles were then annealed at 200 °C. The specific activity of proteinase K of these particles was recorded by the activity assay. Compared with the specific activity of native IM-PK, which was 2.4 U/mg, the specific activity of annealed IM-PK was only 0.05 U/mg. Even though a small fraction of activity was maintained, the values still revealed a significant reduction after annealing.

However, whether the hydrolysis of the substrate with annealed IM-PK was induced enzymatically or just hydrolytically due to the degradation products of proteinase K was still in doubt. Thus, the *N*-Suc-Ala-Ala-Pro-Leu-pNA synthesized with *D*-isomers was used for the activity assay. Notably, the catalytic triad of proteinase K can bind only to the substrate with *L*-conformation. Therefore, a substrate with *D*-conformation can be used to distinguish the degradation type, i.e. enzymatic or hydrolytic. The annealed IM-PK with *D*-conformation displayed no specific activity, implying that the cleavage of the substrate could occur only enzymatically. This conclusion was also further verified by the degradation test of PLLA and PDLA.

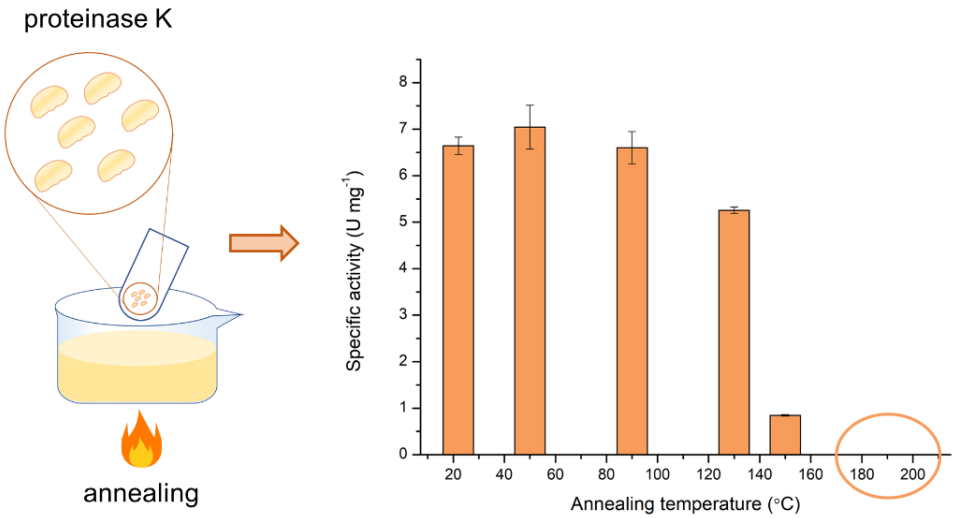


**Figure 2-8**. Specific activity of proteinase K after 5 min of annealing at different temperatures. Assays were done with 200 µM *N*-Suc-Ala-Ala-Pro-Leu-pNA substrate in Tris buffer (pH 8.6) at 25 °C. Activities were determined by evaluating the initial linear absorbance increase at 410 nm in triplicate. The orange circle on the x axis shows that the activity after annealing at 180 and 200 °C is 0 U/mg.

In conclusion, a proteinase K activity assay was established in this work, which allows the determination of the specific activity of proteinase K after being processed in bulk state. The proteinase K could tolerate a relatively high temperature in bulk state (130 °C), but when it reached higher temperatures (over 180 °C), the bare proteinase K denatured and lost its enzyme function. It is also clear from these results that the preparation of PFS by 3D printing is impossible for PLLA/proteinase K composites. When being immobilized in a protective medium, proteinase K could retain little activity at high temperatures, which implies the

importance of the protection medium of proteinase K during processing. However, better protective media for proteinase K for bulk thermal processing are required or other solutions, which are suggested in chapter 2.5.

## 2.5. Cold Processing of Triblock Copolymers under Moderate Pressure

Chengzhang Xu, Chengwei Yi, Dipannita Ghosh, Anja Ramsperger, Julian Brehm, Christian Laforsch, Holger Schmalz, Sabine Rosenfeldt, Seema Agarwal, Andreas Möglich, Andreas Greiner

Manuscript submitted to Nature Sustainability

It is clear from chapter 2.4 that proteinase K could withstand relatively high temperatures (130 °C) in bulk state, but not as high as the processing temperature of PLLA (over 180 °C). Thus, when using proteinase K as an additive for PLLA processing, it is essential to protect it in other media or create an alternative solution. An alternative solution with disruptive consequences for processing could be bulk polymer processing at an ambient temperature. However, it is not possible to process PLLA at a low temperature due to its high melting point. Thus, a new form of degradable polymer is required. In this chapter, a degradable polymer containing a PLLA block which can be processed at an ambient temperature will be discussed in chapter 2.5 and is summarized in a manuscript to be submitted. This polymer consists of a soft segment with a low $T_g$, and a hard segment with high $T_g$. Under pressure, the order-to-disorder transition of the polymer can be achieved at a lower temperature, which is known as baroplastic behavior. I discovered that certain block copolymer compositions of PLLA as a hard segment and poly(ethylene glycol) (PEG) as a soft segment show excellent baroplastic properties.

I synthesized a series of different block copolymers by ring-opening polymerization catalyzed by stannous octoate ($Sn(Oct)_2$). The ROP is schematically illustrated in **Scheme 2-1**. The reaction was initiated by either PEG or methoxy-PEG (mPEG). Therefore, the products were either a polylactide-*block*-poly(ethylene glycol)-*block*-polylactide (PLA-*b*-PEG-*b*-PLA) triblock copolymer or methoxy poly(ethylene glycol)-*block*-polylactide (mPEG-*b*-PLA) diblock copolymer. Different diblock and triblock copolymers with various chain lengths of PLA segment were synthesized. Diblock and triblock copolymers with *L*-isomer *D,L*-isomer were also polymerized for comparison. The structure of the copolymers was analyzed by $^1H$ NMR spectroscopy.

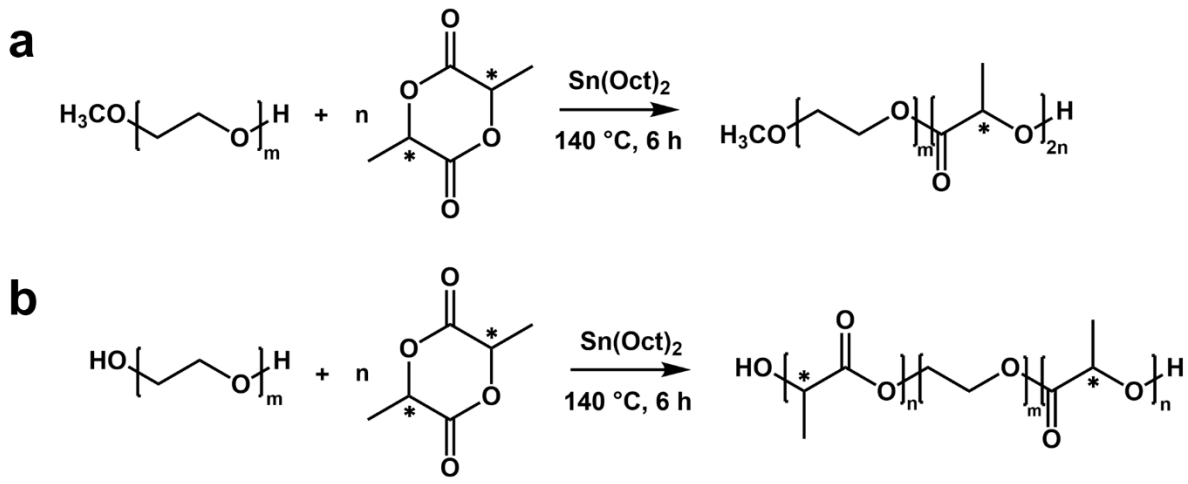


**Scheme 2-1**. Reaction scheme of (a) synthesis of the mPEG-*b*-PLA copolymer and (b) synthesis of PLA-*b*-PEG-*b*-PLA (stereochemistry is not considered in the reaction scheme, as it is a general scheme for both lactide isomers (*D*,*L*- and *L*-lactide)).

The series of PLA-*b*-PEG-*b*-PLA and mPEG-*b*-PLA copolymers were then used for processing at an ambient temperature. The polymers were processed by compression under high pressure (10 MPa) at 37 °C. The latter temperature was chosen for processing based on the melting point of the PEG segment used in this work. In addition, 37 °C is the physiological temperature which is also often used as the enzymatic degradation temperature. Almost all the polymers were able to form a film with these parameters. However, all the films formed by block copolymers with PDLLA segments were rather brittle with poor mechanical stability. Additionally, films with either too short or too long PLA segments also displayed poor mechanical properties. The best baroplastic films were found to be the triblock copolymers with a similar molar mass of lactide and ethylene glycol repeating units. It is noteworthy that baroplastic films were also obtained by pressing at 25 °C.

Two of the best baroplastics, $PLLA_{85}$-*b*-$PEG_{182}$-*b*-$PLLA_{85}$ and $PLLA_{107}$-*b*-$PEG_{182}$-*b*-$PLLA_{107}$, were chosen for further processing. The films were processed at two different temperatures, 37 and 135 °C, both under a pressure of 10 MPa. The mechanical tests of the two films showed that the film processed at the lower temperature (37 °C) had a higher elongation at break than that at the higher temperature (135 °C), implying the possibility of higher crystallinity when being processed at the higher temperature. This assumption was also confirmed by the sharp peaks in the wide-angle X-ray scattering pattern of the film processed at 135 °C.

Yellow fluorescent protein was used as model protein to encapsulate into the baroplastic film

in order to probe YPet fluorescence after the application of temperature and pressure. As shown in the fluorescence microscopic images (**Figure 2-9**), the YPet-encapsulated film processed at 135 °C showed only poor fluorescence, while the fluorescence of YPet-encapsulated film processed at 37 °C was retained.

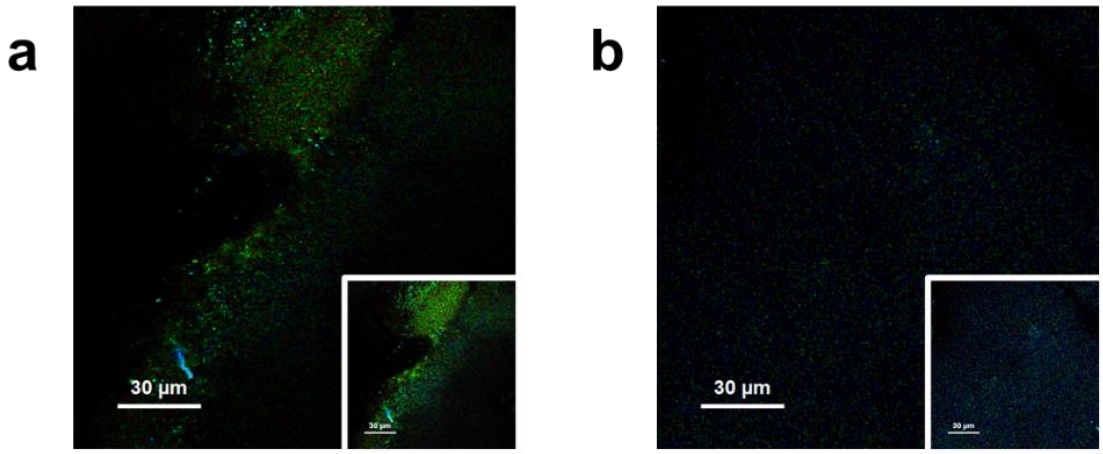


**Figure 2-9**. (a) Fluorescence microscopic image of YPet immobilized $PLLA_{107}$-*b*-$PEG_{182}$-*b*-$PLLA_{107}$ pressed at 37 °C. (b) Fluorescence microscopic image of YPet immobilized $PLLA_{107}$-$PEG_{182}$-$PLLA_{107}$ pressed at 135 °C. The input figures show the same images with higher contrast with better visibility.

In the next step, a proteinase K degradation test of electrospun baroplastic nonwoven was performed to show the degradability of the baroplastic. Furthermore, when being encapsulated in the baroplastic film and after the mild processing, the leachate from the proteinase K-encapsulated baroplastic film displayed enzymatic activity against the nitroanilide substrate used in chapter 2.4, even after a long storage time. This result confirms that the block copolymer presented in this work has the potential to be applied as an encapsulation medium for proteinase K.

In conclusion, PLA-*b*-PEG copolymers were successfully synthesized by ROP. All polymers could be processed at mild temperature, but only the polymers with a similar lactide/ethylene glycol molar mass owned benign mechanical stability. The YPet encapsulation test showed that the protein activity could be retained under the processing conditions with a mild temperature, which was further confirmed by the activity test of proteinase K leached out from the film. Since the PLA-*b*-PEG is easy to produce, it is possible to amplify the product to an industrial scale, therefore, the tunable degradability is possible to commercialize. In addition, the PLA-*b*-PEG is a promising material used as a protection medium for heat-sensitive additives in PLLA processing, such as enzymes. The encapsulated proteinase K has a large

future potential for tuning the degradability of PLLA and related polyesters. I am also convinced that the new baroplastic block copolymer could be very useful for other applications where mild processing conditions are required, for example, in pharmacology.

## 2.6. Author contribution

2.6.1. Contribution to joint publication 1

*Thoroughly Hydrophilized Electrospun Poly(L-Lactide)/ Poly(ε-Caprolactone) Sponges for Tissue Engineering Application*

Chengzhang Xu, Jun Young Cheong, Xiumei Mo, Valérie Jérôme, Ruth Freitag, Seema Agarwal, Reza Gharibi, Andreas Greiner

This work was published in *Macromolecular Bioscience* **2023**, 2300143.

Chengzhang Xu did the main part of the experiments in this work, including electrospinning, and the preparation, hydrophilization and characterization of all the sponges. She also wrote the draft of the manuscript. Dr. Jun Young Cheong supported the design of concept. Prof. Xiumei Mo, Dr. Valérie Jérôme and Prof. Ruth Freitag provided ideas for the cell culture and revised the manuscript. Prof. Seema Agarwal gave suggestions regarding the experiments and revised the manuscript. Dr. Reza Gharibi did experiments about the cells, including the cell toxicity test, cell proliferation and cell penetration. Reza Gharibi also wrote the cell culture part of the manuscript. Prof. Andreas Greiner supervised the whole project, helped with writing and revised the manuscript.

2.6.2. Contribution to joint publication 2

*Investigation of the Thermal Stability of Proteinase K for the Melt Processing of Poly(L-lactide)*

Chengzhang Xu, Alexander Battig, Bernhard Schartel, Renée Siegel, Jürgen Senker, Inge von der Forst, Carlo Unverzagt, Seema Agarwal, Andreas Möglich, Andreas Greiner

This work was published in *Biomacromolecules* **2022**, *23* (11), 4841-4850.

Chengzhang Xu did the main part of experiments in this work, including annealing experiments, part of the spectroscopic analysis, the activity assay, synthesis and characterization of PDLA, electrospinning of PLAs and degradation tests. She also wrote part of the manuscript. Dr. Alexander Battig and Prof. Bernhard Schartel did the thermogravimetric analysis coupled with Fourier transform infrared spectroscopy (TGA-FTIR) experiments and data analysis. Dr. Renée Siegel and Prof. Jürgen Senker did solid-state nuclear magnetic resonance (ss-NMR). Inge von der Forst and Prof. Carlo Unverzagt synthesized the *N*-succinyl-alanine-alanine-proline-leucine-*p*-nitroanilide (*N*-Suc-Ala-Ala-Pro-Leu-pNA) with *D*-isomers. Prof. Seema Agarwal

provided ideas and revised the manuscript. Prof. Andreas Möglich and Prof. Andreas Greiner guided the project, designed the experiments, and wrote and revised the manuscript.

### 2.6.3. Contribution to joint publication 3

*Cold Processing of Triblock Copolymers under Moderate Pressure*

Chengzhang Xu, Chengwei Yi, Dipannita Ghosh, Anja Ramsperger, Julian Brehm, Christian Laforsch, Holger Schmalz, Sabine Rosenfeldt, Seema Agarwal, Andreas Möglich, Andreas Greiner

This work is under peer review of *Nature Sustainability*.

Chengzhang Xu did the main part of the experiments, including the polymer synthesis and characterization, polymer processing, protein encapsulation, enzyme activity, degradation test, mechanical tests, polymer recycling, and wrote the manuscript. Chengwei Yi did the yellow fluorescent protein (YPet) synthesis and characterization. Dr. Sabine Rosenfeldt did the small-angle X-ray scattering and data analysis. Dipannita Ghosh and Prof. Seema Agarwal did the wastewater degradation and data analysis. Anja Ramsperger, Julian Brehm and Prof. Christian Laforsch did the cell toxicity, daphnia toxicity and data analysis. Dr. Holger Schmalz analyzed the data and reviewed the manuscript. Prof. Afndreas Möglich guided the YPet concept, synthesis and characterization. Prof. Andreas Greiner guided the project, designed the experiments, and wrote and revised the manuscript.

# 3. Publications

## 3.1. Publication 1

RESEARCH ARTICLE

Macromolecular Bioscience
www.mbs-journal.de

# Thoroughly Hydrophilized Electrospun Poly(*L*-Lactide)/Poly($\epsilon$-Caprolactone) Sponges for Tissue Engineering Application

*Chengzhang Xu, Jun Young Cheong, Xiumei Mo, Valérie Jérôme, Ruth Freitag, Seema Agarwal, Reza Gharibi,* and Andreas Greiner**

**Biodegradable electrospun sponges are of interest for various applications including tissue engineering, drug release, dental therapy, plant protection, and plant fertilization. Biodegradable electrospun poly(*l*-lactide)/poly($\epsilon$-caprolactone) (PLLA/PCL) blend fiber-based sponge with hierarchical pore structure is inherently hydrophobic, which is disadvantageous for application in tissue engineering, fertilization, and drug delivery. Contact angles and model studies for staining with a hydrophilic dye for untreated, plasma-treated, and surfactant-treated PLLA/PCL sponges are reported. Thorough hydrophilization of PLLA/PCL sponges is found only with surfactant-treated sponges. The MTT assay on the leachates from the sponges does not indicate any cell incompatibility. Furthermore, the cell proliferation and penetration of the hydrophilized sponges are verified by in vitro cell culture studies using MG63 and human fibroblast cells.**

## 1. Introduction

Water insoluble biodegradable polymers are of utmost importance in several application fields, such as tissue engineering,[1,2] gene delivery,[3,4] drug delivery,[5,6] and agriculture.[7,8] Furthermore, biodegradable polymers have gained relevance for microplastic debris.[9–11] Prominent examples of water-insoluble biodegradable polymers are aliphatic polyesters, such as poly (*L*-lactide) (PLLA), polycaprolactone (PCL), polyglycolide, polyhydroxyalkanoates and their copolymers.[12,13] Among biodegradable polyesters, PLLA and its copolymers are frequently used in different biomedical applications like implants, scaffolds for tissue engineering, and as drug-release carriers. The inherent surface hydrophobicity of these polyesters is a drawback in, e.g., tissue engineering since hydrophobic surfaces do not bind proteins.[14] In contrast, a hydrophilic surface promotes cell adhesion and mass transfer of nutrition and metabolism products, which results in cell proliferation.[15]

Numerous efforts have been reported in the literature to tune the surface wetting properties of PLLA by alkaline treatment,[16] coating with hydrophilic materials, such as type-I collagen[17] and chitosan,[18] oxygen, and ammonia plasma treatment.[19,20] The need for surface modification of PLLA is already described well by reviews.[21,22] In previous study, hydrophilicity of biodegradable polyester was increased by plasma treatment on poly(lactic-*co*-glycolic acid) (PLGA) film.[19] After plasma treatment, high

C. Xu, S. Agarwal, A. Greiner
Macromolecular Chemistry and Bavarian Polymer Institute
University of Bayreuth
Universitätsstrasse 30, 95440 Bayreuth, Germany
E-mail: greiner@uni-bayreuth.de
J. Y. Cheong
Bavarian Center for Battery Technology (BayBatt) and Department of Chemistry
University of Bayreuth
Universitätsstrasse 30, 95440 Bayreuth, Germany
X. Mo
State Key Laboratory for Modification of Chemical Fibers and Polymer Materials
College of Biological Science and Medical Engineering,
Donghua University
Shanghai 201620, P. R. China
V. Jérôme, R. Freitag
Chair for Process Biotechnology
University of Bayreuth
Universitätsstrasse 30, 95440 Bayreuth, Germany
R. Gharibi
Department of Organic Chemistry and Polymer, Faculty of Chemistry
Kharazmi University
Tehran 15719-14911, Iran
E-mail: r.gharibi@khu.ac.ir

The ORCID identification number(s) for the author(s) of this article can be found under https://doi.org/10.1002/mabi.202300143



**DOI: 10.1002/mabi.202300143**

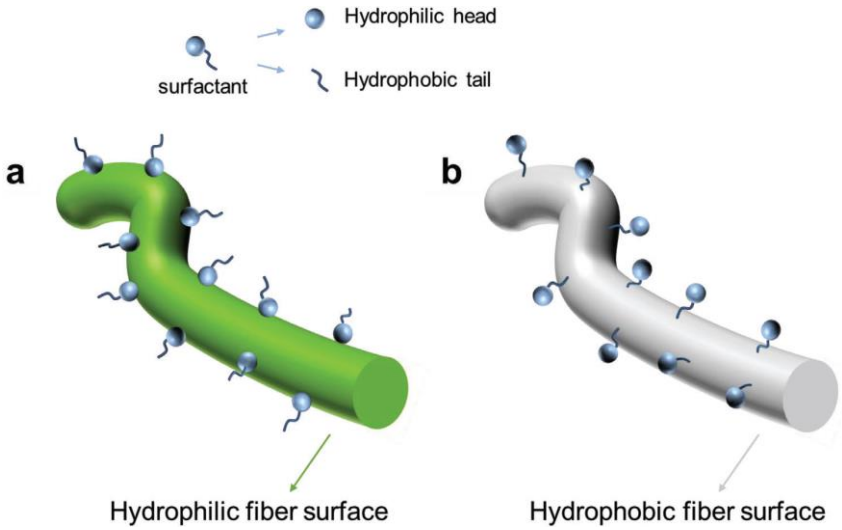


**Scheme 1.** Hydrophilic and hydrophobic fiber surface modified by surfactant a) hydrophilic surface modified by surfactant and b) hydrophobic surface modified by surfactant.

quantities of hydroxyl and peroxyl groups were detected from PLGA film. Another kind of agent, surfactants, which in general can change the wetting properties of the polymer films and particles,[23] are also used for surface modification in recent research. In one of the studies, poly(*D, L*-lactic acid)-*block*-poly(ethylene glycol) particles were coated with surfactant Tween 80 to increase the surface hydrophilicity and the stability, strength and the capacity to penetrate blood–brain barrier of drug-loaded particles.[24]

In some applications, porous structure of polymeric three-dimensional (3D) scaffold is profitable. For example, in the field of tissue engineering, porous structure of material is expected to facilitate cell seeding and proliferation. Additionally, blood vessels invade, thus, to supply enough nutrition and have an efficient mass transfer.[25] Therefore, the porosity of artificial scaffolds for tissue engineering is of importance. Different techniques such as porogene leaching,[26,27] gas foaming,[28] phase separation,[29] and 3D printing[30] have been performed to fabricate scaffolds with porous structure. Recently, a new method combining electrospinning and self-assembly was shown to fabricate low-density 3D open cellular scaffold with hierarchical pore size to mimic natural sponge structure. These scaffolds are named as electrospun sponges. The pores of these sponges with a range of size from 10–400 µm are formed by sublimation of the solvent during freeze-drying step and mechanical stability is realized by self-assembly of electrospun short fibers.[31–34] Following this concept electrospun sponges made of biodegradable polymers, including poly(L-lactide) (PLLA), were reported in recent literature as they are of interest for tissue engineering.[35–41] For example, Chen et al. produced PLLA/gelatin fiber-based sponge with cytocompatibility, which is suitable for cartilage tissue engineering. The hydrophilicity of these sponges was tuned by the addition of gelatin.[35,36] Xu et al. developed a new method (thermally induced self-agglomeration) to fabricate PCL and PCL/PLLA sponges.[37,38] The hydrophilicity of these sponges was achieved by the application of gelatin in short fiber dispersion medium. Miszuk et al. used hydroxyapatite coated PCL sponge for bone tissue regeneration, and in vitro study showed that osteogenic differentiation of cells was improved on the sponge.[39] Recently, we showed the use of PLLA/PCL short fibers to fabricate sponges, in which the self-assembly is achieved by physical cross-linking of PCL with low melting point.[40] The compatibility of these sponges to Jurkat cells and their proliferation worked well but the penetration of the cells into the sponge was limited. The hydrophilization of the sponges was improved by coating with an amphiphilic carbohydrate block copolymer, which resulted in more homogenous cell seeding and proliferation in a perfusion reactor.[41]

Recently, intrinsically hydrophobic polyimide (PI) sponges were hydrophilized by use of the surfactant sodium dodecyl benzenesulfonate (SDBS). PI short electrospun fibers were dispersed in an aqueous solution of SDBS. After freeze drying the PI sponges showed hydrophilic properties on the surface and fast water absorption.[42] The concept of surface wettability of hydrophilic as well as hydrophobic fibers is schematically depicted in **Scheme 1**. While hydrophilic fibers should become hydrophobic by treatment with surfactants, hydrophobic fibers become hydrophilic, which has been applied for two-dimensional (2D electrospun nonwoven for hydrophilization.[43,44] The use of surfactants for the hydrophilization of fibrous scaffolds provides a straightforward and highly efficient approach to achieve a high degree of hydrophilization. Particular advantage of surfactant is the high mass transfer with fibrous scaffold. This advantage of surfactants for the hydrophilization of fibrous scaffolds could be translated to 3D biodegradable PLLA sponges, and thereby could be of advanced interest for PLLA sponges for cartilage, bone tissue, and liver tissue engineering. However, it is crucial to prove the thorough hydrophilization of the PLLA sponges and the cell compatibility for practical use in tissue engineering applications. Therefore, we explored the hydrophilization of PLLA/PCL

**Table 1.** Details of PFSs used in this work.

| PFS | PFS-1 | PFS-2 | PFS-3 |
|---|---|---|---|
| density [mg cm$^{-3}$] | 153 | 80 | 54 |
| porosity[a)] [%] | 87 | 93 | 96 |

[a)] calculated based on Equations S1 and S2

sponges by use of the surfactant Tween 20, which has a relatively low $LD_{50}$ value ($LD_{50}$ of SDBS: 2.3 mg L$^{-1}$ (given for fish, data for human cells are not published to the best of our knowledge),[45] $LD_{50}$ of Tween 20: 40 554 mg kg$^{-1}$).[46] We verified the cell compatibility of the hydrophilized sponges by cell tests with human fibroblast and MG63 cells. The cell tests applied to the sponges are based on our previous evaluation of cell response.[47–50] In contrast to hydrophobic sponges, excellent cell adhesion and cell proliferation were proven for the hydrophilized sponges. However, these sponges could also be of interest for other applications, e.g., dental implant, fertilization, and plant protection. The potential application in agriculture field attributes to its hydrophilicity, thus, it has the possibility to serve as a water reservoir. Besides the importance of hydrophilization of sponges for tissue engineering, it is also of major interest to investigate the cell response to hydrophilized fibrous objects like sponges as it mimics to some extent textile scaffold waste in the environment and address this topic of microplastic debris as well.[51] The result of cell test on sponges will help in understanding the impact of short fibers from textile to organisms, which is important to microplastic.

## 2. Result and Discussion

### 2.1. Sponge Preparation and Hydrophilization

PLLA/PCL (9:1 w/w) blend electrospun nonwoven fibers were used to prepare 3D porous polymer fiber-based sponges (PFSs). PFSs were prepared with different densities and porosities, which are shown in **Table 1** and Table S1 (Supporting Information) (PFSs 4–7). The process of PFSs preparation is illustrated in **Figure 1**a. The PFSs preparation was done in three steps: electrospinning of the nonwoven (step A), cutting of the nonwoven for the preparation of short fibers (step B), and dispersion of the short fibers followed by freeze-drying (step C). In detail, the as-spun PLLA/PCL nonwoven (morphology shown in Figure 1b, fiber diameter at the range of 0.8 – 1 μm) were first cut to short fibers (fiber length 50–150 μm) in water/ice. Homogenization of the resulting short fiber dispersion was achieved by addition of different amount of Tween 20 (0.01 wt.% or 1 wt.%, **Table 2**), which was essential for the preparation of homogeneous PFSs (Figure 1c). In the case of the sponge with lower density, 0.01%

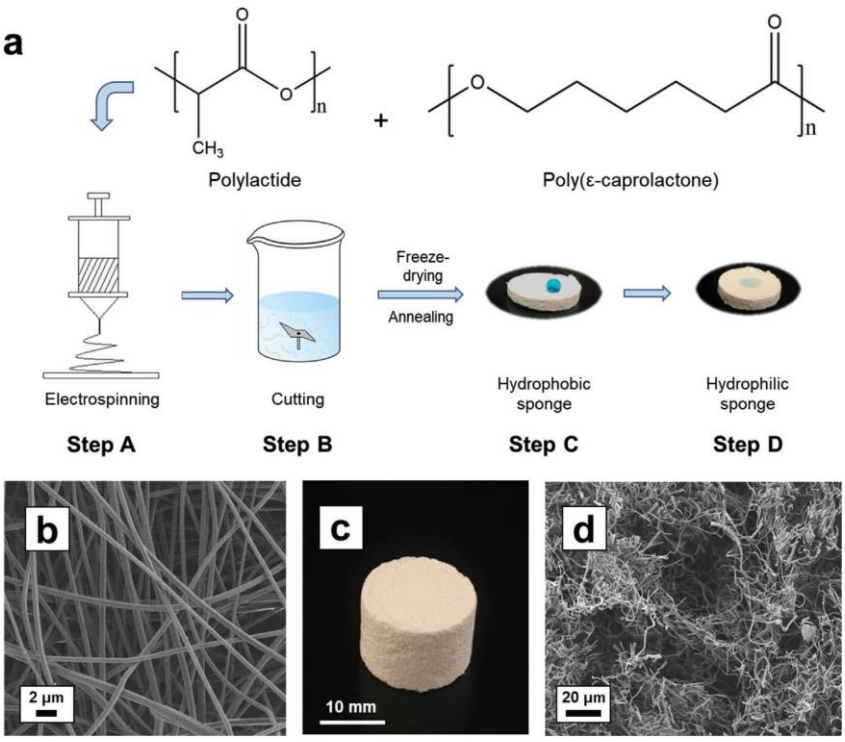


**Figure 1.** a) Schematic illustration of PFS preparation process of PFS (step A: electrospinning of PLLA/PCL blend; step B: cutting nonwoven and dispersing of short fiber; step C: freeze-drying and thermal cross-linking of sponge; step D: dip-coating of sponges in Tween 20 or plasma treatment). b) Morphology of PLLA-PCL as-spun nonwoven. c) Macroscopic appearances of PFS-3 and d) morphology of PFS-3 (scanning electron microscope micrograph).

**Table 2.** Details of Tween 20 treated PFSs.

| PFS | Tween 20 concentration at step B[a)] [%] | Tween 20 concentration at step D[b)] [%] | Plasma treatment |
|---|---|---|---|
| PFS-1 | 1 | 0 | No |
| D-PFS-2 | 0.01 | 1 | No |
| D-PFS-3 | 0.01 | 1 | No |
| P-PFS-3 | 0.01 | 0 | Yes |

[a)] concentration of Tween 20 used to disperse short fibers (step B in Figure 1a); [b)] concentration of Tween 20 used in dip-coating step (step D in Figure 1a).

Tween 20 aqueous solution was added into the short fiber suspension to reach a lower concentration of the short fibers. Contrarily, for higher density sponges, more of the dispersion medium, 0.01% Tween 20 aqueous solution was removed by filtration to get a higher concentration of the short fibers. In contrast, PFSs prepared in aqueous suspension without Tween 20 were inhomogeneous (Figure S1, Supporting Information). Subsequently, the water was removed by freeze-drying at −70 °C. The resulting PFS were bonded by annealing at 60 °C, which is the melting temperature of PCL (Figure S2, Supporting Information) but does not melt PLLA (Figure S3, Supporting Information). At this temperature, PCL melted and formed physical cross-links between the fibers. PCL was chosen due to its rather low melting point, thus, it worked as glue to bind the short fibers together at the annealing temperature. Without the existence of PCL, the pure PLLA fiber had to be annealed at a rather high temperature for a much longer time to maintain the mechanical stability of the sponge. Contrarily, if the PCL content was too high, due to the low melting point, the sponge shrank a lot during the annealing.[40] For hydrophilization of the PFSs, step D was applied: either dip-coating of sponge in 1 wt.% Tween 20 solution or plasma treatment. The sponges treated according to step D are defined as D-PFS-X, whereas is X the specific number of the PFS sample. PFSs were successfully prepared with a density ranging from 54 to 153 mg $cm^{-3}$. SEM measurements demonstrated the porous structure of PFSs. (Figure 1c,d). We have selected PFS-3 for most of the further experiments, because it could be handled well while the porosity is relatively high. PFS-3 in Figure 1d has the porosity of 96% (detail of calculation as Equations S1 and S2, Supporting Information) The pore size of PFS-3 ranged from 20 -160 μm (Figure S4, Supporting Information).

As discussed in detail below, all the as-prepared PFSs which were dispersed in 0.01 wt.% Tween 20 at step B are hydrophobic and require hydrophilization for cell applications. The PFSs were hydrophilized either by dispersion of short fiber in high concentration (1 wt.%) Tween 20 (in step B of Figure 1a), dip-coating of PFSs in Tween 20 (step D), or plasma treatment.

The hydrophobicity/hydrophilicity of the PFSs was analyzed by contact angle measurement on the PFSs' surface and in the middle of the cross-section. PFS-1 prepared from the highest Tween 20 concentration (1%) showed immediate water uptake and thereby high hydrophilicity (Figure S5a, Supporting Information). That result implied, that if the sponge was prepared with a high concentration of Tween 20 (1 wt.%) in step B, the sponge was hydrophilic originally. However, this sponge with high concentration of Tween from step B resulted in obvious shrinkage and the shape of the sponge is irregular (Figure S5b, Supporting Information). Thus, sponge with lower amount of Tween from step B is essential. We analyzed the contact angles of PFS-2 and found the contact angle to be ≈138 ° on the surface and cross-section (**Figure 2**a,b). Although shrinkage was observed to some extent (≈15%) for all PFSs, it was extreme for PFS-1. Therefore, hydrophilization was applied by dip-coating of PFS-3 (here the fiber suspension for sponge preparation (Figure 1a step B) contained only 0.01 wt.% Tween 20) into 1% Tween solution (D-PFS-3). D-PFS-3 takes up water in less than 0.2 seconds according to the video of the contact angle camera, Figure 2c. Due to its immediate water uptake, D-PFS-3 is obviously highly hydrophilic. As a benchmark, we have also analyzed plasma-treated PFS-3 (P-PFS-3) according to a previously published method.[40] The thorough hydrophilization by dip-coating with Tween 20 was demonstrated for D-PFS-3 by dying with an aqueous solution of the hydrophilic dye Wussita blau.[52] After cutting from the middle vertically, the Wusitta blau was found thoroughly distributed all over the cross-section of the D-PFS-3 (**Figure 3**a). In contrast, the untreated PFS (PFS-3, without either dip-coating or plasma treatment in step D) and the plasma-treated sponge P-PFS-3 only absorbed Wusitta blau on its surface (Figure 3a). The hydrophilicity of D-PFS was further verified by dipping the hydrophobic PFS-3 and hydrophilic D-PFS-3 together in water. D-PFS-3 sinks in water within several seconds, whereas the PFS-3 was floating on the surface of water (Figure 3b). D-PFS-3 sinks into water because the water could penetrate the sponges, implying the hydrophilicity of D-PFS-3.

### 2.2. Cytotoxicity Evaluation

Because of the potential application of the prepared sponges for tissue engineering and biomedical application purposes, the absence of leaking substances with toxic effects is essential. To this aim, the possibility of leaking toxic substances from the designed scaffolds was examined by performing the MTT assay after 24 h on MG63 and HDF fibroblast cells cultivated in the growth medium containing the extracted leachates obtained from soaked PFS samples in the culture medium. The model study by hydrophilic dye already verified, that the Wusitta blau could not penetrate the plasma-treated sponge (P-PFS-3). The result indicates that the cell culture medium, which is also aqueous, will not penetrate the sponge either to allow cell infiltration. The high viability of cultured MG63 and HDF cells in the presence of the specific amount of extracted leachates of samples (over 95%) and no significant reduction after 24 h compared to the negative control confirmed the nontoxicity of the extracted leachates (**Figure 4**a,b). For further confirmation, the cell viability was followed at a more extended time on extracted leachates with HDF cells until 10 days. The result showed the viability of cells remained above 90% for one-week extraction, and even after ten days of extraction, only a slight decrease in cell viability was detected (Figure 4c). Therefore, we could conclude that there is no release of toxic material or the released material are lower than the toxicity level, which is another indication of the suitable integration of Tween 20 within the polymeric fiber of PFS's structure. It is worth mentioning that at 24 h, the HDF cell viability on D-PFS-3 leachate is higher. However, at the latter recording points

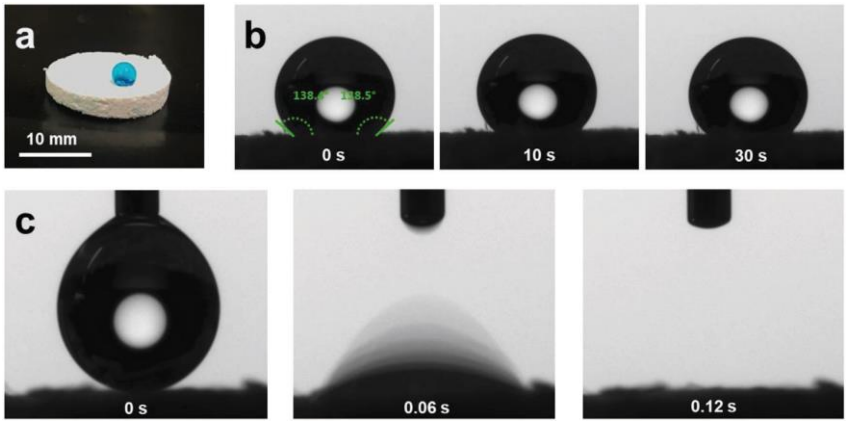


**Figure 2.** a) Image of liquid uptake by PFS-2 (dyed by Wusitta blau). Photographic image of contact angle measurements b) PFS-2 and c) D-PFS-2.

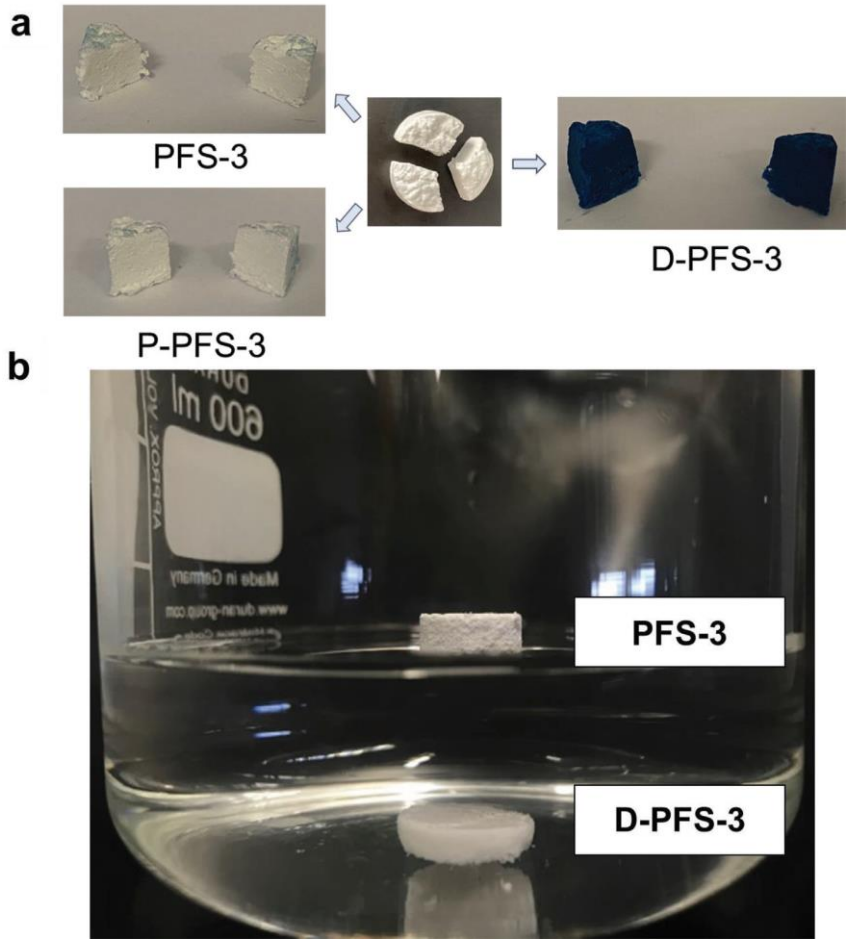


**Figure 3.** a) Cross section of PFS-3 (left) and P-PFS-3 (center) and D-PFS-3 (right) after immersing in hydrophilic dye (Wusitta blau) for 30 min. b) D-PFS-3 (submerged) and PFS-3 (floating) in deionized water.

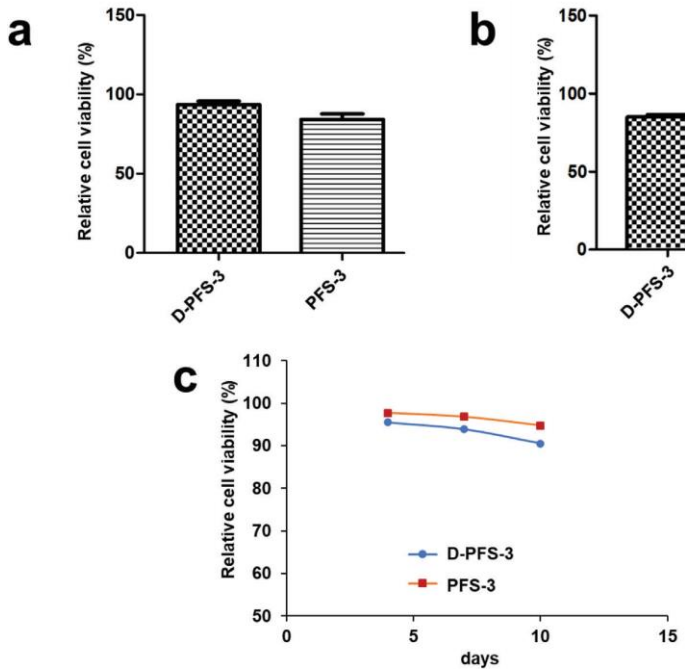


**Figure 4.** a) The cytotoxicity analysis of MG63 cells on leachate extracted from the D-PFS-3 and PFS-3 after 24 h. b) The cytotoxicity analysis of HDF cells on leachate extracted from the D-PFS-3 and PFS-3 after 24 h (Control: cell culture plate = 100% cell viability). c) HDF cell viability monitoring on leachate extracted from the D-PFS-3 and PFS-3 over 10 days.

(96, 168, and 240 h), the HDF cell viability on PFS-3 is higher. The assumption is the HDF cell viability changed slightly between the two recording points (24 and 96 h), which was not further studied. It should be noted at this point, that the PFS did not show any macroscopic morphological changes during the test period for cytotoxicity study (10 days).

### 2.3. Cell Adhesion Study

The absorption and adhesion of cells on the surface of scaffolds have a vital role in the growth and proliferation of cells and, finally, the formation of tissue within the scaffold structure. The effect of surface chemistry, especially hydrophilicity, and hydrophobicity of PFS surface on the biomolecules, protein, and cell adhesion and proliferation, has also been established in previous research.[45–48] The adhesion of MG63 and HDF cells lines (these two cell lines were used to evaluate the potential application of scaffolds for both bone and skin regeneration application) on both D-PFS-3 (hydrophilic) and PFS-3 (hydrophobic) scaffolds was assessed in the present study. The quantitative adhesion result was calculated using cell culture well plate as negative control. The quantified number is shown in **Figure 5**, the morphology, and population of the adhered MG63 and HDF cells on the scaffolds are shown in **Figure 6**, and **Figure 7**. As can be seen in Figure 5, the population of both MG63 and HDF cells on the D-PFS-3 sample is significantly higher than that on the hydrophobic PFS-3 scaffold, and only a few adhered cells were noticed on

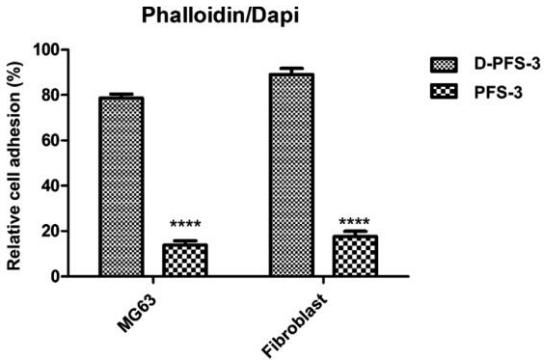


**Figure 5.** The relative adhesion of MG63 and HDF cells on PFS-3 and D-PFS-3 samples (****: *p* value<0.0001, unpaired *t* test, two tailed *p* value).

PFS-3 scaffold. The relative cell adhesion of ≈80% and 92% for MG63 and HDF cells was recorded for the D-PFS-3 sample. In contrast, the relative cell adhesion on the PFS-3 decreased and reached lower than 20% for both cell lines. It is worth noticing that even within the significant drop in relative adhesion of cells on the PFS-3 scaffold, the relatively adhered cells remained viable with spindle-shaped morphology up to 48 h, which confirmed its non--toxicity behavior. The previous reports have shown that the hydrophobic nature of pure PLLA and PCL limits the adhesion and proliferation of cell. The same trend was recorded

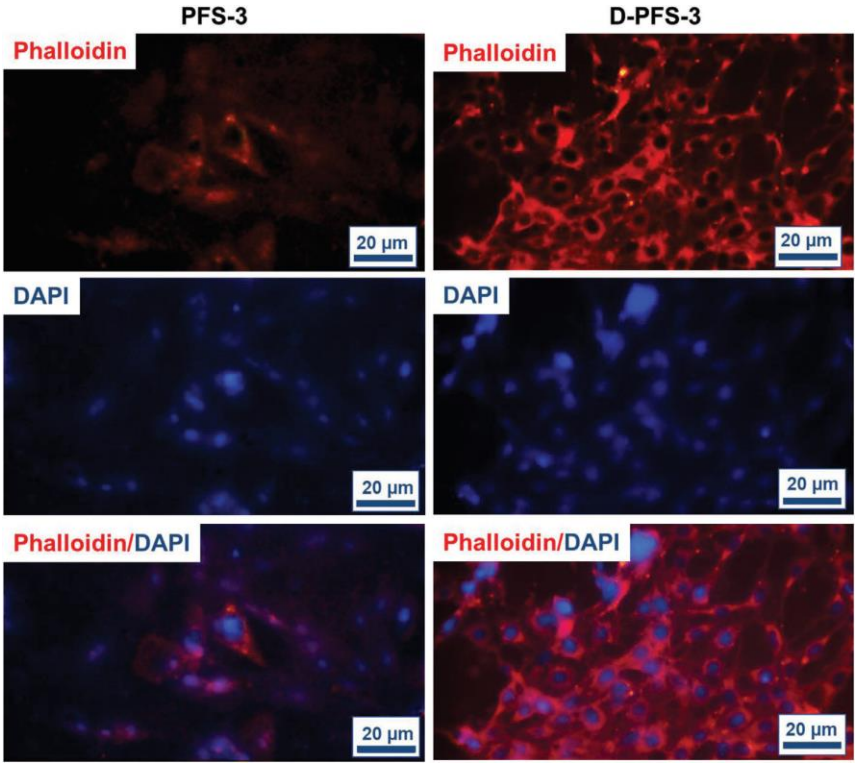


**Figure 6.** Morphology of stained proliferated MG63 cells on scaffolds. Cell nuclei were stained with DAPI, F-actin stained with Alexa Fluor® 488-phalloidin.

for the hydrophobic scaffold in the present study (Figure 6 and Figure 7). The remarkable relative adhesion, growth, and proliferation of both MG63 and HDF on D-PFS-3 scaffolds are attributed to its suitable hydrophilicity that leads to high protein binding to biomolecules, and higher relative cell adhesion. This result verifies that incorporating the Tween 20 within PLLA/PCL scaffold is a promising approach to overcome the limitations mentioned earlier, leading to superior cellular interaction and adhesion. The excellent relative cell adhesion and proliferation of both MG63 and HDF on hydrophilic scaffolds imply their potential application for both skin and bone tissue regeneration.

### 2.4. Penetration and Growth of Cells Within PFSs

Limitations of cell and biomolecule penetration into the scaffolds led to formation of mature tissue on the outer layer and necrotic tissue in the center of scaffolds. The infiltration of cells inside the sponge also relies on the pore structure and pore size of the sponge. To address these issues, designing of porous scaffolds with superior ability to transfer nutrient and cell into their inner layer has prime importance. The penetration of both HDF and MG63 cells into the prepared PFSs was also examined in the present work. To this aim, the cells were seeded onto the PFSs' surfaces, and then the viability, extent and depth of cell growth and penetration were followed by staining of penetrated and grown cells. The images of transverse sections of the cell-seeded PFSs after H&E staining after two days are shown in **Figure 8**a,b. Depth of penetration into the scaffolds was quantified after 48 h. No significant cell penetration was detected for the hydrophobic PFS-3 for both cell lines after 48 h. In contrast, proper number cell/tissue penetration into the middle of the D-PFS-3 was observed. The cell penetration depth of 211 ± 22 and 384 ± 53 µm was recorded for MG63 and HDF cell lines after 48 h, respectively. The observed difference between the depth and extent of cell growth for two different cell lines could be related to the dimensions of cells and hydrophilicity of the seeded cell types. The cells were also properly spread on the edge and surface of D-PFS-3 scaffold. The recorded result proved that the developed scaffolds with tuned hydrophilicity could support tissue formation throughout either surface, edge, or middle of constructed scaffold. Based on recorded results we could conclude that the prepared scaffolds from both physical and biological point of view are properly designed and are enabled to support cell activity and let the cell proliferate. The successful infiltration of the cells in the sponge also indicated that the pore size was suitable for cell penetration.

## 3. Conclusion

Polymer fiber-based PFS was fabricated successfully from the blend polymer system PLLA/PCL. During the cutting process,

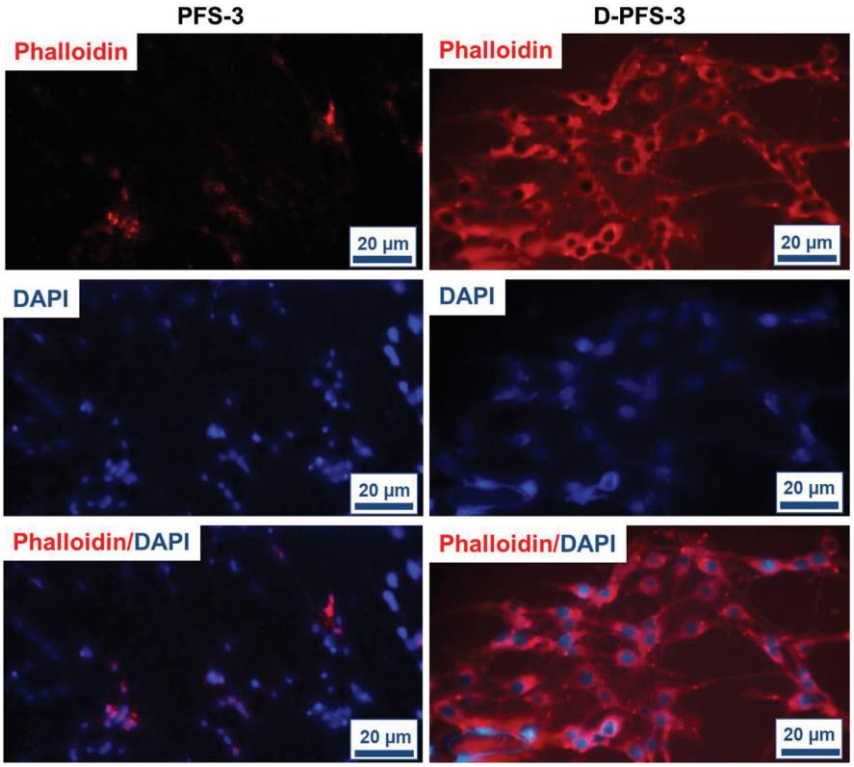


**Figure 7.** Morphology of stained proliferated HDF cells on scaffolds. Cell nuclei were stained with DAPI, F-actin stained with Alexa Fluor® 488-phalloidin (left: PFS-3; right: D-PFS-3).

it was possible to use water as cutting medium instead of harmful organic solvents, but for better dispersion of electrospun short fibers in water, application of surfactant was essential even with a rather low concentration, 0.01% in this work. The PFSs had physically cross-linked structure to maintain the structural integrity after thermal annealing step. PFS without any surface modification showed high hydrophobicity. In contrast, high hydrophilicity of PFS was achieved successfully by surfactant dip coating, which was scalable and fast. The treatment of the PFSs by surfactant resulted in thorough hydrophilization, which was obviously required for successful cell seeding. It was also obvious from our results, that cell seeding did occur inside the sponge within a short time (2 days). In contrast, the model studies showed that untreated PFS and plasma-treated PFS were hydrophobic inside, which was detrimental for cell seeding. The significantly increased high hydrophilicity of surface modified sponge was stable in aqueous state, and the hydrophilicity of PFS was favorable for cell growth, proliferation, and penetration, offering its potential application in fields like hard tissue engineering, and dental material. Fertilization is another potential application, because the hydrophilic sponge could serve as water reservoir for water management. The cell tests also indicated that surfactant dip coating did not harm the cells tested in this work during the test period. This could help to understand the effect of textile-based microplastic waste, such as short fibers, on cells as well. However, this conclusion will need further verification with other scaffolds, fiber geometries, and polymers, which we will follow up in future work. Follow-up future work should surely also address the correlation of the porosity and pore size distribution of hydrophilized PLLA sponges on cell compatibility and cell proliferation.

## 4. Experimental Section

*Materials*: Chloroform ($CHCl_3$, VWR), dimethylformamide (DMF, Fisher Chemical), acetic acid (AA, Sigma-Aldrich), ethanol, (EtOH), polysorbate 20 (Tween 20, Acros, Fisher Scientific), poly($\epsilon$-caprolactone) (PCL, Capa 6800, Perstorp), poly (*L*-lactide) (PLLA, Ingeo Biopolymer PLLA 4043D, Nature-Works LLC) were used as received. Human dermal fibroblast (HDF) cells (Hu02) and human osteosarcoma cell line (MG63) cells were produced from Iranian Biological Resource Centre (IBRC, Tehran, Iran).

*Characterization Methods*: Molecular weight of the PLLA and PCL used for PFSs fabrication was characterized by gel permeation chromatography (GPC) equipped with a Styrene-divinylbenzene (SDV) precolumn (particle size 5 µm; PSS Mainz) and SDV linear XL column (particle size 5 µm, PSS Mainz). Samples were dissolved in $CHCl_3$ with a flow rate of 0.5 mL $min^{-1}$ was used for measurements. The calibration was done with narrowly distributed polystyrene standards (PSS calibration kit). The results were shown in Figures S6 and S7 (Supporting Information). Differential scanning calorimetry (DSC, Netzsch, 204 F1, Phoenix) measurements were

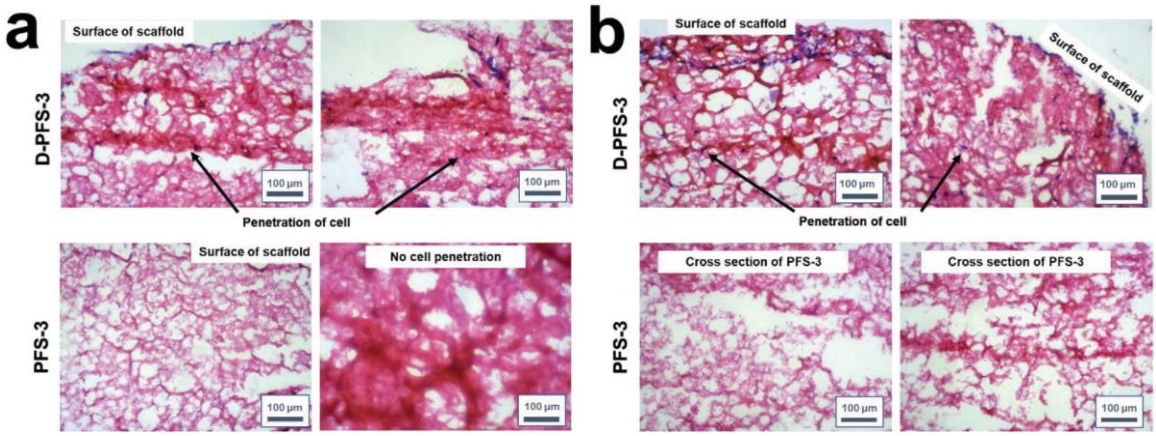


**Figure 8.** The representative images of H&E-stained histological sections of seeded a) MG63 cells and b) HDF cells on surface and cross section of PFSs after 48 h cultivation.

performed on raw polymer material at a heating rate of 10 K $min^{-1}$. Morphology of samples was imaged by scanning electron microscopy (SEM, LEO 1530, Zeiss). The samples were first sputter coated with Pt by sputter coater (208 HR from Cressington, Watford, England). Contact angle measurements were done by Drop Shape Analyzer (Krüss Advance, v1.3.1) at room temperature, and the volume of deionized water drop was 4 µL. For hydrophilic dye staining method, the sponge samples were immersed into hydrophilic dye (Wusitta blau, Erich Wutzig) solution (as received from company) for 30 min at 22 °C. The coated sponges were then cut vertically to check if the internal part was stained by Wusitta blau.

*Preparation of Electrospun Nonwoven*: Electrospinning of PLLA/PCL was done following a previous publication with further modification.[53] In brief, 3.78 g PLLA (6.3 wt.%) and 0.42 g PCL (0.7 wt.%) were dissolved in a solvent mixture containing 39.06 g $CHCl_3$ (65.1 wt.%), 8.37 g AA (13.95 wt.%), and 8.37 g DMF (13.95 wt.%). This solution was filled in a plastic syringe (Injekt, 2 mL, B. Braun) assembled with a blunt-ended stainless steel needle (Sterican, Ø = 0.4 mm, B. Braun). The following conditions were applied for electrospinning: voltage 12.5 kV, flow rate 1.3 mL $h^{-1}$, and the distance between needle and collector 20 cm with relative humidity ≈20% and temperature ≈22 °C. The electrospun nonwoven was collected on a rotating cylinder (diameter 8.5 cm, length 21 cm, rotation speed 100 rpm) covered by slick parchment paper connected to −0.8 kV negative voltage.

*Preparation of Short Fiber Dispersion*: The electrospun nonwoven was stored under ambient conditions (101.3 MPa, 20 °C) for 12 h and cut into 2 × 2 $cm^2$ pieces. 1.5 g nonwoven was then cut into short fibers by a Gastroback kitchen mixer using ≈500 mL ice/water as cutting medium. Higher concentrations of short fiber suspension were reached by selective removal of water by filtration.

*Preparation of PFSs*: The short fibers were dispersed in aqueous solution with different concentrations of Tween 20 (0.01 wt.% or 1 wt.%). Taking polymer fiber-based sponge 3 (PFS-3) as an example, 0.01 g of Tween 20 was added into 100 g dispersion of short fiber, thus, the concentration of Tween 20 is 0.01 wt.% with respect to the dispersion (water as dispersion medium, approximate short fiber concentration 50 mg $mL^{-1}$), and the suspension was stirred vigorously by a Vortex-m shaker at 3000 rpm to realize homogeneity. 5 g of the suspension was then transferred into a cylindrical glass vial with diameter of 19 mm, frozen by immersion in EtOH bath at −30 °C for 15 min. The diameter of the glass vial and the amount of suspension added into the vial will together determine the dimension of the sponges. The frozen suspension was freeze-dried in Christ Beta-2-16 freeze-dryer at −70 °C, 0.1 mbar for 24 h. To achieve physical cross-linking, the dried product was put in oven to subject thermal annealing at 60 °C for 1 h under atmosphere pressure. PFSs with varied densities were prepared by adjustment of the concentration of short fibers in the dispersion (Table 1). For example, in the case of sponges with lower density, 0.01% Tween 20 aqueous solution was added in the short fiber suspension to reach a lower concentration of the short fibers. Contrarily, for higher-density sponges, more of the dispersion medium, 0.01% Tween 20 aqueous solution was removed by filtration to get a higher concentration of the short fibers.

*Dip Coating*: The thermally annealed PFS-3 and PFS-2 were subsequently submerged in 1 wt.% Tween 20/$H_2O$ solution for 30 min. After being taken out from Tween 20 solution, the PFS was dried in freeze-dryer for removal of water. The dip-coated sponge was named as D-PFS-3 and D-PFS-2, respectively.

*Plasma Treatment*: Plasma treatment was done by Air-Plasma oven (MiniFlecto-PC-MFC, Gala Instruments, v. 2.0.9, 2009). PFS-3 were treated under 0.5 mbar pressure with 100% air, the power was 20 W and the duration was 15 min. The plasma-treated sample was named as P-PFS-3.

*In Vitro Cytocompatibility Assay (MTT Assay on Leachate Extracted from Samples)*: The possibility of releasing any toxic material from the prepared PFSs was checked out by applying MTT assay on the cells with existence of extracted leachates of immersed samples in the culture medium at different time intervals. To this aim the freshly synthesized samples were immersed in the culture medium for different time at 37 °C and then MTT assay was applied to cells cultured in the presence of the leachate. The standard culture medium was used as negative control. To check the leaking of any toxic material, the certain amount of standard culture medium with the extracted leachate from sponges at different time intervals was replaced and compared the cell viability with negative control that is standard culture medium with no extracted leachates from sponges. The percentage of relative cell viability was calculated according to Equation 1:

$$\text{cell viability}\% = \frac{OD_{sample}}{OD_{negative\ control}} \quad (1)$$

OD designates the optical density.

*Adhesion of MG63 and Human Dermal Fibroblast (HDF) Cells on the PFSs*: The following procedure was used to analysis the HDF and MG63 cells' relative adhesion and proliferation on the both D-PFS-3 and PFS-3 scaffolds. First, the scaffold specimens were cut in a suitable size (0.3 $cm^2$ basal area and 0.5 cm height) to cover the bottom of each well and then seeded with culture medium with density of 5× $10^4$ cells $mL^{-1}$. After certain time intervals, the PFS/cells were removed and washed at least three times to remove the unattached cells from sample surfaces. The number of adhered cells was quantified by MTT assay. The standard calibration

curve was plotted by applying MTT assay on an identified number of cells on a 96-well plate. Then, MTT assay was performed on each sample with adhered cells, and the number of attached cells was calculated from the standard calibration curve.

The number of adhered cells on the PFSs was quantified through the MTT assay on the PFS/cells construct. Then, the relative cell viability and relative cell adhesion percent were calculated by Equation 2.

$$\text{relative cell adhesion}\% = \frac{OD_{sample} - OD_{positive\ control}}{OD_{negative\ control}} \quad (2)$$

OD designates the optical density.

The standard tissue culture plate (TCP) was tested as a negative control, and the scaffolds with no cells were tested as a positive control.

Finally, the adhered cells were stained with DAPI/Phalloidin and imaged under a Confocal microscope for DAPI (359 nm) and Phalloidin (550 nm).

*Cell Penetration Assay*: The cell penetration depth into the PFSs samples was assessed by staining of penetrated cells and formed tissue via histological analyses. The constructed PFSs/cell samples (The PFSs/cell samples were prepared based on the procedure described in the previous section, the same cell number and same cell culture medium and incubation time) were separately fixed in 10% formalin and then dehydrated through graded alcohol series and fixed in paraffin wax. Serial sections of 5 µm thickness were cut via microtome and the grown cells and were stained with Hematoxylin and Eosin (H&E). These stained sections were observed under a microscope, and photomicrographs were captured. The depth of stained area that were the penetrated cells were analyzed by Image J software to evaluate the depth of cell growth and penetration into the PFS samples.

*Statistical Analysis*: The analysis of recorded data was performed with One-Way ANOVA with the Tukey post hoc test. The significance level was set at $p \leq 0.05$.

## Supporting Information

Supporting Information is available from the Wiley Online Library or from the author.

## Acknowledgements

This study was funded in part by the Deutsche Forschungsgemeinschaft (DFG, German Research Foundation), CRC Microplastic, project number SFB 1357-391977956. Dr. Qimeng Song, Tobias Lauster and Stefan Rettinger from Department of Physical Chemistry I were kindly acknowledged for the support with the plasma machine. The authors were thankful for the support of SEM measurement from the Keylabs for Optical and Electron Microscopy of the Bavarian Polymer Institute.

Open access funding enabled and organized by Projekt DEAL.

## Conflict of Interest

The authors declare no conflict of interest.

## Data Availability Statement

The data that support the findings of this study are available in the supplementary material of this article.

## Keywords

electrospun sponges, human cell tests, hydrophilization, polylactide

Received: April 3, 2023
Revised: June 19, 2023
Published online:

[1] G. J. Christ, J. M. Saul, M. E. Furth, K.-E. Andersson, *Pharmacol. Rev.* **2013**, *65*, 1091.
[2] A. Joraku, C. A. Sullivan, J. J. Yoo, A. Atala, *Laryngoscope* **2005**, *115*, 244.
[3] S. D. Patil, D. G. Rhodes, D. J. Burgess, *AAPS J.* **2005**, *7*, E61.
[4] A. Nagarsekar, H. Ghandehari, *J. Drug Targeting* **1999**, *7*, 11.
[5] B. Amsden, A. Hatefi, D. Knight, E. Bravo-Grimaldo, *Biomacromolecules* **2004**, *5*, 637.
[6] O. Dechy-Cabaret, B. Martin-Vaca, D. Bourisssou, *Chem. Rev.* **2004**, *104*, 6147.
[7] M. Sander, *Environ. Sci. Technol.* **2019**, *53*, 2304.
[8] Z. Majeed, K. Ramli Nur, N. Mansor, Z. Man, *Rev. Chem. Eng.* **2015**, *31*, 69.
[9] J. M. Millican, S. Agarwal, *Macromolecules* **2021**, *54*, 4455.
[10] X.-F. Wei, M. Bohlén, C. Lindblad, M. Hedenqvist, A. Hakonen, *Water Res.* **2021**, *198*, 117123.
[11] A. Kumar, A. R. Weig, S. Agarwal, *Macromol. Mater. Eng.* **2022**, *307*, 2100602.
[12] W. Amass, A. Amass, B. Tighe, *Polym. Int.* **1998**, *47*, 89.
[13] I. Vroman, L. Tighzert, *Materials* **2009**, *2*, 307.
[14] X. Wang, B. Ding, B. Li, *Mater. Today* **2013**, *16*, 229.
[15] H. Amani, H. Arzaghi, M. Bayandori, A. S. Dezfuli, H. Pazoki-Toroudi, A. Shafiee, L. Moradi, *Adv. Mater. Interfaces* **2019**, *6*, 1900572.
[16] N. Yoon Sung, Y. Joon Jin, L. Jae Gwan, P. Tae Gwan, *J. Biomater. Sci., Polym. Ed.* **1999**, *10*, 1145.
[17] X. Garric, J.-P. Molès, H. Garreau, J.-J. Guilhou, M. Vert, *J. Biomed. Mater. Res.* **2005**, *72A*, 180.
[18] A. Zhu, M. Zhang, J. Wu, J. Shen, *Biomaterials* **2002**, *23*, 4657.
[19] Y. Wan, X. Qu, J. Lu, C. Zhu, L. Wan, J. Yang, J. Bei, S. Wang, *Biomaterials* **2004**, *25*, 4777.
[20] S. Sarapirom, L. D. Yu, D. Boonyawan, C. Chaiwong, *Appl. Surf. Sci.* **2014**, *310*, 42.
[21] Y.-P. Jiao, F.u-Z. Cui, *Biomed. Mater.* **2007**, *2*, R24.
[22] Y. Cheng, S. Deng, P. Chen, R. Ruan, *Front. Chem. China* **2009**, *4*, 259.
[23] T. Sritapunya, B. Kitiyanan, J. F. Scamehorn, B. P. Grady, S. Chavadej, *Colloids Surf., A* **2012**, *409*, 30.
[24] T. Ren, N. Xu, C. Cao, W. Yuan, X. Yu, J. Chen, J. Ren, *J. Biomater. Sci., Polym. Ed.* **2009**, *20*, 1369.
[25] A. G. Mikos, G. Sarakinos, S. M. Leite, J. P. Vacant, R. Langer, *Biomaterials* **1993**, *14*, 323.
[26] S.-J. Liu, C.-L. Hsueh, S. Wen-Neng Ueng, S.-S.u Lin, J.-K. Chen, *Asia-Pac. J. Chem. Eng.* **2009**, *4*, 154.
[27] I. O. Smith, X. H. Liu, L. A. Smith, P. X. Ma, *WIREs Nanomed. Nanobiotechnol.* **2009**, *1*, 226.
[28] Y. S. Nam, J. J. Yoon, T. G. Park, *J. Biomed. Mater. Res.* **2000**, *53*, 1.
[29] P. X. Ma, R. Zhang, *J. Biomed. Mater. Res.* **1999**, *46*, 60.
[30] W. Yu, X. Sun, H. Meng, B. Sun, P. Chen, X. Liu, K. Zhang, X. Yang, J. Peng, S. Lu, *Biomater. Sci.* **2017**, *5*, 1690.
[31] Y. Si, J. Yu, X. Tang, J. Ge, B. Ding, *Nat. Commun.* **2014**, *5*, 5802.
[32] G. Duan, S. Jiang, V. Jérôme, J. H. Wendorff, A. Fathi, J. Uhm, V. Altstädt, M. Herling, J. Breu, R. Freitag, S. Agarwal, A. Greiner, *Adv. Funct. Mater.* **2015**, *25*, 2850.
[33] S. Jiang, S. Agarwal, A. Greiner, *Angew. Chem., Int. Ed.* **2017**, *56*, 15520.
[34] F. Deuber, S. Mousavi, M. Hofer, C. Adlhart, *ChemistrySelect* **2016**, *1*, 5595.
[35] W. Chen, S. Chen, Y. Morsi, H. El-Hamshary, M. El-Newhy, C. Fan, X. Mo, *ACS Appl. Mater. Interfaces* **2016**, *8*, 24415.
[36] W. Chen, J. Ma, L. Zhu, Y. Morsi, H. El-Hamshary, S. S. Al-Deyab, X. Mo, *Colloids Surf., B* **2016**, *142*, 165.
[37] T. Xu, J. M. Miszuk, Y. Zhao, H. Sun, H. Fong, *Adv. Healthcare Mater.* **2015**, *4*, 2238.
[38] T. Xu, Q. Yao, J. M. Miszuk, H. J. Sanyour, Z. Hong, H. Sun, H. Fong, *Colloids Surf., B* **2018**, *171*, 31.

[39] J. Miszuk, Z. Liang, J. Hu, H. Sanyour, Z. Hong, H. Fong, H. Sun, *ACS Appl. Bio Mater.* **2021**, *4*, 3639.
[40] M. Mader, V. Jérôme, R. Freitag, S. Agarwal, A. Greiner, *Biomacromolecules* **2018**, *19*, 1663.
[41] M. Mader, M. Helm, M. Lu, M. H. Stenzel, V. Jérôme, R. Freitag, S. Agarwal, A. Greiner, *Biomacromolecules* **2020**, *21*, 4094.
[42] J. Y. Cheong, M. Mafi, L. Benker, J. Zhu, M. Mader, C. Liang, H. Hou, S. Agarwal, I.-D. Kim, A. Greiner, *ACS Appl. Mater. Interfaces* **2020**, *12*, 18002.
[43] R. S. Kurusu, N. R. Demarquette, *Eur. Polym. J.* **2017**, *89*, 129.
[44] R. Vasita, G. Mani, C. M. Agrawal, D. S. Katti, *Polymer* **2010**, *51*, 3706.
[45] J. Jensen, *Sci. Total Environ.* **1999**, *226*, 93.
[46] G. Wypych, in *Databook of Antistatics*, (Ed: G. Wypych), Elsevier, Oxford, UK **2014**, Ch. 3.1.
[47] H. Gholami, H. Yeganeh, R. Gharibi, M. Jalilian, M. Sorayya, *Polymer* **2015**, *62*, 94.
[48] N. Baheiraei, R. Gharibi, H. Yeganeh, M. Miragoli, N. Salvarani, E. Di Pasquale, G. Condorelli, *J. Biomed. Mater. Res. Part A* **2016**, *104*, 1570.
[49] A. Rezapour-Lactoee, H. Yeganeh, S. N. Ostad, R. Gharibi, Z. Mazaheri, J. Ai, *Mater. Sci. Eng., C* **2016**, *69*, 804.
[50] A. Meydani, S. Yousefi, R. Gharibi, S. Kazemi, M. B. Teimouri, *ChemistrySelect* **2019**, *4*, 3315.
[51] A. P. Periyasamy, A. Tehrani-Bagha, *Polym. Degrad. Stab.* **2022**, *199*, 109901.
[52] N. B. Haro-Mares, J. C. Meza-Contreras, F. A. López-Dellamary, A. Richaud, F. Méndez, B. G. Curiel-Olague, G. Buntkowsky, R. Manríquez-González, *Surf. Interfaces* **2022**, *35*, 102412.
[53] J. Zhu, A. Kumar, P. Hu, C. Habel, J. Breu, S. Agarwal, *Global Challenges* **2020**, *4*, 2000030.

# Supporting Information

## Thoroughly hydrophilized electrospun poly(*L*-lactide)/ poly(ε-caprolactone) sponges for tissue engineering application

*Chengzhang Xu, Jun Young Cheong, Xiumei Mo, Valérie Jérôme, Ruth Freitag, Seema Agarwal, Reza Ghabiri*, Andreas Greiner**

C. Xu, Prof. A. Greiner, Prof. S. Agarwal
Macromolecular Chemistry and Bavarian Polymer Institute,
University of Bayreuth, Universitätsstrasse 30, 95440 Bayreuth, Germany
E-mail: greiner@uni-bayreuth.de

Dr. J. Y. Cheong
Bavarian Center for Battery Technology (BayBatt) and Department of Chemistry,
University of Bayreuth, Universitätsstrasse 30, 95440 Bayreuth, Germany

Prof. X. Mo
State Key Laboratory for Modification of Chemical Fibers and Polymer Materials,
College of Biological Science and Medical Engineering, Donghua University, Shanghai 201620, P.R. China

Dr. Valérie Jérôme, Prof. R. Freitag
Chair for Process Biotechnology,
University of Bayreuth, Universitätsstrasse 30, 95440 Bayreuth, Germany

Dr. R. Ghabiri
Department of Organic Chemistry and Polymer, Faculty of Chemistry,
Kharazmi University, 15719-14911 Tehran, Iran
E-mail: r.gharibi@khu.ac.ir

**Figure S1** is a photographic image of polymer fiber-based sponge (PFS) prepared in pure water without any additives. It could be seen that many big pores are on the sponge. The reason is that the short fibers could not disperse well without any surfactant.

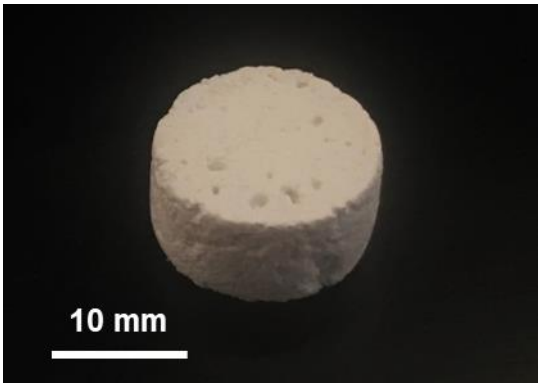


**Figure S1.** As-prepared PFS dispersed in pure water.

**Figure S2** and **S3** show the thermal behavior measured by differential scanning calorimetry (DSC) of poly(*L*-lactide (PLLA) and poly(*ε*-caprolactone) (PCL) used in this work. It can be seen from DSC results that the melting point of PCL is around 60 °C while the melting point of PLLA is around 150 °C. The annealing temperature of sponges (60 °C) was decided based on DSC results.

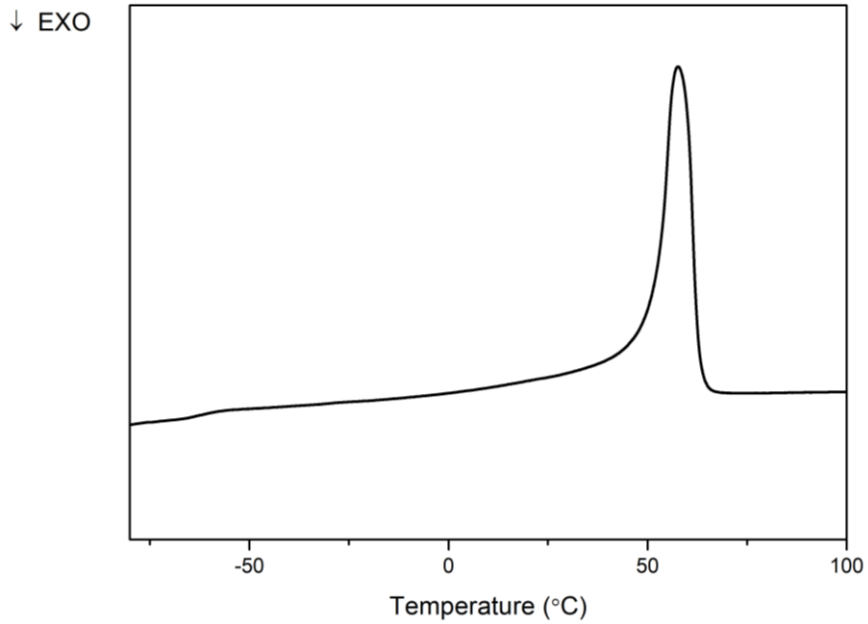


**Figure S2.** DSC measurement of PCL raw material (PCL Capa 6800).

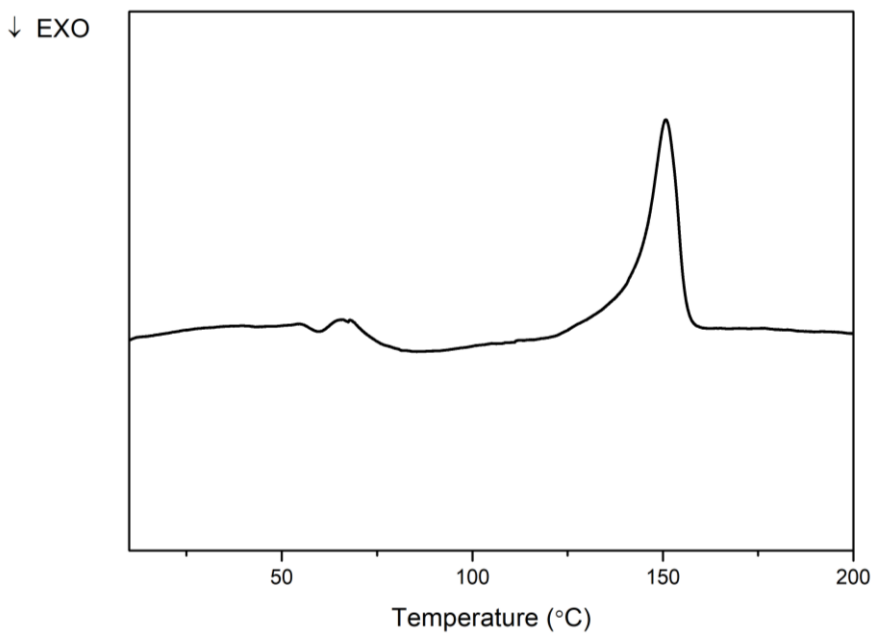


**Figure S3.** DSC measurement of PLLA raw material (PLLA 4043D).

**Figure S4** shows the statistical result of pore size distribution of PFS-3. The pore size was measured by ImageJ from the PFS cross-section images obtained by scanning electron microscope (SEM). 50 pores were chosen from the cross-section images of PFS-3, and the statistic calculation was done by OriginLab 8.1 software.

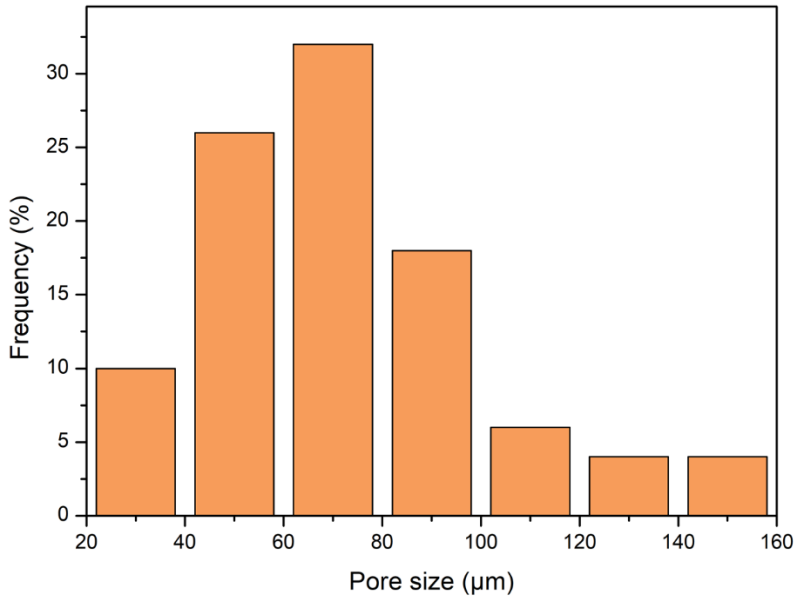


**Figure S4.** Range of pore size of PFS-3 measured by ImageJ.

Albeit PFS-1 is hydrophilic (**Figure S5**a), the shrinkage of PFS-1 was too high after annealing

and the shape is irregular, which is shown in Figure S5b (prepared by dispersing short fibers in 1 wt.% Tween 20).

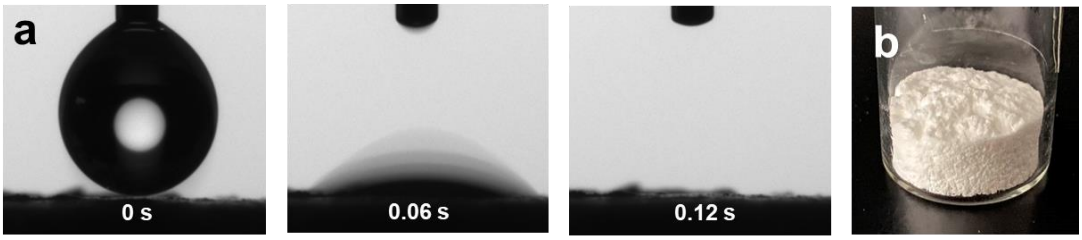


**Figure S5.** (a) Photographic image of contact angle measurements of PFS-1 and (b) PFS dispersed in 1 wt.% Tween 20 (PFS-1).

**Figure S6** and **Figure S7** show the molecular weight of PLLA and PCL used in this work.

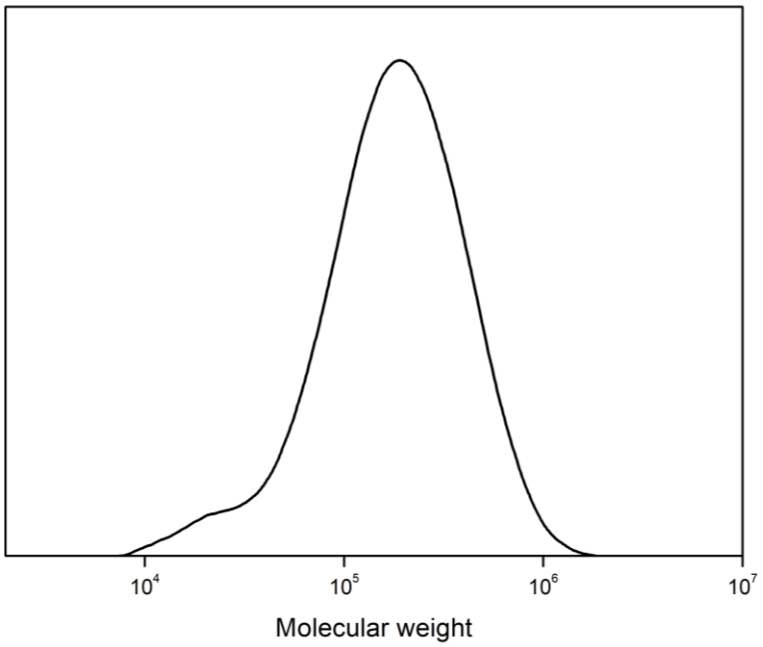


**Figure S6.** Molecular weight measurement of PLLA used in this work by GPC ($M_n$ = 116000, $M_w$ = 235000).

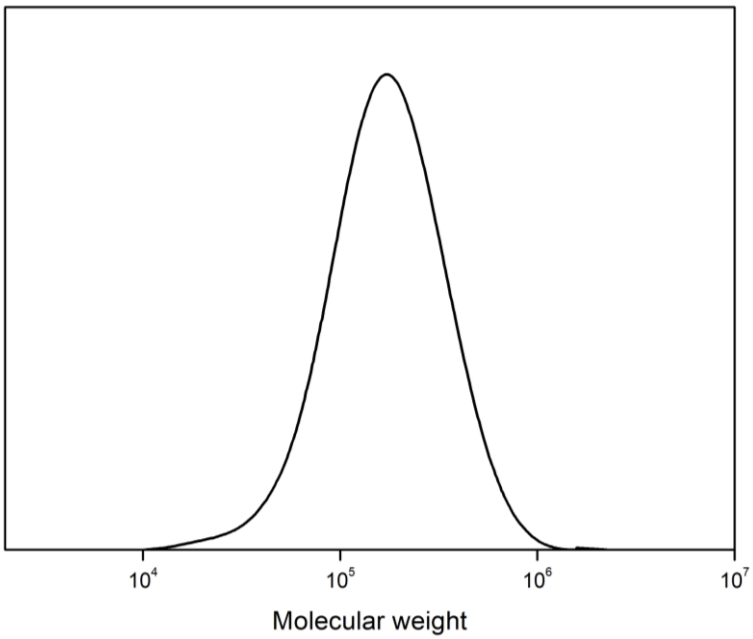


**Figure S7.** Molecular weight measurement of PCL used in this work by GPC (Mn = 134000, Mw = 211000).

**Table S1.** Details of PFSs used in this work.

| Sponge | PFS-4 | PFS-5 | PFS-6 | PFS-7 |
|---|---|---|---|---|
| density [mg $cm^{-3}$] | 23 | 31 | 65 | 104 |
| porosity[a)] [%] | 98 | 97 | 95 | 91 |

[a)] calculated based on **Equation S1** and **S2**

Calculation of porosity (P)

$$P=\left(1-\frac{\rho_{PFS}}{\rho_{bulk}}\right)\times 100\% \quad (1)$$

$$\rho_{PFS}=\frac{m}{V_{PFS}}=\frac{m}{\pi r^2 h} \quad (2)$$

The radius r and height h of PFS were measured by a spiral micrometer. The density of bulk polymer PLLA 4043D (1.24 g/$cm^3$) and PCL Capa 6800 (1.13g/$cm^3$) is kindly provided by the manufacturers. Taking PFS-3 as example, the porosity of 96% is calculated from an

average of triplicate based on the density of PFS-3 which is 54 ± 2 mg $cm^{-3}$ and the density of bulk PLLA/PCL mixture, which is 1.23 g $cm^{-3}$, taking a weight average of 90% PLLA (1.24 g $cm^{-3}$) and 10% PCL (1.13 g $cm^{-3}$)

## 3.2. Publication 2

BioMACROMOLECULES



pubs.acs.org/Biomac
Article

# Investigation of the Thermal Stability of Proteinase K for the Melt Processing of Poly(L-lactide)

Chengzhang Xu, Alexander Battig, Bernhard Schartel, Renée Siegel, Jürgen Senker, Inge von der Forst, Carlo Unverzagt, Seema Agarwal, Andreas Möglich,* and Andreas Greiner*

Cite This: *Biomacromolecules* 2022, 23, 4841−4850
Read Online



**ABSTRACT:** The enzymatic degradation of aliphatic polyesters offers unique opportunities for various use cases in materials science. Although evidently desirable, the implementation of enzymes in technical applications of polyesters is generally challenging due to the thermal lability of enzymes. To prospectively overcome this intrinsic limitation, we here explored the thermal stability of proteinase K at conditions applicable for polymer melt processing, given that this hydrolytic enzyme is well established for its ability to degrade poly(L-lactide) (PLLA). Using assorted spectroscopic methods and enzymatic assays, we investigated the effects of high temperatures on the structure and specific activity of proteinase K. Whereas in solution, irreversible unfolding occurred at temperatures above 75−80 °C, in the dry, bulk state, proteinase K withstood prolonged incubation at elevated temperatures. Unexpectedly little activity loss occurred during incubation at up to 130 °C, and intermediate levels of catalytic activity were preserved at up to 150 °C. The resistance of bulk proteinase K to thermal treatment was slightly enhanced by absorption into polyacrylamide (PAM) particles. Under these conditions, after 5 min at a temperature of 200 °C, which is required for the melt processing of PLLA, proteinase K was not completely denatured but retained around 2% enzymatic activity. Our findings reveal that the thermal processing of proteinase K in the dry state is principally feasible, but equally, they also identify needs and prospects for improvement. The experimental pipeline we establish for proteinase K analysis stands to benefit efforts directed to this end. More broadly, our work sheds light on enzymatically degradable polymers and the thermal processing of enzymes, which are of increasing economical and societal relevance.

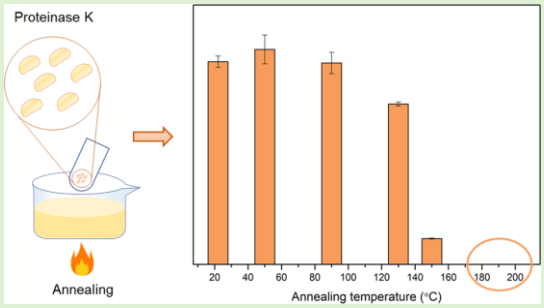


## INTRODUCTION

Degradable polymers have received considerable attention for applications in healthcare,[1] agriculture,[2] and packaging.[3] Recently, they attracted added significance in the context of microplastic particle reduction in the environment. It is anticipated that degradable polymers could help in the reduction of microplastic environmental debris originating from packaging applications,[3] which is, however, also under dispute.[4] Generally, polymers can be degraded by different routes, e.g., by light,[5] photooxidation,[6] chemical hydrolysis,[7] microbial action,[8] and enzymatic degradation.[8] Closely related to microbial degradation, enzymatic degradation is of particular interest as it can molecularly break macromolecular chains into bioavailable oligomers, monomers, or other degradation products, which can then be assimilated and mineralized by microbes. The fast molecular breakage of polymers by enzymes thus augurs new avenues for biotechnological approaches. However, enzymes often exhibit narrow substrate ranges and sensitivity to temperature and solvent conditions, which can limit their technical processing and application.

Well-known examples of enzymatically degradable polymers are aliphatic polyesters, with poly(L-lactide) (PLLA) receiving most attention due its technical relevance for numerous applications.[9] Whereas PLLA can be hydrolyzed by a variety of enzymes,[10] the serine protease proteinase K (PK) from the fungus *Tritirachium album*[11] has been found highly efficient in this regard.[10] Proteinase K hydrolyzes a broad range of proteins including recalcitrant ones such as keratin, from which its name derives. Its enzymatic activity can be routinely analyzed with chromogenic oligopeptide substrates, especially nitroanilides, which release a colored compound upon hydrolysis.[12−14] Besides peptides and proteins, proteinase K also degraded partially crystalline PLLA within a few days[10,15]

Received: August 15, 2022
Revised: September 14, 2022
Published: November 3, 2022





https://doi.org/10.1021/acs.biomac.2c01008
*Biomacromolecules* 2022, 23, 4841−4850

and amorphous PLLA films (thickness = 100 nm) within only a few hours.[16] By contrast, the non-enzymatic abiotic hydrolysis of PLLA in water takes several months.[17,18] The fast enzymatic degradation of PLLA by proteinase K is unique among proteases[19] and highly specific as poly(D-lactide) (PDLA) is not degraded by proteinase K.[15,20] Apparently, the catalytic triad (serine−histidine−aspartate) and the substrate-binding pocket of proteinase K, evolved to mediate the proteolysis of poly(L-amino acids),[19,21] accommodate very well the molecular structure of PLLA. The similar molecular shapes of L-lactic acid and L-alanine arguably explain the high reactivity of proteinase K toward PLLA.

In common with other enzymes, the efficient hydrolysis of substrates by proteinase K strictly depends on the preservation of its native structure and active-site geometry.[8] The molecular structure of proteinase K in aqueous media is affected by numerous factors and in turn profoundly governs the catalytic proficiency; even small structural changes can have detrimental effects on proteinase K activity. For instance, removal of $Ca^{2+}$ ions induces small rearrangements within proteinase K that entail significant activity reduction.[12,22] In aqueous medium, proteinase K shows the highest enzymatic activity toward protein substrates between 50 and 70 °C. At higher temperatures, the activity is successively lost due to the onset of irreversible protein denaturation.[14,22] Using differential scanning calorimetry, the midpoint for thermal denaturation of proteinase K was determined to be 77 °C in aqueous solution,[14] with complete unfolding and activity loss occurring above 80 °C.

Much less is known about the thermal stability of proteinase K in bulk, i.e., in the dry state, which is of major interest for the processing of proteinase K by polymer melt extrusion. Although polymer melt extrusion of enzymes has gained significant interest not least for pharmaceutical purposes,[23] pertinent applications are often limited by the thermal lability of enzymes. Several concepts were suggested for facilitating the processing of proteins in general.[21,24] In one recent study, proteinase K was mixed with a so-called random heterogeneous polymer and embedded in solvent-cast PLLA films.[25] Incubation of these films in aqueous solution led to their near-complete degradation within 7 days at ambient temperature. Another study proposed the absorption of proteinase K inside (or on) polyacrylamide (PAM) microparticles.[26] Incorporation of these particles in melt-extruded PLLA yielded films that underwent partial weight loss during extended incubation in aqueous solution. It is hard to rationalize how proteinase K can withstand exposition to temperatures of 200 °C for several minutes, required for PLLA extrusion, without complete loss of activity due to enzyme degradation. Alternatively, the observed weight loss of the PLLA film might be due to the non-enzymatic hydrolytic decomposition catalyzed by PK degradation products. Therefore, it is unclear if the PLLA films degraded because of enzymatic degradation or non-enzymatic actions. To address this pivotal question, incited by the abovementioned work, a reliable protocol is required to study the activity of melt-processed proteinase K and to understand the PLLA degradation mechanism.

To reliably gauge the properties of proteinase K and to assess its potential for polymer melt processing with degradable polymers like PLLA, the precise monitoring of enzyme integrity and activity upon thermal treatment is required. Only with this understanding, measures can be developed, and concepts can be verified for this promising approach. Most importantly, the presence and extent of enzymatic activity must be verified since degradation products of the enzyme itself could promote hydrolytic degradation and thus mimic enzymatic degradation.

Against this backdrop, we here investigated the thermal stability of proteinase K in the bulk state in detail. Potential changes in proteinase K integrity after thermal treatment in bulk were assessed by different spectroscopic techniques and thermal gravimetric analysis. In parallel, the enzymatic activity of native and thermally treated proteinase K samples was quantified using nitroanilide peptide substrates and was assessed qualitatively by the degradation of electrospun PLLA and PDLA nonwovens. Using this setup, we also investigated the thermal stability of proteinase K absorbed to PAM particles. These measurements revealed that in combination with PAM particles, but not without, residual proteinase K activity was retained after 5 min exposure to 200 °C. While the remaining activity is currently too low to promote the rapid degradation of PLLA materials, our studies pinpoint a viable strategy for the melt processing of proteinase K and, by inference, other enzymes. The protocols we establish for the precise and quantitative analysis of enzyme integrity and activity upon processing will help the design and implementation of measures to overcome the inherent thermal lability of proteinase K. Doing so is of fundamental importance as it would enable the melt processing of proteinase K and other enzymes with polymers.

## MATERIAL AND METHODS

**Materials.** Native proteinase K (lyophilized powder, from *T. album*, 28.9 kDa, GeneOn, Germany, stored at −20 °C in a deep freezer), *N*-succinyl-L-phenylalanine-*p*-nitroanilide (*N*-Suc-Phe-pNA), *N*-succinyl-alanine-alanine-proline-leucine-*p*-nitroanilide (*N*-Suc-Ala-Ala-Pro-Leu-pNA), alanine-alanine-proline-phenylalanine-chloromethyl ketone (MeOSuc-Ala-Ala-Pro-Phe-CMK), and tin(II) 2-ethylhexanoate were obtained from Sigma-Aldrich, Germany. *N*-Succinyl-phenylalanine-alanine-alanine-phenylalanine-*p*-nitroanilide (*N*-Suc-Phe-Ala-Ala-Phe-pNA) was obtained from Bachem, Germany. 4-Nitrophenyl acetate (98%) was obtained from Thermo Fisher, Germany. 1 M Tris buffer solution (pH 9.0) was obtained from Abcr, Germany. D-Lactide was purchased from Haihang Industry Co., Ltd., China. Poly(L-lactide) (PLLA) was purchased from Ingeo Biopolymer PLA 4043D, Nature-Works LLC. Tritylchloride−polystyrene (TCP, 1.04 mmol/g, 200−400 mesh, 1% divinylbenzene (DV)) resin was purchased from PepChem, Germany. Fmoc-D-Ala-OH (≥99%) and Fmoc-D-Pro-OH (≥ 99%) were purchased from Sigma-Aldrich, Germany. Fmoc-D-Leu-OH (≥99%) and *O*-(1*H*-6-chlorobenzotriazole-1-yl)-1,1,3,3-tetramethyluronium hexafluorphosphate (HCTU, ≥99%) were obtained from Iris Biotech, Germany. *N*,*N*-diisopropylethylamine (DIPEA, 99.5%), piperidine (≥ 99.5%), trifluoroacetic acid (TFA, ≥99.9%), and dimethylformamide (DMF, ≥99.8%) were purchased from Carl Roth, Germany. Succinic anhydride and 1,4-phenylenediamine were purchased from Carbolution Chemicals, Germany. Potassium peroxomonosulfate (oxone, ≥4.5% active oxygen) was purchased from Acros, Belgium. High-pressure liquid chromatography−mass spectroscopy (HPLC-MS)-grade acetonitrile and formic acid (≥99%) were obtained from VWR Chemicals, Germany. All of the above compounds were used as received. The solvents dichloromethane (DCM) and methanol (MeOH) were of technical grade and purified by distillation over phosphorus pentoxide or magnesium before use. All of the above compounds were used as received. Tris buffer was diluted into a concentration of 50 mM, and the pH was adjusted to 8.6 by hydrochloric acid. Micro Bio-Spin 30 columns were obtained from Bio-Rad, Germany.

**Synthesis of *N*-Suc-Ala-Ala-Pro-Leu-pNA (all-D).** Tritylchloride−polystyrene (TCP) resin (1 g, 1.04 mmol/g, 1 eq) was swollen in


https://doi.org/10.1021/acs.biomac.2c01008
*Biomacromolecules* 2022, 23, 4841−4850

8 mL of DCM and subsequently in 8 mL of dimethylformamide (DMF) for 20 min. A solution of 1,4-phenylenediamine (0.890 g, 8.32 mmol, 8 eq) and *N*,*N*-diisopropylethylamine (DIPEA) (1.45 mL, 8.32 mmol, 8 eq) in 8 mL of DMF was added to the swollen TCP resin and shaken at room temperature for 16 h.[27] The resin was washed with 8 mL of DMF, and the unreacted sites were capped by shaking with 6 mL of DMF/MeOH/DIPEA (17:2:1) at room temperature for 10 min (3 repetitions). The resin loaded with 1,4-phenylenediamine was washed with 6 mL of DMF for 1 min (5 repetitions) and then 6 mL of DCM for 1 min (10 repetitions). The Fmoc solid-phase peptide synthesis was carried out on a Tribute peptide synthesizer (PTI) using 1.22 g of resin. The Fmoc-D-amino acids (5 eq, 0.5 M) were coupled for 45 min at room temperature with HCTU (4.8 eq) and DIPEA (6 eq) in DMF. The Fmoc groups were cleaved using a solution of 20% piperidine in DMF, and deprotection was monitored by UV absorption. After the final Fmoc deprotection, the resin was washed with 6 mL of DCM. A solution of 341 mg of succinic anhydride (3.41 mmol, 4 eq) in 7 mL of DCM/DMF (9:1) was added to the resin and shaken for 15 min at room temperature.[28] The succinyl peptide *p*-aminoanilide was cleaved from the TCP resin with 5 mL of trifluoroacetic acid (TFA) for 1 h, dried in vacuo, and washed three times with 10 mL of cold diethylether (−24 °C). The final oxidation of the peptide *p*-aminoanilide (66.3 mg, 0.118 mmol) to the peptide *p*-nitroanilide was performed by adding oxone (436 mg, 0.709 mmol, 6 eq) in 3.3 mL of $H_2O$ and shaking for 16 h.[27]

**Polymerization of PDLA and Electrospinning of PDLA and PLLA Nonwovens.** Polarimetry measurements showed that the specific rotation of D-lactide used for polymerization is $[\alpha]_D^{20} = -288.8 \pm 0.2°$ in toluene. The monomer D-lactide (14.4 g) was dried in a pre-dried Schlenk flask under vacuum for 3 h. Afterward, the flask was heated by oil bath until it reached 185 °C. After the monomer melted, initiator 1-decanol and catalyst tin(II) 2-ethylhexanoate ($Sn(Oct)_2$) were added into the molten monomer with molar ratios of monomer-to-initiator at 1000 and monomer-to-catalyst at 2000. The reaction was run for 30 min under an argon atmosphere. The molecular weight of the PDLA was characterized by gel permeation chromatography (GPC) equipped with a Styrene-DV (SDV) precolumn (particle size 5 $\mu$m; PSS Mainz) and an SDV linear XL column (particle size 5 $\mu$m, PSS Mainz). The sample was dissolved in $CHCl_3$, and a flow rate of 0.5 mL/min was used for the measurements. The molecular weight of PDLA was 95.000 according to GPC analysis versus polystyrene standard (PSS Mainz). The PDLA and PLLA were used for electrospinning following a previous recipe.[29] The electrospun nonwoven was collected on a rotating plate collector for 30 min. The fiber diameter of electrospun PLLA fibers is in the range of 800−1000 nm.

**Immobilization of Proteinase K (According to a Previously Published Procedure).**[26] Proteinase K was dissolved at 0 °C in Tris buffer (50 mM, pH 8.6) with a concentration of 1 mg/mL. Micro Bio-Spin columns (2 cm working bed height and 0.8 mL bed volume) containing 70 mg polyacrylamide (PAM) (Figure S1) particles were used for encapsulation of proteinase K. The Tris buffer inside the column was first removed by centrifugation for 2 min at 5000 rpm. Tris buffer (0.5 mL, 50 mM, pH 8.6) was added inside the column and removed by centrifugation for 2 min at 5000 rpm. This step was repeated two more times in order to replace the remaining buffer inside the column. Then, 0.5 mL of 1 mg/mL proteinase K solution was added into the column and centrifuged at 3500 rpm for 2 min. After centrifugation, the filtrate was added back to the Bio-Spin column and centrifuged again at 3500 rpm for 2 min. This step was repeated for a total of five times. After centrifugation, the column was frozen at −26 °C, and the solution was removed by freeze-drying (−70 °C, 0.1 mbar) for 48 h. The proteinase K-immobilized PAM particle is named IM-PK. IM-PK was stored at −26 °C prior to use. The immobilization efficiency, which was 2 mg per 1 g PAM particles, was determined by absorption spectroscopy. The absorbance at 280 nm was used for analysis of the immobilization efficiency by comparison of the proteinase K concentration in Tris buffer before and after treatment of the PAM particles. The absorbance was determined using an Agilent 8453 diode-array spectrophotometer. The following equation is used to calculation the immobilization ratio *I*:[26]

$$I = \frac{(C_0 - C) \times V}{W}$$

where $C_0$ is the concentration of PK before immobilization, $C$ is the concentration of PK after immobilization, $V$ is the volume of PK solution, and $W$ is the weight of PAM particles used for immobilization.

**Annealing of Proteinase K.** Ten milligrams of proteinase K powder was heated in a 10 mL preheated glass vial with open lid in a water bath (50−90 °C) and in an oil bath (130−200 °C). The annealing was done for 5 min at the following temperatures: 22, 50, 90, 130, 150, 180, and 200 °C (the setup of annealing is shown in Figure S2). After annealing, the vials were transferred immediately into an ice bath at 0 °C. This procedure results in a cooling rate of less than 200 °C/min (from 200 to 0 °C). Native proteinase K (kept at −20 °C) and 22 °C 5 min incubated proteinase K powder was also used for comparison. The IM-PK was annealed by the same method but only at 200 °C.

**Circular Dichroism Spectroscopy.** Native proteinase K and annealed proteinase K were dissolved at a concentration of 15 mg/mL in phosphate-buffered saline (PBS, pH 7.4). For subsequent measurements, the solutions were diluted in PBS to an absorbance at 210 nm of between 0.5 and 0.9 in a 1 mm cuvette. Circular dichroism spectra were then acquired on a CD spectrometer (J-715, Jasco Corp.) within the range of 190−250 nm with a scan speed of 100 nm/min. The unfolding of proteinase K was monitored by the CD signal at 222 nm. To this end, the temperature was increased from 15 to 90 °C at a speed of 0.5 °C/min.

**PK Enzymatic Activity Assay.** Proteinase K activity was determined by an absorbance measurement assay using as substrates 4-nitrophenyl acetate, *N*-succinyl-phenylalanine-*p*-nitroanilide (N-Suc-Phe-pNA), *N*-succinyl-alanine-alanine-proline-leucine-*p*-nitroanilide (*N*-Suc-Ala-Ala-Pro-Leu-pNA), and *N*-succinyl-phenylalanine-alanine-alanine-phenylalanine-*p*-nitroanilide (*N*-Suc-Phe-Ala-Ala-Phe-pNA).[14] All the above-listed substrates are commercial and with L-configuration. The self-synthesized *N*-Suc-Ala-Ala-Pro-Leu-pNA with D-configuration was used for the activity assay of IM-PK. The activity assay was performed in 96-well clear microtiter plates by dissolving 0.005 mg of native or annealed proteinase K in 1 mL of Tris buffer (50 mM tris(hydroxymethyl)aminomethane/HCl (pH 8.6) and 1 mM $Ca^{2+}$), and the concentration of proteinase K assay is close to the concentration used in the publication of Numata et al.;[30] for native and annealed IM-PK, 10 mg of either native or annealed particles were dispersed in 1 mL of Tris buffer. The assay of IM-PK was done by *N*-Suc-Ala-Ala-Pro-Leu-pNA with both L- and D-configurations. The assay was done at 25 °C, and absorbance at 410 nm was monitored over time. Specific proteinase K activity was determined according to the equation below:

$$\text{specific activity} = \Delta A/(\varepsilon \times h \times \Delta t \times C)$$

in which $\Delta A$ represents the difference of absorbance at 410 nm relative to time zero, $\varepsilon$ is the molar extinction coefficient of *p*-nitroaniline at a wavelength of 410 nm ($\varepsilon$ = 8800 $M^{-1}$ $cm^{-1}$), $h$ is the thickness of the sample solution, $\Delta t$ is the elapsed time, and $C$ is the concentration of proteinase K in the assay solution. The initial, linear region of the absorbance signal was fitted linearly to determine the slope $\Delta A/\Delta t$. Proteinase K activity is reported as enzymatic unit U, where 1 U corresponds to the hydrolysis of 1 $\mu$mol of substrate per minute.

To assess the influence of proteinase K inhibitors, 10 mg of annealed proteinase K-immobilized PAM particles were first suspended in 0.95 mL of Tris buffer. Before doing the activity assay, 0.05 mL (0.5 mg/mL) of the proteinase K-specific inhibitor, methoxysuccinyl-alanine-alanine-proline-phenylalanine-chloromethyl ketone (MeOSuc-Ala-Ala-Pro-Phe-CMK) in Tris buffer was added, resulting in final concentrations of 10 mg/mL IM-PK and 0.005 mg/


https://doi.org/10.1021/acs.biomac.2c01008
Biomacromolecules 2022, 23, 4841−4850

mL inhibitor. The suspension was then incubated at 22 °C for 60 min before conducting the activity assay as described above.

**Degradation of PDLA and PLLA by IM-PK.** Round pieces of the sample were cut at a diameter of 10 mm from the nonwoven and used for degradation in 10 mg/mL by IM-PK suspension, as listed below: (1) PDLA nonwoven in native IM-PK suspension, (2) PDLA nonwoven in annealed IM-PK suspension, (3) PLLA nonwoven in native IM-PK suspension, and (4) PLLA nonwoven in annealed IM-PK suspension. Each sample was in 2 mL of suspension. All the samples were incubated in a water bath at 37 °C. The appearance of the samples was observed visually after 24 h to qualitatively determine the degradation of the PLA nonwoven. Once the nonwoven was obviously disintegrated completely, the sample was rated as degraded.

**Solid-State Nuclear Magnetic Resonance.** $^{1}$H solid-state NMR spectroscopic experiments were performed on a Bruker Avance III HD spectrometer operating at an external magnetic field, $B_0$, of 14.1 T ($\nu_0$ = 600.1 MHz) using a 1.3 mm HFX double resonance probe. The samples were spun at 62.5 kHz, and the spectra were obtained after a 90° pulse of 1.3 $\mu$s using a recycle delay of 10 s. $^{13}$C and $^{15}$N solid-state NMR spectra were acquired on a Bruker Avance III HD spectrometer operating at a $B_0$ field of 9.4 T ($\nu_0(^{13}C)$ = 100.6 MHz; $\nu_0(^{15}N)$ = 40.6 MHz). The MAS NMR spectra were obtained with ramped cross-polarization (CP) experiments, where the $^{13}$C/$^{15}$N nutation frequency was set to 50/45 kHz. The $^{1}$H nutation frequency ($\nu_{nut}$) was varied linearly from 50 to 100%, on average matching the Hartmann−Hahn conditions. The contact time was adjusted to 1.0 ms/5.0 ms ($^{13}$C/$^{15}$N). The samples were spun at 12.5/10.0 kHz ($^{13}$C/$^{15}$N) in a 3.2 mm HXY MAS triple-resonance probe. Proton broadband decoupling using a spinal-64 sequence with $\nu_{nut}$ = 70 kHz was applied during acquisition of the FID. The $^{1}$H and $^{13}$C spectra were referenced with respect to tetramethylsilane (TMS) using the secondary standard adamantane, and the $^{15}$N spectra were referenced to $CH_3NO_2$ using glycine.

**Thermogravimetric Analysis−Fourier Transfer Infrared Spectroscopy.** Thermogravimetric analysis was performed using a Netzsch Instruments (Selb, Germany) TG 209 F1 Iris. Isothermal measurements of proteinase K sample (10 mg) were achieved via heating at a high rate (100 °C/min) and then maintaining $T$ = 200 °C for at least $t$ = 20 min. The uncertainty of the results is always below < ±1 °C and ±1 wt %.

Evolved gas analysis measurements were conducted using a Bruker Optics (Ettlingen, Germany) Tensor27 Fourier transform infrared spectrometer. Effluents from thermogravimetric measurements passed through a preheated ($T$ = 270 °C) transfer line ($L$ = 1 m) into the FTIR gas cell.

## RESULTS AND DISCUSSION

**Annealing of Proteinase K in the Dry State.** To gauge the principal compatibility of proteinase K with thermal processing of PLLA, in particular by melt extrusion, we characterized how elevated temperatures impact enzyme integrity and activity. Notably, a large body of work reports on the properties, activity, and thermal stability of proteinase K in solution. By contrast, only sparse data are available on how temperature exposure alters the integrity and activity of proteinase K in the bulk phase. It is, however, precisely these aspects that are relevant for the envisioned proteinase K use cases in PLLA processing. We hence assessed the response of proteinase K, purchased as freeze-dried powder with an average particle size of about 100 $\mu$m (Figure S3a), to thermal treatment in the bulk, dry state (note that the observed size corresponds to proteinase K clumps and does not reflect the size of individual enzyme molecules). To this end, proteinase K powder was placed in 10 mL vials preheated in a water or oil bath at temperatures between 22 and 200 °C and annealed for between 1 and 5 min. The maximum temperature of 200 °C and time of 5 min resemble the conditions relevant for PLLA processing. Upon rapid cooling, we investigated the annealed proteinase K samples spectroscopically and compared them to non-annealed, native proteinase K.

After undergoing annealing at 200 °C for 5 min, proteinase K powder particles shrank slightly (Figure S3b). The infrared (IR) spectrum of annealed proteinase K (Figure S4) exhibited signals characteristic for proteins[31] and resembled that of native, non-annealed proteinase K. These observations indicate that the thermal treatment did not cause the complete decomposition of proteinase K. To glean additional insight, we employed multinuclear magic-angle-spinning (MAS) solid-state NMR spectroscopy. The $^{1}$H, $^{13}$C, and $^{15}$N MAS NMR spectra of the native and annealed samples are remarkably similar with only subtle differences (Figure 1 and Figures S5 and S6). This suggests that the primary structure of proteinase K is largely retained despite the harsh temperature treatment. Two trends emerge from the NMR data. First, the $^{1}$H, $^{13}$C, and $^{15}$N NMR signals of the annealed sample are significantly broadened compared to native proteinase K. Second, a peak shoulder at 8−8.5 ppm vanished in the $^{1}$H MAS NMR spectra of the annealed sample (Figure 1).Together with a high-field shift of the NH resonances, this change suggests a weaker hydrogen-bond network for the annealed sample and likely reflects partial denaturation upon annealing and loss of secondary and tertiary structure.[32−35] The additional decrease of the small shoulder at about 4.8 ppm in the $^{1}$H spectrum for the native sample is typical for the removal of residual adsorbed water upon annealing. The significant broadening of the $^{1}$H, $^{13}$C, and $^{15}$N NMR peaks in the annealed sample relative to the native one is most likely caused by increased chemical shift dispersion induced by the partial denaturation of the protein. In the $^{13}$C cross-polarization MAS spectrum (Figure S5), the broadening is most pronounced within the region between 50 and 70 ppm, corresponding to the aliphatic $C_\alpha$ groups.[33,36] These resonances are strongly affected by the denaturation since their chemical shifts can vary by 2−3 ppm depending on whether their amide groups engage in hydrogen bonds or not. Taken together, the solid-state NMR data reveal that proteinase K undergoes partial denaturation upon thermal treatment. Additionally, the observed spectral changes may stem from covalent changes induced in proteinase K by thermal treatment.

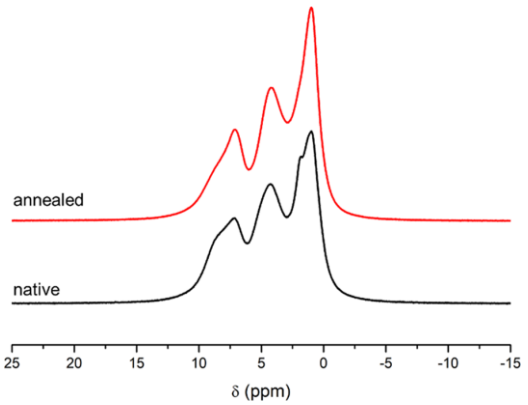


**Figure 1.** $^{1}$H-NMR MAS spectra of native (black) and annealed proteinase K (red, annealed at 200 °C for 5 min).


https://doi.org/10.1021/acs.biomac.2c01008
Biomacromolecules 2022, 23, 4841−4850

We therefore further characterized the response of proteinase K to high temperatures in the bulk phase by thermogravimetric analysis coupled to Fourier transform IR spectroscopy (TGA-FTIR). The isothermal mass-loss curve from TGA measurements on bulk proteinase K under air atmosphere are shown in Figure 2. During the initial heating to

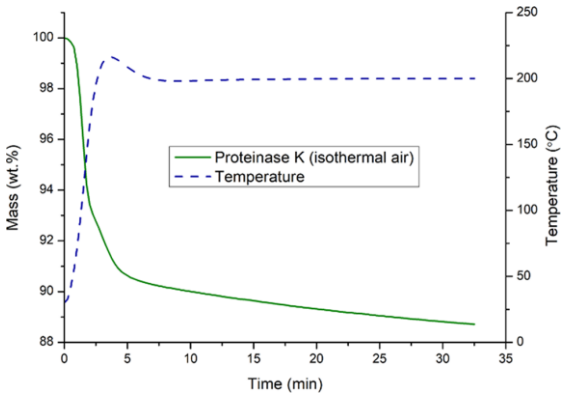


**Figure 2.** Mass of the proteinase K sample (green solid line) and temperature (blue dashed line) over time from isothermal gravimetric measurements under air flow.

200 °C within the first 6 min of the experiment, a mass loss of nearly 10% occurred. Two distinct regimes can be identified, the first between 0 and 2 min, entailing a ∼7% mass reduction, and the second between 2 and 6 min with an additional mass loss of 2%. The FTIR analyses (Figure 3) of the effluents

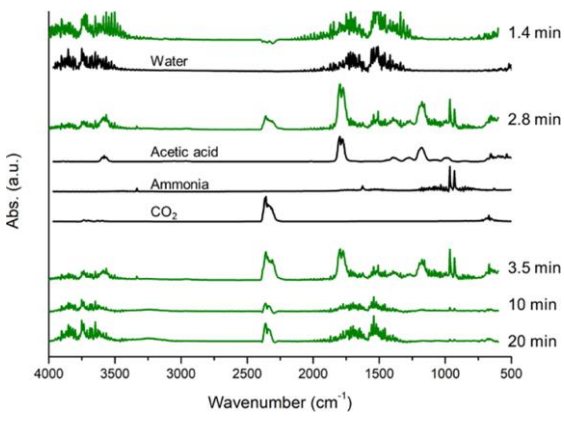


**Figure 3.** FTIR spectra of the effluents at different time points in isothermal gravimetric measurements on proteinase K under air (green lines). Reference spectra of small molecules (water, acetic acid, ammonia, and $CO_2$) are shown for comparison as black lines.

identified the decomposition products as water in the first regime and a mixture of water, ammonia, carbon dioxide, and acetic acid within the second phase. The initial release of water is arguably mainly owed to the dehydration of the hygroscopic proteinase K powder used in the experiments.[37] The subsequent detection of ammonia, carbon dioxide, and acetic acid reflects the deamidation and decarboxylation of amide side chains of the protein based on comparison to literature data.[38] In proteinase K, amines are found in lysine (Lys, K), amides in asparagine (Asn, N) and glutamine (Gln, Q), guanidino groups in arginine (Arg, R), and imidazole groups in histidine (His, H). These amino acids combined make up about 17.5% of the residues of proteinase K.[39] Thus, the presence of ammonia in the effluents (Figure 3) points to the cleavage of these residues, accounting for the mass loss in the regime between 2 and 6 min in Figure 2. Successive isothermal incubation at 200 °C resulted in a gradual mass loss and a remaining mass of ∼89% of the starting material after 30 min. In agreement with the NMR data, the TGA-FTIR experiments show that proteinase K slowly decays when exposed to temperatures above around 150 °C. At even higher temperatures, proteinase K fully degraded with the main decomposition step occurring at 304 °C in air and 322 °C in nitrogen atmosphere. (Figure S7).

The above experiments indicated partial and gradual decomposition of proteinase K when incubated in the dry state at temperatures above 150 °C. We next addressed the consequences of these covalent changes on the structure of proteinase K in solution. Notably, enzymes must generally fold to their native three-dimensional structure to exert their catalytic activity. To assess intact protein folding, we next recorded far-UV circular dichroism (CD) spectra on the native and annealed samples solubilized in PBS buffer (Figure 4).

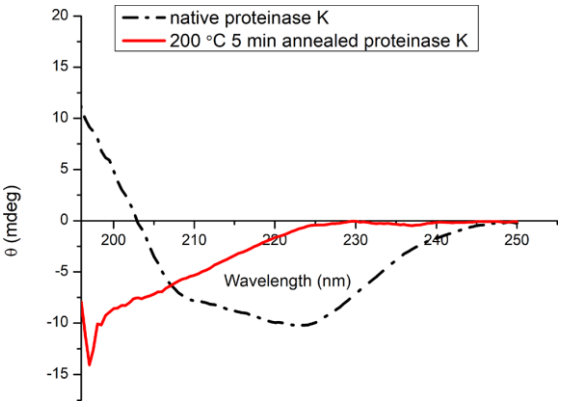


**Figure 4.** Far-UV circular dichroism spectra of native (black) and annealed proteinase K (red, 200 °C for 5 min).

Whereas the native proteinase K readily and completely dissolved, the thermally treated sample did so only partially and contained an insoluble fraction of 44% of the total weight (Figure S8). Native proteinase K exhibited a CD spectrum characteristic of a folded protein with mixed $\alpha/\beta$ fold and consistent with its three-dimensional structure.[22] By contrast, the annealed sample displayed an utterly different CD spectrum of an unfolded protein, as indicated by the loss of the peaks at around 208 and 222 nm and negative ellipticity below 200 nm. Evidently, the exposure to high temperatures incurred the unfolding of proteinase K, likely connected to the partial decomposition evidenced above. As an ensemble method, circular dichroism spectroscopy however reports on the average properties of the sample molecules. The data thus cannot rule out that a minor fraction of proteinase K retained native structure and function. For reference, we also examined the thermal unfolding of proteinase K in solution by monitoring by the CD signal at 222 nm while increasing the


https://doi.org/10.1021/acs.biomac.2c01008
Biomacromolecules 2022, 23, 4841−4850

temperature from 15 to 90 °C at a rate of 0.5 °C/min. The fit to the experimental data yielded a midpoint of unfolding of 72.6 ± 0.1 °C (Figure S9). The thermal unfolding curve was fitted to a two-state unfolding transition using the Fit-o-mat software.[40,41]

**Activity Analysis of Native and Annealed Proteinase K.** We therefore assessed next the enzymatic activity of proteinase K before and after annealing. To achieve sufficient sensitivity and facilitate the experiments, we opted for *para*-nitroanilide (pNA)-containing oligopeptides as substrates. To this end, we first tested different nitroanilide peptide sequences that were reported in the literature as substrates for proteinase K and other proteases.[14,42−44] Whereas *N*-succinyl-Phe-pNA and *N*-succinyl-Phe-Ala-Ala-Phe-pNA exhibited only sluggish enzymatic degradation (Figures S10 and S11), proteinase K rapidly hydrolyzed *N*-succinyl-Ala-Ala-Pro-Leu-pNA (Figure S12). Of particular advantage, the reaction progress can be continuously monitored via the absorbance of the hydrolysis product *para*-nitroaniline. We also tested the reactivity of proteinase K toward 4-nitrophenyl acetate, which contains an ester bond to the nitrobenzyl moiety rather than an amide bond and thus more closely resembles the scissile link in PLLA. Although proteinase K could catalyze the hydrolysis, the compound was inherently prone to spontaneous hydrolysis in aqueous solution, thus precluding its use in these experiments (Figure S13). All subsequent activity assays were hence conducted with *N*-succinyl-Ala-Ala-Pro-Leu-pNA as substrate at 25 °C, at a proteinase K concentration of 5 $\mu$g mL$^{-1}$ and in reaction buffer (50 mM Tris/HCl (pH 8.6) and 1 mM $CaCl_2$). We initially recorded reactions for native proteinase K at different substrate concentrations to determine Michaelis−Menten parameters (Figure S14). The initial reaction velocity $v_0$ increased hyperbolically with substrate concentration and yielded a Michaelis constant $K_m$ of (1.29 ± 0.02) mM.[45] While relatively weak, the substrate affinity agrees with previous reports.[43] From the initial kinetics, we calculated a specific activity of around (6.5 ± 0.2) U mg$^{-1}$ for native proteinase K, where one enzymatic activity unit is defined as the hydrolysis of 1 $\mu$mol substrate per minute. We then assessed the enzymatic activity of annealed proteinase K samples at a substrate concentration of 200 $\mu$M. Strikingly, annealing of bulk-state proteinase K at temperatures up to 130 °C incurred little loss in catalytic proficiency and yielded nearly unchanged specific activities (Table 1, Figure 5, and Figures S15−S19; recorded curves shown in Figure S20). By contrast, when annealed at 150 °C, proteinase K was severely impaired but still exhibited a specific activity of (0.85 ± 0.02) U mg$^{-1}$, i.e., more than 10% that of the native enzyme. At even higher temperatures, the annealed proteinase K samples were only partially soluble. Moreover, the proteinase K samples treated at 180 and 200 °C did not display any catalytic turnover, indicating complete and irreversible destruction of the enzyme. That notwithstanding, the activity measurements pinpointed a remarkable thermal stability of proteinase K in the dry state. These observations contrast with the properties in aqueous solution where proteinase K irreversibly unfolded with a midpoint of 72.6 ± 0.1 °C, as seen above.

**Table 1. Specific Activity of Proteinase K after 5 Min of Annealing in the Dry State at Different Temperatures**

| annealing temperature (°C) | specific activity[a] (U mg$^{-1}$) |
|---|---|
| native | 6.5 ± 0.2 |
| 22 | 6.6 ± 0.2 |
| 50 | 7.0 ± 0.5 |
| 90 | 6.6 ± 0.4 |
| 130 | 5.3 ± 0.1 |
| 150 | 0.85 ± 0.02 |
| 180 | 0 |
| 200 | 0 |

[a]Assays were done with 200 $\mu$M *N*-Suc-Ala-Ala-Pro-Leu-pNA in Tris buffer (pH 8.6) at 25 °C. Activities were determined by evaluating the absorbance signal at 410 nm within the initial linear regime. All experiments were done in triplicate.

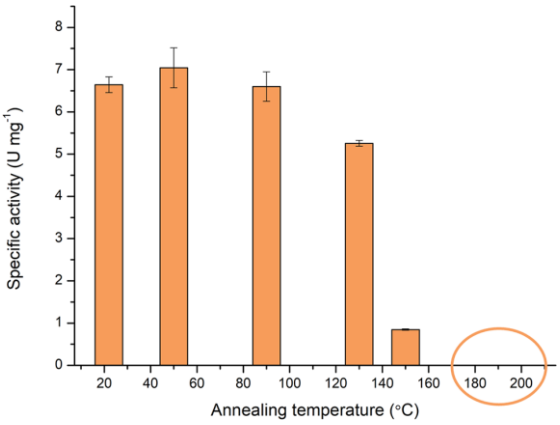


**Figure 5.** Specific activity of proteinase K after 5 min of annealing at different temperatures. Assays were done with 200 $\mu$M *N*-Suc-Ala-Ala-Pro-Leu-pNA substrate in Tris buffer (pH 8.6) at 25 °C. Activities were determined by evaluating the initial linear absorbance increase at 410 nm in triplicate. The orange circle on the *x* axis shows that the activity after annealing at 180 and 200 °C is 0.

**Thermal Stabilization of Proteinase K by PAM Microparticles.** The above experiments revealed pronounced resistance of proteinase K to thermal treatment when in the dry, bulk state. Even so, the catalytic activity of proteinase K was entirely lost at 180 and 200 °C. Unless the thermal stability can be further enhanced, the processing of proteinase K at conditions relevant for manufacturing of PLLA plastics is thus not possible. As PLLA materials are routinely processed by melt extrusion at around 200 °C, proteinase K would need to withstand such conditions for several minutes. Recent work indicated that embedding proteinase K in PAM particles may bestow added thermal stability.[26] However, as the specific activity of proteinase K was not assessed, it remained unclear as to what extent the catalytic proficiency could be maintained. Using the experimental setup we established above, we hence investigated a potential stabilization of proteinase K by absorption in PAM microparticles according to the previously published procedure.[26] To this end, proteinase K solution was added to PAM particles, followed by filtration and freeze-drying. Based on evaluating the amount of proteinase K remaining in the filtrate, we estimate that around 2 mg proteinase K was absorbed per gram of PAM particle. The proteinase K-absorbed PAM particles are referred to as IM-PK particles (immobilized proteinase K) hereon.

The IM-PK particles were annealed in preheated glass vials at 200 °C for 5 min. As a control, IM-PK particles were incubated at 22 °C for 5 min. We note that while this approach


https://doi.org/10.1021/acs.biomac.2c01008
Biomacromolecules 2022, 23, 4841−4850

mimics the conditions during PLLA processing, it neglects the mechanical stress during melt extrusion and the desorption of proteinase K in a PLLA matrix. After annealing, the thermally treated and control IM-PK particles were dispersed in buffer and assessed for activity as above (Figure 6).

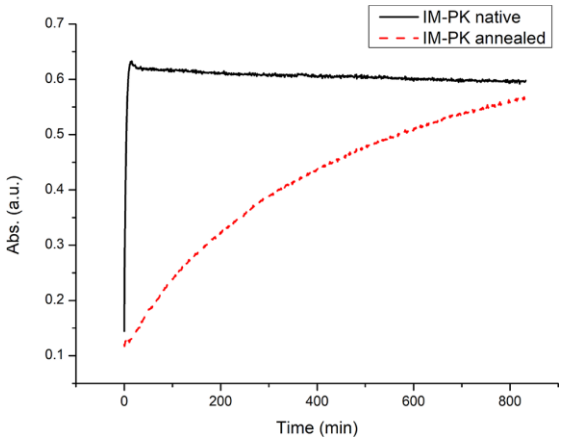


**Figure 6.** Catalytic activity of IM-PK particles. A suspension of 10 mg $mL^{-1}$ IM-PK particles, either annealed at 200 °C for 5 min (red) or not (black), was incubated with 200 $\mu$M *N*-Suc-Ala-Ala-Pro-Leu-pNA in Tris buffer (pH 8.6) at 25 °C. The reaction was followed by absorbance at 410 nm. Based on the amount of PK embedded in the PAM particles, we estimated specific activities of 2.4 U $mg^{-1}$ of enzyme for native IM-PK and 0.05 U $mg^{-1}$ of enzyme for annealed IM-PK.

The non-annealed control IM-PK particles showed clear-cut activity as indicated by an absorbance increase due to hydrolysis of the nitroanilide peptide substrate. Based on the amount of proteinase K embedded in the IM-PK samples, we estimate that the observed kinetics correspond to a specific activity of 2.4 U $mg^{-1}$ of proteinase K, i.e., similar levels as non-embedded PK. Strikingly, the IM-PK particles that were exposed to 200 °C also exhibited some turnover of the peptide substrate, albeit at much reduced velocity and an apparent specific activity of 0.05 U $mg^{-1}$ of proteinase K.

Notably, our above analyses (see Figures 2−4) showed partial decomposition of proteinase K at temperatures above 130 °C. We hence entertained the possibility that the observed hydrolysis of the nitroanilide peptide may have occurred non-enzymatically, mediated by proteinase K degradation products. To discriminate between the two principal scenarios of enzymatic hydrolysis by remaining, intact proteinase K vs non-enzymatic hydrolysis by proteinase K degradation products, we employed a specific chloromethyl ketone (CMK) inhibitor. Notably, the inhibitor reacts by binding to the active site of folded proteinase K, followed by formation of a covalent adduct with two enzyme residues, which irreversibly destroys the active site.[46] Indeed, addition of the inhibitor methoxysuccinyl-alanine-alanine-proline-phenylalanine-chloromethyl ketone (MeOSuc-Ala-Ala-Pro-Phe-CMK) resulted in a strong activity reduction of native proteinase K (Figure S21). To assess the hydrolysis mechanism of thermally treated IM-PK particles, we incubated these particles in the presence of the CMK inhibitor. The nitroanilide substrate was then added to start the reaction, and the kinetics were followed spectrophotometrically (Figure 7).

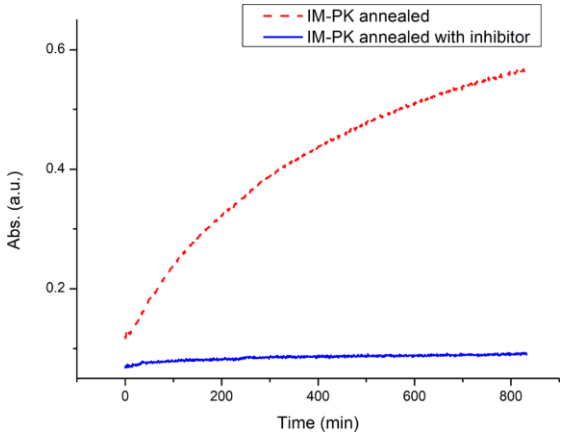


**Figure 7.** Catalytic activity of IM-PK particles in the presence (solid line) or absence (dashed line) of the inhibitor MeOSuc-Ala-Ala-Pro-Phe-CMK. Assays were performed with 200 $\mu$M of *N*-Suc-Ala-Ala-Pro-Leu-pNA in Tris buffer (pH 8.6) at 25 °C. The reaction was followed by absorbance at 410 nm.

Strikingly, the velocity and extent of substrate hydrolysis were much reduced when the CMK inhibitor was added. These observations point toward enzymatic catalysis and thus indicate that a portion of the particle-embedded proteinase K withstood thermal treatment. Furthermore, the non-annealed and annealed IM-PKs were tested for their ability to hydrolyze *N*-Suc-Ala-Ala-Pro-Leu-pNA with D-isomers (Figure 8). Neither native nor annealed IM-PK exhibited activity against the *p*-nitroanilide (D-peptide), indicating that the above hydrolysis of the L-peptide substrate (see Figure 6) occurred enzymatically. By contrast, had the reaction proceeded non-enzymatically, similar reactivities against the D- and L-isomers

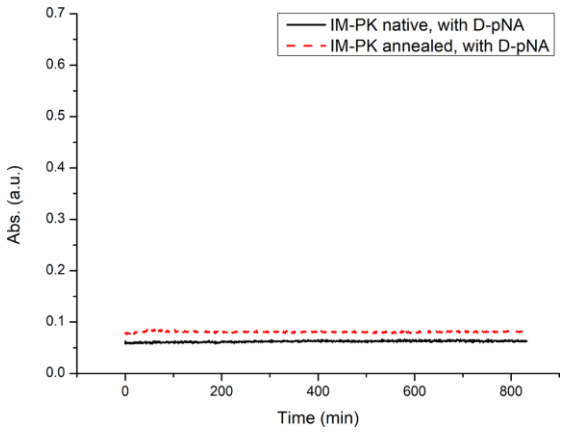


**Figure 8.** Catalytic activity of IM-PK particles against D-peptides. A suspension of 10 mg $mL^{-1}$ IM-PK particles, either annealed at 200 °C for 5 min (dashed line) or not (solid line), was incubated with 200 $\mu$M *N*-Suc-Ala-Ala-Pro-Leu-pNA (D-peptide) in Tris buffer (pH 8.6) at 25 °C. The reaction was followed by absorbance at 410 nm.



https://doi.org/10.1021/acs.biomac.2c01008
*Biomacromolecules* 2022, 23, 4841−4850

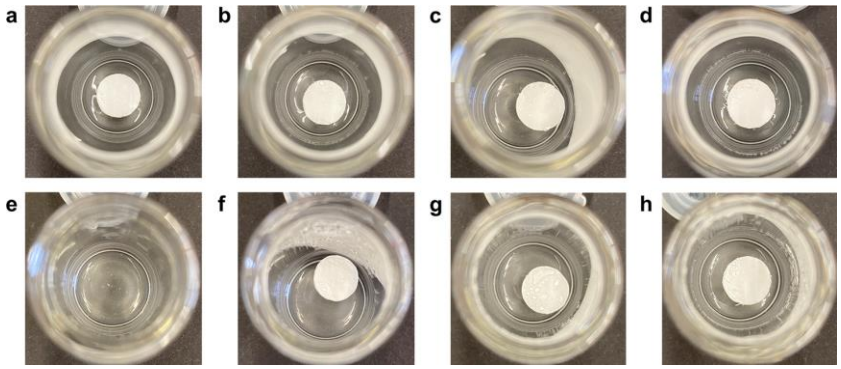


**Figure 9.** PLLA and PDLA electrospun nonwoven in IM-PK suspensions. Original status of PLLA in (a) native IM-PK and (b) annealed IM-PK suspensions, original status of PDLA in (c) native IM-PK and (d) annealed IM-PK suspensions, status after 24 h of PLLA in (e) native IM-PK and (f) annealed IM-PK suspensions, and status after 24 h of PDLA in (g) native IM-PK and (h) annealed IM-PK suspensions.

would have emerged. These data also nicely match the previous findings on the degradation reactivity of proteinase K toward PDLA.[15]

**Degradation Behavior of IM-PK on PLLA/PDLA Electrospun Nonwoven.** We next addressed the reactivity of annealed IM-PK against PLLA (Figure 9 and Figure S22). For this study, we applied PLLA nonwoven because it is degraded by native proteinase K within ca. 12 h, compared to ca. 168 h required for PLLA films. The reason for the faster reaction with the PLLA nonwoven is the higher surface area. As a control, we also manufactured PDLA nonwovens made of the enantiomer D-lactide by electrospinning under same conditions as for PLLA nonwovens. In common with other enzymes, proteinase K exhibits exquisite stereospecificity. In particular, for degradation to occur, the polylactide chain has to be recognized and bound within the active site of proteinase K. Once precisely coordinated, a catalytic triad of three proteinase K residues (Asp 39, His 69, and Ser 224) mediates the hydrolysis of the polylactide ester bonds, with a reaction intermediate stabilized by the so-called oxyanion hole. These processes are highly specific for the L-isomer (PLLA), whereas for the D-isomer (PDLA), productive binding to the active site is hindered by steric effects of the methyl group in the polylactide chain.[8]

When incubated with native IM-PK particles, the PLLA nonwoven was completely degraded within only 1 day (Figure 9e). By contrast, the PDLA nonwoven persisted after 24 h (Figure 9g) and was not visibly affected even after 10 days of incubation (not shown here). These observations showed that polylactide degradation occurs enzymatically when incubated with native IM-PK. We next examined the reaction of PLLA and PDLA nonwovens with thermally treated IM-PK particles. However, degradation occurred neither for PLLA (Figure 9f) nor for PDLA (Figure 9h) after 24 h. Even after 10 days, no visible degradation was observed for either polymer despite the sensitivity of this qualitative test. We attribute the lack of overall degradation to strongly reduced IM-PK activity after annealing (see Figure 6).

## CONCLUSIONS

Surprisingly, proteinase K withstood high temperatures in the bulk phase up to 130 °C for 5 min in an enzymatically active state. By contrast, at temperatures of 150 °C and higher, the activity of proteinase K was strongly reduced. Given that the melt processing of PLLA requires temperatures larger than 180 °C, the direct use of PK under conditions relevant for melt processing is precluded unless additional measures are taken. That notwithstanding, the pronounced thermal stability of proteinase K in the dry phase gives a promising outlook for the application of proteinase K, especially when it is encapsulated and thereby protected within proper encapsulation media. The experiments on proteinase K immobilized in PAM particles verified the principal concept but also identified the need for further improvement as the enzyme activity levels retained after thermal treatment were too low to readily cause PLLA degradation. Nevertheless, there are many other potential candidate options for the encapsulation of proteinase K that can be combined with the advanced melt processing of PLLA to open promising perspectives for future work. Crucially, we have at present established methodologies for the precise assessment and quantitative measurement of enzymatic activity after annealing. We note that our studies did not yet consider the mechanical stress on the enzyme during melt extrusion at higher temperatures, which could have further impact on the stability and activity of proteinase K. Likewise, we did not yet examine the effect of immobilized proteinase K on the mechanical properties of PLLA. Armed with the experimental framework established at present, these questions will be addressed in upcoming work. Moreover, we intend to explore new encapsulation methods for proteinase K, which reliably allow the melt processing of proteinase K with PLLA as verified by the approaches reported in the current manuscript.

The results obtained here for proteinase K could be transferrable to other enzymes and proteins, thus benefitting the burgeoning field of melt processing of proteins. Pertinent efforts augur a new and promising class of hybrid materials based on enzymatically degradable thermoplastics and proteins. These materials are relevant for a variety of applications like drug formulation, scaffolds for tissue engineering, plastic materials, and battling microplastic debris.

## ASSOCIATED CONTENT

### Supporting Information

The Supporting Information is available free of charge at https://pubs.acs.org/doi/10.1021/acs.biomac.2c01008.

SEM images of PAM particles and native/annealed PK, IR of native/annealed PK, NMR spectra of native/annealed PK, mass loss curves and FTIR spectra of



https://doi.org/10.1021/acs.biomac.2c01008
Biomacromolecules 2022, 23, 4841−4850

decomposition products of PK, photographic image of PK solutions, CD thermal unfolding of PK, activity assay curves of PK, electrospun PLA nonwoven (PDF)

## AUTHOR INFORMATION


### Corresponding Authors

**Andreas Möglich** − *Department of Biochemistry, University of Bayreuth, Bayreuth 95447, Germany;* orcid.org/0000-0002-7382-2772; Email: andreas.moeglich@uni-bayreuth.de

**Andreas Greiner** − *Macromolecular Chemistry and Bavarian Polymer Institute, University of Bayreuth, Bayreuth 95440, Germany;* orcid.org/0000-0002-5310-3850; Email: andreas.greiner@uni-bayreuth.de

### Authors

**Chengzhang Xu** − *Macromolecular Chemistry and Bavarian Polymer Institute, University of Bayreuth, Bayreuth 95440, Germany*

**Alexander Battig** − *Bundesanstalt für Materialforschung und -prüfung (BAM), Berlin 12205, Germany;* orcid.org/0000-0002-9461-1368

**Bernhard Schartel** − *Bundesanstalt für Materialforschung und -prüfung (BAM), Berlin 12205, Germany;* orcid.org/0000-0001-5726-9754

**Renée Siegel** − *Inorganic Chemistry III and Northern Bavarian NMR Centre (NBNC), University of Bayreuth, Bayreuth 95440, Germany;* orcid.org/0000-0003-1412-5237

**Jürgen Senker** − *Inorganic Chemistry III and Northern Bavarian NMR Centre (NBNC), University of Bayreuth, Bayreuth 95440, Germany;* orcid.org/0000-0002-7278-7952

**Inge von der Forst** − *Bioorganic Chemistry, University of Bayreuth, Bayreuth 95447, Germany*

**Carlo Unverzagt** − *Bioorganic Chemistry, University of Bayreuth, Bayreuth 95447, Germany*

**Seema Agarwal** − *Macromolecular Chemistry and Bavarian Polymer Institute, University of Bayreuth, Bayreuth 95440, Germany*

Complete contact information is available at: https://pubs.acs.org/10.1021/acs.biomac.2c01008


### Author Contributions

The manuscript is based on contributions of all authors. C.X. wrote the manuscript, designed part of the experiments, and did part of the spectroscopic analysis, annealing experiments, enzymatic assays, synthesis and electrospinning of PDLA, and degradation tests of the PLAs. A.G. guided the project, wrote the manuscript, and designed the experiments. A.M. guided the project, wrote the manuscript, and designed the experiments. J.S. and R.S. did ss-NMR, B.S. and A.B. did TG-FTIR, and C.U. and I.v.d.F. synthesized *N*-Suc-Ala-Ala-Pro-Leu-pNA with D-isomers. All authors have given approval to the final version of the manuscript.


### Funding

This study was funded by the Deutsche Forschungsgemeinschaft (DFG, German Research Foundation), CRC Microplastic, project number 391977956-SFB 1357.


### Notes

The authors declare no competing financial interest.

## ACKNOWLEDGMENTS


The authors thank Tobias Lauster in Physical Chemistry I for kind help with UV−vis measurement, Prof. Dr. Matthias Breuning and Christian Jürgen Müller in Organische Chemie I/2 for kind help with polarimetry, Rika Schneider for kind help with GPC measurement, and Dr. Qianzhao Xu and Andrés García de Fuentes in Biochemistry II for help with lab work. The authors also thank Patrick Klack for his help with the TG-FTIR device and Lea Dämpfling for fruitful discussions on TG-FTIR of proteinase K.


## REFERENCES


(1) Anju, S.; Prajitha, N.; Sukanya, V. S.; Mohanan, P. V. Complicity of degradable polymers in health-care applications. *Mater. Today Chem.* **2020**, *16*, No. 100236.

(2) Zaaba, N. F.; Jaafar, M. A review on degradation mechanisms of polylactic acid: Hydrolytic, photodegradative, microbial, and enzymatic degradation. *Polym. Eng. Sci.* **2020**, *60*, 2061−2075.

(3) Siracusa, V.; Rocculi, P.; Romani, S.; Rosa, M. D. Biodegradable polymers for food packaging: a review. *Trends Food Sci. Technol.* **2008**, *19*, 634−643.

(4) Millican, J. M.; Agarwal, S. Plastic Pollution: A Material Problem? *Macromolecules* **2021**, *54*, 4455−4469.

(5) Lesaffre, N.; Bellayer, S.; Vezin, H.; Fontaine, G.; Jimenez, M.; Bourbigot, S. Recent advances on the ageing of flame retarded PLA: Effect of UV-light and/or relative humidity. *Polym. Degrad. Stab.* **2017**, *139*, 143−164.

(6) Salač, J.; Šerá, J.; Jurča, M.; Verney, V.; Marek, A. A.; Koutný, M. Photodegradation and Biodegradation of Poly(Lactic) Acid Containing Orotic Acid as a Nucleation Agent. *Materials* **2019**, *12*, 481.

(7) Ozdemir, E.; Lekesiz, T. O.; Hacaloglu, J. Polylactide/organically modified montmorillonite composites; effects of organic modifier on thermal characteristics. *Polym. Degrad. Stab.* **2016**, *134*, 87−96.

(8) Qi, X.; Ren, Y.; Wang, X. New advances in the biodegradation of Poly(lactic) acid. *Int. Biodeterior. Biodegrad.* **2017**, *117*, 215−223.

(9) Sin, L. T.; Tueen, B. S. In *Polylactic Acid*, 2nd Ed.; Sin, L. T.; Tueen, B. S.; Eds. William Andrew Publishing: 2019; pp. xv-xvi.

(10) Williams, D. F. Enzymic Hydrolysis of Polylactic Acid. *Proc. Inst. Mech. Eng., Part H* **1981**, *10*, 5−7.

(11) Ebeling, W.; Hennrich, N.; Klockow, M.; Metz, H.; Orth, H. D.; Lang, H. Proteinase K from Tritirachium album Limber. *Eur. J. Biochem.* **1974**, *47*, 91−97.

(12) Bajorath, J.; Hinrichs, W.; Saenger, W. The enzymatic activity of proteinase K is controlled by calcium. *Eur. J. Biochem.* **1988**, *176*, 441−447.

(13) Liu, S.-Q.; Tao, Y.; Meng, Z.-H.; Fu, Y.-X.; Zhang, K.-Q. The effect of calciums on molecular motions of proteinase K. *J. Mol. Model.* **2011**, *17*, 289−300.

(14) Yazawa, K.; Sugahara, M.; Yutani, K.; Takehira, M.; Numata, K. Derivatization of Proteinase K with Heavy Atoms Enhances Its Thermal Stability. *ACS Catal.* **2016**, *6*, 3036−3046.

(15) Reeve, M. S.; McCarthy, S. P.; Downey, M. J.; Gross, R. A. Polylactide stereochemistry: effect on enzymic degradability. *Macromolecules* **1994**, *27*, 825−831.

(16) Yamashita, K.; Kikkawa, Y.; Kurokawa, K.; Doi, Y. Enzymatic degradation of poly(L-lactide) film by proteinase K: quartz crystal microbalance and atomic force microscopy study. *Biomacromolecules* **2005**, *6*, 850−857.

(17) Tsuji, H.; Eto, T.; Sakamoto, Y. Synthesis and Hydrolytic Degradation of Substituted Poly(DL-Lactic Acid)s. *Materials* **2011**, *4*, 1384−1398.

(18) Andersson, S. R.; Hakkarainen, M.; Albertsson, A.-C. Tuning the Polylactide Hydrolysis Rate by Plasticizer Architecture and Hydrophilicity without Introducing New Migrants. *Biomacromolecules* **2010**, *11*, 3617−3623.

(19) Oda, Y.; Yonetsu, A.; Urakami, T.; Tonomura, K. Degradation of Polylactide by Commercial Proteases. *J. Polym. Environ.* **2000**, *8*, 29−32.
(20) Kawai, F.; Nakadai, K.; Nishioka, E.; Nakajima, H.; Ohara, H.; Masaki, K.; Iefuji, H. Different enantioselectivity of two types of poly(lactic acid) depolymerases toward poly(l-lactic acid) and poly(d-lactic acid). *Polym. Degrad. Stab.* **2011**, *96*, 1342−1348.
(21) Hedstrom, L. Serine Protease Mechanism and Specificity. *Chem. Rev.* **2002**, *102*, 4501−4524.
(22) Bajorath, J.; Raghunathan, S.; Hinrichs, W.; Saenger, W. Long-range structural changes in proteinase K triggered by calcium ion removal. *Nature* **1989**, *337*, 481−484.
(23) Zheng, Y.; Pokorski, J. K. Hot melt extrusion: An emerging manufacturing method for slow and sustained protein delivery. *Wiley Interdiscip. Rev.: Nanomed. Nanobiotechnol.* **2021**, *13*, No. e1712.
(24) Lee, P.; Towslee, J.; Maia, J.; Pokorski, J. PEGylation to Improve Protein Stability During Melt Processing. *Macromol. Biosci.* **2015**, *15*, 1332−1337.
(25) DelRe, C.; Jiang, Y.; Kang, P.; Kwon, J.; Hall, A.; Jayapurna, I.; Ruan, Z.; Ma, L.; Zolkin, K.; Li, T.; Scown, C. D.; Ritchie, R. O.; Russell, T. P.; Xu, T. Near-complete depolymerization of polyesters with nano-dispersed enzymes. *Nature* **2021**, *592*, 558−563.
(26) Huang, Q.; Hiyama, M.; Kabe, T.; Kimura, S.; Iwata, T. Enzymatic Self-Biodegradation of Poly(l-lactic acid) Films by Embedded Heat-Treated and Immobilized Proteinase K. *Biomacromolecules* **2020**, *21*, 3301−3307.
(27) Abbenante, G.; Leung, D.; Bond, T.; Fairlie, D. P. An efficient Fmoc strategy for the rapid synthesis of peptide para-nitroanilides. *Lett. Pept. Sci.* **2000**, *7*, 347−351.
(28) Burdick, D. J.; Struble, M. E.; Burnier, J. P. Solid phase synthesis of peptide para -nitroanilides. *Tetrahedron Lett.* **1993**, *34*, 2589−2592.
(29) Zhu, J.; Kumar, A.; Hu, P.; Habel, C.; Breu, J.; Agarwal, S. Layering-Triggered Delayering with Exfoliated High-Aspect Ratio Layered Silicate for Enhanced Gas Barrier, Mechanical Properties, and Degradability of Biodegradable Polymers. *Global Challenges* **2020**, *4*, 2000030.
(30) Numata, K.; Finne-Wistrand, A.; Albertsson, A.-C.; Doi, Y.; Abe, H. Enzymatic Degradation of Monolayer for Poly(lactide) Revealed by Real-Time Atomic Force Microscopy: Effects of Stereochemical Structure, Molecular Weight, and Molecular Branches on Hydrolysis Rates. *Biomacromolecules* **2008**, *9*, 2180−2185.
(31) Barth, A. Infrared spectroscopy of proteins. *Biochim. Biophys. Acta, Bioenerg.* **2007**, *1767*, 1073−1101.
(32) Wüthrich, K. *NMR of Proteins and Nucleic Acids*; Wiley: New York, 1986.
(33) Ulrich, E. L.; Akutsu, H.; Doreleijers, J. F.; Harano, Y.; Ioannidis, Y. E.; Lin, J.; Livny, M.; Mading, S.; Maziuk, D.; Miller, Z.; Nakatani, E.; Schulte, C. F.; Tolmie, D. E.; Kent Wenger, R.; Yao, H.; Markley, J. L. BioMagResBank. *Nucleic Acids Res.* **2008**, *36*, D402−D408.
(34) Wishart, D. S.; Sykes, B. D.; Richards, F. M. The chemical shift index: a fast and simple method for the assignment of protein secondary structure through NMR spectroscopy. *Biochemistry* **1992**, *31*, 1647−1651.
(35) Harding, M. M.; Williams, D. H.; Woolfson, D. N. Characterization of a partially denatured state of a protein by two-dimensional NMR: reduction of the hydrophobic interactions in ubiquitin. *Biochemistry* **1991**, *30*, 3120−3128.
(36) Wishart, D. S.; Nip, A. M. Protein chemical shift analysis: a practical guide. *Biochem. Cell Biol.* **1998**, *76*, 153−163.
(37) Wehrli, M. C.; Kratky, T.; Schopf, M.; Scherf, K. A.; Becker, T.; Jekle, M. Thermally induced gluten modification observed with rheology and spectroscopies. *Int. J. Biol. Macromol.* **2021**, *173*, 26−33.
(38) Weiss, I. M.; Muth, C.; Drumm, R.; Kirchner, H. O. K. Thermal decomposition of the amino acids glycine, cysteine, aspartic acid, asparagine, glutamic acid, glutamine, arginine and histidine. *BMC Biophys.* **2018**, *11*, 2.
(39) Jany, K.-D.; Lederer, G.; Mayer, B. Amino acid sequence of proteinase K from the mold Tritirachium album Limber. *FEBS Lett.* **1986**, *199*, 139−144.
(40) Schmid, F. X. In *Protein Structure: A Practical Approach*; 2nd ed.; Creighton, T. E., Ed.; IRL Press at Oxford University Press: Oxford, 1997; p 261.
(41) Möglich, A. An Open-Source, Cross-Platform Resource for Nonlinear Least-Squares Curve Fitting. *J. Chem. Educ.* **2018**, *95*, 2273−2278.
(42) Liao, J.; Warmuth, M. K.; Govindarajan, S.; Ness, J. E.; Wang, R. P.; Gustafsson, C.; Minshull, J. Engineering proteinase K using machine learning and synthetic genes. *BMC Biotechnol.* **2007**, *7*, 16.
(43) Georgieva, D.; Genov, N.; Voelter, W.; Betzel, C. Catalytic Efficiencies of Alkaline Proteinases from Microorganisms. *Z. Naturforsch., C: J. Biosci.* **2006**, *61*, 445−452.
(44) Stone, L. A.; Jackson, G. S.; Collinge, J.; Wadsworth, J. D. F.; Clarke, A. R. Inhibition of Proteinase K Activity by Copper(II) Ions. *Biochemistry* **2007**, *46*, 245−252.
(45) Johnson, K. A.; Goody, R. S. The Original Michaelis Constant: Translation of the 1913 Michaelis−Menten Paper. *Biochemistry* **2011**, *50*, 8264−8269.
(46) Betzel, C.; Pal, G. P.; Struck, M.; Jany, K.-D.; Saenger, W. Active-site geometry of proteinase K. *FEBS Lett.* **1986**, *197*, 105−110.




https://doi.org/10.1021/acs.biomac.2c01008
*Biomacromolecules* 2022, 23, 4841−4850

# Supporting Information

## Investigation of the Thermal Stability of Proteinase K for the Melt Processing with Poly(*L*-lactide)

*Chengzhang Xu,[a] Alexander Battig,[b] Bernhard Schartel,[b] Renée Siegel,[c] Jürgen Senker,[c] Inge v. d. Forst,[d] Carlo Unverzagt,[d] Seema Agarwal,[a] Andreas Möglich[e]* and Andreas Greiner,[a]**

[a] University of Bayreuth, Macromolecular Chemistry and Bavarian Polymer Institute, Universitätsstrasse 30, 95440 Bayreuth, Germany

[b] Bundesanstalt für Materialforschung und -prüfung (BAM), Unter den Eichen 87, 12205 Berlin, Germany

[c] University of Bayreuth, Inorganic Chemistry III and Northern Bavarian NMR Centre (NBNC), Universitätsstrasse 30, 95440 Bayreuth, Germany

[d] University of Bayreuth, Bioorganic Chemistry, Universitätsstrasse 30, 95447 Bayreuth, Germany

[e] University of Bayreuth, Department of Biochemistry, Universitätsstrasse 30, 95447 Bayreuth, Germany

*Corresponding authors

Figure S1 shows native PAM particles (Bio-Rad). The image was taken by scanning electron microscopy (SEM, LEO 1530, Zeiss). The samples were first sputter coated with Pt by sputter coater (208 HR from Cressington, Watford, England).

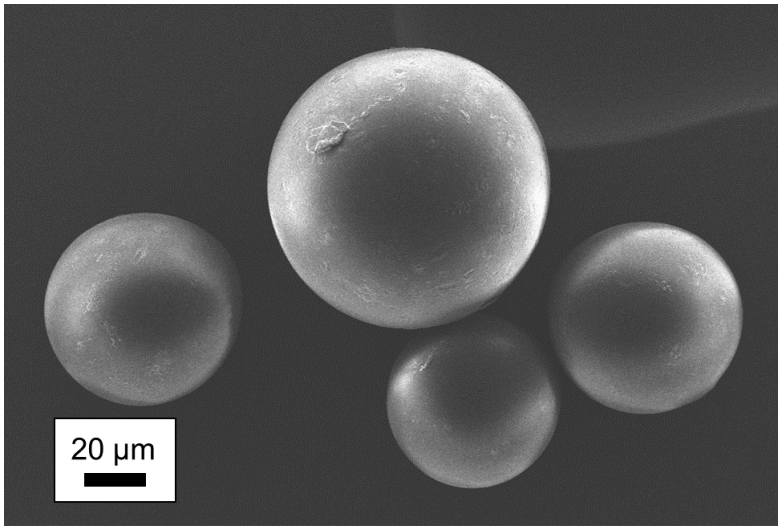


**Figure S1.** SEM micrograph of PAM particles without proteinase K.

Figure S2 illustrates the setup for annealing of proteinase K and IM-PK. A 10 mL vial was immersed either in water bath (50 °C – 90 °C) or in oil bath (130 °C – 200 °C) with a stirring bar until the expected temperatures were reached, and the whole setup was left still for 30 min prior to the addition of proteinase K powder. Around 10 mg of proteinase K were added to the preheated vial and kept there for 5 min. The temperature was controlled by a digital thermometer attached to the wall of the vial. After annealing the vial was shock frozen in ice-water kept at 0 °C for 10 minutes.

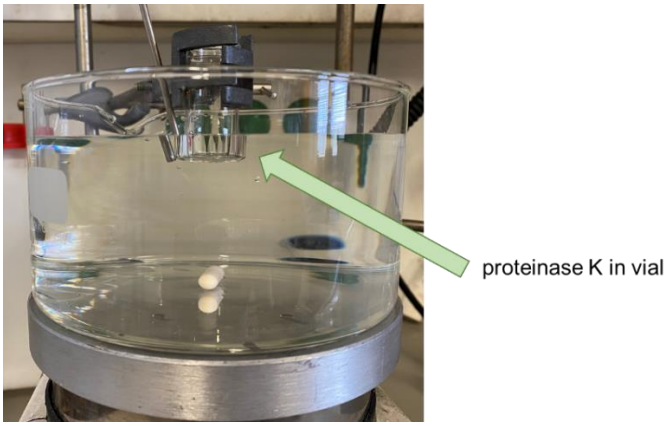


**Figure S2.** Photographic image of the setup for annealing of proteinase K powder at different temperatures for 5 min (see table 1 in manuscript).

Figure S3 shows the native (Figure S3a) and annealed proteinase K powder particles (annealed at 200 °C for 5 min, Figure S3b). The images were taken by SEM. Qualitative visual comparison of native and annealed proteinase K powder particles showed minor shrinkage of the particles after annealing.

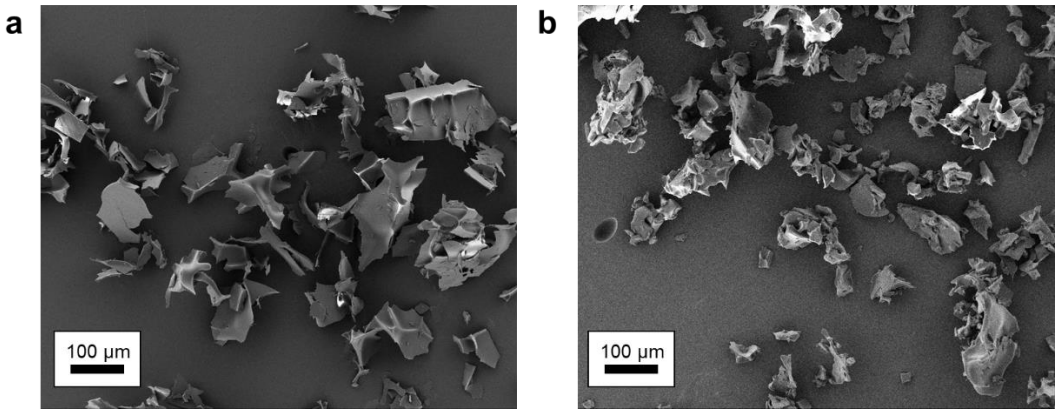


**Figure S3.** SEM micrograph of native (a) and annealed (b, 200 °C for 5 min) proteinase K powder particles.

Figure S4 shows the infrared (IR) spectra of native (dashed line) and annealed (solid line, 200°C for 5 minutes) proteinase K.

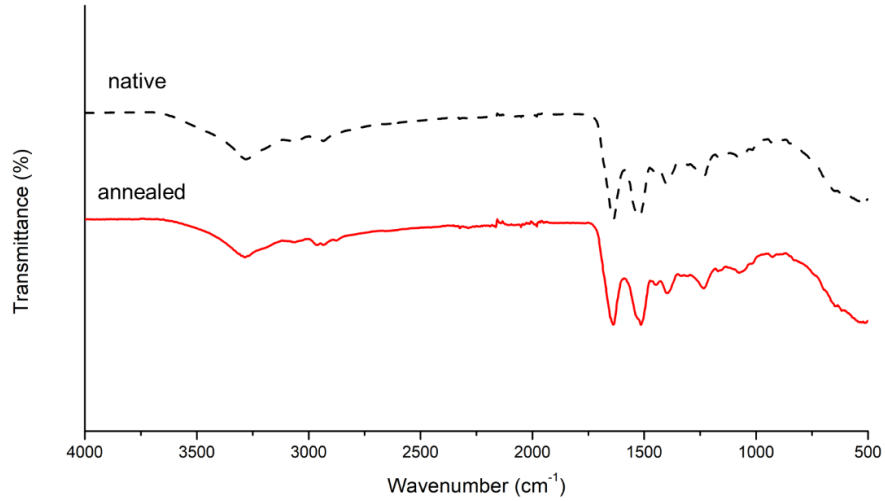


**Figure S4.** IR of native (black dashed line) and annealed (red solid line, 200 °C for 5 min) proteinase K.

Figure S5 and S6 show the $^{13}C$ and $^{15}N$ MAS NMR spectra of native and annealed (200 °C 5 min) proteinase K powder.

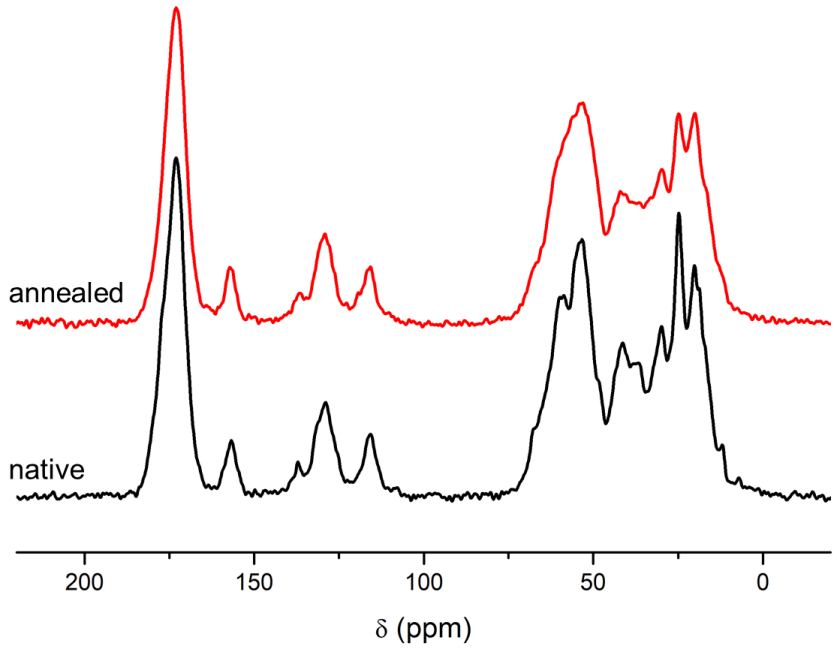


**Figure S5.** $^{13}C$ CP MAS NMR spectra of native and annealed proteinase K.

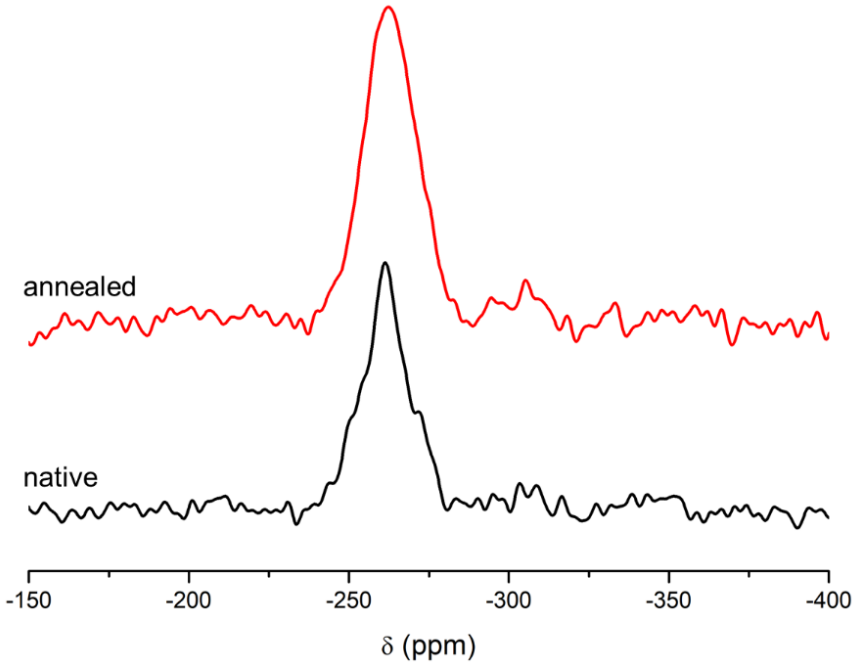


**Figure S6.** $^{15}$N CP MAS NMR spectra of native and annealed proteinase K

Figure S7a and S7c show the mass loss of proteinase K powder under different conditions (Figure S7a under nitrogen and Figure S7c under air). In Figure S7a and S7c, the solid line with triangles is the mass loss of proteinase K powder, and the dashed line is the first derivative of mass loss (DTG). Figure S7b and S7d show the FITR spectra of detected products from proteinase K at different temperatures. In Figure S7b and S7d, the solid lines with triangles show the FTIR spectra of detected compound from proteinase K powder at different temperatures, and the black solid lines show the reference spectra of small molecules. In Figure S7b and S7d, $T_1$ corresponds to the temperature where the first peak of DTG is, and $T_{max}$ is the temperature where the maximum DTG is.

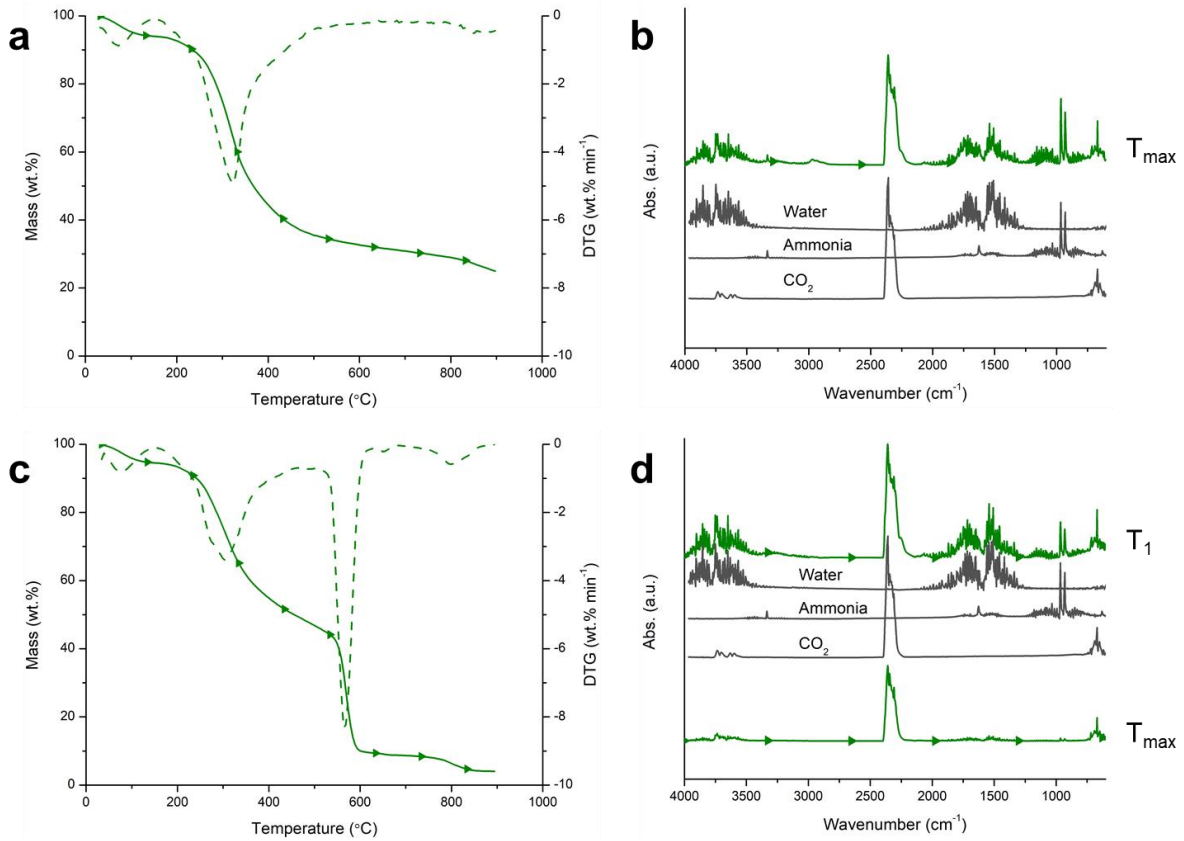


**Figure S7**. Mass loss curves of proteinase K under $N_2$ (a) and under air (c) and FTIR spectra of decomposition products at various temperatures under $N_2$ (b) and under air (d) of proteinase K powder via TG-FTIR. Heating rate: 10 K $min^{-1}$. In figure a and c, the solid line with triangles is the mass loss of proteinase K powder, and the dashed line is the first derivative of mass loss (DTG). In figure b and d, the solid lines with triangles show the FTIR spectra of detected compound from proteinase K powder at different temperatures, and the black solid lines show the reference spectra of small molecules. In figure b and d, $T_1$ corresponds to the temperature where the first peak of DTG is, and $T_{max}$ is the temperature where the maximum DTG is.

Figure S8 shows the photographic image of native (S8a) and annealed (S8b, 180 °C, 5 min) proteinase K after attempts of dissolution in tris(hydroxymethyl)aminomethane (tris) buffer. The native proteinase K dissolved in tris buffer solution rather fast (with 1 min at 25 °C), while

the annealed proteinase K dissolved only partially (56 wt.%) in buffer solution even after 12 hours in tris buffer solution.

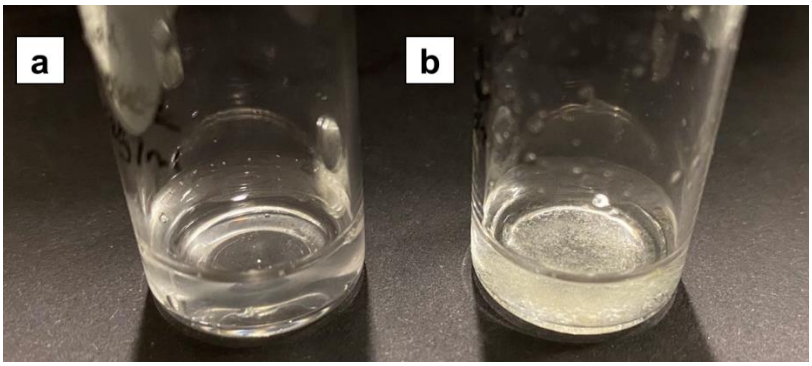


**Figure S8.** Photograph image of 5 mg native (a) and annealed (b, 180 °C for 5 min) proteinase K in vials with 1 mL tris buffer solution.

Figure S9 shows the plot of dynamic CD signal at 222 nm of proteinase K in phosphate buffer at a concentration of 0.6 mg/mL. Here phosphate buffer was used instead of tris buffer because tris buffer generated too much noise at this range of wavelength. The signal was recorded from 15 °C - 90 °C at a rate of 0.5 °C/min. The curve is fitted by Ft-o-mat software. In Figure S9 only the CD signal at the range of 40 °C – 90 °C is shown. A midpoint of unfolding at 72.6 ± 0.1 °C is yielded by the data fitting.

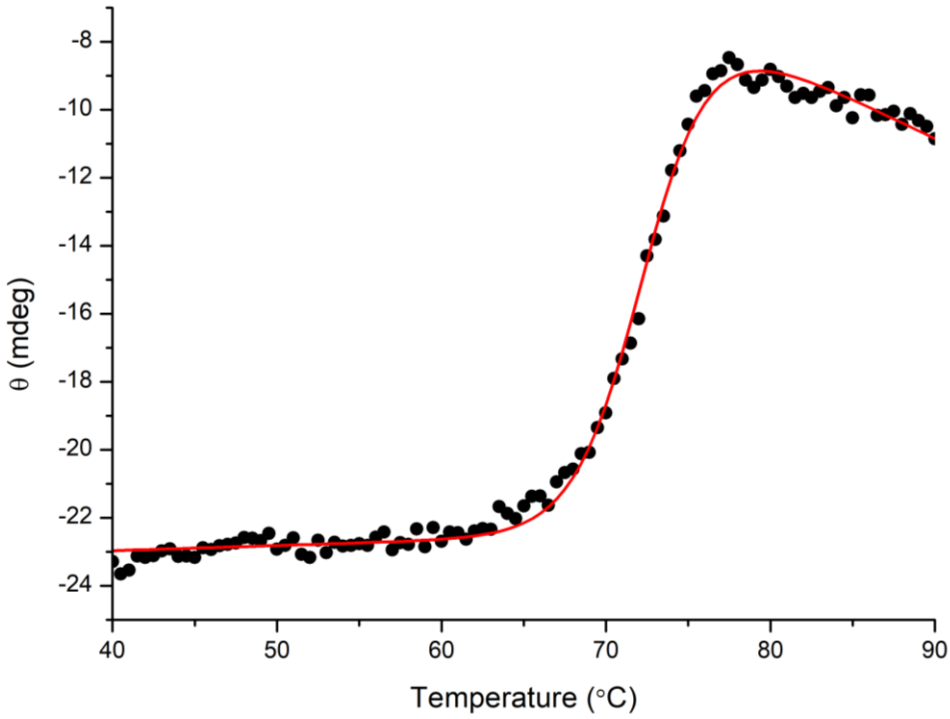


**Figure S9.** Dynamic CD spectra of the signal of proteinase K at 222 nm in phosphate buffer at a concentration of 0.6 mg/mL.

Figure S10 and S11 show the data plotting of activity assay of 0.005 mg/mL proteinase K using *N*-Succinyl-phenylalanine-*p*-nitroanilide (*N*-Suc-Phe-pNA) and *N*-Succinyl-Phenylalanine-Alanine-Alanine-Phenylalanine-*p*-nitroanilide (*N*-Suc-Phe-Ala-Ala-Phe-pNA) as substrates. The absorbance at 410 nm was recorded dynamically. For the substrate *N*-Suc-Phe-pNA, the absorbance at 410 nm increased a bit, but the increased value is too small, comparing with the noise. The absorbance at 410 nm against the substrate *N*-Suc-Phe-Ala-Ala-Phe-pNA shows almost no increase, thus, the calculation of specific activity using these two substrates is not reliable.

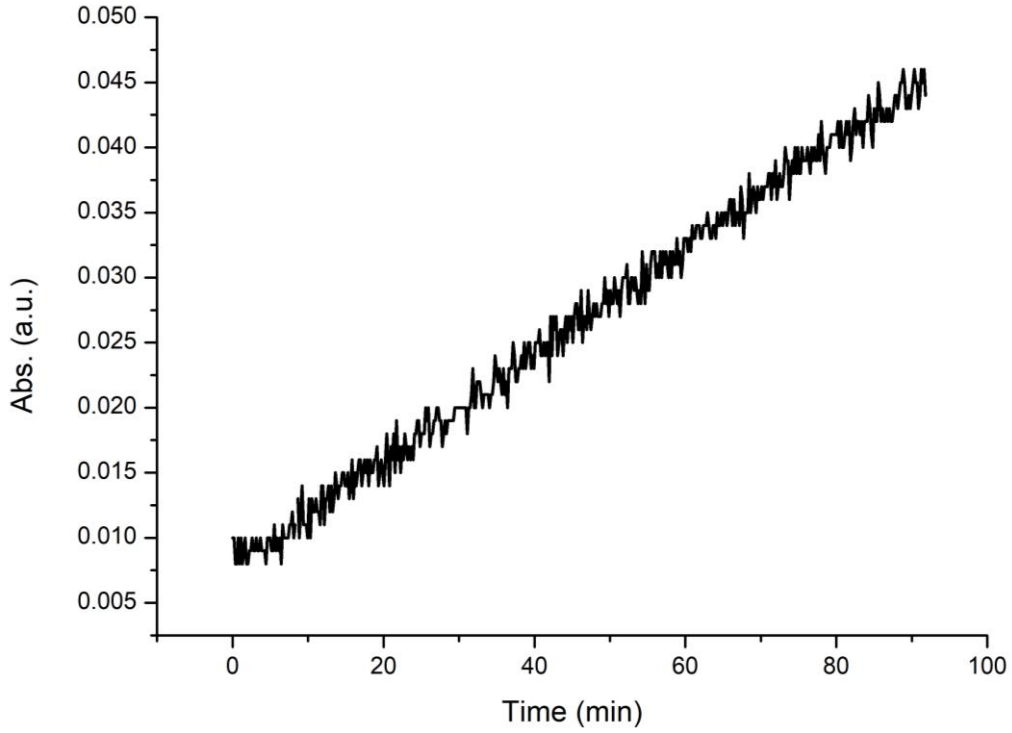


**Figure S10.** The hydrolysis of substrate (*N*-Suc-Phe-pNA, 1 M) by native proteinase K (1 mg/mL) monitored by absorbance spectroscopy versus time at wavelength of 410 nm at 25 °C.

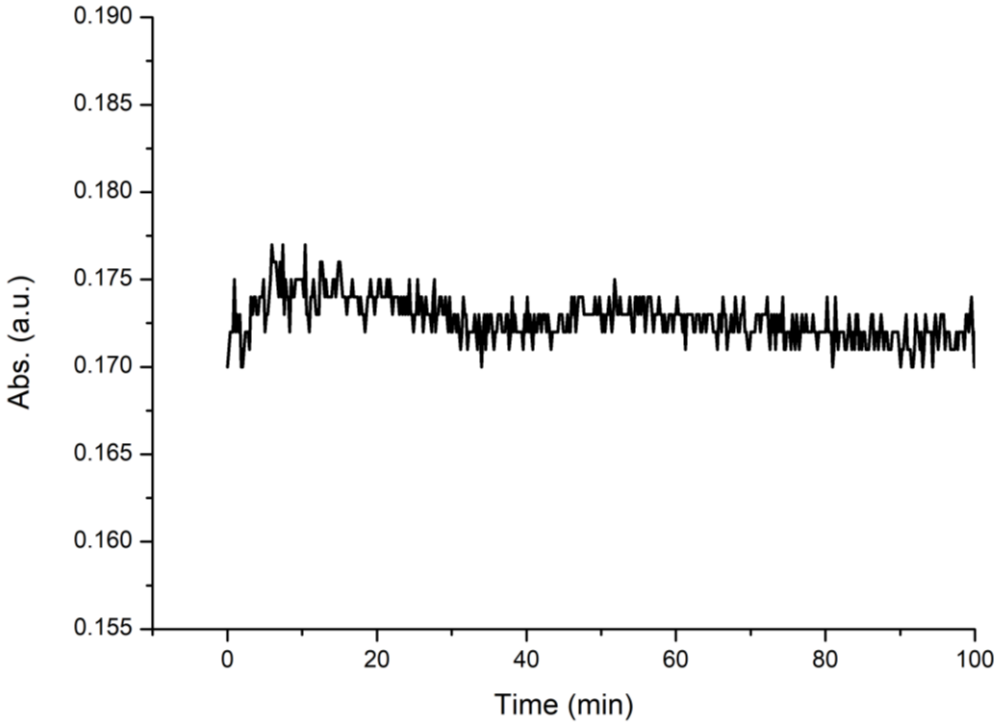

**Figure S11.** The hydrolysis of substrate (*N*-Suc-Phe-Ala-Ala-Phe-pNA, 1 M) by native proteinase K (1 mg/mL) monitored by absorbance spectroscopy versus time at wavelength of 410 nm at 25 °C.

Figure S12 shows the absorbance at 410 nm recorded dynamically, using *N*-Suc-Ala-Ala-Pro-Leu-pNA as substrate. The increase of the absorbance can be clearly observed comparing with the other two substrates (*N*-Suc-Phe-pNA and *N*-Suc-Phe-Ala-Ala-Phe-pNA), indicating enough amount of product *p*-nitroaniline generated during the activity assay. The slope at the beginning of the recorded curve can be therefore used for specific activity calculation. The slope of the curve is fitted by OriginLab 8.1.

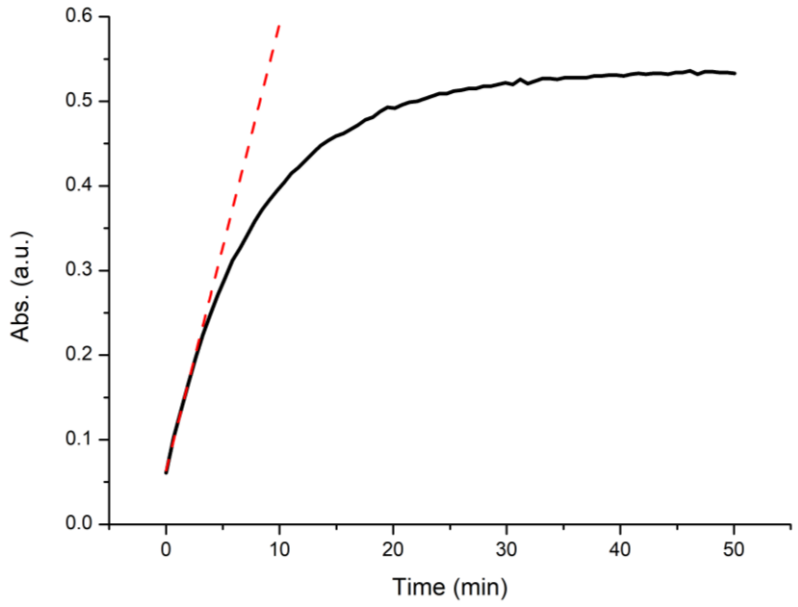


**Figure S12.** The hydrolysis of substrate (N-Suc-Ala-Ala-Pro-Leu-pNA, 200 μM) by native proteinase K (0.005 mg/mL) monitored by absorbance spectroscopy versus time at wavelength of 410 nm at 25 °C (solid line). The red dashed line shows the fitted slope of hydrolysis at the linear region.

Figure S13 shows the solution of 4-nitrophenyl acetate dissolved in tris buffer. After dissolving, the solution is not colorless anymore. The yellowish color implies the hydrolysis of 4-nitrophenyl acetate in aqueous solution even without proteinase K. Thus, this substrate is not used for the activity assay.

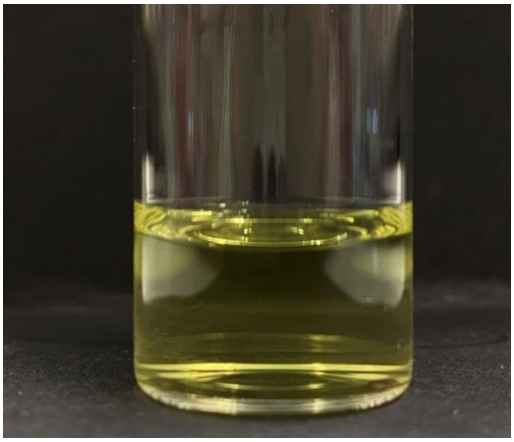

**Figure S13.** Solution of 4-nitrophenyl acetate dissolved in tris buffer at 25 °C with the concentration of 200 μM.

Figure S14 shows the velocity of *p*-nitroaniline generation by 0.005 mg/mL of proteinase K vs. the substrate (N-Suc-Ala-Ala-Pro-Leu-pNA) concentration. The dashed curve is the data fitting done by OriginLab 8.1. The data fitting shows that the increase of velocity is in accordance with hyperbola function.

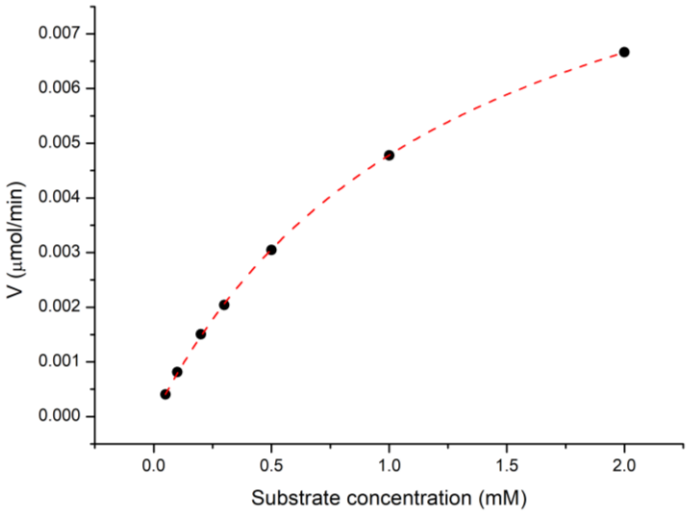


**Figure S14.** Proteinase K activity assay with different concentrations of the substrate *N*-Suc-Ala-Ala-Pro-Leu-pNA, data fitted by hyperbola function (dashed line).

Figure S15 – S19 show the activity assay results of proteinase K annealed at different temperatures using *N*-Suc-Ala-Ala-Pro-Leu-pNA as substrate. The dashed lines in each figure are linear data fitting at the linear region done by OriginLab 8.1. The slopes of the fitted data are used to calculate the specific activity of the samples. For the proteinase K samples annealed at 180 °C and 200 °C, there is no increase of the absorbance at 410 nm, thus the data fitting of the samples annealed at those two temperatures cannot be used for calculation.

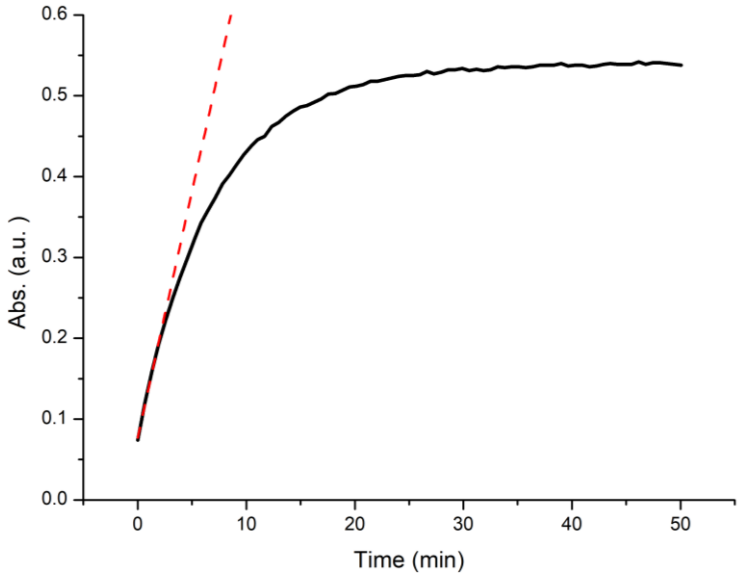

**Figure S15.** The hydrolysis of substrate (*N*-Suc-Ala-Ala-Pro-Leu-pNA, 200 μM) by proteinase K annealed at 22 °C for 5 min (0.005 mg/mL) monitored by absorbance spectroscopy versus time at wavelength of 410 nm at 25 °C (solid line). The red dashed line shows the fitted slope of hydrolysis at the linear region.

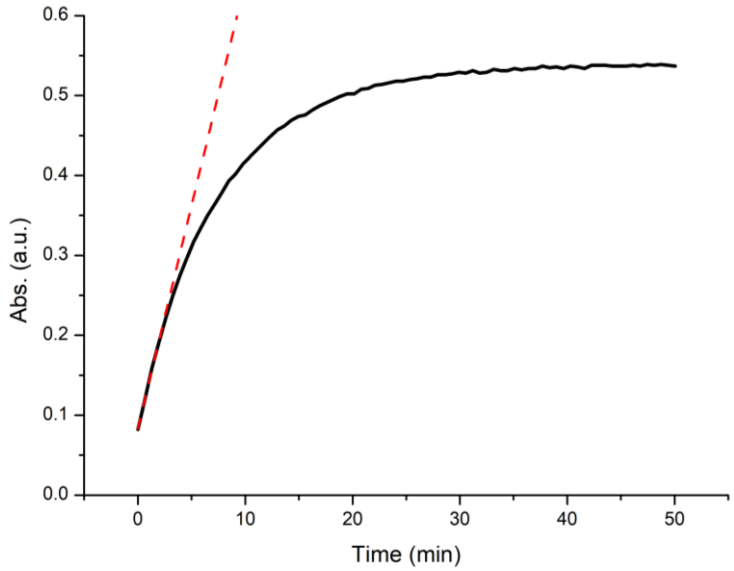


**Figure S16.** The hydrolysis of substrate (*N*-Suc-Ala-Ala-Pro-Leu-pNA, 200 μM) by proteinase K annealed at 50 °C for 5 min (0.005 mg/mL) monitored by absorbance spectroscopy versus time at wavelength of 410 nm at 25 °C (solid line). The red dashed line shows the fitted slope of hydrolysis at the linear region.

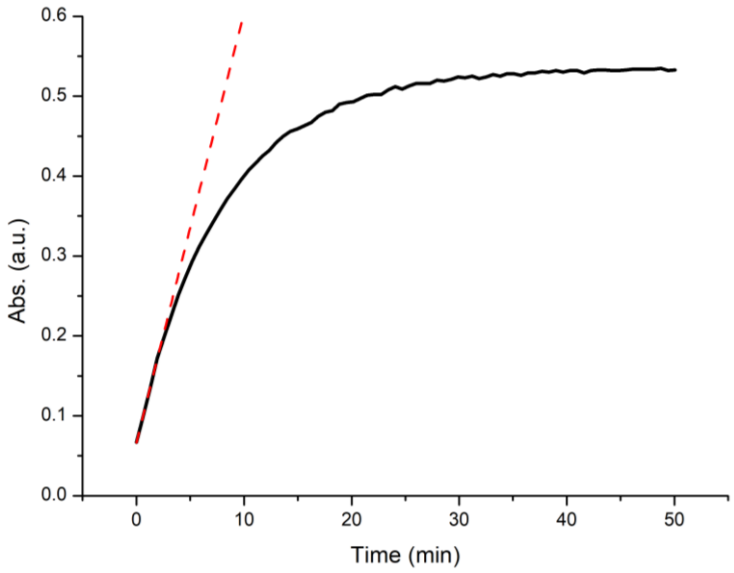


**Figure S17.** The hydrolysis of substrate (*N*-Suc-Ala-Ala-Pro-Leu-pNA, 200 μM) by proteinase K annealed at 90 °C for 5 min (0.005 mg/mL) monitored by absorbance spectroscopy versus time at wavelength of 410 nm at 25 °C (solid line). The red dashed line shows the fitted slope of hydrolysis at the linear region.

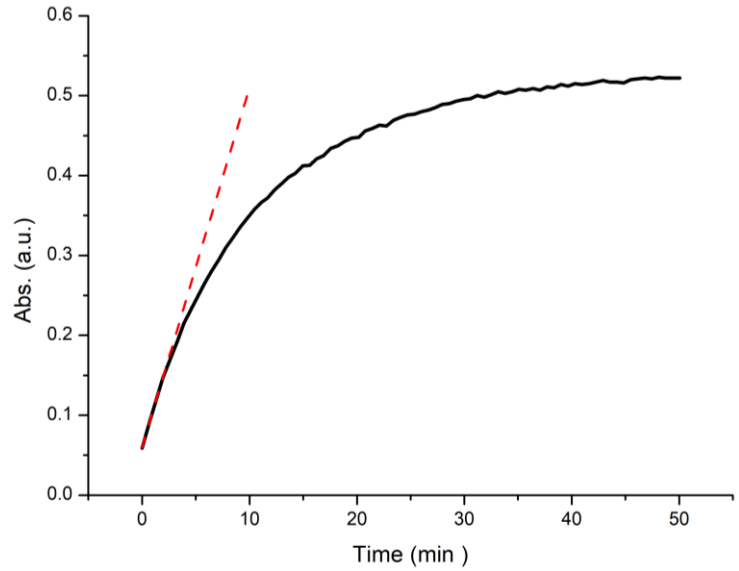


**Figure S18.** The hydrolysis of substrate (*N*-Suc-Ala-Ala-Pro-Leu-pNA, 200 μM) by proteinase K annealed at 130 °C for 5 min (0.005 mg/mL) monitored by absorbance spectroscopy versus time at wavelength of 410 nm at 25 °C (solid line). The red dashed line shows the fitted slope of hydrolysis at the linear region.

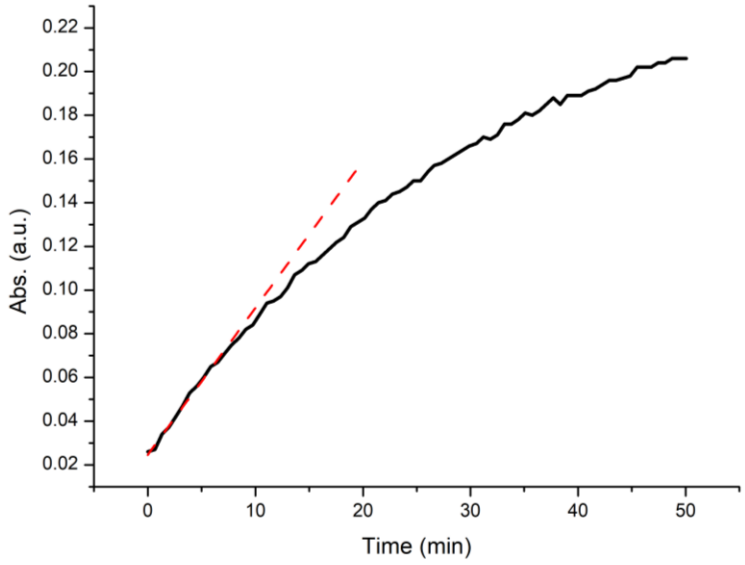


**Figure S19.** The hydrolysis of substrate (*N*-Suc-Ala-Ala-Pro-Leu-pNA, 200 μM) by proteinase K annealed at 150 °C for 5 min (0.005 mg/mL) monitored by absorbance spectroscopy versus time at wavelength of 410 nm at 25 °C (solid line). The red dashed line shows the fitted slope of hydrolysis at the linear region.

Figure S20b is the collection of activity assay of all proteinase K samples annealed at different temperatures, and the amplified starting region of the curves is shown in Figure S20a. The activities of proteinase K annealed at 22 °C, 50 °C and 90 °C are almost the same as that of native proteinase K. At higher annealing temperatures, with the increasing of annealing temperature, the activity of proteinase K decreases. When proteinase K is annealed at 180 °C or 200 °C, there is no activity left at all.

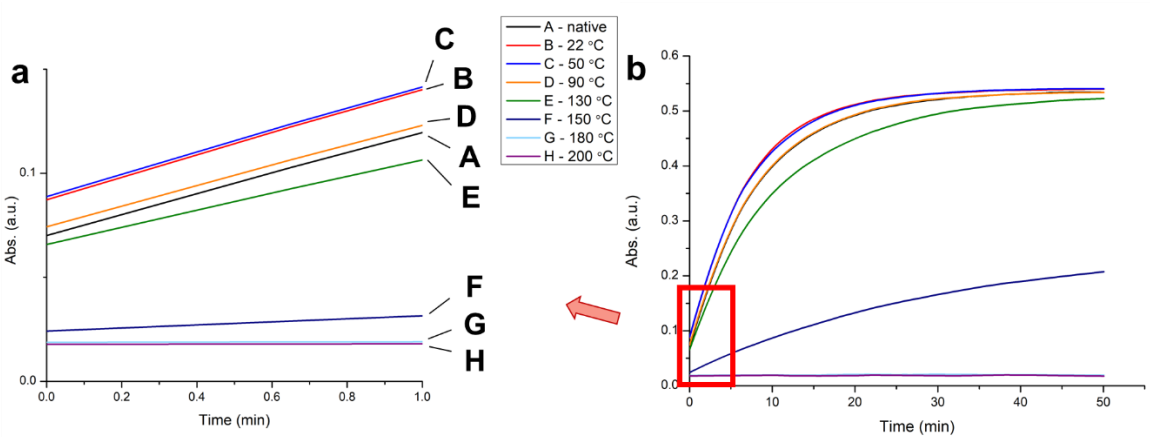


**Figure S20.** Activity of 0.005 mg/mL proteinase K annealed at different temperatures for 5 min (all experiments were done in triplicate, exemplarily only one experiment is shown here). (a) the absorbance recorded at starting region of (b), and (b) the recorded curves of the hydrolysis of substrate (N-Suc-Ala-Ala-Pro-Leu-pNA, 200 μM) by proteinase K annealed at different temperatures (0.005 mg/mL) monitored by absorbance spectroscopy versus time at wavelength of 410 nm at 25 °C (solid line). The absorbance started not at 0 point because the time was required to put the sample into the machine, thus, there was a "dead time" before data recording.

Figure S21 shows the proteinase K activity assay curves with/without the inhibitor MeOSuc-Ala-Ala-Pro-Phe-CMK. The inhibitor/ tris buffer solution was mixed with proteinase K/ tris buffer solution (0.005 mg/mL) 60 min ahead of the assay, and the reaction mixture was incubated at 22 °C. Accordingly, the proteinase K/tris buffer solution without any inhibitor was also incubated under the same condition for the same time. The recorded curves show clearly that with the inhibitor MeOSuc-Ala-Ala-Pro-Phe-CMK (0.005 mg/mL), no *p*-nitroaniline has been generated.

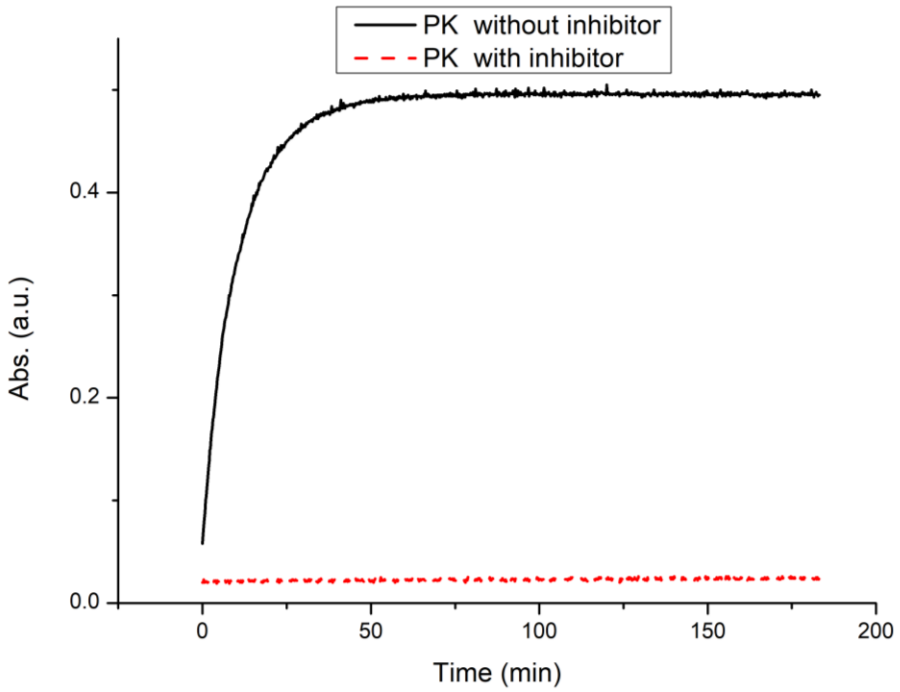


**Figure S21.** Activity of 0.005 mg/mL proteinase K with (dashed line) and without (solid line) inhibitor MeOSuc-Ala-Ala-Pro-Phe-CMK (concentration of inhibitor: 0.005 mg/mL).

Figure S22 shows the electrospun PLLA nonwoven used for degradation test. The sample is collected on a rotating plate, and small pieces with diameter of 10 mm is cut off from the electrospun PLLA or PDLA nonwoven for the degradation tests.

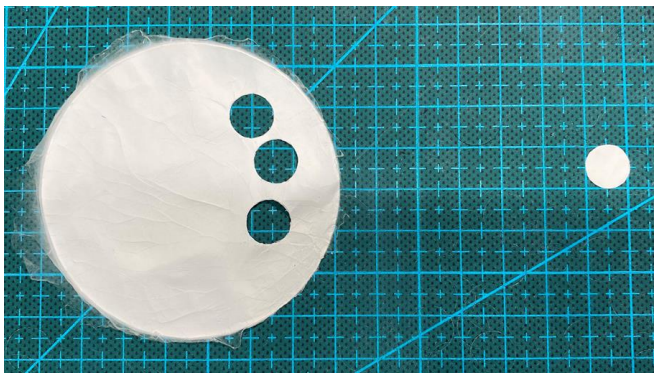

**Figure S22.** Sample of PLLA electrospun nonwoven with diameter of 10 mm obtained by punching of a larger sample used for degradation studies. Samples for PDLA were obtained the same way.

## 3.3. Publication 3 (to be submitted)

Submitted Manuscript: Confidential
Template revised November 2022

# Cool processing of triblock copolymers under pressure

**Authors:** Chengzhang Xu[1], Chengwei Yi[2], Dipannita Ghosh[1], Anja Ramsperger[3], Julian Brehm[3], Christian Laforsch[3], Holger Schmalz[1], Sabine Rosenfeldt[4], Seema Agarwal[1]*, Andreas Möglich[2]*, Andreas Greiner[1]*

**Affiliations:**

[1]Macromolecular Chemistry and Bavarian Polymer Institute, University of Bayreuth; Bayreuth 95440, Germany.

[2]Department of Biochemistry, University of Bayreuth; Bayreuth 95440, Germany.

[3]Animal Ecology I, University of Bayreuth; 95440 Bayreuth, Germany.

[4]Physical Chemistry 1, University of Bayreuth; 95440 Bayreuth, Germany.

*Corresponding authors. Email: agarwal@uni-bayreuth.de, andreas.moeglich.uni-bayreuth.de, greiner@uni-bayreuth.de

**Abstract:**

The intrinsic requirement of high temperatures for film processing of thermoplastic polymers was overcome by applying elevated pressure at an ambient temperature on triblock copolymers far below their melting points. This phenomenon is known as baroplasticity. Out of a series of polylactide-*block*-poly(ethylene glycol) block copolymers the triblock copolymers poly(*L*-lactide)-*b*-poly(ethylene glycol)-*b*-poly(*L*-lactide) (PLLA-*b*-PEG-*b*-PLLA) of distinct compositions exhibited surprisingly baroplasticity, i.e., they assumed their plastic state under these conditions, and could be processed to polymer films. Heat sensitive compounds, like proteins, could be processed with the triblock copolymers to films without degradation. We expect that many more block copolymers exist with unrevealed and, hence, untapped potential for baroplastic processing. Baroplastic processing saves energy, facilitates recycling, and enables the embedding of heat-sensitive compounds, like proteins. Therefore, baroplastic polymers exhibit a large potential for sustainable polymer processing and for design of functional of polymers.

**One-Sentence Summary:** PLLA-*b*-PEG-*b*-PLLA block copolymers show surprisingly baroplasticity and can be sustainably processed to films at ambient temperatures and elevated pressure.

**Main Text:** The state-of-the art technical method for the continuous processing of thermoplastic polymers is melt extrusion once plasticity is reached in the melt state (*1*), which is an energy intensive process. Importantly, chain entanglement is enhanced in the plastic state, which is important for the formation of polymer films, fibers, and engineered objects. Thermoplastic polymers include, for example, polyethylene, polypropylene, poly(ethylene terephthalate), polyamide 66, polylactide (PLA), poly(butylene adipate-*co*-terephthalate), and polycaprolactone. The thermal stability of polymers under shear conditions and their melt viscosity are most crucial for their melt processability. Similar criteria also apply for additives of melt-extruded polymers and may curtail the embedding of thermally sensitive compounds such as drugs, enzymes, pheromones, catalysts, or even living cells and bacteria. The introduction of these agents is, however, desirable as they add highly valuable functionality to polymers. To date, the processing of thermolabile compounds with polymers has been mostly restricted to solution or dispersion-based methods, such as film casting (*2*), electrospinning (*3*), and spray-drying (*4*). Due to the limitation and hurdles given by solution / dispersion-based methods, there is a strong interest in the hot melt processing of thermally sensitive compounds with thermoplastic polymers (*2,5-7*). Apart from the thermolability of additives, the energy required for the melt processing of polymers and the microplastic debris caused by polymers calls for alternatives to decrease the carbon footprint and environmental pollution.

Against this backdrop, we found that polylactide-*block*-poly(ethylene glycol)-*block*-polylactide (PLA-*b*-PEG-*b*-PLA) block copolymers unexpectedly show plasticity far below their melting point at elevated pressure. The phenomenon of processability under high pressure far below the melting point has been defined as baroplasticity (*8,9*) which is different from a sintering process (*10,11*). Some block copolymers were reported to display baroplastic properties (*8,9,12,13*) including enzymatically degradable polyesters with blended protein, which requires a special synthesis approach (*14*). The PLA-*b*-PEG-*b*-PLA represents a well-known polymer class, which can be synthesized on a large scale in widely varying derivatives, and is therefore, of technical interest for numerous applications in the fields of medicine, pharmacy, agriculture, and packaging. We found surprisingly that some PLA-*b*-PEG block copolymers show baroplasticity. In order to gauge the structural requirements for the baroplasticity of PLA-*b*-PEG block copolymers in general, we systematically synthesized a series of block copolymers and analyzed their potential for film formation under baroplastic conditions (ambient temperature/elevated pressure). Film formation under baroplastic conditions in combination with acceptable mechanical properties depends greatly on the structure and composition of the different blocks whereas higher temperature/pressure just reduce the time required for film formation (not reported in detail here). The PLLA-*b*-PEG-*b*-PLLA with similar LA/EG ratio displayed good formability, and the tensile test of the obtained films showed similar behavior to the high-temperature processed film.

Understanding the requirements for baroplastic polymers will pave the way towards a large variety of different block copolymers different from PLA-*b*-PEG. Novel polymers of that kind stand to provide ample opportunities for applications, sustainable processing, and recycling as a future class of engineering plastics. In order to assess the potential of baroplastic PLA-*b*-PEG block copolymers for the functionalization with heat-sensitive additives, we encapsulated proteins in PLA-*b*-PEG block copolymers and assayed their functionality after baroplastic processing.

Details of the PLA-*b*-PEG block copolymer synthesis and characterization are provided in the supplementary material (fig. S1-S6). Only poly(*L*-lactide)-based PLLA-*b*-PEG-*b*-PLLA triblock

copolymers showed processability under baroplastic conditions which result in polymer films with decent mechanical properties (Table S1), depending on the length of the PLLA block. By contrast, examples of poor film formation are given in fig. S7. Dogbone test specimens of the block copolymer $PLLA_{85}$-*b*-$PEG_{182}$-*b*-$PLLA_{85}$ (Fig. 1A) processed at 37 °C/10 MPa/5 min (baroplastic conditions) showed the same strength but much higher toughness (95) than the sample processed at 135 °C/10MPa/5 min (22, Fig. 1B). The analysis by small-angle (fig. S8-S10) and wide-angle X-ray diffraction (XRD, Fig. 1C) and differential scanning calorimetry (DSC) showed relatively small crystallites formed by the PEG block (Fig. 1D). This observation is quantitatively confirmed by the comparison of the heat of the fusion of the hot-pressed (135 °C, heat of fusion PEG block = 23.6 J/g), the cold-pressed (37 °C, heat of fusion PEG block = 3.7 J/g), and the as-precipitated sample (heat of fusion PEG block = 17 J/g). The strong heating exotherm in the first heating ramp of the cold-pressed (37 °C) and as-precipitated samples indicate that the PLLA block was in the crystallized state upon processing (Fig. 1D). By contrast, the hot-pressed sample showed no exotherm upon heating but a pronounced melting endotherm at 160 °C, indicating that the sample was already crystalline. It is noteworthy that shorter PLLA blocks in tri-block copolymers do not crystallize but still formed films under baroplastic conditions (fig. S11-S13).

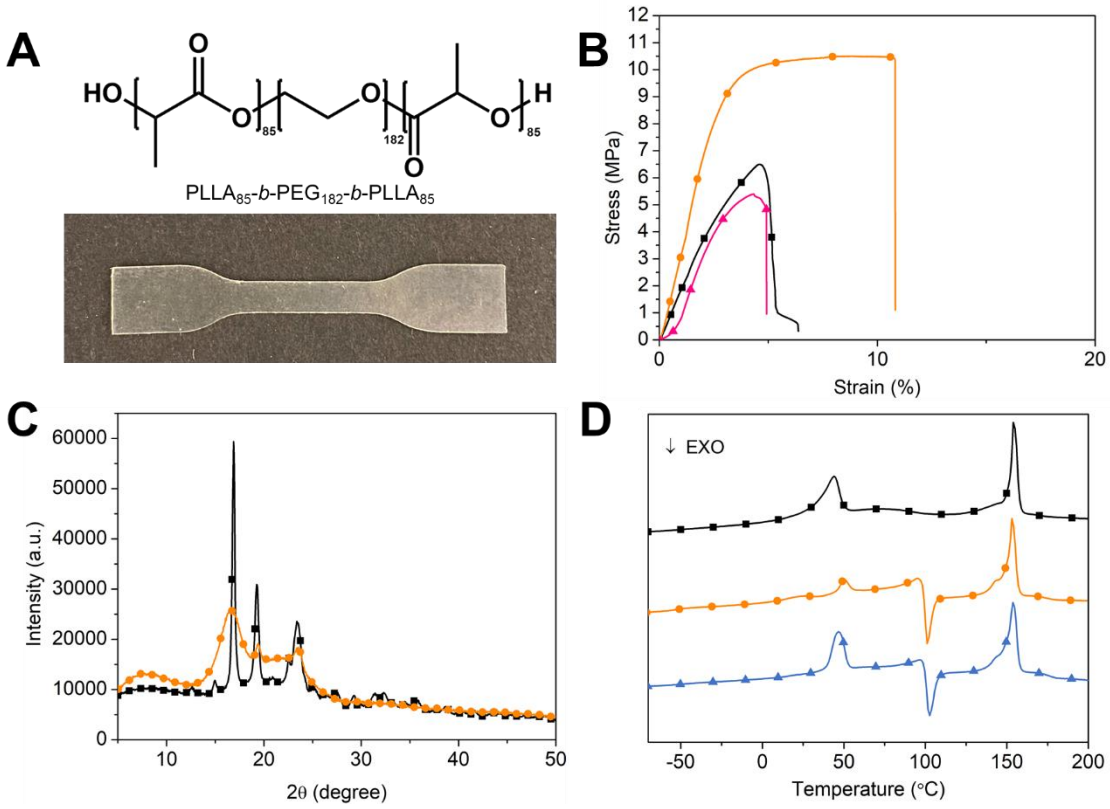


**Fig. 1. Structural analysis of $PLLA_{85}$-*b*-$PEG_{182}$-*b*-$PLLA_{85}$ (sample 20) pressed at different temperatures.** (**A**) Chemical formula of the $PLLA_n$-*b*-$PEG_{182}$-*b*-$PLLA_n$ (sample 18, sample 20, and sample 21, n = 68, 85, and 107, respectively) triblock copolymer (indices denote the degree of polymerization of the respective blocks) used for analysis and photograph of a dogbone sample pressed at 37 °C/10 MPa/5 min (sample 20, Table S1). (**B**) Comparison of stress-versus

strain of a $PLLA_{85}$-*b*-$PEG_{182}$-*b*-$PLLA_{85}$ dogbone sample obtained by pressing (10 MPa) at different temperatures (pink triangle line: pressed at 22 °C under 10 MPa for 14 h, orange dot line: pressed at 37 °C under 10 MPa for 14 h, and black square line: pressed at 135 °C under 10 MPa for 5 min). (**C**) Comparison of the XRD of $PLLA_{85}$-*b*-$PEG_{182}$-*b*-$PLLA_{85}$ dogbone sample obtained under different conditions (orange dot line: pressed at 37 °C under 10 MPa for 14 hand black square line: pressed at 135 °C under 10 MPa for 5 min). (**D**) Comparison of DSC traces (heating rate 10 K/min under nitrogen atmosphere, first heating run) of a $PLLA_{85}$-*b*-$PEG_{182}$-*b*-$PLLA_{85}$ dogbone sample obtained under different conditions (blue triangle line: as-precipitated powder, orange dot line: pressed at 37 °C under 10 MPa for 14 h and black square line: pressed at 135 °C under 10 MPa for 5 min).

We employed the yellow-fluorescent YPet and the enzyme proteinase K to assess the stability of proteins under baroplastic processing conditions. $PLLA_{107}$-*b*-$PEG_{182}$-*b*-$PLLA_{107}$ (sample 21) was used as a baroplastic probe, which is very similar to sample 20 used above, for all the following bio-related tests. The fluorescence analysis of YPet encapsulated in sample 21 processed at 37 °C under a pressure of 10 MPa for 5 min retained fluorescence (fig. S14A), whereas the sample annealed at the 135 °C for 5 minutes showed a near-complete loss of the yellow fluorescence (fig. S14B). The fluorescence lifetime of YPet (fig. S15) within the hot-pressed samples was essentially unchanged from that within to the baroplastic samples and the isolated protein (fig. S15, Table S3). This observation suggests that the loss of the fluorescence intensity reflects a deterioration of the vast majority of the proteins. Pure proteinase K powder incubated at 37 °C for 14 h, and powder pressed at 37 °C even under 35 MPa for 14 h showed no loss in enzymatic activity, as assessed by the reaction with proteolysis of a chromogenic substrate (*N*-Suc-Phe-Ala-Ala-Phe-pNA) (*15*) (Fig. 2A).

Powdered $PLLA_{107}$-*b*-$PEG_{182}$-*b*-$PLLA_{107}$ (sample 21) and proteinase K were mixed in a mass ratio of 19:1 and processed at 37 °C/10 MPa/5 min into a composite film to simulate processing conditions. We determined via the enzymatic assay above, that proteinase K retained activity and gradually leached out from the composite film (Fig. 2B and 2C). After 504 h, the activity of the leached proteinase K amounted to 40% of the activity of the enzyme used for the film preparation (Fig. 2D).

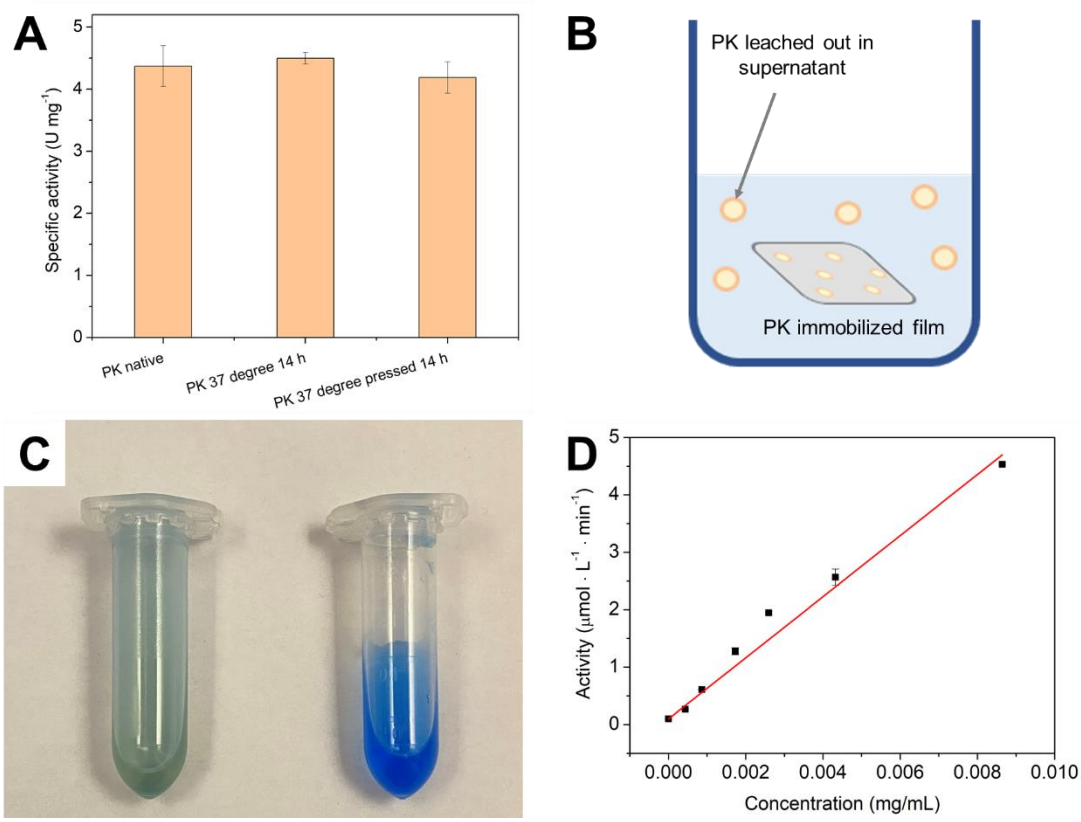


**Fig. 2. Proteinase K for processing.** (**A**) Plot of the specific activity of proteinase K (PK) powder for native proteinase K (first column), proteinase K powder annealed at 37 °C in air for 14 h (second column), and proteinase K powder pressed at 37 °C under 35 MPa for 14 h (third column). The specific activity was normalized by proteinase K concentration determined by absorption spectroscopy. (**B**) Schematic illustration of the proteinase K leaching test from sample 21. (**C**) Photograph of the Coomassie Brilliant Blue staining test with Tris buffer (left) and with Tris buffer / proteinase K leachate from $PLLA_{107}$-*b*-$PEG_{182}$-*b*-$PLLA_{107}$ (sample 21, right). The proteinase K-encapsulated film in Tris buffer solution was incubated at 37 °C. (**D**) Plot of the calibration of proteinase K activity vs. concentration of proteinase K in buffer solution. The value was fitted by linear fitting using OriginLab 8 (y = ax+b, where a = 531.79 µmol/(g · min), b = 0.10 µmol/(L · min), $R^2$ = 0.993). The function was used for the calculation of the concentration of proteinase K leachate from baroplastic film. The leachate of proteinase K is 0.3 mg/mL based on the calibration curve, which corresponds to 40% of active proteinase K leached out from sample 21 after 504 h. The leachate was diluted 100-fold before testing.

A potential environmental impact of the baroplastic polymer $PLLA_{107}$-*b*-$PEG_{182}$-*b*-$PLLA_{107}$ (sample 21, without encapsulated proteinase K) was probed by biodegradation experiments and compatibility studies with cells and aquatic organisms (fig. S17). Sludge water degradation showed slow biodegradation of sample 21, which is consistent with results previously published (*16*). The baroplastic film showed a somewhat faster degradation compared to the pristine powder of sample 21 (fig. S17 sludge water degradation). It is clear from our results obtained by sludge water degradation, that the current degradation rate is too slow and could lead to microplastic particle formation. More detailed investigations and material optimizations are

required here. Baroplastic films of sample 21 were also degraded by proteinase K in Tris buffer solution within 10 days. The degradation of sample 21 is fast, although the proteinase K is not an optimized enzyme for the degradation of PLLA-*b*-PEG-*b*-PLLA triblock copolymers which compares well with literature (*17,18*).

The unique processing behavior of baroplastic triblock copolymers also offers the potential of physical recycling at an ambient temperature. In fact, the latter should prevent the formation of unwanted degradation products due to the lower thermal stress of the polymer. We did the physical recycling of our triblock copolymers films of $PLLA_{68}$-*b*-$PEG_{182}$-*b*-$PLLA_{68}$ (sample 18) by cryo-milling and pressing at 37 °C/10 MPa/14 h (Fig. 3). The molecular analysis of the recycled films by $^{1}H$ nuclear magnetic resonance spectroscopy showed no significant changes of the molecular parameters and formation of a film (fig. S18).

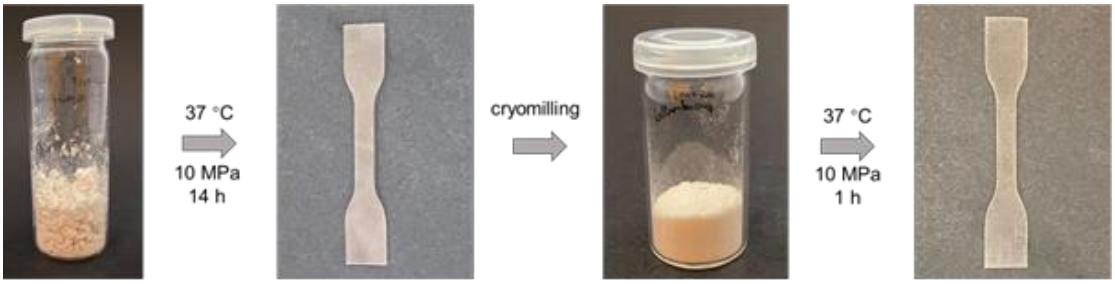


**Fig. 3. Recycling of $PLLA_{68}$-*b*-$PEG_{182}$-*b*-$PLLA_{68}$ (sample 18).** Photographs of the sample 18,pressed at 37 °C under 10 MPa for 16 h, the cryomilled powder of the film of sample 18 (milled for 30 s), and for the film of the cryomilled powder of sample 18 obtained by pressing at 37 °C under 10 MPa for 1 h. The films were cut by a hydraulic sample puncher to give dogbone shaped films.

Our results underpin the great potential of baroplastic polymers for sustainable polymer processing under ambient temperature. The use of lower processing temperatures in combination with recyclability under baroplastic conditions could delay the end of life of polymers and thereby contribute to the reduction of microplastic debris. The baroplastic properties are probably not restricted to the known baroplastic block copolymers but extend to other compounds. In fact, many block copolymers known already might be waiting for discovery as baroplastic polymers. Surely, many new baroplastic polymers could be designed following the general concept of covalently linking soft (low $T_g$) and hard (high $T_g$) blocks in appropriate ratio. The options for the design of baroplastic polymers are manifold and could be adapted well to technical needs. With this in mind, a class of polymers could be accessible which fulfills environmental demands and opens avenues for a wide range of functionalities by chemical or biological additives in combination with a sustainable processing approach.

Reference

1. D. G. Baird, D. I. Collias, *Polymer Processing: Principles and Design, 2nd Edition*. (Wiley, the United States of America, 2014).
2. S. Karki *et al.*, Thin films as an emerging platform for drug delivery. *Asian Journal of*

*Pharmaceutical Sciences* **11**, 559-574 (2016).
hdoi.org/10.1016/j.ajps.2016.05.004
3. A. Luraghi, F. Peri, L. Moroni, Electrospinning for drug delivery applications: A review. *Journal of Controlled Release* **334**, 463-484 (2021).
doi.org/10.1016/j.jconrel.2021.03.033
4. A. da S. Pereira, C. P. L. Souza, L. Moraes, G. C. Fontes-Sant'Ana, P. F. F. Amaral, Polymers as encapsulating agents and delivery vehicles of enzymes. *Polymers* **13**, 4061 (2021).
10.3390/polym13234061
5. Y. Zheng, J. K. Pokorski, Hot melt extrusion: An emerging manufacturing method for slow and sustained protein delivery. *WIREs Nanomedicine and Nanobiotechnology* **13**, e1712 (2021).
doi.org/10.1002/wnan.1712
6. H. Patil, R. V. Tiwari, M. A. Repka, Hot-Melt Extrusion: from theory to application in pharmaceutical formulation. *AAPS PharmSciTech* **17**, 20-42 (2016).
10.1208/s12249-015-0360-7
7. D. Douroumis, *Hot-Melt Extrusion: Pharmaceutical Applications*. (Wiley, United Kingdom, 2012).
8. A. V. G. Ruzette *et al.*, Phase behavior of diblock copolymers between styrene and n-alkyl methacrylates. *Macromolecules* **31**, 8509-8516 (1998).
10.1021/ma981055c
9. J. A. Gonzalez-Leon, M. H. Acar, S.-W. Ryu, A.-V. G. Ruzette, A. M. Mayes, Low-temperature processing of 'baroplastics' by pressure-induced flow. *Nature* **426**, 424-428 (2003).
10.1038/nature02140
10. T. Tomkovic, S. G. Hatzikiriakos, Rheology and processing of polytetrafluoroethylene (PTFE) paste. *The Canadian Journal of Chemical Engineering* **98**, 1852-1865 (2020).
doi.org/10.1002/cjce.23816
11. S.-W. Jin *et al.*, Preparation of polyimide powders via hydrothermal polymerization and post-heat treatment for application to compression-molding materials. *ACS Sustainable Chemistry & Engineering* **10**, 1910-1919 (2022).
10.1021/acssuschemeng.1c07621
12. Z. Lv *et al.*, Baroplastics with robust mechanical properties and reserved processability through hydrogen-bonded interactions. *ACS Applied Materials & Interfaces* **11**, 12008-12016 (2019).
10.1021/acsami.8b20676
13. J.-N. Qiao *et al.*, Baroplastics with ultrahigh strength and modulus via hydrogen-bonding interactions with agar. *ACS Applied Polymer Materials* **2**, 5550-5557 (2020).
10.1021/acsapm.0c00892
14. Y. Iwasaki, K. Takemoto, S. Tanaka, I. Taniguchi, Low-temperature processable block copolymers that preserve the function of blended proteins. *Biomacromolecules* **17**, 2466-2471 (2016).
10.1021/acs.biomac.6b00641
15. C. Xu *et al.*, Investigation of the thermal stability of proteinase K for the melt processing of poly(l-lactide). *Biomacromolecules* **23**, 4841-4850 (2022).
10.1021/acs.biomac.2c01008
16. K.-S. Kim, S. Chung, I.-J. Chin, M.-N. Kim, J.-S. Yoon, Crystallization behavior of biodegradable amphiphilic poly(ethylene glycol)-poly(L-lactide) block copolymers. *Journal of Applied Polymer Science* **72**, 341-348 (1999).
doi.org/10.1002/(SICI)1097-4628(19990418)72:3<341::AID-APP4>3.0.CO;2-D
17. C.-H. Wang, K.-R. Fan, G.-H. Hsiue, Enzymatic degradation of PLLA-PEOz-PLLA triblock

copolymers. *Biomaterials* **26**, 2803-2811 (2005).
doi.org/10.1016/j.biomaterials.2004.07.064
18. X. Li *et al.*, Self-accelerated biodegradation of electrospun poly(ethylene glycol)–poly(l-lactide) membranes by loading proteinase K. *Polymer Degradation and Stability* **93**, 618-626 (2008).
doi.org/10.1016/j.polymdegradstab.2008.01.003
19. S. Förster *et al.*, Calculation of scattering-patterns of ordered nano- and mesoscale materials. *Advances in Colloid and Interface Science* **163**, 53-83 (2011).
doi.org/10.1016/j.cis.2010.12.003
20. S. Michael, SAXSutilities, version 1.024, PyPI (2021);
https://doi.org/10.5281/zenodo.5825707.
21. E. Multamäki *et al.*, Optogenetic Control of bacterial expression by red light. *ACS Synthetic Biology* **11**, 3354-3367 (2022).
10.1021/acssynbio.2c00259
22. J. Baumann, Y. Sakka, C. Bertrand, J. Köser, J. Filser, Adaptation of the daphnia sp. acute toxicity test: miniaturization and prolongation for the testing of nanomaterials. *Environmental Science and Pollution Research* **21**, 2201-2213 (2014).
10.1007/s11356-013-2094-y
23. R. C. Team, R, version 4.2.0, CRAN (2022); https://www.R-project.org/.

**Acknowledgments:** The authors thank Rika Schneider for the help with the polymer synthesis and GPC measurements. The authors are indebted to Prof. Jürgen Köhler and Lisa Günther for fluorescence microcopy and fluorescence lifetime measurement of YPet. The authors thank Bavarian Polymer Institute Keylab: Electron and Optical Microscopy for the help with fluorescence microscopy and the Bavarian Polymer Institute Keylab: Small Scale Polymer Processing for the help with sample pressing.

**Funding:** Deutsche Forschungsgemeinschaft (DFG, German Research Foundation), CRC Microplastic, project number 391977956-SFB 1357.

**Author contributions:**

Conceptualization: CX, SA, AM, AG

Methodology: CX, DG, AR, JB, CL, HS

Investigation: CX, SR

Visualization: CX, CW

Funding acquisition: CL, SA, AM, AG

Project administration: AG

Supervision: HS, SA, AM, AG

Writing – original draft: CX, AG

Writing – review & editing: all authors

**Competing interests:** The authors declare no competing interests

**Data and materials availability:** All data are available in the main text or the supplementary materials.

**Supplementary Materials**

Materials and Methods

Supplementary Text

Figs. S1 to S18

Tables S1 to S3

Science
AAAS

# Supplementary Materials for

## Cool processing of triblock copolymers under pressure

Chengzhang Xu, Chengwei Yi, Dipannita Ghosh, Anja Ramsperger, Julian Brehm, Christian Laforsch, Holger Schmalz, Sabine Rosenfeldt, Seema Agarwal*, Andreas Möglich*, Andreas Greiner*

*Corresponding authors. Email: agarwal@uni-bayreuth.de, andreas.moeglich.uni-bayreuth.de, greiner@uni-bayreuth.de

**The PDF file includes:**

**Materials**

Dichloromethane (DCM, technical grade), diethyl ether (technical grade), stannous octoate ($Sn(Oct)_2$, Thermo Scientific, Germany), chloroform (VWR, Germany), aniline (≥99.5%, Carl Roth, Germany), native proteinase K (PK, lyophilized powder, from *T. album*, 28.9 kDa, GeneOn, Germany, stored at − 20 °C in a deep freezer), tris(hydroxymethyl)-aminomethane (Tris buffer, 1 M, pH 9.0 abcr, Germany), *N*-succinyl-alanine-alanine-proline-leucine-*p*-nitroanilide (*N*-Suc-Ala-Ala-Pro-Leu-pNA, Sigma Aldrich, Germany), and aniline (≥99.5%, Carl Roth, Germany) were used without further treatment. 1-Decanol (synthesis grade, Merck, Germany) was distilled before use. Poly(ethylene glycol) methyl ether 5000 (mPEG 5000, Sigma-Aldrich, Germany), poly (ethylene glycol) 8000 (PEG 8000, Sigma-Aldrich, Germany), poly (ethylene glycol) 20000 (PEG 20000, Sigma-Aldrich, Germany), *L*-lactide and *D, L*-lactide (PURASORB L, PURASOB DL, Corbion, Netherland) were dried under vacuum for 12 h before polymerization. Tris buffer was diluted to a concentration of 50 mM by purified water (Milli-Q® Reference A+), and the pH was adjusted to 8.6 by hydrochloric acid (37%, VWR, Germany). The *Daphnia magna* clone BL2.2 utilized in this study was initially sourced from a small pond (Oud Meren in Leuven, Belgium), and has been under continuous laboratory culture since 1997. The animals were reared in M4 medium under controlled conditions at 20 ± 0.5 °C, following a light-dark cycle of 16 h light and 8 h dark. The green algae *Acutodesmus obliquus* was fed *ad libitum*. Following the OECD guideline 202, the clone is regularly tested (minimum twice a year) for acute toxicity with sodium chloride for quality assurance and quality control. The resulting $EC_{50}$ (48 h) value of 4.925 µg/mL is in line to the clones used in other related studies and therefore suitable for testing the acute toxicity of various substances. The murine macrophage cell line J774A.1 (ACC170, DSMZ, Braunschweig, Germany), the human adenocarcinoma epithelial cell line Caco2 (ACC169, DSMZ, Braunschweig, Germany), and human macrophages derived from the differentiation of monocytic cells THP-1 (ACC16, DSMZ, Braunschweig, Germany) were passaged two (Caco2 and THP-1) or three (J774A.1) times per week to an appropriate number and cultured in T-75 culture flasks (Corning, New York, USA) under cell culture conditions (37 °C, 5% $CO_2$). The J774A.1 were cultured in 90% Dulbecco's Modified Eagle Medium (DMEM) + 10% h.i. fetal bovine serum (FBS), the Caco2 in 90% DMEM + 10% heat-inactivated FBS and the THP-1 in 80-90% Roswell Park Memorial Institute 1640 (RPMI 1640) + 10% heat-inactivated FBS. Before the experiments, the J774A.1 cells were scraped off the culture flask surfaces into the culture media, centrifuged (200 g, 2 min, 20 °C), and resuspended with 5 mL of cell culture medium in a Falcon tube (Corning, Corning, New York, USA). The Caco2 cells were washed with Dulbecco's Phosphate Buffer Saline (DPBS) and subsequently collected via trypsinization for 2 min at cell culture condition. The THP-1 suspension was passaged into new cell culture medium.

**Methods**

Polymerization

Ring-opening polymerization (ROP) was conducted in a flame-dried and argon-purged Schlenk tube. Different amounts of mPEG/PEG and lactide (Table S1) were dried under reduced pressure for 12 h, then 2.5 µL of $Sn(Oct)_2$ was added into the reaction mixture and the reaction temperature was kept at 140 °C for 6 h. After the reaction, the product was dissolved in DCM and precipitated in cold diethyl ether (cooled by ice bath at 0 °C). After filtration, the rest of solvent was removed by vacuum drying at 37 °C for 24 h.

Polymer characterization

Proton nuclear magnetic resonance ($^1H$ NMR) spectra of the polymers were recorded by a Bruker Ultrashield-300 spectrometer. $CDCl_3$ was used as solvent, and the signal of residual

non-deuterated solvent was used as internal standard. The thermal properties of the synthesized polymers were characterized by differential scanning calorimetry (DSC) performed on a NETZSCH DSC 204 F1 Phoenix at a rate of 10 K/min under a nitrogen atmosphere (flow rate 20 mL per min). Gel permeation chromatography (GPC) as conducted on a system equipped with a styrene-divinylbenzene (SDV) precolumn (particle size 5 μm, PSS Mainz), a SDV linear XL column (particle size 5 μm, PSS Mainz), and a refractive index detector (RI, Agilent Technologies). Samples were dissolved in $CHCl_3$ with toluene (HPLC grade) as an internal standard in a concentration of 2 mg/mL and filtered through a 0.22 μm polytetrafluoroethylene filter (BGB, China) before injection, and a flow rate of 0.5 mL/min was used for measurements. The calibration was done with narrowly distributed polystyrene standards (PSS calibration kit, PSS Standard Service). Wide-angle X-ray scattering (WAXS) experiments were carried out with a Bragg-Brentano geometry employing an Empyrean diffractometer equipped with a pixel detector using copper $K_\alpha$ ($\lambda = 0.15406$ nm) radiation by Malvern Panalytical BV. Small angle X-ray (SAXS) measurements were performed using a lab-based Ganesha AIR system (SAXSLAB/ Xenoc) equipped with a copper rotating anode (MicroMax 007HF by Rigaku Corporation with a wavelength of $\lambda = 1.54$ Å) and position-sensitive Pilatus detector (300K, Dectris LTd.). If needed, the 2D scattering patterns were converted to 1D profiles of $I(q)$ vs. $q$, where $q$ is given as $q = 4\pi/\lambda \cdot \sin(\theta/2)$ with $\theta$ being the scattering angle. Data treatment were performed with the software provided by the instrument for WAXS, and by the software packages SAXSutili-ties or for SAXS (*19*,*20*).

Protein expression and purification

The light-regulated pREDown-YPet system encoding YPet which was tagged with 6x histidine N-terminally was constructed as introduced before *(21)*. The pREDown-YPet plasmid was transformed chemically into the *E.coli* CmpX 13 strain. *E.coli* CmpX 13 cells containing pREDown-YPet were cultured by lysogeny broth (LB) medium supplemented with 50 μg/mL kanamycin at 37 °C and 225 rpm shaking in darkness. When the optical density at 600 nm reached 0.6, 660 nm light with 100 μW/cm intensity was applied to illuminate the cells for 18 h. The cultivation temperature was kept at 37 °C. After 18 h incubation, the cells were harvested by centrifugation and lysed by sonication. The lysate was separated by centrifugation and the supernatant was purified via $Co^{2+}$ immobilized metal ion affinity chromatography. The imidazole with gradient concentration from 20 to 500 mM was used to elute His-YPet protein. The elution fractions were analyzed by denaturing polyacrylamide gel electrophoresis (PAGE). Based on the purity and yield, fractions were pooled and dialyzed in Tris buffer (50 mM Tris/HCl, 20 mM NaCl, 5 mM β-mercaptoethanol, pH = 8.0) overnight at 4 °C. After dialysis, the YPet protein was dried into powders.

Polymer processing

Polymer films were pressed by a P/O Weber-H HDP300 hydraulic press. The samples were pressed at 10 MPa and either 22 °C, 37 °C, or 135 °C. The samples were placed between two sheets of reusable Teflon paper reinforced by glass fibers (High-tech-flon, Germany). After pressing, the film was cooled to room temperature using refluxing cooling water (22 °C, 1 MPa). When the block copolymer was processed together with YPet, a ratio of 99 / 1 (w/w) polymer/protein was used. YPet was coated on $PLLA_{107}$-*b*-$PEG_{182}$-*b*-$PLLA_{107}$ (sample 21) powder by an airbrush and the samples were pressed at 37 °C, and 135 °C as comparison.

Fluorescence microscope

For the fluorescence lifetime experiments, the commercial optical microscope MicroTime 200 (PicoQuant) was used. The setup accommodated a laser diode operated in pulsed mode

with a repetition rate of 20 MHz providing an excitation wavelength of 482 nm (LDH-D-C-485, PicoQuant). The spectral profile of the laser is cleaned using a bandpass filter ET480/20m (AHF/Croma), the radiation from the laser is directed into the main optical unit via a single mode optical fiber, and then reflected by a dichroic mirror (ZT405/485rpc, AHF/Croma) into an inverted confocal optical microscope, and focused onto the sample using an objective (MPLFLN100, NA = 0.9, Olympus). Fluorescence lifetime images were collected by scanning the focal spot across 150 μm × 150 μm on the sample using a galvo scanner (FLIMbee unit, PicoQuant). The signal from the sample is transmitted to the dichroic mirror, passes a long pass filter (488 LP Edge Basic, Semrock). The signal was detected by a single-photon counting avalanche diode (SPCM-AQRH-14-TR, Excelitas) and a time correlated single photon counting unit (TCSPC TimeHarp 260 PICO Dual, PicoQuant, temporal resolution of 250 ps) was used for time tagged time-resolved (TTTR) fluorescence data collection. The obtained transients were deconvoluted with the instrument response function and fitted using the commercial software SymPhoTime 64 (Picoquant).

Tensile test

$PLLA_{85}$-*b*-$PEG_{182}$-*b*-$PLLA_{85}$ (sample 20) was pressed by hydraulic press at 37 °C for 14 h at a pressure of 10 MPa. As comparison, a film was also pressed at 135 °C. To compare with diblock copolymer, $mPEG_{113}$-$PLLA_{247}$ (sample 7) was pressed at 37 °C and 70 °C for 48 h. The pressed films were cut by a hydraulic sample puncher according to DIN 53 504 S3A (Coesfeld Materialtest, Germany) for tensile test. The thickness of the test specimens was measured using a Series digital micrometer (0 – 25 mm, Mitutoyo, Neuss, Germany), taken average at 3 different points in the gauge area. The tensile test was performed using a tensile tester (BT1-FR0.5TN.D14, Zwick/Roell, Germany) at a rate of 0.2 mm/min at Young's modulus region and afterwards 1 mm/min.

Proteinase K activity test

Proteinase K powder was pressed at 37 °C under 35 MPa for 14 h. As comparison, proteinase K powder in a centrifuge tube was incubated in 37 °C water bath for 14 h. The both samples were dissolved in Tris buffer (50 mM tris(hydroxymethyl)aminomethane/HCl (pH 8.6) and 1 mM $Ca^{2+}$) and used for activity assay. The concentration of proteinase K was determined by Agilent 8435 diode-array spectrophotometer. The activity assay was performed in a 96-well clear microtiter plate in multi-mode microplate reader (CLARIOstar, BMG Labtech) using *N*-Suc-Ala-Ala-Pro-Leu-pNA as substrate. The activity was done at 25 °C, kinetic absorbance at 410 nm was recorded. The specific activity was calculated using Equation (1):

$$Specific\ activity = \Delta A/(\varepsilon \cdot h \cdot \Delta t \cdot C) \quad (1)$$

Where $\Delta A$ represents the difference of absorbance at $\lambda = 410$ nm relative to time zero, $\varepsilon$ is the molar extinction coefficient of *p*-nitroaniline at a wavelength of $\lambda = 410$ nm ($\varepsilon = 8800\ M^{-1}\ cm^{-1}$), $h$ is the thickness of the solution, $\Delta t$ is the monitoring time, and $C$ is the concentration of proteinase K in the solution.

Proteinase K leaching test

10 mg proteinase K powder was dissolved in 4 mL Tris buffer solution and mixed with 200 mg of sample 21 (table S1) powder. The mixture was freeze-dried for 24 h, and the dry

mixture was pressed at 37 °C under 10 MPa for 5 min. Then a piece of the pressed film with a weight of 30 mg was immersed in 2 mL Tris buffer and incubated at 37 °C in a water bath. After 504 h, the supernatant was taken out for proteinase K leaching test. The calibration curve of the proteinase K was done with proteinase K/Tris buffer solution at different concentrations. The concentration of the calibration samples was determined by UV absorbance at $\lambda = 280$ nm. The calibration curve was plotted with proteinase K activity vs. proteinase K concentration, fitted by OriginLab 8 software.

Wastewater degradation monitored by Micro-Oxymax

Sample 21 powder and film were tested for biodegradation in wastewater in triplicate for 42 days according to the test method based on DIN ISO 14851:2019. From the wastewater treatment plant at Bayreuth, activated sludge water (after nitrification) was collected and used in the test as an inoculum. Around 95 mg of sample was taken and added into the 100 mL test medium, consisting of a mixture of 95 mL standard medium, and 5 mL supernatant of the activated sludge. For blank measurements activated sludge in the same concentration was used and aniline was used as a positive control. The percentage production of $CO_2$ was monitored at different time intervals with Micro-Oxymax Respirometer (Columbus Instruments International, USA) using an IR $CO_2$ detector and the percentage of biodegradation was calculated according to the following Equation (2):

$$Biodegradation\% = \frac{(mgCO_2\ produced)_T - (mgCO_2\ produced)_B}{ThCO_2} \cdot 100\% \quad (2)$$

Where, $(mgCO_2\ produced)_T$ is the amount of $CO_2$ evolved in the test material flask in milligrams, and $(mgCO_2\ produced)_B$ is the amount of $CO_2$ evolved in the blank flask between the start to the end of the test, in milligrams. $ThCO_2$ is the theoretical amount of $CO_2$ evolved by the test material, expressed in milligrams, which is calculated by the following Equation (3):

$$ThCO_2 = Specimen\ (mg) \cdot \frac{TOC\%}{100} \cdot \frac{44}{12} \quad (3)$$

Where, 44 is the molar mass of $CO_2$ and 12 is the molar mass of C, *TOC%* is the carbon content of the test specimen determined by elemental analysis (CHNS elemental analyser vario EL cube, Elementar Analysensysteme GmbH, Langenselbold, Germany).

Daphnia acute toxicity test

The sample 21 was dispersed in M4 medium by a solvent replacement method to get particles with a size of 50 µm for *Daphnia* acute toxicity test with a final concentration of 60 mg/mL.

Third brood neonates (≤ 24h) were used for the experiment. These age-synchronized animals were randomly distributed into groups of five individuals, each placed in 10 mL of M4 medium within individual sample wells of a six-well plate. A total of 120 animals were subjected to exposure to five different concentrations of the sample 21 (31.25 µg/mL, 62.5 µg/mL, 125 µg/mL, 250 µg/mL, and 500 µg/mL + control (0 µg/mL)), each with four independent replicates. Following the OECD Guideline 202, no supplementary food was provided, and no medium exchanges were performed during the exposure period. The

experiment was extended to a duration of 96 h as recommended by Baumann et al. (*22*), with the animals being visually assessed for immobilization at 24, 48, and 96 h.

Alamar blue assay

The sample 21 was dispersed in MilliQ water by a solvent replacement method to get particles with a size of 50 µm for Alamar blue viability cell test to a final concentration of 60 mg/mL.

Three cell lines were used to test for potential cytotoxicity of the PLLA-*b*-PEG-*b*-PLLA triblock copolymer: the murine macrophage cell line J774A.1 (ACC170), the human adenocarcinoma epithelial cell line Caco2 (ACC169), and human macrophages derived from the differentiation of monocytic cells THP-1 (ACC16). Each cell line was counted using a hemocytometer (Neubauer improved, Brand, Wertheim, Germany). For each treatment, 6 sample wells of a 96 well plates (CellStar, Greiner Bio-One, Frickenhausen, Germany) for each cell line in 100 µL of the corresponding cell culture medium were tested. Since the cell lines have different proliferation rates the J774A.1 were seeded as 50,000 colony-forming unit and for Caco2 and THP-1 100,000 colony-forming unit were added and allowed to adhere under standard culture conditions (37 °C, 5% $CO_2$, humidified) overnight. The THP-1 were differentiated into macrophages using 100mM 12-O-tetradecanoylphorbol-13 acetate (TPA).

The cells were treated with increasing concentrations of the sample 21 suspension to 0 (control), 0.1, 1, 10, 100, 500 and 1000 µg/mL and with a 0.2% Triton X solution as a positive control treatment. The cells were incubated for 24 h under cell culture conditions, and subsequently, 10 µL of the Alamar blue dye (Invitrogen, ThermoFisher Scientific) was added and further incubated for 5 h. The well plates were measured at $\lambda = 530$-560 nm excitation and $\lambda = 590$ nm emission using a plate reader (Varioskan LUX, ThermoFisher Scientific). The experiments were performed three times and the data are shown as blank subtracted mean values of the three individual experiments in % in relation to control viability (≙ 100 %).

The statistical analysis was performed in R studio (*23*) using the packages “rstatix”, “stats”, and “rcompanion”. The data was tested for normal distribution and heteroskedacity and subsequently a Kruskal Wallis test with a Games Howell post hoc test was performed.

**Supplementary Text**

The molecular characteristics of PLLA, PDLLA, PEG, mPEG, and block copolymers are presented in Table S1.

**Table S1**. Molecular characterization of the synthesized block copolymers

| Sample | Polymer | Yield/ % | EG:LA (in feed, molar ratio) | EG:LA ($^1$H NMR integral ratio) | $\bar{M}_n$ ($^1$H NMR) | $\bar{M}_n$ (GPC) | $Đ$ |
|---|---|---|---|---|---|---|---|
| 1 | $mPEG_{113}$-*b*-$PDLLA_{46}$ | 78 | 113:90 | 113:46 | 8300 | 16600 | 1.17 |
| 2 | $mPEG_{113}$-*b*-$PDLLA_{134}$ | 82 | 113:150 | 113:134 | 14600 | 33500 | 1.36 |
| 3 | $mPEG_{113}$-*b*-$PDLLA_{178}$ | 81 | 113:200 | 113:178 | 17800 | 32400 | 1.33 |
| 4 | $mPEG_{113}$-*b*-$PDLLA_{291}$ | 88 | 113:300 | 113:291 | 25900 | 32600 | 1.57 |
| 5 | $mPEG_{113}$-*b*-$PDLLA_{384}$ | 88 | 113:400 | 113:384 | 32600 | 47900 | 1.68 |
| 6 | $mPEG_{113}$-*b*-$PLLA_{148}$ | 91 | 113:150 | 113:148 | 15600 | 24500 | 1.30 |
| 7 | $mPEG_{113}$-*b*-$PLLA_{247}$ | 89 | 113:250 | 113:247 | 22800 | 29600 | 1.52 |
| 8 | $PDLLA_{14}$-*b*-$PEG_{182}$-*b*-$PDLLA_{14}$ | 79 | 182:100 | 182:28 | 10000 | 34200 | 1.25 |
| 9 | $PDLLA_{49}$-*b*-$PEG_{182}$-*b*-$PDLLA_{49}$ | 61 | 182:180 | 182:98 | 15000 | 38800 | 1.14 |
| 10 | $PDLLA_{100}$-*b*-$PEG_{182}$-*b*-$PDLLA_{100}$ | 94 | 182:226 | 182:200 | 22400 | 35600 | 1.24 |
| 11 | $PDLLA_{117}$-*b*-$PEG_{182}$-*b*-$PDLLA_{117}$ | 86 | 182:300 | 182:234 | 24800 | 52500 | 1.16 |
| 12 | $PDLLA_{182}$-*b*-$PEG_{182}$-*b*-$PDLLA_{182}$ | 78 | 182:400 | 182:364 | 34200 | 35900 | 1.45 |
| 13 | $PDLLA_{236}$-*b*-$PEG_{182}$-*b*-$PDLLA_{236}$ | 81 | 182:500 | 182:472 | 42000 | 31300 | 1.86 |
| 14 | $PDLLA_{291}$-*b*-$PEG_{182}$-*b*-$PDLLA_{291}$ | 88 | 182:600 | 182:582 | 49900 | 73500 | 1.92 |
| 15 | $PLLA_{28}$-*b*-$PEG_{182}$-*b*-$PLLA_{28}$ | 75 | 182:100 | 182:56 | 12000 | 23200 | 1.09 |
| 16 | $PLLA_{58}$-*b*-$PEG_{182}$-*b*-$PLLA_{58}$ | 83 | 182:128 | 182:116 | 16300 | 29800 | 1.09 |
| 17 | $PLLA_{64}$-*b*-$PEG_{182}$-*b*-$PLLA_{64}$ | 78 | 182:180 | 182:128 | 17200 | 28300 | 1.12 |
| 18[a)] | $PLLA_{68}$-*b*-$PEG_{182}$-*b*-$PLLA_{68}$ | 76 | 182:180 | 182:136 | 17800 | 30800 | 1.10 |
| 19 | $PLLA_{71}$-*b*-$PEG_{182}$-*b*-$PLLA_{71}$ | 79 | 182:190 | 182:142 | 18200 | 29700 | 1.12 |
| 20 | $PLLA_{85}$-*b*-$PEG_{182}$-*b*-$PLLA_{85}$ | 96 | 182:180 | 182:170 | 20200 | 34400 | 1.12 |
| 21 | $PLLA_{107}$-*b*-$PEG_{182}$-*b*-$PLLA_{107}$ | 96 | 182:226 | 182:214 | 23400 | 45700 | 1.14 |
| 22 | $PLLA_{182}$-*b*-$PEG_{182}$-*b*-$PLLA_{182}$ | 91 | 182:400 | 182:364 | 34200 | 76300 | 1.09 |
| 23 | $PLLA_{35}$-*b*-$PEG_{455}$-*b*-$PLLA_{35}$ | 87 | 455:100 | 455:70 | 25000 | 44900 | 1.09 |
| 24 | PDLLA | 64 | - | - | - | 20300 | 1.68 |
| 25 | PLLA | 88 | - | - | - | 10600 | 1.90 |

a) precipitated in cold diethyl ether/methanol (volume ratio 1:1)

**Table S2**. Thermal properties of the synthesized PLA-*b*-PEG block copolymers

| Sample | Polymer | $T_m$ (PEG)/ °C | $T_g$ (PLA)/ °C | $T_m$ (PLA)/ °C |
|---|---|---|---|---|
| 1 | $mPEG_{113}$-*b*-$PDLLA_{46}$ | 56 | - | - |
| 2 | $mPEG_{113}$-*b*-$PDLLA_{134}$ | 54 | - | - |
| 3 | $mPEG_{113}$-*b*-$PDLLA_{178}$ | 53 | - | - |
| 4 | $mPEG_{113}$-*b*-$PDLLA_{291}$ | 53 | - | - |
| 5 | $mPEG_{113}$-*b*-$PDLLA_{384}$ | 54 | - | - |
| 6 | $mPEG_{113}$-*b*-$PLLA_{148}$ | 56 | - | 163 |
| 7 | $mPEG_{113}$-*b*-$PLLA_{247}$ | 56 | - | 170 |
| 8 | $PDLLA_{14}$-*b*-$PEG_{182}$-*b*-$PDLLA_{14}$ | 55 | - | - |
| 9 | $PDLLA_{49}$-*b*-$PEG_{182}$-*b*-$PDLLA_{49}$ | 53 | - | - |
| 10 | $PDLLA_{100}$-*b*-$PEG_{182}$-*b*-$PDLLA_{100}$ | 52 | - | - |
| 11 | $PDLLA_{117}$-*b*-$PEG_{182}$-*b*-$PDLLA_{117}$ | 51 | - | - |
| 12 | $PDLLA_{182}$-*b*-$PEG_{182}$-*b*-$PDLLA_{182}$ | 51 | - | - |
| 13 | $PDLLA_{236}$-*b*-$PEG_{182}$-*b*-$PDLLA_{236}$ | 50 | - | - |
| 14 | $PDLLA_{291}$-*b*-$PEG_{182}$-*b*-$PDLLA_{291}$ | 52 | - | - |
| 15 | $PLLA_{28}$-*b*-$PEG_{182}$-*b*-$PLLA_{28}$ | 56 | - | - |
| 16 | $PLLA_{58}$-*b*-$PEG_{182}$-*b*-$PLLA_{58}$ | 50 | - | 141 |
| 17 | $PLLA_{64}$-*b*-$PEG_{182}$-*b*-$PLLA_{64}$ | 53 | - | 141 |
| 18 | $PLLA_{71}$-*b*-$PEG_{182}$-*b*-$PLLA_{71}$ | - | - | 141 |
| 19 | $PLLA_{85}$-*b*-$PEG_{182}$-*b*-$PLLA_{85}$ | 47 | - | 154 |
| 20 | $PLLA_{107}$-*b*-$PEG_{182}$-*b*-$PLLA_{107}$ | 47 | - | 157 |
| 21 | $PLLA_{182}$-*b*-$PEG_{182}$-*b*-$PLLA_{182}$ | - | - | 164 |
| 22 | $PLLA_{35}$-*b*-$PEG_{455}$-*b*-$PLLA_{35}$ | 61 | - | - |
| 23 | PDLLA | - | 54 | - |
| 24 | PLLA | - | 62 | 160 |

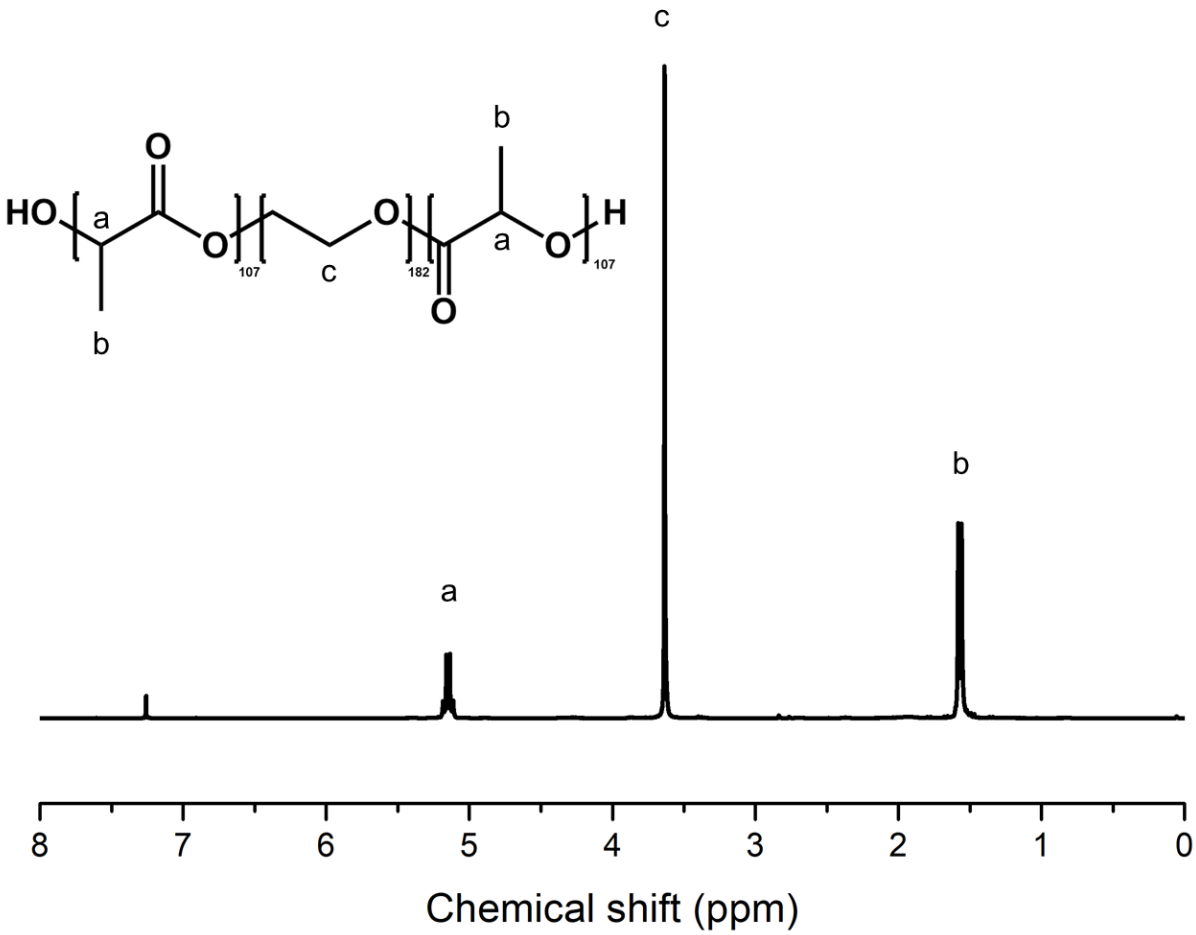


**Fig. S1. $^{1}$H NMR spectrum for triblock copolymers with PLA$_{107}$-*b*-PEG$_{182}$-*b*-PLA$_{107}$ (sample 21) as representative**. The as-precipitated sample was dissolved in $CDCl_3$, and the signal of residual non-deuterated solvent was used as internal standard. The characteristic peaks for the PLLA block (1.6 ppm, 5.1 ppm) and for the PEG block (3.6 ppm) of mPEG-*b*-PLA were clearly identified. The spectra of all diblock and triblock copolymers are shown in Fig. S2-S5. The composition of EG/*L*-LA (ethylene glycol/*L*-lactic acid repeating unit) of block copolymer is calculated based on Equation S4-S6:

$$I_{LA} = I_a \tag{4}$$

$$I_{EG} = I_c/4 \tag{5}$$

$$n_{LA} = \frac{I_{LA}}{I_{EG}} \bullet n_{EG} \tag{6}$$

Where $n_{LA}$ is the number of repeating units of *L*-lactic acid, $n_{EG}$ is the number of repeating unit of ethylene glycol calculated from the given $M_n$ of PEG precursors, $I_{LA}$ is the calculated integral of the proton in methine group of lactic acid repeating unit, $I_{EG}$ is the integral in the methylene groups in the ethylene glycol repeating unit normalized by 4 protons, $I_a$ is the integral of NMR peak at 5.1 ppm, $I_c$ is the integral of NMR peak at 3.6 ppm. The composition for all other block copolymers were calculated accordingly. The code for the assignment of the different block copolymers is given by the subscript for the particular block copolymers. The

experimental composition of most of the block copolymers compares well to the composition in feed for all educts except for mPEG$_{113}$-*b*-PDLLA$_{46}$, PDLLA$_{14}$-*b*-PEG$_{182}$-*b*-PDLLA$_{14}$, and for PDLLA$_{49}$-*b*-PEG$_{182}$-*b*-PDLLA$_{49}$ (Table S1). The reason for the deviation of the feed and experimental ratio could be explained by the extraction of unreacted mPEG homopolymer or block copolymers with short PLA blocks or sublimation lactide during polymerization. The number average molecular weights ($\bar{M}_n$) of the block copolymer were calculated based on $^1$H NMR (Equation 7).

$$\bar{M}_n = 72\ g/mol \bullet n_{LA} + \bar{M}_{n\,(PEG)} \tag{7}$$

Where 72 g/mol is the molar mass of LA repeating unit. $M_{n(PEG)}$ is the molecular weight of either PEG (8000/20000) or mPEG (5000) used as *co*-initiator. The molecular weight of block copolymers calculated from NMR ranges from 8300 to 49900. NMR result also shows that in order to reach the expected composition, it is necessary to use an over stoichiometry of equivalent of LA fraction with respect to the PEG or mPEG fraction.

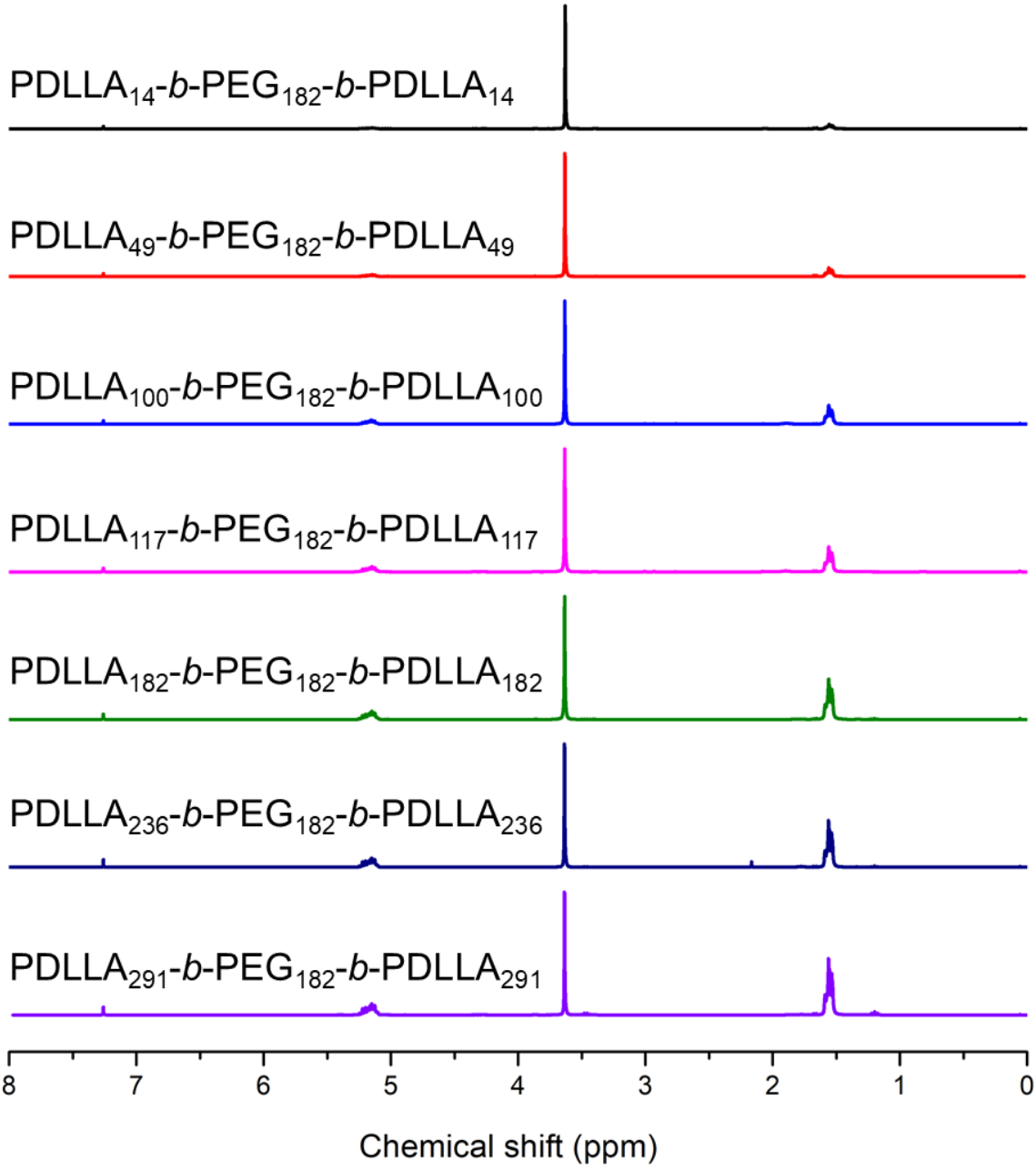


**Fig. S2. $^{1}$H NMR spectra of PDLLA-*b*-PEG-*b*-PDLLA triblock copolymers.** The as-precipitated samples were dissolved in $CDCl_3$, and the signal of the residual non-deuterated solvent was used as internal standard.

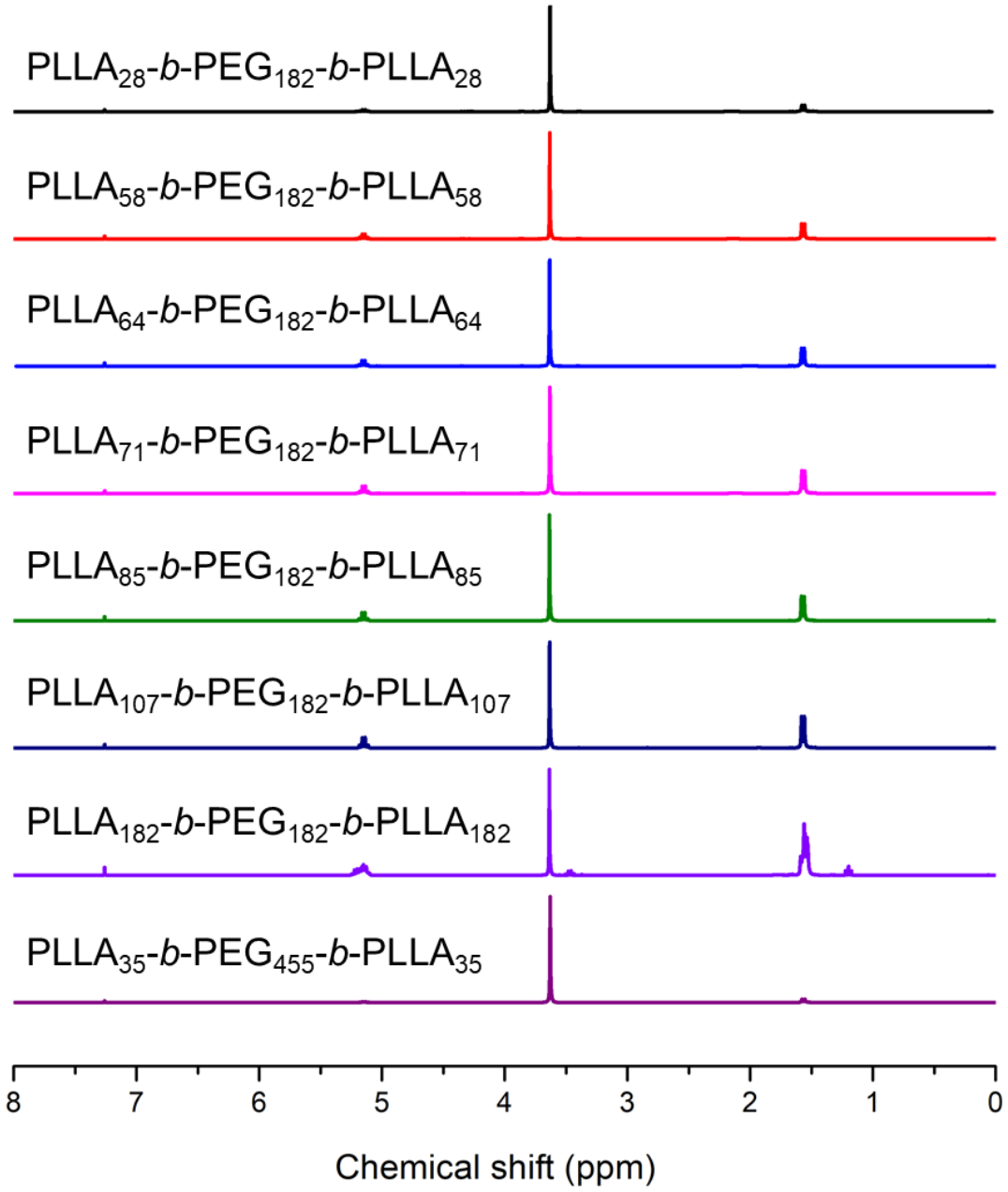


**Fig. S3. $^{1}$H NMR spectra of PLLA-*b*-PEG-*b*-PLLA triblock copolymers.** The as-precipitated samples were dissolved in $CDCl_3$, and the signal of residual non-deuterated solvent was used as internal standard.

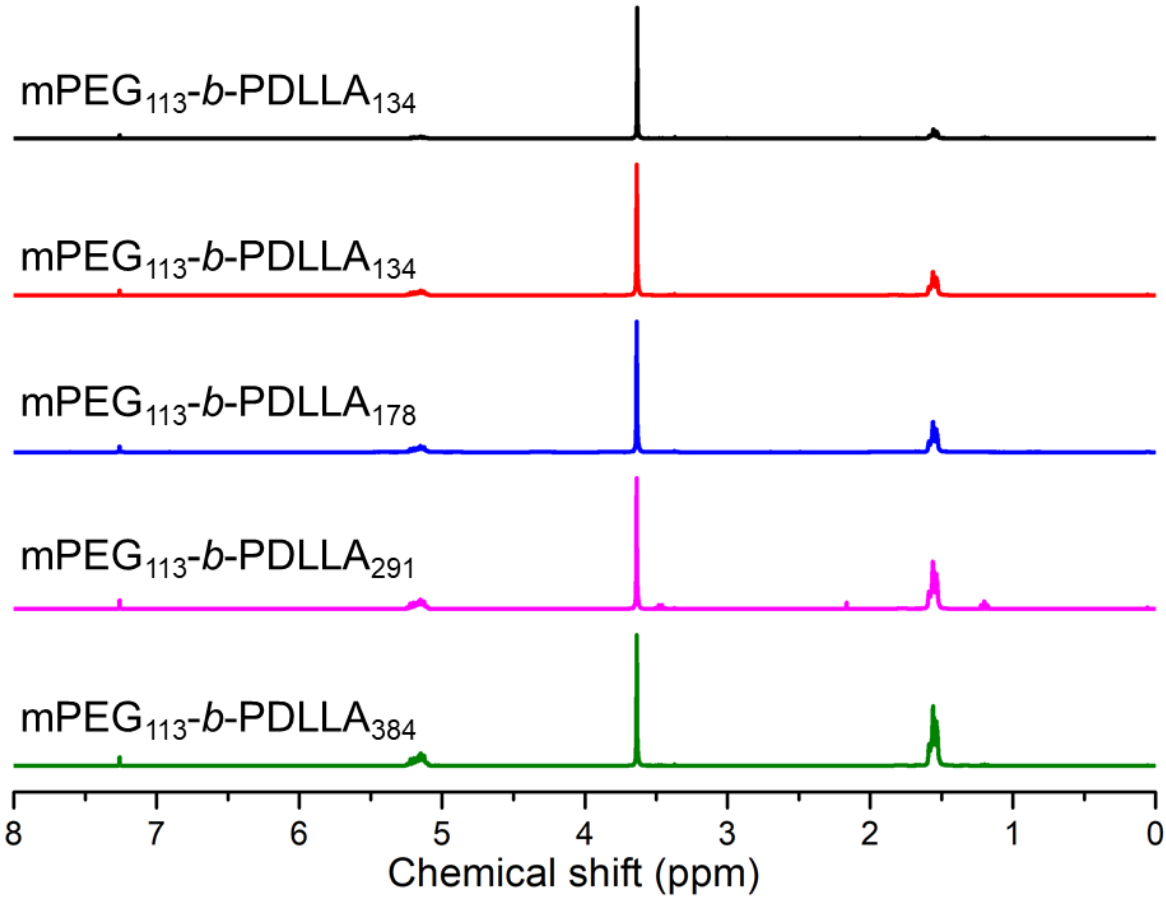


**Fig. S4. $^{1}$H NMR spectra of mPEG-*b*-PDLLA diblock copolymers.** The as-precipitated samples were dissolved in $CDCl_3$, and the signal of residual non-deuterated solvent was used as internal standard.

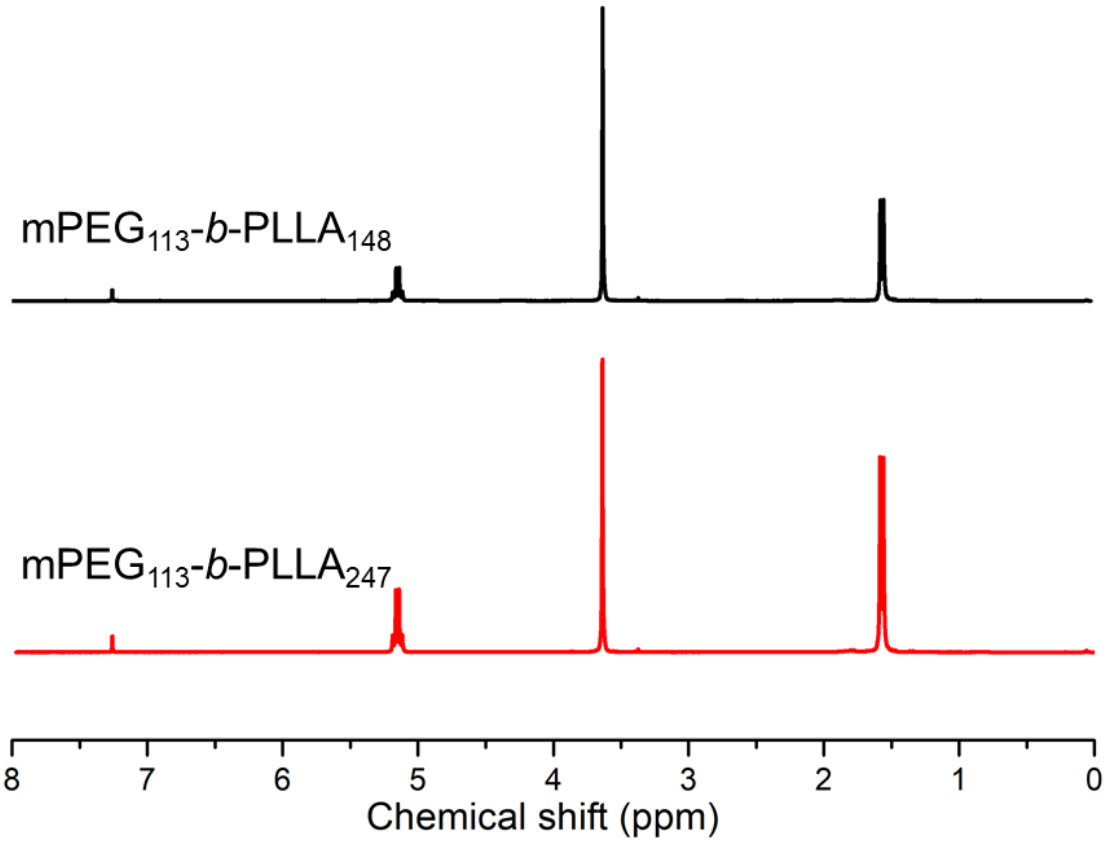


**Fig. S5. $^{1}$H NMR spectra of mPEG-PLLA diblock copolymers.** The as-precipitated samples were dissolved in $CDCl_3$, and the signal of residual non-deuterated solvent was used as internal standard.

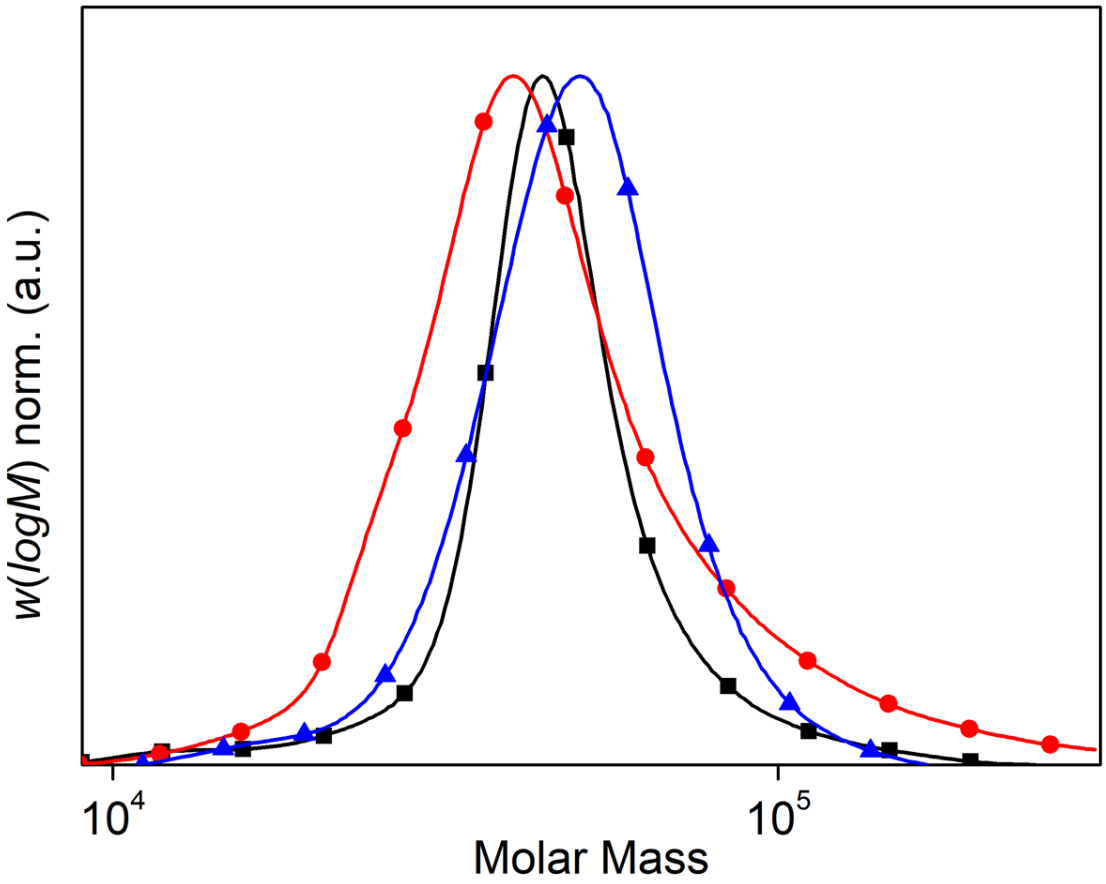


**Fig. S6. Apparent molecular weight distribution of representative block copolymers.** Normalized molecular weight distributions of the mPEG$_{113}$-*b*-PDLLA$_{134}$ (sample 2, black square) diblock, as well as PDLLA$_{117}$-*b*-PEG$_{182}$-*b*-PDLLA$_{117}$ (sample 11, red dot), and PLLA$_{107}$-*b*-PEG$_{182}$-*b*-PLLA$_{107}$ (sample 21, blue triangle) triblock copolymers as determined by GPC. The molecular weight of the block copolymers based on GPC are significantly higher as compared to the molecular weight obtained by $^{1}$H NMR data, which could be explained by the calibration of the GPC against polystyrene standards. The GPC traces of all block copolymers (representatively shown in Fig. S6) are unimodal with relatively low dispersity, which supports the block copolymer structure.

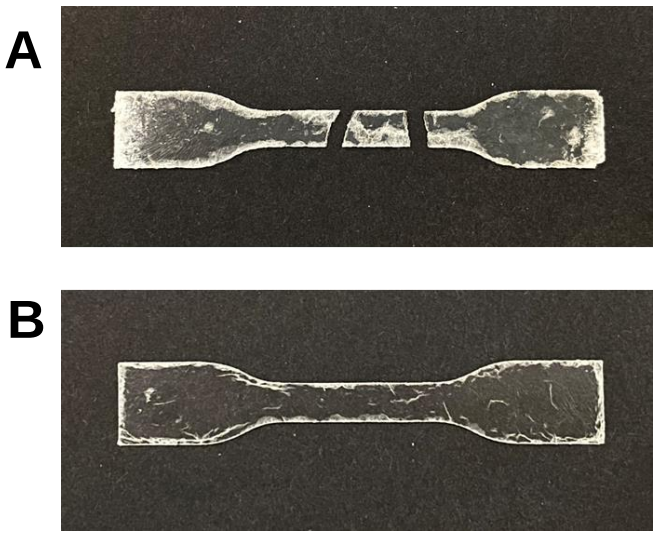


**Fig. S7. Dogbone samples.** (**A**) mPEG$_{113}$-*b*-PLLA$_{247}$ (sample 7) pressed at 37 °C under 10 MPa for 48 h. (**B**) mPEG$_{113}$-*b*-PLLA$_{247}$ (sample 7) pressed at 70 °C under 10 MPa for 48 h. Cracks were generated during the punching of the both dogbone specimens. Dogbone specimen shown in (A) broke into pieces during punching.

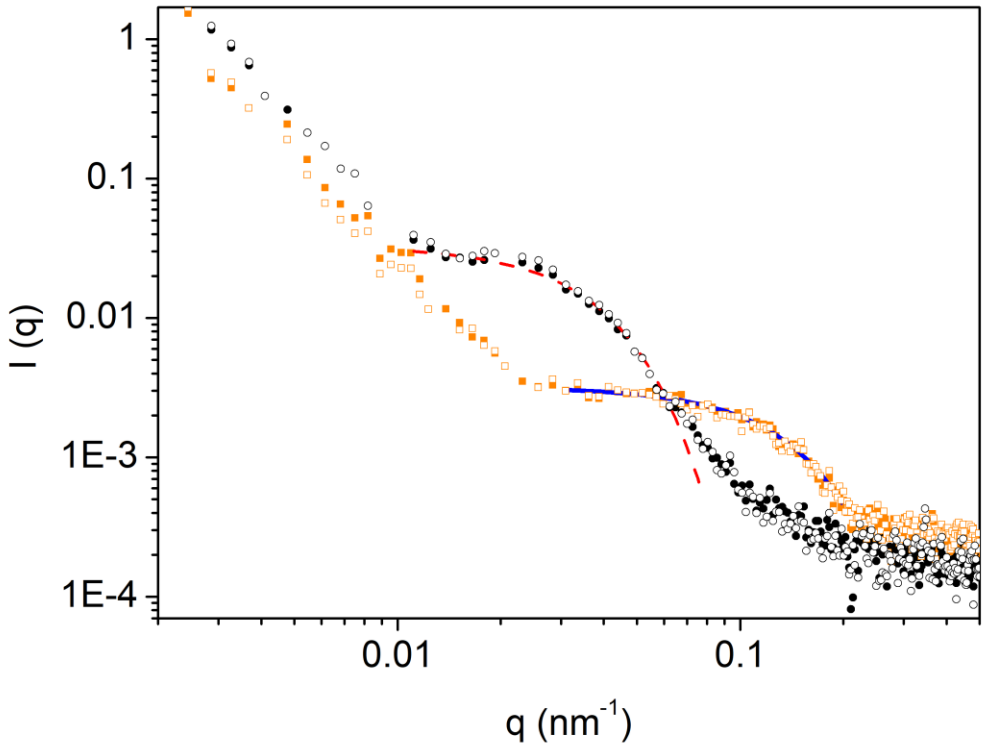


**Fig. S8: SAXS data with beam at different directions relative to film plane.** SAXS data of $PLLA_{85}$-*b*-$PEG_{182}$-*b*-$PLLA_{85}$ (sample 20) after pressing at different temperatures (black circles: film pressed at 135 °C under 10 MPa for 5 min, orange squares: film pressed at 37 °C under 10 MPa for 14 h). The data were taken with X-ray beam parallel (open symbols) or perpendicular (filled symbols) to the main film surface. The red dashed line is fitting curve of film pressed at 135 °C, and blue line is fitting curve of film pressed at 37 °C, both under 10 MPa pressure for 14 h. As consequence in a PLLA-*b*-PEG-*b*-PLLA triblock copolymer where PLLA and PEG are covalently bounded, the phase segregation may change dramatically with temperature. Small angle X-ray scattering (SAXS) with x-ray beam parallel or perpendicular to the film surface was performed to investigate the possibility of block segregation in $PLLA_{85}$-*b*-$PEG_{182}$-*b*-$PLLA_{85}$ films (see Fig. 1C and Fig. S8). The radial averaged intensities (1D SAXS) are independent from the beam-sample geometry. The scattering intensities show a $q^{-3}$ power law at low q and a shoulder at intermediate $q$ values. The $q^{-3}$ scaling hints to the existence of a pore-like structure in the nano- and mesoscale, whereas the shoulder is characteristic for an immiscible block (here PEG in PLLA). In a first approximation the averaged size of the PEG blocks may be described by Guinier's law using a radius of gyration of $R_g$ = 12 nm for film 37 and of $R_g$ = 45 nm for film pressed at 135 °C. These values correspond to the radius of a sphere of $R$ = 15 nm for film pressed at 37 °C and $R$ = 58 for film pressed at 135 °C, respectively based on Equation (8):

$$R_g^2 = (3/5)R^2 \qquad (8)$$

Therefore, we conclude that indeed a phase separation took place, leading to significant smaller PEG aggregated in film pressed at 37 °C (compared to film pressed at 135 °C). Unfortunately, due to the low contrast and bad signal to noise ratio, the determination of the exact geometrical structure of the PEG pre-aggregates from the corresponding 2D patterns is beyond scope, but the 2D SAXS obtained in parallel beam geometry points to an anisometric

structure (exemplarily shown for film pressed at 37 °C and 135 °C in Fig. S9 and S10, where this feature is most pronounced).

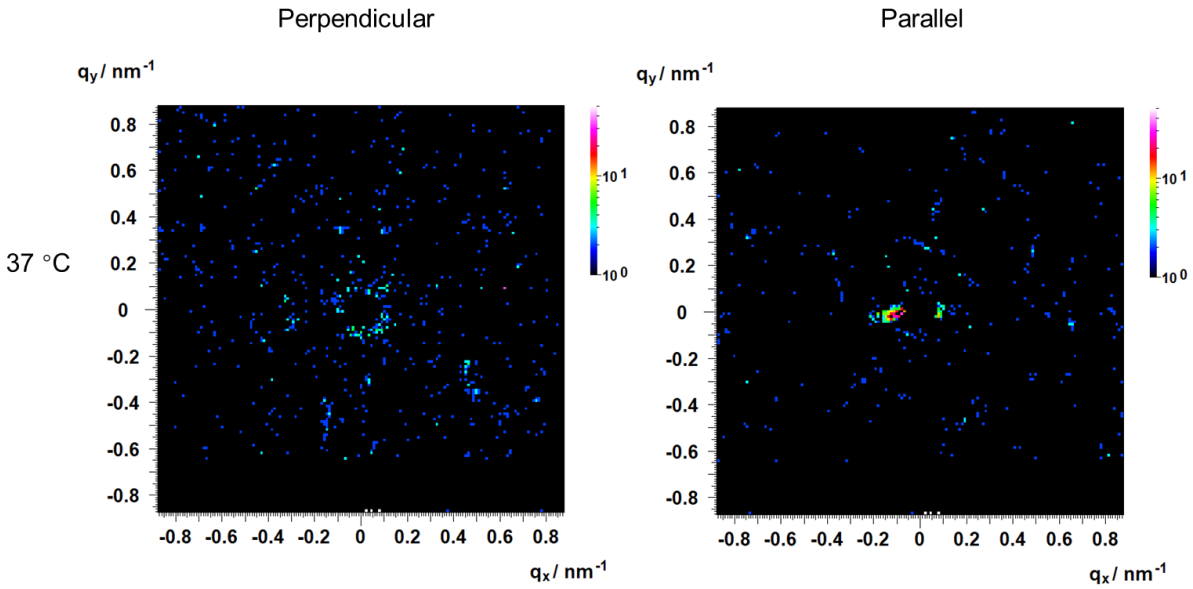


**Fig. S9: 2D SAXS intensities with beam at different directions relative to film plane.** SAXS intensities of PLLA$_{85}$-*b*-PEG$_{182}$-*b*-PLLA$_{85}$ (sample 20) film pressed at 37 °C under 10 MPa for 14 h. The data are taken with X-ray beam perpendicular (left, isotropic) and parallel (right, anisotropic) to the main film surface. The scattering contribution of air is subtracted. The differences between both pattern points to an anisotropic feature inside the sample, as it may for example result from worm-like or lamellar substructures inside the sample.

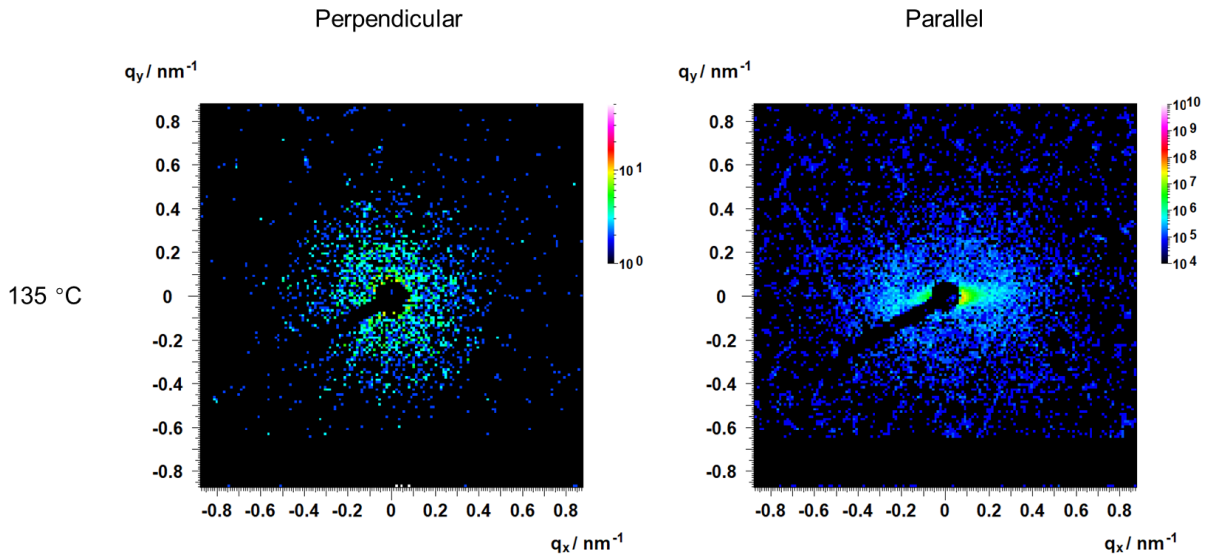


**Fig. S10: 2D SAXS intensities with beam at different directions relative to film plane.** SAXS intensities of PLLA$_{85}$-*b*-PEG$_{182}$-*b*-PLLA$_{85}$ (sample 20) film pressed at 135 °C under 10 MPa for 5 min. The data are taken with X-ray beam perpendicular (left, isotropic) and parallel (right, anisotropic) to the main film surface. The scattering contribution of air is subtracted. The differences between both pattern points to an anisotropic feature inside the sample, as it may for example result from worm-like or lamellar substructures inside the sample.

The glass transition temperatures and melting points of the block polymers were studied by DSC. The respective DSC are shown in Fig. S11-13. The results are summarized in Table S1.

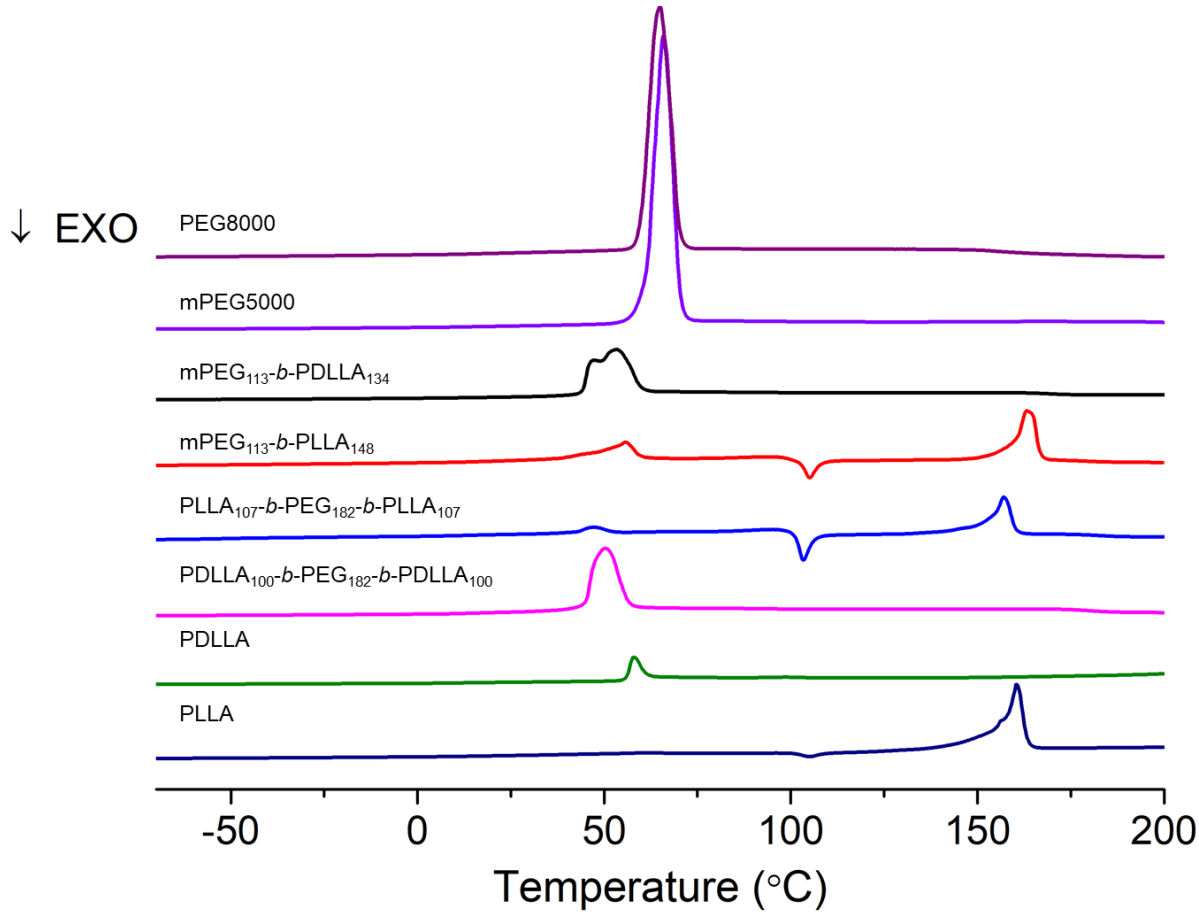


**Fig. S11**. **First heating curves of the polymers.** DSC thermograms of PEG8000, mPEG5000, mPEG$_{113}$-*b*-PDLLA$_{134}$ (sample 2, black), mPEG$_{113}$-*b*-PLLA$_{148}$ (sample 6, red), PLLA$_{107}$-*b*-PEG$_{182}$-*b*-PDLLA$_{107}$ (sample 21, blue), PDLLA$_{100}$-*b*-PEG$_{182}$-*b*-PDLLA$_{100}$ (sample 10, magenta), PDLLA (sample 24, green), and PLLA (sample 25, navy). Measurements were performed at a rate of 10 K/min under a nitrogen atmosphere with 20 mL per min flow.

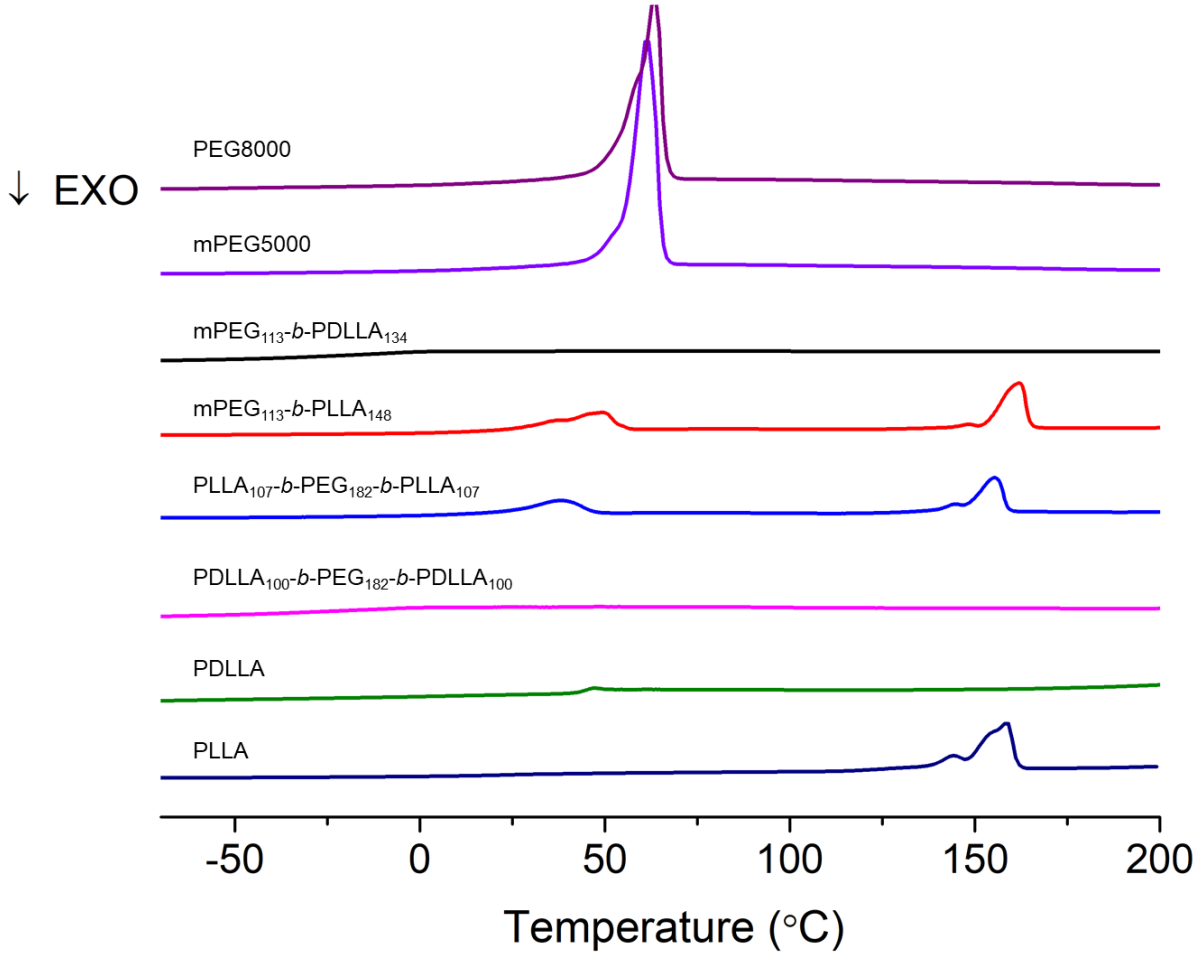


**Fig. S12. Second heating curves of the polymers.** DSC thermograms of PEG8000, mPEG5000, mPEG$_{113}$-PDLLA$_{134}$ (sample 2, black), mPEG$_{113}$-*b*-PLLA$_{148}$ (sample 6, red), PLLA$_{107}$-*b*-PEG$_{182}$-*b*-PDLLA$_{107}$ (sample 21, blue), PDLLA$_{100}$-*b*-PEG$_{182}$-*b*-PDLLA$_{100}$ (sample 10, magenta), PDLLA (sample 24, green), and PLLA (sample 25, navy).

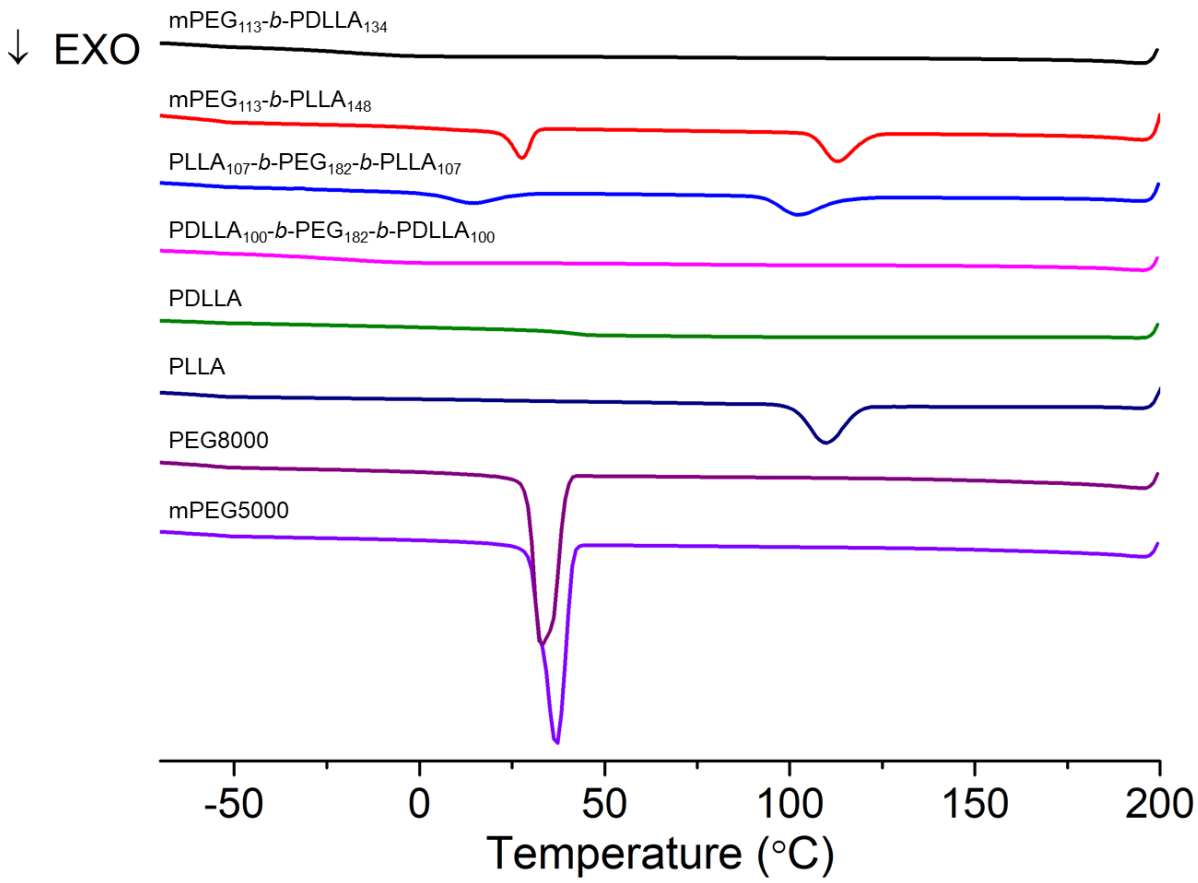


**Fig. S13. First cooling curves of the polymers.** DSC thermograms of $mPEG_{113}$-*b*-$PDLLA_{134}$ (sample 2, black), $mPEG_{113}$-*b*-$PLLA_{148}$ (sample 6, red), $PLLA_{107}$-*b*-$PEG_{182}$-*b*-$PDLLA_{107}$ (sample 21, blue), $PDLLA_{100}$-*b*-$PEG_{182}$-*b*-$PDLLA_{100}$ (sample 10, magenta), PDLLA (sample 24, green), PLLA (sample 25, navy), PEG8000, and mPEG5000.

Protein encapsulation in baroplastic

To assess the functionality of the YPet protein within the polymer film after pressing/heating treatment, measuring the fluorescence lifetime of the protein can provide valuable insights. This parameter is sensitive to the local environment of the fluorescence unit and therefore to the conformation of the protein.

If the native conformation of the protein is preserved within the polymer film, it is highly likely that neither the fluorescence quantum yield (i.e. the emitted intensity) nor the fluorescence lifetime will change significantly. In contrast, for a denatured protein it is expectable that these parameters will be altered.

The lifetimes extracted from the data in fig. S14 of the YPet protein in film are similar to the one of the native YPet powder (see Table S3). The decrease of the fluorescence intensity of the pressed film at 135 °C under 10 MPa for 5 min suggests that only a minority of the proteins remains intact and contributes to the signal.

**Table. S3.** Fluorescence lifetime of native YPet powder and YPet-immobilized $PLLA_{107}$-*b*-$PEG_{182}$-*b*-$PLLA_{107}$ (sample 21) pressed film at 37 °C and at 135 °C under 10 MPa pressure for 5 min (ratio YPet : sample 21 = 99:1).

| Sample | Lifetime τ/ns |
|---|---|
| YPet powder | 2.61 ± 0.05 |
| YPet in sample 21 pressed at 37 °C | 2.56 ± 0.05 |
| YPet in sample 21 pressed at 135 °C | 2.48 ± 0.08 |

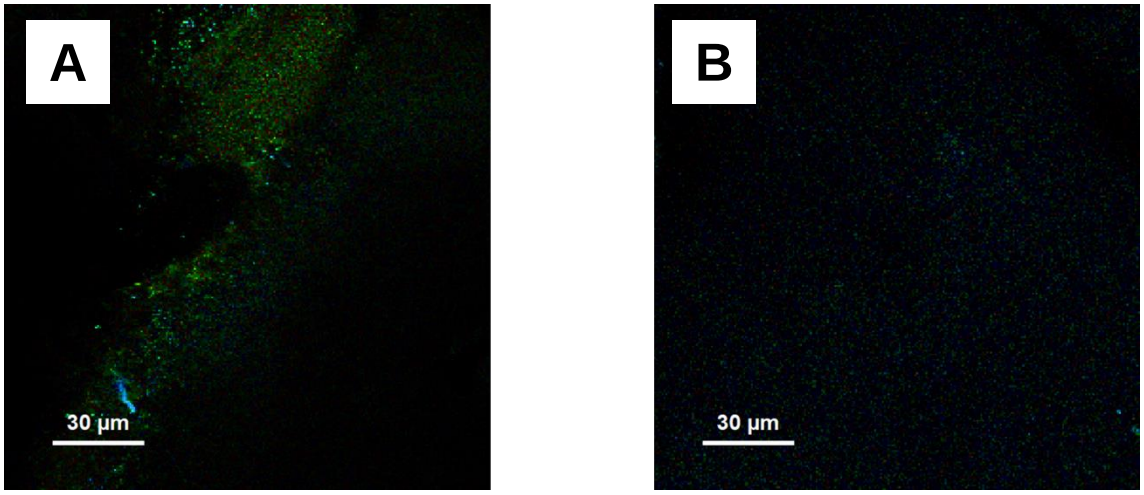


**Fig. S14. Fluorescence analysis with PLLA$_{85}$-*b*-PEG$_{182}$-*b*-PLLA$_{85}$.** (**A**) Fluorescence microscopic image of YPet immobilized PLLA$_{107}$-*b*-PEG$_{182}$-*b*-PLLA$_{107}$ (sample 21) pressed at 37 °C under 10 MPa for 5 min. (**B**) Fluorescence microscopic image of YPet immobilized PLLA$_{107}$-*b*-PEG$_{182}$-*b*-PLLA$_{107}$ pressed at 135 °C under 10 MPa for 5 min. The brightness of the color in the images represents the fluorescence intensity of YPet.

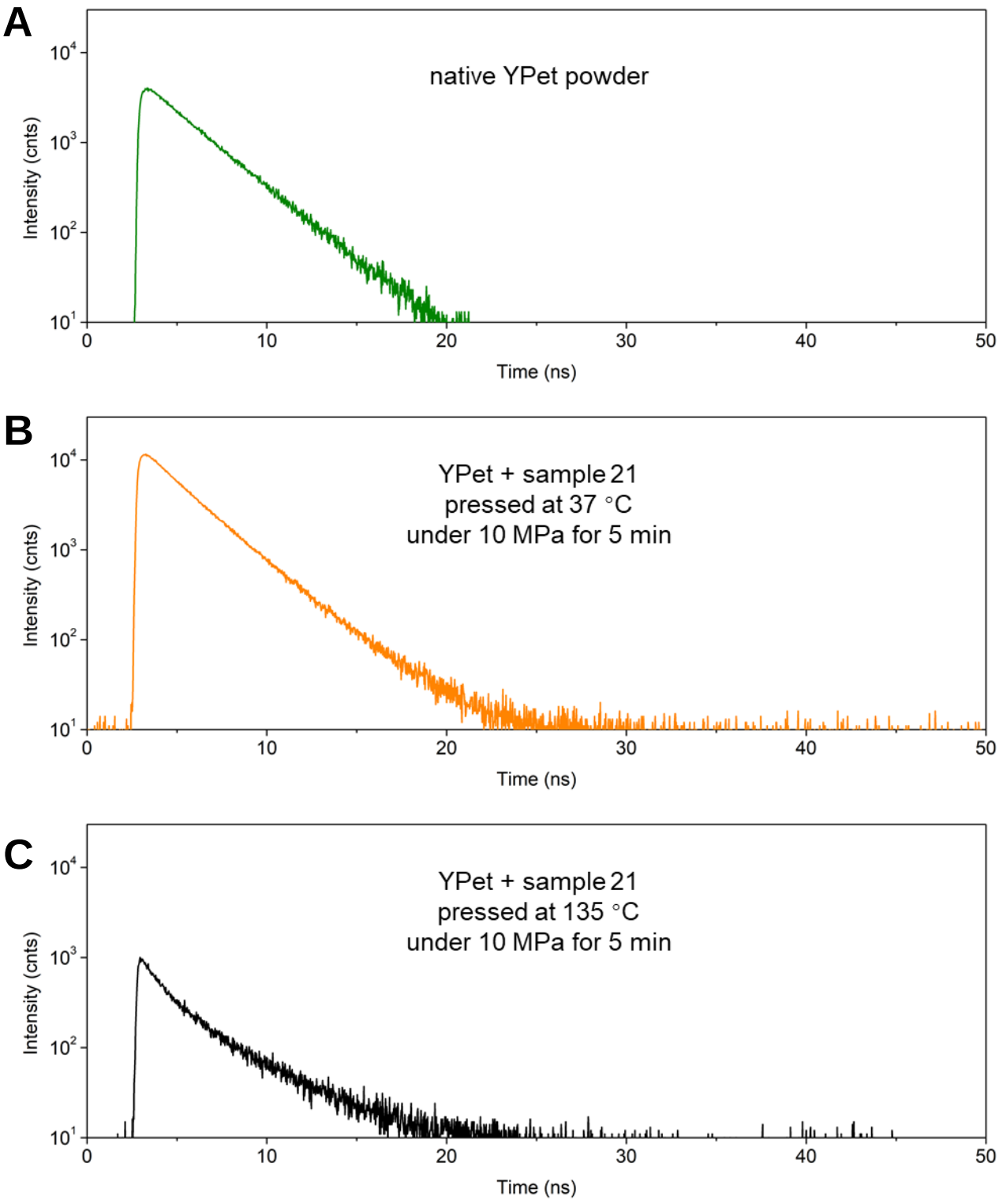


**Fig. S15. YPet lifetime measurement.** (**A**) Lifetime histogram of native YPet powder. Lifetime histogram of YPet-immobilized PLLA$_{107}$-*b*-PEG$_{182}$-*b*-PLLA$_{107}$ (sample 21) pressed films, (**B**) pressed at 37 °C under 10 MPa for 5 min, and (**C**) pressed at 135 °C under 10 MPa for 5 min. The intensity represents if YPet could kept its complete topological structure during processing.

Environmental investigation

The cell viability was the lowest for 100 µg/mL for Caco2 (87.9 % of control viability) and the highest for 1000 µg/mL in dTHP-1 (106.8 % of control viability). The increase in cell viability for the highest concentration in dTHP-1 could be explained by a stimulation of the cells and therefore higher metabolic activity, which consequently did not result in acute cytotoxicity. For the J774A.1 all treatment concentrations, for the Caco2 all concentrations higher than 10 µg/mL, and for the dTHP-1 0.1, 1 and 100 µg/mL were significantly lower than the untreated cells (Kruskal Wallis test and Games Howell post hoc testing: J774A.1: 0.1 = $p < 0.01$, 1, 10, 100, 500, 1000 = $p < 0.001$; Caco2: 10, 100, 500, 1000 = $p < 0,01$; dTHP-1: 0.1 & 1 = $p < 0.05$, 100 = $p < 0,001$). However, there were no significant differences between the used concentrations (J774A.1 and Caco2) indicating no acute dose-dependent cytotoxicity of the PLLA-*b*-PEG-*b*-PLLA triblock copolymer particles in suspension with particle size 50 µm. For the dTHP-1 cells the cell viability after exposing the cells to concentrations of 0.1, 1, 10 ($p < 0.05$) and 100µg/mL ($p < 0.001$) were significantly lower than 1000 µg/mL and 1µg/mL was significantly higher than 100 µg/mL ($p < 0.05$). The significant values can be explained by the significant increase in cell viability compared to untreated cells for 1000 µg/mL. Overall, no severe acute cytotoxicity was observed for all cell lines and concentrations.

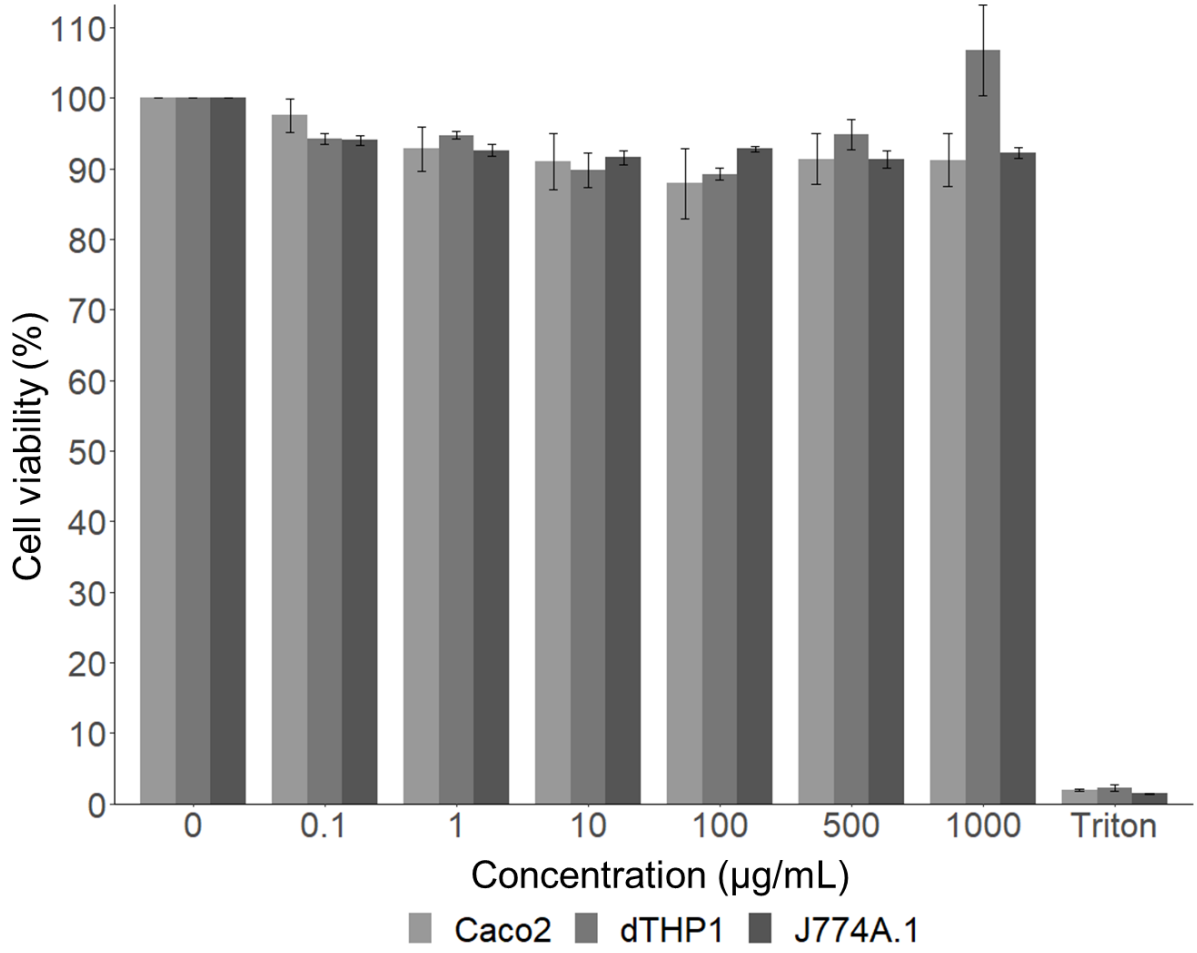


**Fig. S16. Cell toxicity test.** Suspension of PLLA$_{107}$-*b*-PEG$_{182}$-*b*-PLLA$_{107}$ (sample 21) with a size of 50 µm was used for cell toxicity test with three different cell lines: the murine macrophage cell line J774A.1, the human adenocarcinoma epithelial cell line Caco2, and human macrophages derived from the differentiation of monocytic cells THP-1. The cells were incubated with the triblock copolymer suspension for 24 h. The cell viability was determined by Alamar blue assay. In the *Daphnia* acute toxicity test, no immobilization of *D. magna* was detected for any of the tested concentrations and time points. Therefore, no $EC_{50}$ of the PLLA$_{107}$-*b*-PEG$_{182}$-*b*-PLLA$_{107}$ (sample 21) can be given here up to a concentration of 500 µg / mL.

Wastewater degradation results

Wastewater degradation of $PLLA_{107}$-b-$PEG_{182}$-b-$PLLA_{107}$ (sample 21) powder was performed in order to investigate the degradation of the triblock copolymers.

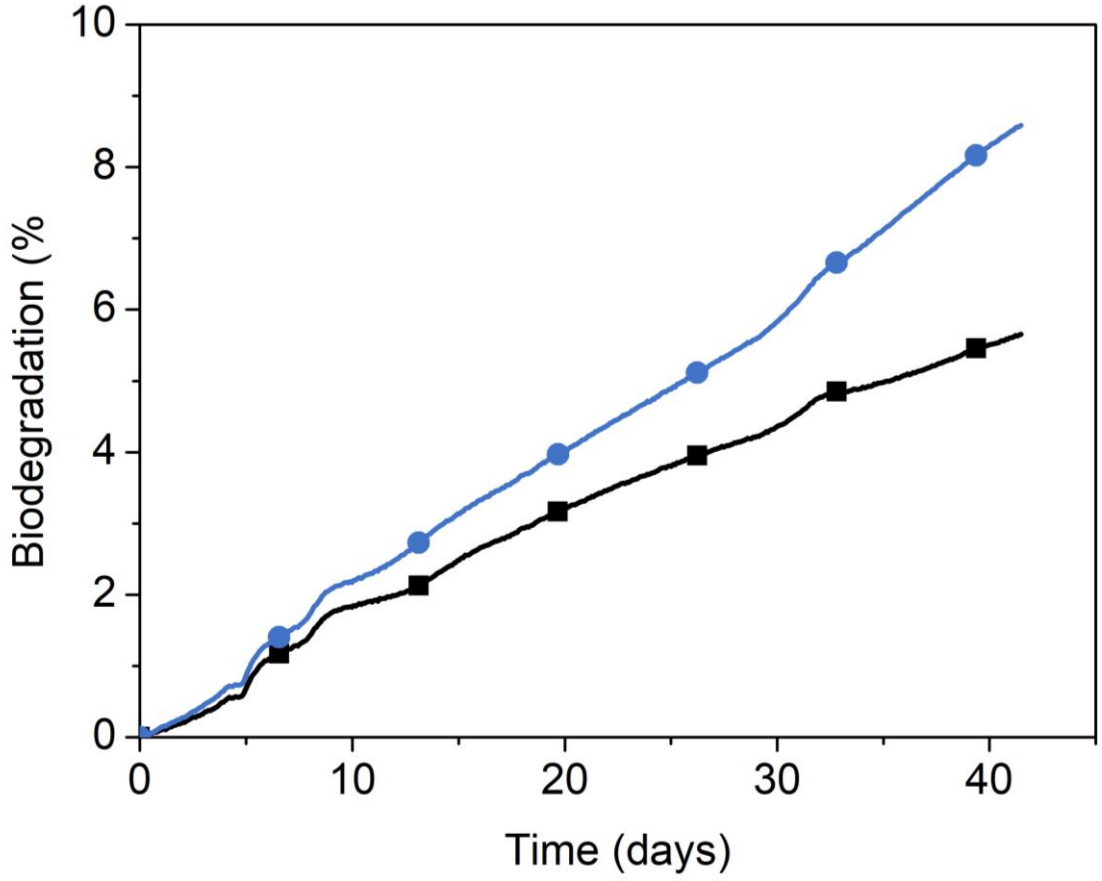


**Fig. S17. Wastewater degradation results.** Wastewater degradation of $PLLA_{107}$-b-$PEG_{182}$-b-$PLLA_{107}$ (sample 21) powder and film samples in Micro-Oxymax Respirometer. Aniline was used as positive control (blue line with circles: $PLLA_{107}$-b-$PEG_{182}$-b-$PLLA_{107}$ film pressed at 37 °C and black line with squares: $PLLA_{107}$-b-$PEG_{182}$-b-$PLLA_{107}$ powder).

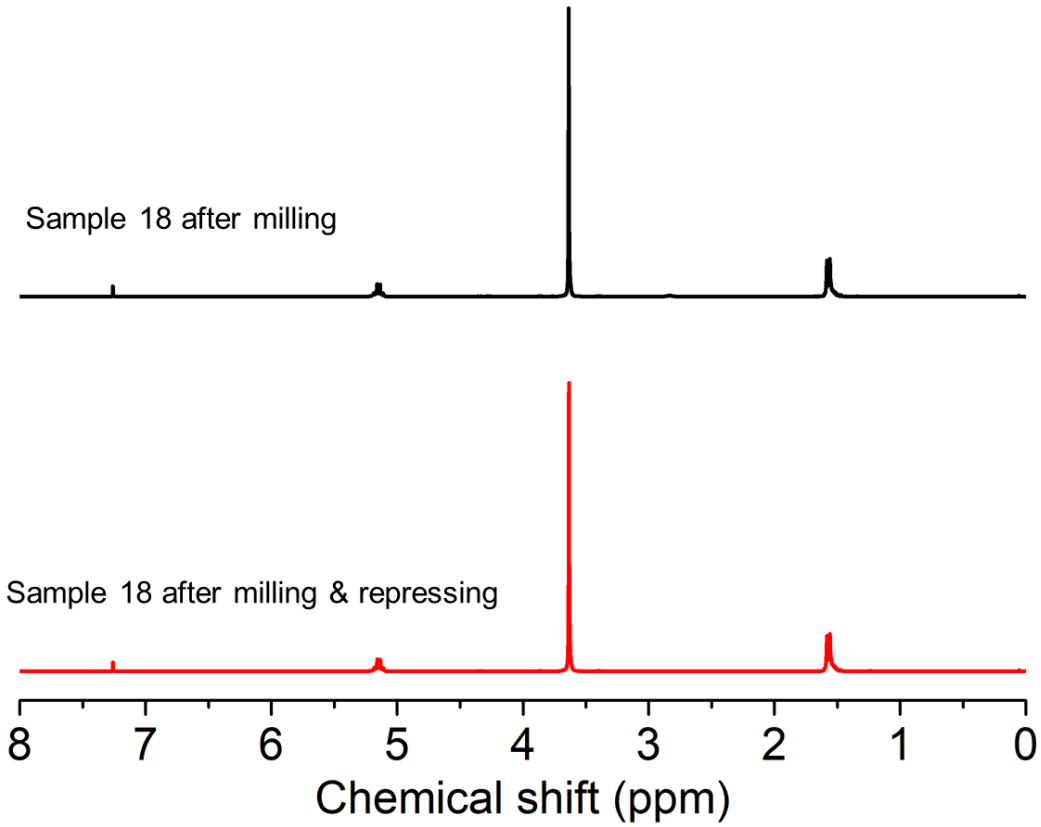


**Fig. S18. $^{1}$H NMR spectra of PLLA$_{68}$-*b*-PEG$_{182}$-*b*-PLLA$_{68}$ (sample 18) powder after cryomilling (upper), and cryomilled and repressed film (down).** The repressing was done using the milled powder at 37 °C under 10 MPa pressure for 1 h.

## 4. References


[1] J. Yu, A. Corma, Y. Li, *Advanced Materials* **2020**, *32*, 2006277.

[2] A. G. Slater, A. I. Cooper, *Science* **2015**, *348*, aaa8075.

[3] U. G. T. M. Sampath, Y. C. Ching, C. H. Chuah, J. J. Sabariah, P.-C. Lin, *Materials* **2016**, *9*, 991.

[4] T. D. Bennett, F.-X. Coudert, S. L. James, A. I. Cooper, *Nature Materials* **2021**, *20*, 1179.

[5] D. H. Everett, **1972**, *31*, 577.

[6] C. T. Kresge, M. E. Leonowicz, W. J. Roth, J. C. Vartuli, J. S. Beck, *Nature* **1992**, *359*, 710.

[7] S. Wang, Y. Peng, *Chemical Engineering Journal* **2010**, *156*, 11.

[8] H.-C. Zhou, J. R. Long, O. M. Yaghi, *Chemical Reviews* **2012**, *112*, 673.

[9] K. Rezwan, Q. Z. Chen, J. J. Blaker, A. R. Boccaccini, *Biomaterials* **2006**, *27*, 3413.

[10] H. Zheng, F. Gao, V. Valtchev, *Journal of Materials Chemistry A* **2016**, *4*, 16756.

[11] M. E. Medina, A. E. Platero-Prats, N. Snejko, A. Rojas, A. Monge, F. Gándara, E. Gutiérrez-Puebla, M. A. Camblor, *Advanced Materials* **2011**, *23*, 5283.

[12] B. M. Weckhuysen, J. Yu, *Chemical Society Reviews* **2015**, *44*, 7022.

[13] V. Van Speybroeck, K. Hemelsoet, L. Joos, M. Waroquier, R. G. Bell, C. R. A. Catlow, *Chemical Society Reviews* **2015**, *44*, 7044.

[14] D. W. Breck, W. G. Eversole, R. M. Milton, *Journal of the American Chemical Society* **1956**, *78*, 2338.

[15] Z. Liu, J. Zhu, C. Peng, T. Wakihara, T. Okubo, *Reaction Chemistry & Engineering* **2019**, *4*, 1699.

[16] C. Martínez, A. Corma, *Coordination Chemistry Reviews* **2011**, *255*, 1558.

[17] J. Wen, H. Dong, G. Zeng, *Journal of Cleaner Production* **2018**, *197*, 1435.

[18] J. Qin, Q. Chen, C. Yang, Y. Huang, *Journal of Alloys and Compounds* **2016**, *654*, 39.

[19] M. A. Atwater, L. N. Guevara, K. A. Darling, M. A. Tschopp, *Advanced Engineering Materials* **2018**, *20*, 1700766.

[20] F. García-Moreno, M. Mukherjee, E. Solórzano, J. Banhart, *Dedicated to Prof. Dr. H.-P. Degischer on the occasion of his 65th birthday* **2010**, *101*, 1134.

[21] B. Parveez, N. A. Jamal, A. Maleque, F. Yusof, N. H. Jamadon, S. Adzila, *Journal of Materials Research and Technology* **2021**, *14*, 2017.

[22] R. Zhang, H. Olin, *Materials* **2014**, *7*, 3834.

[23] S. Cherevko, C.-H. Chung, *Electrochemistry Communications* **2011**, *13*, 16.

[24] M. Yazdimamaghani, M. Razavi, D. Vashaee, K. Moharamzadeh, A. R. Boccaccini, L. Tayebi, *Materials Science and Engineering: C* **2017**, *71*, 1253.
[25] N. T. Kirkland, N. Birbilis, M. P. Staiger, *Acta Biomaterialia* **2012**, *8*, 925.
[26] G. Song, S. Song, *Advanced Engineering Materials* **2007**, *9*, 298.
[27] M. Salman, S. Jahan, S. Kanwal, F. Mansoor, *Environmental Science and Pollution Research* **2019**, *26*, 21065.
[28] G. Singh, K. S. Lakhi, I. Y. Kim, S. Kim, P. Srivastava, R. Naidu, A. Vinu, *ACS Applied Materials & Interfaces* **2017**, *9*, 29782.
[29] L. F. Giraldo, B. L. López, L. Pérez, S. Urrego, L. Sierra, M. Mesa, *Macromolecular Symposia* **2007**, *258*, 129.
[30] E. Doustkhah, S. Rostamnia, N. Tsunoji, J. Henzie, T. Takei, Y. Yamauchi, Y. Ide, *Chemical Communications* **2018**, *54*, 4402.
[31] S. Shi, M. Wang, C. Chen, F. Lu, X. Zheng, J. Gao, J. Xu, *RSC Advances* **2013**, *3*, 1158.
[32] C. Meng, W. Zhikun, L. Qiang, L. Chunling, S. Shuangqing, H. Songqing, *Journal of Hazardous Materials* **2018**, *341*, 198.
[33] T. Yanagisawa, T. Shimizu, K. Kuroda, C. Kato, *Bulletin of the Chemical Society of Japan* **1990**, *63*, 988.
[34] M. Manzano, M. Vallet-Regí, *Advanced Functional Materials* **2020**, *30*, 1902634.
[35] S.-H. Wu, C.-Y. Mou, H.-P. Lin, *Chemical Society Reviews* **2013**, *42*, 3862.
[36] Z. Cai, Z. Ye, X. Yang, Y. Chang, H. Wang, Y. Liu, A. Cao, *Nanoscale* **2011**, *3*, 1974.
[37] C. Bharti, U. Nagaich, A. K. Pal, N. Gulati, *International journal of pharmaceutical investigation* **2015**, *5*, 124.
[38] L. Liu, K. Shinozaki, *Journal of Alloys and Compounds* **2023**, *940*, 168874.
[39] S. Kitagawa, R. Kitaura, S.-i. Noro, *Angewandte Chemie International Edition* **2004**, *43*, 2334.
[40] O. Shekhah, J. Liu, R. A. Fischer, C. Wöll, *Chemical Society Reviews* **2011**, *40*, 1081.
[41] Q. Wang, D. Astruc, *Chemical Reviews* **2020**, *120*, 1438.
[42] X.-Y. Yang, L.-H. Chen, Y. Li, J. C. Rooke, C. Sanchez, B.-L. Su, *Chemical Society Reviews* **2017**, *46*, 481.
[43] H. Furukawa, K. E. Cordova, M. O'Keeffe, O. M. Yaghi, *Science* **2013**, *341*, 1230444.
[44] C. R. Kim, T. Uemura, S. Kitagawa, *Chemical Society Reviews* **2016**, *45*, 3828.
[45] N. L. Rosi, J. Eckert, M. Eddaoudi, D. T. Vodak, J. Kim, M. O'Keeffe, O. M. Yaghi, *Science* **2003**, *300*, 1127.
[46] H. K. Chae, D. Y. Siberio-Pérez, J. Kim, Y. Go, M. Eddaoudi, A. J. Matzger, M. O'Keeffe,

O. M. Yaghi, D. Materials, G. Discovery, *Nature* **2004**, *427*, 523.
[47] J. H. Cavka, S. Jakobsen, U. Olsbye, N. Guillou, C. Lamberti, S. Bordiga, K. P. Lillerud, *Journal of the American Chemical Society* **2008**, *130*, 13850.
[48] K. S. Park, Z. Ni, A. P. Côté, J. Y. Choi, R. Huang, F. J. Uribe-Romo, H. K. Chae, M. O'Keeffe, O. M. Yaghi, *Proceedings of the National Academy of Sciences* **2006**, *103*, 10186.
[49] C. Wang, X. Liu, N. Keser Demir, J. P. Chen, K. Li, *Chemical Society Reviews* **2016**, *45*, 5107.
[50] B. Chen, Z. Yang, Y. Zhu, Y. Xia, *Journal of Materials Chemistry A* **2014**, *2*, 16811.
[51] M. Peller, K. Böll, A. Zimpel, S. Wuttke, *Inorganic Chemistry Frontiers* **2018**, *5*, 1760.
[52] P. Horcajada, C. Serre, M. Vallet-Regí, M. Sebban, F. Taulelle, G. Férey, *Angewandte Chemie International Edition* **2006**, *45*, 5974.
[53] A. Dhakshinamoorthy, M. Alvaro, A. Corma, H. Garcia, *Dalton Transactions* **2011**, *40*, 6344.
[54] J.-X. Jiang, A. Trewin, F. Su, C. D. Wood, H. Niu, J. T. A. Jones, Y. Z. Khimyak, A. I. Cooper, *Macromolecules* **2009**, *42*, 2658.
[55] T. Ben, H. Ren, S. Ma, D. Cao, J. Lan, X. Jing, W. Wang, J. Xu, F. Deng, J. M. Simmons, S. Qiu, G. Zhu, *Angewandte Chemie International Edition* **2009**, *48*, 9457.
[56] H. M. El-Kaderi, J. R. Hunt, J. L. Mendoza-Cortés, A. P. Côté, R. E. Taylor, M. O'Keeffe, O. M. Yaghi, *Science* **2007**, *316*, 268.
[57] B. Beiler, Á. Vincze, F. Svec, Á. Sáfrány, *Polymer* **2007**, *48*, 3033.
[58] C. D. Wood, B. Tan, A. Trewin, F. Su, M. J. Rosseinsky, D. Bradshaw, Y. Sun, L. Zhou, A. I. Cooper, *Advanced Materials* **2008**, *20*, 1916.
[59] M. Rose, N. Klein, I. Senkovska, C. Schrage, P. Wollmann, W. Böhlmann, B. Böhringer, S. Fichtner, S. Kaskel, *Journal of Materials Chemistry* **2011**, *21*, 711.
[60] F. Svec, *Journal of Chromatography A* **2010**, *1217*, 902.
[61] P. M. Budd, B. S. Ghanem, S. Makhseed, N. B. McKeown, K. J. Msayib, C. E. Tattershall, *Chemical Communications* **2004**, 230.
[62] B. S. Ghanem, N. B. McKeown, P. M. Budd, D. Fritsch, *Macromolecules* **2008**, *41*, 1640.
[63] J. Weber, Q. Su, M. Antonietti, A. Thomas, *Macromolecular Rapid Communications* **2007**, *28*, 1871.
[64] N. Du, G. P. Robertson, J. Song, I. Pinnau, S. Thomas, M. D. Guiver, *Macromolecules* **2008**, *41*, 9656.
[65] X. Hu, Q. An, G. Li, S. Tao, J. Liu, *Angewandte Chemie International Edition* **2006**, *45*, 8145.

[66] J. Rzayev, M. A. Hillmyer, *Macromolecules* **2005**, *38*, 3.

[67] B. Li, X. Huang, L. Liang, B. Tan, *Journal of Materials Chemistry* **2010**, *20*, 7444.

[68] A. P. Côté, A. I. Benin, N. W. Ockwig, M. O'Keeffe, A. J. Matzger, O. M. Yaghi, *Science* **2005**, *310*, 1166.

[69] F.-L. Jin, M. Zhao, M. Park, S.-J. Park, *Polymers* **2019**, *11*, 953.

[70] S. Zhang, Y. Lin, L. Ye, Y. Gu, J. Qiu, T. Tang, M. Li, *Polymer* **2018**, *146*, 304.

[71] R. Li, H. Lin, P. Lan, J. Gao, Y. Huang, Y. Wen, W. Yang, *Polymers* **2018**, *10*, 1319.

[72] L. Wang, Y.-K. Wu, F.-F. Ai, J. Fan, Z.-P. Xia, Y. Liu, *Polymers* **2018**, *10*, 1310.

[73] W. Gong, H. Fu, C. Zhang, D. Ban, X. Yin, Y. He, L. He, X. Pei, *Polymers* **2018**, *10*, 1375.

[74] D. Zhou, Y. Xiong, H. Yuan, G. Luo, J. Zhang, Q. Shen, L. Zhang, *Composites Part B: Engineering* **2019**, *165*, 272.

[75] G. Wang, G. Zhao, L. Zhang, Y. Mu, C. B. Park, *Chemical Engineering Journal* **2018**, *350*, 1.

[76] S. Pérez-Tamarit, E. Solórzano, A. Hilger, I. Manke, M. A. Rodríguez-Pérez, *European Polymer Journal* **2018**, *109*, 169.

[77] V. Kakumanu, S. Srinivas Sundarram, *Materials Letters* **2018**, *213*, 366.

[78] R. Kuska, S. Milovanovic, S. Frerich, J. Ivanovic, *The Journal of Supercritical Fluids* **2019**, *144*, 71.

[79] S. Wang, A. Ameli, V. Shaayegan, Y. Kazemi, Y. Huang, H. E. Naguib, C. B. Park, *Polymers* **2018**, *10*, 261.

[80] M. Barmouz, A. H. Behravesh, *Journal of the Mechanical Behavior of Biomedical Materials* **2019**, *91*, 266.

[81] J. Heimann, A. M. Matz, B. S. Matz, N. Jost, *Science and Technology of Materials* **2018**, *30*, 23.

[82] V. Volpe, S. Lanzillo, G. Affinita, B. Villacci, I. Macchiarolo, R. Pantani, *Polymers* **2019**, *11*, 326.

[83] M. Yuan, L.-S. Turng, *Polymer* **2005**, *46*, 7273.

[84] M. J. Yuan, L. S. Turng, *Plastics, Rubber and Composites* **2006**, *35*, 129.

[85] J. Hári, F. Horváth, K. Renner, J. Móczó, B. Pukánszky, *Polymer Testing* **2018**, *72*, 178.

[86] W. Xiao, X. Liao, Q. Jiang, Y. Zhang, J. Chen, Q. Yang, G. Li, *The Journal of Supercritical Fluids* **2018**, *142*, 52.

[87] W. Tang, J. Bai, X. Liao, W. Xiao, Y. Luo, Q. Yang, G. Li, *The Journal of Supercritical Fluids* **2018**, *141*, 78.

[88] T. Grätzl, Y. van Dijk, N. Schramm, L. Kroll, *Composite Structures* **2019**, *208*, 557.
[89] K. Friedrich, A. A. Almajid, *Applied Composite Materials* **2013**, *20*, 107.
[90] G. Wang, G. Zhao, G. Dong, Y. Mu, C. B. Park, *Composites Science and Technology* **2018**, *168*, 38.
[91] P. Nejat, F. Jomehzadeh, M. M. Taheri, M. Gohari, M. Z. Abd. Majid, *Renewable and Sustainable Energy Reviews* **2015**, *43*, 843.
[92] P. Gong, G. Wang, M.-P. Tran, P. Buahom, S. Zhai, G. Li, C. B. Park, *Carbon* **2017**, *120*, 1.
[93] E. S. Weiser, T. F. Johnson, T. L. St Clair, Y. Echigo, H. Kaneshiro, B. W. Grimsley, *High Performance Polymers* **2000**, *12*, 1.
[94] S.-J. Park, F.-L. Jin, J.-R. Lee, *Macromolecular Chemistry and Physics* **2004**, *205*, 2048.
[95] S.-J. Park, F.-L. Jin, J.-R. Lee, *Macromolecular Rapid Communications* **2004**, *25*, 724.
[96] Y.-C. Chen, W. Tai, *Polymers* **2018**, *10*, 1100.
[97] W. Jiang, F.-L. Jin, S.-J. Park, *Journal of Industrial and Engineering Chemistry* **2015**, *27*, 40.
[98] S.-J. Park, *Bulletin of the Korean Chemical Society* **2009**, *30*, 2643.
[99] G. Yang, W.-H. Wu, Y.-H. Wang, Y.-H. Jiao, L.-Y. Lu, H.-Q. Qu, X.-Y. Qin, *Journal of Hazardous Materials* **2019**, *366*, 78.
[100] J.-F. Yue, L. Gan, C.-H. Liu, X.-Z. Ma, D. Wang, J. Huang, *Polymer* **2018**, *155*, 50.
[101] Ö. C. Önder, E. Yilgör, I. Yilgör, *Polymer* **2016**, *107*, 240.
[102] J. Li, A. Zhang, S. Zhang, Q. Gao, W. Zhang, J. Li, *Composites Part B: Engineering* **2019**, *156*, 368.
[103] S.-X. Wang, H.-B. Zhao, W.-H. Rao, S.-C. Huang, T. Wang, W. Liao, Y.-Z. Wang, *Polymer* **2018**, *153*, 616.
[104] K. Chen, C. Tian, S. Liang, X. Zhao, X. Wang, *Polymer Degradation and Stability* **2018**, *150*, 105.
[105] L. A. Capadona, M. A. B. Meador, A. Alunni, E. F. Fabrizio, P. Vassilaras, N. Leventis, *Polymer* **2006**, *47*, 5754.
[106] N. Hüsing, U. Schubert, *Angewandte Chemie International Edition* **1998**, *37*, 22.
[107] R. Ciriminna, A. Fidalgo, V. Pandarus, F. Béland, L. M. Ilharco, M. Pagliaro, *Chemical Reviews* **2013**, *113*, 6592.
[108] M. Antonietti, N. Fechler, T.-P. Fellinger, *Chemistry of Materials* **2014**, *26*, 196.
[109] A. C. Pierre, G. M. Pajonk, *Chemical Reviews* **2002**, *102*, 4243.
[110] A. Soleimani Dorcheh, M. H. Abbasi, *Journal of Materials Processing Technology* **2008**,

*199*, 10.
[111] S. S. Kistler, *Nature* **1931**, *127*, 741.
[112] A. D. McNaught, A. Wilkinson, **1997**.
[113] G. M. Pajonk, *Journal of Non-Crystalline Solids* **1998**, *225*, 307.
[114] I. Smirnova, P. Gurikov, *The Journal of Supercritical Fluids* **2018**, *134*, 228.
[115] H. Choi, V. G. Parale, T. Kim, Y.-S. Choi, J. Tae, H.-H. Park, *Microporous and Mesoporous Materials* **2020**, *298*, 110092.
[116] V. G. Parale, T. Kim, K.-Y. Lee, V. D. Phadtare, R. P. Dhavale, H.-N.-R. Jung, H.-H. Park, *Ceramics International* **2020**, *46*, 4939.
[117] V. D. Phadtare, V. G. Parale, K.-Y. Lee, T. Kim, V. R. Puri, H.-H. Park, *Journal of Alloys and Compounds* **2019**, *805*, 120.
[118] V. G. Parale, T. Kim, V. D. Phadtare, H. M. Yadav, H.-H. Park, *Journal of Molecular Liquids* **2019**, *277*, 424.
[119] V. G. Parale, K.-Y. Lee, H.-N.-R. Jung, H.-Y. Nah, H. Choi, T.-H. Kim, V. D. Phadtare, H.-H. Park, *Ceramics International* **2018**, *44*, 3966.
[120] R. W. Pekala, *Journal of Materials Science* **1989**, *24*, 3221.
[121] H. P. S. Abdul Khalil, A. S. Adnan, E. B. Yahya, N. G. Olaiya, S. Safrida, M. S. Hossain, V. Balakrishnan, D. A. Gopakumar, C. K. Abdullah, A. A. Oyekanmi, D. Pasquini, *Polymers* **2020**, *12*, 1759.
[122] C. Ziegler, A. Wolf, W. Liu, A. K. Herrmann, N. Gaponik, A. Eychmüller, *Angewandte Chemie (International ed. in English)* **2017**, *56*, 13200.
[123] I. Surya, N. G. Olaiya, S. Rizal, I. Zein, N. A. Sri Aprilia, M. Hasan, E. B. Yahya, K. K. Sadasivuni, H. P. S. Abdul Khalil, *Polymers* **2020**, *12*, 115.
[124] T. M. Tamer, M. N. Collins, K. Valachová, M. A. Hassan, A. M. Omer, M. S. Mohy-Eldin, K. Švík, R. Jurčík, Ľ. Ondruška, C. Biró, A. B. Albadarin, L. Šoltés, *Materials* **2018**, *11*, 569.
[125] H. P. S. A. Khalil, F. Jummaat, E. B. Yahya, N. G. Olaiya, A. S. Adnan, M. Abdat, N. N. A. M, A. S. Halim, U. S. Kumar, R. Bairwan, A. B. Suriani, *Polymers* **2020**, *12*, 2043.
[126] J. Wang, T. Higashihara, *Polymer Chemistry* **2013**, *4*, 5518.
[127] J. Wang, M. Ueda, T. Higashihara, *Journal of Polymer Science Part A: Polymer Chemistry* **2014**, *52*, 1139.
[128] J. Wang, P. Gao, L. Ye, A.-y. Zhang, Z.-g. Feng, *The Journal of Physical Chemistry B* **2010**, *114*, 5342.
[129] J. Wang, L. Ye, A.-y. Zhang, Z.-g. Feng, *Journal of Materials Chemistry* **2011**, *21*, 3243.

[130] J. Wang, S. Li, L. Ye, A.-Y. Zhang, Z.-G. Feng, *Macromolecular Rapid Communications* **2012**, *33*, 1143.
[131] S. Wei, X. Cui, *Journal of Porous Materials* **2021**, *28*, 751.
[132] M. Sajjad, R. Tao, K. Kang, S. Luo, L. Qiu, *ACS Applied Energy Materials* **2021**, *4*, 828.
[133] M. Guastaferro, E. Reverchon, L. Baldino, *Materials* **2021**, *14*, 1631.
[134] J. Holländer, R. Hakala, J. Suominen, N. Moritz, J. Yliruusi, N. Sandler, *International Journal of Pharmaceutics* **2018**, *544*, 433.
[135] S. Pulapura, J. Kohn, *Journal of Biomaterials Applications* **1992**, *6*, 216.
[136] J. Wang, C. Zong, D. Shi, W. Wang, D. Shen, L. Liu, X. Tong, Q. Zheng, C. Gao, *Journal of Tissue Engineering and Regenerative Medicine* **2012**, *6*, 29.
[137] L. Zhang, L. Rao, P. Wang, Z. Shi, P. Wang, *Applied Surface Science* **2021**, *536*, 147726.
[138] P. Sun, M. Wang, T. Wu, L. Guo, W. Han, "Covalent Crosslinking Cellulose/Graphene Aerogels with High Elasticity and Adsorbability for Heavy Metal Ions Adsorption", in *Polymers* **2023**, 15, 2434.
[139] C. I. Idumah, A. C. Ezika, V. U. Okpechi, *Surfaces and Interfaces* **2021**, *25*, 101258.
[140] L. J. Gibson, *MRS Bulletin* **2003**, *28*, 270.
[141] S. Jiang, S. Agarwal, A. Greiner, *Angewandte Chemie International Edition* **2017**, *56*, 15520.
[142] Z. Xue, Y. Cao, N. Liu, L. Feng, L. Jiang, *Journal of Materials Chemistry A* **2014**, *2*, 2445.
[143] S. Jiang, G. Duan, U. Kuhn, M. Mörl, V. Altstädt, A. L. Yarin, A. Greiner, *Angewandte Chemie International Edition* **2017**, *56*, 3285.
[144] Q. Fu, Y. Si, C. Duan, Z. Yan, L. Liu, J. Yu, B. Ding, *Advanced Functional Materials* **2019**, *29*, 1808234.
[145] G. Duan, M. Koehn-Serrano, A. Greiner, *Macromolecular Rapid Communications* **2017**, *38*, 1600511.
[146] S. Jiang, B. Uch, S. Agarwal, A. Greiner, *ACS Applied Materials & Interfaces* **2017**, *9*, 32308.
[147] M. Mader, V. Jérôme, R. Freitag, S. Agarwal, A. Greiner, *Biomacromolecules* **2018**, *19*, 1663.
[148] G. Duan, A. R. Bagheri, S. Jiang, J. Golenser, S. Agarwal, A. Greiner, *Biomacromolecules* **2017**, *18*, 3215.
[149] N. V. Gama, A. Ferreira, A. Barros-Timmons, *Materials* **2018**, *11*, 1841.
[150] Y. Liu, X. Zhao, L. Ye, *Industrial & Engineering Chemistry Research* **2016**, *55*, 8743.

[151] R. Starbird, C. A. García-González, I. Smirnova, W. H. Krautschneider, W. Bauhofer, *Materials Science and Engineering: C* **2014**, *37*, 177.
[152] W. Chen, Y.-X. Huang, D.-B. Li, H.-Q. Yu, L. Yan, *RSC Advances* **2014**, *4*, 21619.
[153] X. Zhang, D. Chang, J. Liu, Y. Luo, *Journal of Materials Chemistry* **2010**, *20*, 5080.
[154] T. A. Schaedler, A. J. Jacobsen, A. Torrents, A. E. Sorensen, J. Lian, J. R. Greer, L. Valdevit, W. B. Carter, *Science* **2011**, *334*, 962.
[155] D. Jang, L. R. Meza, F. Greer, J. R. Greer, *Nature Materials* **2013**, *12*, 893.
[156] Y.-G. Ko, N. Kawazoe, T. Tateishi, G. Chen, *Journal of Biomedical Materials Research Part B: Applied Biomaterials* **2010**, *93B*, 341.
[157] Y. S. Nam, J. J. Yoon, T. G. Park, *Journal of Biomedical Materials Research* **2000**, *53*, 1.
[158] R. Baetens, B. P. Jelle, A. Gustavsen, *Energy and Buildings* **2011**, *43*, 761.
[159] C. Li, G. Shi, *Advanced Materials* **2014**, *26*, 3992.
[160] A. Vintiloiu, J.-C. Leroux, *Journal of Controlled Release* **2008**, *125*, 179.
[161] N. Job, A. Théry, R. Pirard, J. Marien, L. Kocon, J.-N. Rouzaud, F. Béguin, J.-P. Pirard, *Carbon* **2005**, *43*, 2481.
[162] R. Pirard, A. Rigacci, J. C. Maréchal, D. Quenard, B. Chevalier, P. Achard, J. P. Pirard, *Polymer* **2003**, *44*, 4881.
[163] V. I. Lozinsky, *Russian Chemical Reviews* **2002**, *71*, 489.
[164] F. Ak, Z. Oztoprak, I. Karakutuk, O. Okay, *Biomacromolecules* **2013**, *14*, 719.
[165] R. G. Weiss, *Journal of the American Chemical Society* **2014**, *136*, 7519.
[166] M. Suzuki, K. Hanabusa, *Chemical Society Reviews* **2010**, *39*, 455.
[167] M. Kobayashi, T. Nakaoki, N. Ishihara, *Macromolecules* **1990**, *23*, 78.
[168] A. Saiani, J.-M. Guenet, *Macromolecules* **1997**, *30*, 966.
[169] A. Pich, N. Schiemenz, V. Boyko, H.-J. P. Adler, *Polymer* **2006**, *47*, 553.
[170] H. Kodama, *Review of Scientific Instruments* **1981**, *52*, 1770.
[171] E. Saygili, A. A. Dogan-Gurbuz, O. Yesil-Celiktas, M. S. Draz, *Bioprinting* **2020**, *18*, e00071.
[172] R. Schipani, D. R. Nolan, C. Lally, D. J. Kelly, *Connective Tissue Research* **2020**, *61*, 174.
[173] S. V. Murphy, A. Atala, *Nature Biotechnology* **2014**, *32*, 773.
[174] M. Nakamura, S. Iwanaga, C. Henmi, K. Arai, Y. Nishiyama, *Biofabrication* **2010**, *2*, 014110.
[175] S. Pina, V. P. Ribeiro, C.F. Marques, F.R. Maia, T.H. Silva, R. L. Reis, J. M. Oliveira,

*Materials* **2019**, *12*, 1824.
[176] Z. Xie, M. Gao, A. O. Lobo, T. J. Webster, *Polymers* **2020**, *12*, 1717.
[177] S. Zhang, H. Wang, *SLAS Technology* **2019**, *24*, 70.
[178] A. R. Akkineni, T. Ahlfeld, A. Lode, M. Gelinsky, *Biofabrication* **2016**, *8*, 045001.
[179] A. Sorkio, L. Koch, L. Koivusalo, A. Deiwick, S. Miettinen, B. Chichkov, H. Skottman, *Biomaterials* **2018**, *171*, 57.
[180] X. Yang, Z. Lu, H. Wu, W. Li, L. Zheng, J. Zhao, *Materials Science and Engineering: C* **2018**, *83*, 195.
[181] M. Kesti, M. Müller, J. Becher, M. Schnabelrauch, M. D'Este, D. Eglin, M. Zenobi-Wong, *Acta Biomaterialia* **2015**, *11*, 162.
[182] Y. Si, J. Yu, X. Tang, J. Ge, B. Ding, *Nature Communications* **2014**, *5*, 5802.
[183] T. Xu, J. M. Miszuk, Y. Zhao, H. Sun, H. Fong, *Advanced Healthcare Materials* **2015**, *4*, 2238.
[184] G. Duan, S. Jiang, V. Jérôme, J. H. Wendorff, A. Fathi, J. Uhm, V. Altstädt, M. Herling, J. Breu, R. Freitag, S. Agarwal, A. Greiner, *Advanced Functional Materials* **2015**, *25*, 2850.
[185] G. M. Bose, "*Recherches sur la cause et sur la veritable teorie de l'electricite publies par George Mathias Bose prof. en phisique"*, de l'imprimerie de Jean Fred. Slomac, 1745.
[186] N. Bhardwaj, S. C. Kundu, *Biotechnology Advances* **2010**, *28*, 325.
[187] C. V. Boys, *The London, Edinburgh, and Dublin Philosophical Magazine and Journal of Science* **1887**, *23*, 489.
[188] A. Greiner, J. H. Wendorff, *Angewandte Chemie International Edition* **2007**, *46*, 5670.
[189] A. Formhals, **1934**.
[190] B. Vonnegut, R. L. Neubauer, *Journal of Colloid Science* **1952**, *7*, 616.
[191] G. I. Taylor, *Proceedings of the Royal Society of London. Series A. Mathematical and Physical Sciences* **1997**, *280*, 383.
[192] H. M. Ibrahim, A. Klingner, *Polymer Testing* **2020**, *90*, 106647.
[193] H. Fong, I. Chun, D. H. Reneker, *Polymer* **1999**, *40*, 4585.
[194] D. H. Reneker, A. L. Yarin, H. Fong, S. Koombhongse, *Journal of Applied Physics* **2000**, *87*, 4531.
[195] Y. M. Shin, M. M. Hohman, M. P. Brenner, G. C. Rutledge, *Applied Physics Letters* **2001**, *78*, 1149.
[196] A. L. Yarin, S. Koombhongse, D. H. Reneker, *Journal of Applied Physics* **2001**, *89*, 3018.
[197] M. M. Hohman, M. Shin, G. Rutledge, M. P. Brenner, *Physics of Fluids* **2001**, *13*, 2201.
[198] M. M. Hohman, M. Shin, G. Rutledge, M. P. Brenner, *Physics of Fluids* **2001**, *13*, 2221.

[199] G. Larsen, R. Velarde-Ortiz, K. Minchow, A. Barrero, I. G. Loscertales, *Journal of the American Chemical Society* **2003**, *125*, 1154.
[200] D. Li, Y. Wang, Y. Xia, *Nano Letters* **2003**, *3*, 1167.
[201] A. Theron, E. Zussman, A. L. Yarin, *Nanotechnology* **2001**, *12*, 384.
[202] J. M. Deitzel, J. D. Kleinmeyer, J. K. Hirvonen, N. C. Beck Tan, *Polymer* **2001**, *42*, 8163.
[203] R. Dersch, T. Liu, A. K. Schaper, A. Greiner, J. H. Wendorff, *Journal of Polymer Science Part A: Polymer Chemistry* **2003**, *41*, 545.
[204] Z. Sun, E. Zussman, A. L. Yarin, J. H. Wendorff, A. Greiner, *Advanced Materials* **2003**, *15*, 1929.
[205] J. Xue, T. Wu, Y. Dai, Y. Xia, *Chemical Reviews* **2019**, *119*, 5298.
[206] S. Jiang, Y. Chen, G. Duan, C. Mei, A. Greiner, S. Agarwal, *Polymer Chemistry* **2018**, *9*, 2685.
[207] R. K. Mishra, P. Mishra, K. Verma, A. Mondal, R. G. Chaudhary, M. M. Abolhasani, S. Loganathan, *Environmental Chemistry Letters* **2019**, *17*, 767.
[208] R. Khajavi, M. Abbasipour, in *Electrospun Nanofibers*, Vol. 186 (Ed. M. Afshari), Elsevier, Duxford, UK **2017**, Ch. 5.
[209] C. Mit-uppatham, M. Nithitanakul, P. Supaphol, *Macromolecular Chemistry and Physics* **2004**, *205*, 2327.
[210] S. T. M, A. B. Arshad, P. T. Lin, J. Widakdo, M. H. K, H. F. M. Austria, C.-C. Hu, J.-Y. Lai, W.-S. Hung, *RSC Advances* **2021**, *11*, 9638.
[211] T. Mazoochi, S. M. Ahmadi, M. hamadnian, V. jabbari, *International Journal of Industrial Chemistry* **2012**, *3*, 2.
[212] A. Haider, S. Haider, I.-K. Kang, *Arabian Journal of Chemistry* **2018**, *11*, 1165.
[213] S. Megelski, J. S. Stephens, D. B. Chase, J. F. Rabolt, *Macromolecules* **2002**, *35*, 8456.
[214] C. Angammana, S. Jayaram, *Particulate Science and Technology* **2015**, *34*, 150511123627003.
[215] M. Lauricella, D. Pisignano, S. Succi, *The Journal of Physical Chemistry A* **2016**, *120*, 4884.
[216] G. Eda, S. Shivkumar, *Journal of Applied Polymer Science* **2007**, *106*, 475.
[217] A. Abdelrasoul, *Advances in Membrane Technologies*, IntechOpen, London, UK **2020**.
[218] Inamuddin, R. Boddula, M. Ahamed, A. M. Asiri, *Electrospun Materials and Their Allied Applications*, John Wiley & Sons, Hoboken, NJ, USA **2020**.
[219] C. Wang, C.-H. Hsu, J.-H. Lin, *Macromolecules* **2006**, *39*, 7662.
[220] O. Akampumuza, H. Gao, H. Zhang, D. Wu, X.-H. Qin, *Macromolecular Materials and*

*Engineering* **2018**, *303*, 1700269.
[221] Y. Ding, H. Hou, Y. Zhao, Z. Zhu, H. Fong, *Progress in Polymer Science* **2016**, *61*, 67.
[222] Y. Zheng, R. H. Gong, Y. Zeng, *RSC Advances* **2015**, *5*, 48533.
[223] G. Kim, Y.-S. Cho, W. D. Kim, *European Polymer Journal* **2006**, *42*, 2031.
[224] A. Varesano, R. Carletto, G. Mazzuchetti, *Journal of Materials Processing Technology* **2009**, *209*, 5178.
[225] N. M. Thoppey, J. R. Bochinski, L. I. Clarke, R. E. Gorga, *Polymer* **2010**, *51*, 4928.
[226] J. S. Varabhas, G. G. Chase, D. H. Reneker, *Polymer* **2008**, *49*, 4226.
[227] I. Partheniadis, I. Nikolakakis, I. Laidmäe, J. Heinämäki, *Processes* **2020**, *8*, 673.
[228] O. Jirsak, F. Sanetrnik, D. Lukas, V. Kotek, L. Martinova, J. Chaloupek, *US 7585437*, **2009**.
[229] A. Ahmad, U. Ali, A. Nazir, A. Shahzad, Z. Khaliq, M. B. Qadir, M. A. Khan, S. Ali, M. Aamir Hassan, S. Abid, R. Tahir, B. Mushtaq, *Journal of Materials Science* **2019**, *54*, 13834.
[230] L. Wei, C. Liu, X. Mao, J. Dong, W. Fan, C. Zhi, X. Qin, R. Sun, *Polymers* **2019**, *11*, 2052.
[231] Y. Kara, H. He, K. Molnár, *Journal of Applied Polymer Science* **2020**, *137*, 49104.
[232] J. H. Yu, S. Fridrikh, G. C. Rutledge, *Advanced Materials* **2004**, *16*, 1562.
[233] M. Wang, J. Yu, D. Kaplan, G. Rutledge, *Macromolecules* **2006**, *39*.
[234] S. Agarwal, A. Greiner, J. Wendorff, *Advanced Functional Materials* **2009**, *19*, 2863.
[235] Y. Dror, J. Kuhn, R. Avrahami, E. Zussman, *Macromolecules* **2008**, *41*.
[236] S. Klein, J. Kuhn, R. Avrahami, S. Tarre, M. Beliavski, M. Green, E. Zussman, *Biomacromolecules* **2009**, *10*, 1751.
[237] R. Korehei, J. F. Kadla, *Carbohydrate polymers* **2014**, *100*, 150.
[238] J. P. F. Lagerwall, J. T. McCann, E. Formo, G. Scalia, Y. Xia, *Chemical Communications* **2008**, 5420.
[239] L. Liu, F. Zhang, S. Hu, L. Zhang, S. Wen, *Macromolecular Materials and Engineering* **2012**, *297*, 298.
[240] X. Wang, W. J. Zhang, D. Yu, X. Y. Li, H. Yang, *Macromolecular Materials and Engineering* **2013**, *298*.
[241] B. M. Thamer, A. Aldalbahi, A. M. Moydeen, M. Rahaman, M. H. El-Newehy, *Polymers (Basel)* **2020**, *13*.
[242] D. Han, A. J. Steckl, *ACS applied materials & interfaces* **2013**, *5*, 8241.
[243] L. Peng, J. Shaohua, M. Seuß, A. Fery, G. Lang, T. Scheibel, S. Agarwal, *Macromolecular Materials and Engineering* **2015**, *301*.

[244] X. Zhang, R. Lv, L. Chen, R. Sun, Y. Zhang, R. Sheng, T. Du, Y. Li, Y. Qi, *ACS applied materials & interfaces* **2022**, *14*, 12984.
[245] J. Yang, K. Wang, D.-G. Yu, Y. Yang, S. W. A. Bligh, G. R. Williams, *Materials Science and Engineering: C* **2020**, *111*, 110805.
[246] Y. Huang, N. Bu, Y. Duan, Y. Pan, H. Liu, Z. Yin, Y. Xiong, *Nanoscale* **2013**, *5*, 12007.
[247] T. P. Lei, X. Z. Lu, F. Yang, *AIP Advances* **2014**, *5*, 041301.
[248] Y. K. Fuh, H. S. Hsu, *Journal of Micro/Nanolithography, MEMS, and MOEMS* **2011**, *10*, 043004.
[249] X. Wang, G. Zheng, L. Xu, W. Cheng, B. Xu, Y. Huang, D. Sun, *Applied Physics A* **2012**, *108*, 825.
[250] S. Peng, G. Jin, L. Li, K. Li, M. Srinivasan, S. Ramakrishna, J. Chen, *Chemical Society Reviews* **2016**, *45*, 1225.
[251] J. Xue, J. Xie, W. Liu, Y. Xia, *Accounts of Chemical Research* **2017**, *50*, 1976.
[252] S. Agarwal, A. Greiner, J. H. Wendorff, *Progress in Polymer Science* **2013**, *38*, 963.
[253] Y. Chen, M. Shafiq, M. Liu, Y. Morsi, X. Mo, *Bioactive Materials* **2020**, *5*, 963.
[254] B. Sun, Y. Z. Long, H. D. Zhang, M. M. Li, J. L. Duvail, X. Y. Jiang, H. L. Yin, *Progress in Polymer Science* **2014**, *39*, 862.
[255] C. A. Bonino, K. Efimenko, S. I. Jeong, M. D. Krebs, E. Alsberg, S. A. Khan, *Small* **2012**, *8*, 1928.
[256] Q. Yao, J. G. L. Cosme, T. Xu, J. M. Miszuk, P. H. S. Picciani, H. Fong, H. Sun, *Biomaterials* **2017**, *115*, 115.
[257] F. Deuber, S. Mousavi, M. Hofer, C. Adlhart, *ChemistrySelect* **2016**, *1*, 5595.
[258] W. Chen, S. Chen, Y. Morsi, H. El-Hamshary, M. El-Newhy, C. Fan, X. Mo, *ACS Applied Materials & Interfaces* **2016**, *8*, 24415.
[259] J. Zhu, S. Jiang, H. Hou, S. Agarwal, A. Greiner, *Macromolecular Materials and Engineering* **2018**, *303*, 1700615.
[260] W. Chen, J. Ma, L. Zhu, Y. Morsi, H. Ei-Hamshary, S. S. Al-Deyab, X. Mo, *Colloids and Surfaces B: Biointerfaces* **2016**, *142*, 165.
[261] M. Mader, M. Helm, M. Lu, M. H. Stenzel, V. Jérôme, R. Freitag, S. Agarwal, A. Greiner, *Biomacromolecules* **2020**, *21*, 4094.
[262] L. Berhan, A. M. Sastry, *Physical Review E* **2007**, *75*, 041120.
[263] G. Duan, S. Jiang, T. Moss, S. Agarwal, A. Greiner, *Polymer Chemistry* **2016**, *7*, 2759.
[264] S. Mohaghegh, H. Sadat Haeri Boroojeni, H. Nokhbatolfoghahaei, A. Khojasteh, *British Journal of Oral and Maxillofacial Surgery* **2023**, *61*, 587.

[265] A. Krzan, S. Hemjinda, S. Miertus, A. Corti, E. Chiellini, *Polymer Degradation and Stability* **2006**, *91*, 2819.
[266] J. M. Millican, S. Agarwal, *Macromolecules* **2021**, *54*, 4455.
[267] S. Agarwal, *Macromolecular Chemistry and Physics* **2020**, *221*, 2000017.
[268] I. Vroman, L. Tighzert, *Materials* **2009**, *2*, 307.
[269] W. Zhao, X. Jin, Y. Cong, Y. Liu, J. Fu, *Journal of Chemical Technology & Biotechnology* **2013**, *88*, 327.
[270] J. Xu, N. Hadjichristidis, *Progress in Polymer Science* **2023**, *139*, 101656.
[271] S. Pack, M. Lewin, M. H. Rafailovich, in *Fire and Polymers VI: New Advances in Flame Retardant Chemistry and Science*, Vol. 1118 (Eds. A.B. Morgan, C.A. Wilkie, G.L. Nelson), American Chemical Society, Washington, DC, USA **2012**, Ch. 27.
[272] S. Doppalapudi, A. Jain, W. Khan, A. J. Domb, *Polymers for Advanced Technologies* **2014**, *25*, 427.
[273] F. Hajiali, S. Tajbakhsh, A. Shojaei, *Polymer Reviews* **2018**, *58*, 164.
[274] F. Gironi, V. Piemonte, *Environmental Progress & Sustainable Energy* **2011**, *30*, 459.
[275] S. Saeidlou, M. A. Huneault, H. Li, C. B. Park, *Progress in Polymer Science* **2012**, *37*, 1657.
[276] M. Okamoto, B. John, *Progress in Polymer Science* **2013**, *38*, 1487.
[277] M. J. Krause, T. G. Townsend, *Environmental Science & Technology Letters* **2016**, *3*, 166.
[278] T. A. Hottle, M. L. Agüero, M. M. Bilec, A. E. Landis, *Compost Science & Utilization* **2016**, *24*, 159.
[279] J. P. G. L. Frias, R. Nash, *Marine Pollution Bulletin* **2019**, *138*, 145.
[280] A. R. Bagheri, C. Laforsch, A. Greiner, S. Agarwal, *Global Challenges* **2017**, *1*, 1700048.
[281] Y.-N. Chang, R. E. Mueller, E. L. Iannotti, *Plant Growth Regulation* **1996**, *19*, 223.
[282] R. E. Drumright, P. R. Gruber, D. E. Henton, *Advanced Materials* **2000**, *12*, 1841.
[283] M.-A. Paul, C. Delcourt, M. Alexandre, P. Degée, F. Monteverde, P. J. P. d. Dubois, stability, **2005**, *87*, 535.
[284] H. T. Oyama, Y. Tanaka, A. Kadosaka, *Polymer Degradation and Stability* **2009**, *94*, 1419.
[285] J. Siepmann, A. Göpferich, *Advanced Drug Delivery Reviews* **2001**, *48*, 229.
[286] I. Grizzi, H. Garreau, S. Li, M. Vert, *Biomaterials* **1995**, *16*, 305.
[287] M. J. A. i. P. S. Hakkarainen, **2002**, *157*, 113.
[288] Q. Zhou, M. Xanthos, *Polymer Degradation and Stability* **2008**, *93*, 1450.

[289] Y.-B. Luo, X.-L. Wang, Y.-Z. Wang, *Polymer Degradation and Stability* **2012**, *97*, 721.
[290] F. Iñiguez-Franco, R. Auras, M. Rubino, K. Dolan, H. Soto-Valdez, S. Selke, *Polymer Degradation and Stability* **2017**, *146*, 287.
[291] B. S. Ndazi, S. Karlsson, *EXPRESS POLYMER LETTERS* **2011**, *5*, 119.
[292] E. Ozdemir, T. O. Lekesiz, J. Hacaloglu, *Polymer Degradation and Stability* **2016**, *134*, 87.
[293] M. Karamanlioglu, R. Preziosi, G. D. Robson, *Polymer Degradation and Stability* **2017**, *137*, 122.
[294] F. Iñiguez-Franco, R. Auras, G. Burgess, D. Holmes, X. Fang, M. Rubino, H. Soto-Valdez, *Polymer* **2016**, *99*, 315.
[295] Y. Matsusue, T. Yamamuro, M. Oka, Y. Shikinami, S. H. Hyon, Y. Ikada, *Journal of biomedical materials research* **1992**, *26*, 1553.
[296] H. Tsuji, K. Ikarashi, *Biomaterials* **2004**, *25*, 5449.
[297] N. F. Zaaba, M. Jaafar, *Polymer Engineering & Science* **2020**, *60*, 2061.
[298] X. Qi, Y. Ren, X. Wang, *International Biodeterioration & Biodegradation* **2017**, *117*, 215.
[299] C.-C. Lin, K. S. Anseth, in *Biomaterials Science (Third Edition)*, (Eds. B.D. Ratner, A.S. Hoffman, F.J. Schoen, and J.E. Lemons), Elsevier Academic Press, San Diego, USA **2013**.
[300] D. F. Williams, *Engineering in Medicine* **1981**, *10*, 5.
[301] Y. Oda, A. Yonetsu, T. Urakami, K. Tonomura, *Journal of Polymers and the Environment* **2000**, *8*, 29.
[302] S. H. Lee, I. Y. Kim, W. S. Song, *Macromolecular Research* **2014**, *22*, 657.
[303] A. Kumar, A. R. Weig, S. Agarwal, *Macromolecular Materials and Engineering* **2022**, *307*, 2100602.
[304] J. Zhu, A. Kumar, P. Hu, C. Habel, J. Breu, S. Agarwal, *Global Challenges* **2020**, *4*, 2000030.
[305] L. T. Lim, R. Auras, M. Rubino, *Progress in Polymer Science* **2008**, *33*, 820.
[306] N. D. Rawlings, A. J. Barrett, R. Finn, *Nucleic Acids Research* **2016**, *44*, D343.
[307] A. Koterwa, I. Kaczmarzyk, S. Mania, M. Cieslik, R. Tylingo, T. Ossowski, R. Bogdanowicz, P. Niedziałkowski, J. Ryl, *Applied Surface Science* **2022**, *574*, 151587.
[308] F. Kawai, K. Nakadai, E. Nishioka, H. Nakajima, H. Ohara, K. Masaki, H. Iefuji, *Polymer Degradation and Stability* **2011**, *96*, 1342.
[309] S. Obuchi, S. Ogawa, in *Poly(Lactic Acid)* (Eds. R.F. Grossman, D. Nwabunma, R. Auras, L.-T. Lim, S.E.M. Selke, H. Tsuji), Wiley, Hoboken, NJ, USA **2010**, Ch. 25.

[310] S. R. Andersson, M. Hakkarainen, A.-C. Albertsson, *Biomacromolecules* **2010**, *11*, 3617.
[311] A. Höglund, M. Hakkarainen, A.-C. Albertsson, *Biomacromolecules* **2010**, *11*, 277.
[312] Y. Whulanza, A. Azadi, S. Supriadi, S. F. Rahman, M. Chalid, M. Irsyad, M. H. Nadhif, P. Kreshanti, *Heliyon* **2022**, *8*, e08600.
[313] M. Tang, Y. Dong, M. M. Stevens, C. K. Williams, *Macromolecules* **2010**, *43*, 7556.
[314] Q. Huang, M. Hiyama, T. Kabe, S. Kimura, T. Iwata, *Biomacromolecules* **2020**, *21*, 3301.
[315] S. Böhler, S. Rosencrantz, K. Wolf, R. Heinemann, P. Schmidt, J. Ganster, T. Büsse, J. Balko, R. R. Rosencrantz, *Materials Today Communications* **2023**, *34*, 105018.
[316] J. Bajorath, W. Hinrichs, W. Saenger, *European Journal of Biochemistry* **1988**, *176*, 441.
[317] K. Yazawa, M. Sugahara, K. Yutani, M. Takehira, K. Numata, *ACS Catalysis* **2016**, *6*, 3036.
[318] A. V. G. Ruzette, P. Banerjee, A. M. Mayes, T. P. Russell, *J. Chem. Phys.* **2001**, *114*, 8205.
[319] A. M. Mayes, A.-v. Ruzette, T. Russell, P. Banerjee (Massachusetts Institute of Technology) *WO2010092126A1*, **2001**.
[320] T. P. Russell, T. E. Karis, Y. Gallot, A. M. Mayes, *Nature* **1994**, *368*, 729.
[321] M. Pollard, T. P. Russell, A. V. Ruzette, A. M. Mayes, Y. Gallot, *Macromolecules* **1998**, *31*, 6493.
[322] D. Y. Ryu, D. J. Lee, J. K. Kim, K. A. Lavery, T. P. Russell, Y. S. Han, B. S. Seong, C. H. Lee, P. Thiyagarajan, *Physical Review Letters* **2003**, *90*, 235501.
[323] J. Dudowicz, K. F. Freed, *Macromolecules* **1993**, *26*, 213.
[324] J. A. González-León, *Doctoral Thesis*, Massachusetts Institute of Technology, February **2006**.
[325] M. Rabeony, D. Lohse, R. Garner, S. Han, W. Graessley, M. Kalman, **1998**.
[326] A.-V. G. Ruzette, *Doctoral Thesis*, Massachusetts Institute of Technology, June **2000**.
[327] J.-N. Qiao, Q.-C. Yang, Y. Li, Z. lv, J.-H. Tang, J. Lei, Z.-M. Li, *ACS Applied Polymer Materials* **2020**, *2*, 5550.
[328] A. V. G. Ruzette, A. M. Mayes, M. Pollard, T. P. Russell, B. Hammouda, *Macromolecules* **2003**, *36*, 3351.
[329] J. A. Gonzalez-Leon, M. H. Acar, S.-W. Ryu, A.-V. G. Ruzette, A. M. Mayes, *Nature* **2003**, *426*, 424.
[330] A. Wong, S. N. Leung, G. Y. G. Li, C. B. Park, *Industrial & Engineering Chemistry Research* **2007**, *46*, 7107.
[331] A. V. G. Ruzette, P. Banerjee, A. M. Mayes, M. Pollard, T. P. Russell, R. Jerome, T.

Slawecki, R. Hjelm, P. Thiyagarajan, *Macromolecules* **1998**, *31*, 8509.
[332] Z. Lv, J.-N. Qiao, Y.-N. Song, X. Ji, J.-H. Tang, D.-X. Yan, J. Lei, Z.-M. Li, *ACS Applied Materials & Interfaces* **2019**, *11*, 12008.
[333] I. Taniguchi, N. G. Lovell, *Macromolecules* **2012**, *45*, 7420.
[334] Z. Lv, C.-L. Jia, X. Ji, D.-X. Yan, J. Lei, Z.-M. Li, *Journal of Materials Chemistry C* **2018**, *6*, 12955.
[335] Y. Iwasaki, K. Takemoto, S. Tanaka, I. Taniguchi, *Biomacromolecules* **2016**, *17*, 2466.
[336] J. Y. Cheong, M. Mafi, L. Benker, J. Zhu, M. Mader, C. Liang, H. Hou, S. Agarwal, I.-D. Kim, A. Greiner, *ACS Applied Materials & Interfaces* **2020**, *12*, 18002.
[337] Q. Huang, M. Hiyama, T. Kabe, S. Kimura, T. Iwata, *Biomacromolecules* **2020**, *21*, 3301.

# 5. Conclusion and outlook

The thesis clearly showed the potential of electrospun degradable PLLA sponges in different application fields, such as tissue engineering and agricultural materials. The intrinsic hydrophobicity of PLLA was conquered by dip-coating the surfactant Tween 20 in a sustainable way. The hydrophilization was efficient and notably persistent even after immersion in aqueous medium for a long time. The hydrophilic PLLA sponges displayed benign cell compatibility and were favorable for cell proliferation and penetration. Nevertheless, there are also other surfactants which might have the potential for the hydrophilization of PLLA sponges based on their HLB or CMC values. Some preliminary work of this thesis showed that Tween 20 could increase the enzymatic activity of proteinase K. Therefore, the integration of surfactants into sponge could be another promising topic to design the sponge system with the tailored degradation rate of PLLA. The assumption of the increased activity is that the surfactant can change the tertiary structure of proteinase K, which will, in turn, benefit the infiltration of the substrate. Nonetheless, the stretching of chains results in the reduced thermal stability of proteinase K during thermal processing, eventually causing a loss of enzymatic activity. Remarkably, the enzymatic activity of proteinase K in a dry state could be retained at a rather high temperature, but still not high enough for PLLA thermal processing. It was clearly demonstrated by the activity assay established in this thesis that proteinase K could not withstand the processing temperature of PLLA, even after being encapsulated. The inadequate thermal stability of proteinase K at high temperatures hinders its possibility for thermal processing together with PLLA, such as for 3D printing. Rather than encapsulating proteinase K, processing it at an ambient temperature would be a better solution to the problem. The processing of proteinase K at an ambient temperature was achieved by utilizing the baroplastic concept, which was used as a promising processing method in the thesis. Processing at an ambient temperature offered the possibility of composite processing using proteinase K as an additive. Surprisingly, PLLA-PEG block copolymers were found to be suitable baroplastic polymers. They behave differently compared to other known baroplastic polymers. Only the amorphous parts of PLLA/PEG segments melt under high pressure, while the crystallites of the PLLA segment remain intact under high pressure. When the pressure is released, the crystallites serve as hard blocks in a solid state. The enhanced mechanical properties are attributed to the hard blocks in the PLLA segment. This behavior is similar to the thermoplastic elastomer concept, which consists of a hard and soft segment. It could be anticipated that there are still many block copolymers containing crystallites and amorphous

segments, where the latter are miscible. This decisive factor would provide those block copolymers with the potential to be used as baroplastic polymers. The baroplastic concept reduces energy consumption during processing, accordingly, offering the opportunity for environmentally friendly processing. Therefore, it is well worth investigating this kind of baroplastic copolymers. The design of baroplastic polymers would also allow the continuous processing in a sustainable way, which is promising for polymer applications.

## 6. Acknowledgements

I would like to give my sincere appreciation to all the people who gave me support to finish this thesis.

First of all, I would like to thank my supervisor, Prof. Andreas Greiner, for giving me this opportunity to work on this exciting topic. I would also like to thank him for his patience, enthusiasm and inspiration during the supervision of my work. Besides scientific work, I was also affected by his optimism, from which I learned how to face failures and enjoy success. In addition, I also learned many useful competencies from him, such as communication and presentation skills, which will definitely be beneficial to my future work and life.

Next, I would like to thank Prof. Seema Agarwal for her warm support during my work in the group. She has always been helpful and creative during scientific discussions, and extremely efficient when doing revision and proofreading of my manuscript. She is always passionate and innovative when providing research ideas, and takes care of all the group members ardently.

I would like to thank Prof. Andreas Möglich for his helpful support in the biochemical work field. He provided many useful ideas during discussions, did manuscript revision, and gave high quality and elegant language optimizations for the manuscripts. He also offered me the chance to use many instruments in his lab and gave enormous support when I was working there. Additionally, he offered help with devices and chemicals in my scientific work. During the cooperation with him, I gained more interest in biochemistry and had a deeper understanding of this field.

I would like to thank several colleagues for their cooperation and discussions in different areas: Prof. Bernhard Schartel and Dr. Battig Alexander for TGA-FTIR; Prof. Jürgen Senker and Dr. Renée Siegel for ss-NMR; Prof. Carlo Unverzagt and Inge von der Forst for the synthesis of an oligo peptide; Dr. Jun Young Cheong for providing ideas for sponge hydrophilization; Prof. Xiumei Mo, Prof. Ruth Freitag and Dr. Valérie Jérôme for revision of the sponge manuscript; Dr. Reza Gharibi for cell culture tests; Chengwei Yi for YPet synthesis and analysis; Prof. Jürgen Köhler and Dr. Lisa Günter for fluorescence microscopy; Dipannita Gosh and Prof. Seema Agarwal for sludge water degradation tests; Prof. Christian Laforsch, Anja Ramsperger and Julian Brehm for Daphnia and cell toxicity tests; Dr. Sabine Rosenfeldt for SAXS measurement; Dr. Ulrich Mansfeld and Martina Heider for TEM and SEM measurements; Tobias Lauster and Dr. Qimeng Song for plasma treatment; and Christian Müller for his help with the polarimeter in the group of Prof. Matthias Breuning.

I would like to thank the following group members for their support with the research work on different issues. I would like to thank Dr. Holger Schmalz for all the discussions about polymer synthesis and characterization; Rika Schneider for her support with GPC and the synthesis of block copolymers; Lothar Benker for his great help with Raman spectroscopy; Maximillian Rist and Marcel Höferth for their help with LC-MS; Adrian Wambach and Thomas Schmidt for their IT support; Gaby Olivier, Niko Plocher, Ramona Lechner and Christina Lindörfer for all their help with the administrative work; and Annette Krökel for her assistance with chemicals and equipment. Moreover, I would like to thank my direct labmates Elmar Sehl, Sören Schumacher, Sagar Joshi, Daina Damberger, Sophia Däbritz, Lars Schwarzer, Dr. Sivaraj Pazhaniswamy, Mohamed Albashkar and Shweta Hiwase for their support, valuable discussions and all the wonderful time together. Furthermore, I would like to thank all our group members for all their support and the joyful hours, and for the pleasant working atmosphere.

In addition, I would like to thank CRC1357 Microplastics for the financial support regarding my research work, and all the organization and kind help within the project.

Last but not least, I would like to show my appreciation to my friends and all my family members, especially my parents, my husband and his family, who have always been unconditionally supportive and encouraging during my thesis work.

## 7. (Eidesstattliche) Versicherungen und Erklärungen

(§ 9 Satz 2 Nr. 3 PromO BayNAT)

*Hiermit versichere ich eidesstattlich, dass ich die Arbeit selbstständig verfasst und keine anderen als die von mir angegebenen Quellen und Hilfsmittel benutzt habe (vgl. Art. 97 Abs. 1 Satz 8 BayHIG).*

(§ 9 Satz 2 Nr. 3 PromO BayNAT)

*Hiermit erkläre ich, dass ich die Dissertation nicht bereits zur Erlangung eines akademischen Grades eingereicht habe und dass ich nicht bereits diese oder eine gleichartige Doktorprüfung endgültig nicht bestanden habe.*

(§ 9 Satz 2 Nr. 4 PromO BayNAT)

*Hiermit erkläre ich, dass ich Hilfe von gewerblichen Promotionsberatern bzw. -vermittlern oder ähnlichen Dienstleistern weder bisher in Anspruch genommen habe noch künftig in Anspruch nehmen werde.*

(§ 9 Satz 2 Nr. 7 PromO BayNAT)

*Hiermit erkläre ich mein Einverständnis, dass die elektronische Fassung meiner Dissertation unter Wahrung meiner Urheberrechte und des Datenschutzes einer gesonderten Überprüfung unterzogen werden kann.*

(§ 9 Satz 2 Nr. 8 PromO BayNAT)

*Hiermit erkläre ich mein Einverständnis, dass bei Verdacht wissenschaftlichen Fehlverhaltens Ermittlungen durch universitätsinterne Organe der wissenschaftlichen Selbstkontrolle stattfinden können.*

…….

Ort, Datum, Unterschrift